LUT
Lappeenranta
University of Technology

Olga Oleksiienko

PHYSICO-CHEMICAL PROPERTIES OF SOL-GEL SYNTHESIZED TITANOSILICATES FOR THE UPTAKE OF RADIONUCLIDES FROM AQUEOUS SOLUTIONS

Thesis for the degree of Doctor of Science (Technology) to be presented with due permission for public examination and criticism in the Mikkeli University Consortium (MUC) auditorium, Mikkeli, Finland on the 16th of August, 2016, at noon.

Acta Universitatis
Lappeenrantaensis 709

Supervisor Professor Mika Sillanpää
LUT School of Engineering Science
Lappeenranta University of Technology
Finland

Reviewers Professor Shaobin Wang
Curtin University of Technology
Australia

Professor Ulla Lassi
University of Oulu
Finland

Opponent Assistant Professor Amit Bhatnagar
Department of Environmental and Biological Sciences
University of Eastern Finland
Finland

ISBN 978-952-265-987-3
ISBN 978-952-265-988-0 (PDF)
ISSN-L 1456-4491
ISSN 1456-4491

Lappeenrannan teknillinen yliopisto
Yliopistopaino 2016

Abstract

Olga Oleksiienko

Physico-chemical properties of sol-gel synthesized titanosilicates for the uptake of radionuclides from aqueous solutions

Lappeenranta 2016
100 pages
Acta Universitatis Lappeenrantaensis 709
Diss. Lappeenranta University of Technology
ISBN 978-952-265-987-3, ISBN 978-952-265-988-0 (PDF), ISSN-L 1456-4491, ISSN 1456-4491

Harnessing the power of nuclear reactions has brought huge benefits in terms of nuclear energy, medicine and defence as well as risks including the management of nuclear wastes. One of the main issues for radioactive waste management is liquid radioactive waste (LRW). Different methods have been applied to remediate LRW, thereunder ion exchange and adsorption. Comparative studies have demonstrated that $Na_2Ti_2O_3SiO_4 \cdot 2H_2O$ titanosilicate sorption materials are the most promising in terms of Cs^+ and Sr^{2+} retention from LRW. Therefore these TiSi materials became the object of this study. The recently developed in Ukraine sol-gel method of synthesizing these materials was chosen among the other reported approaches since it allows obtaining the TiSi materials in the form of particles with size $\geq$ 4mm. utilizing inexpensive and bulk stable inorganic precursors and yielded the materials with desirable properties by alteration of the comparatively mild synthesis conditions.

The main aim of this study was to investigate the physico-chemical properties of sol-gel synthesized titanosilicates for radionuclide uptake from aqueous solutions. The effect of synthesis conditions on the structural and sorption parameters of TiSi xerogels was planned to determine in order to obtain a highly efficient sorption material. The ability of the obtained TiSis to retain Cs^+, Sr^{2+} and other potentially toxic metal cations from the synthetic and real aqueous solutions was intended to assess. To our expectations, abovementioned studies will illustrate the efficiency and profitability of the chosen synthesis approach, synthesis conditions and the obtained materials.

X-ray diffraction, low temperature adsorption/desorption surface area analysis, X-ray photoelectron spectroscopy, infrared spectroscopy and scanning electron microscopy with energy dispersive X-ray spectroscopy was used for xerogels characterization. The sorption capability of the synthesized TiSi gels was studied as a function of pH, adsorbent mass, initial concentration of target ion, contact time, temperature, composition and concentration of the background solution.

It was found that the applied sol-gel approach yielded materials with a poorly crystalline sodium titanosilicate structure under relatively mild synthesis conditions. The temperature of HTT has the strongest influence on the structure of the materials and consequently was concluded to be the control factor for the preparation of gels with the desired properties. The obtained materials proved to be effective and selective for both Sr^{2+} and Cs^+ decontamination from synthetic and real aqueous solutions like drinking, ground, sea and mine waters, blood plasma and liquid radioactive wastes.

Keywords: titanosilicates, sol-gel method, kinetic studies, sorption mechanism, separation factor, selectivity coefficient, caesium, strontium, toxic metal cations, radionuclides

Acknowledgements

First of all, I thank my supervisor, Professor Mika Sillanpää, for giving me the opportunity to work in his well-equipped and internationally staffed laboratory. Thanks to your kind support and encouragement -– I learned a great deal and met a lot of new great friends and colleagues. Without your trust in me this thesis would never have been possible.

My sincere gratitude also goes to Prof. Dr habil. Christian Wolkersdorfer for his kind support, countless patience in explaining and endless inspiration for my studies. And of course, additional thanks for opening up the world of mine water to me and illustrating how passionate a researcher shall be.

Additionally, I want to thank Prof. Volodymyr V. Strelko and all my Ukrainian colleagues for their assistance with sample synthesis and pore structure characterization. In particular I wish to name Svitlana I. Meleshevych, Valentyn A. Kanibolotsky, Nadiya M. Patryliak, Yuriy M. Kylivnyk, and Valeriy I. Yakovlev; I learned a lot from you.

Also I thank Prof. Maciej Sitarz for his invaluable advice on material characterization, fruitful discussions of my work and excellent collaboration on our papers. It was a true pleasure to have such a co-author.

I greatly appreciate Prof. Galina Lujaniene for her kind assistance with radionuclide studies, fruitful discussions and interesting ideas on our research and paper.

Furthermore, I thank my dearest teachers, Olena M. Kovtyn and Olena V. Mityaeva, from the bottom of my heart. Learning from you is an honour and a great pleasure. Thank you for sharing your love to chemistry, support and trust and for inspiring me to continue my education

Especially, I thank my friends and colleagues Heikki, Mahmoud, Kwena and Taras. You inspired me, taught me and blessed me with your friendship ─ thank you.

Ultimately, the greatest appreciation, from all my heart, I express to Irina Levcuk: for the amazing chance to change my life, to discover the Laboratory of Green Chemistry and Finland for me. Never-ever before have I met such a wonderful, intelligent, helpful and kind person. Thank you from the bottom of my heart for bringing so much new knowledge and happiness into my life!

Finally, I want to thank my family for their understanding, support, care and trust in me during all these years.

Olga Oleksiienko
March 2016
Malyn, Ukraine

Contents

List of publications

This thesis is based on the following papers. The rights have been granted by the publishers to include the papers in this dissertation.

I. **Oleksiienko**, **O.,** Meleshevych, S., Strelko, V., Wolkersdorfer, Ch., Tsyba, M. M., Kylivnyk, Yu. M., Levchuk, I., Sitarz, M., Sillanpää, M. (2015). Pore structure and sorption characterization of titanosilicates obtained from concentrated precursors by the sol–gel method. *Royal Society of Chemistry Advances,* 5, pp. 72562–72571, DOI: 10.1039/c5ra06985h.

II. **Oleksiienko**, **O.,** Levchuk, I., Sitarz, M., Meleshevych, S., Strelko, V., Sillanpää, M. (2015). Removal of strontium (Sr^{2+}) from aqueous solutions with titanosilicates obtained by sol-gel method. *Journal of Colloid and Interface Science*, 438, pp. 159–168, DOI: 10.1016/j.jcis.2014.09.075.

III. **Oleksiienko**, **O.,** Levchuk, I., Sitarz, M., Meleshevych, S., Strelko, V., Sillanpää, M. (2015). Adsorption of caesium (Cs^{+}) from aqueous solution by porous titanosilicate xerogels. *Desalination and Water Treatment*. Published online: 19 Jan 2015, DOI: 10.1080/19443994.2014.1003103.

IV. Lujaniene G., Meleshevych S., Kanibolotskyy V., Mazeika K., Strelko V., Remeikis V., **Oleksienko O.**, Sapolaite J. (2009). Application inorganic sorbents for removal Cs, Sr, Pu and Am from contaminated solutions. *Journal of radioanalytical and nuclear chemistry*, 282(3), pp. 787–791, DOI: 10.1007/s10967-009-0170-z.

V. Ivanets, A.I., Kitikova, N.V., Shashkova, I.L., **Oleksiienko**, **O.V.,** Levchuk, I., Sillanpää, M. (2014). Removal of Zn^{2+}, Fe^{2+}, Cu^{2+}, Pb^{2+}, Cd^{2+}, Ni^{2+} and Co^{2+} ions from aqueous solutions using modified phosphate dolomite. *Journal of Environmental Chemical Engineering,* 2, pp. 981–987, DOI: 10.1016/j.jece.2014.03.018.

Author's contribution

I—III The author carried out all the experimental work, analysed the data and prepared the first draft of the manuscript.

IV The author carried out the synthesis of sorbents and material characterization. The data was analysed and the manuscript prepared together with the co-authors.

V The author carried out all the sorption experiments. The data was analysed and the manuscript prepared together with the co-authors.

Related publications

1. Oleksiienko O.V., Meleshevych S.I., Strelko V.V., V'yunov O.I., Matkovsky O.K., Milgrandt V.G., Tsyba M.M. and Kanibolotsky V.A., Effect of hydrothermal treatment on the formation of the titanosilicates` porous structure. Probl. Chem. Chem. Technol., 2013, 2, pp. 101–105. (Ukrainian)

2. Kalenchuk V.G., Meleshevych S.I., Kanibolotsky V.A., Strelko V.V., Oleksiienko O.V. and Patryliak N.M., A method for producing titanosilicate ion exchangers, Patent UA48457U, 2010. (Ukrainian)

3. Strelko V.V., Meleshevych S.I., Kanibolotsky V.A. and OleksiienkoO.V., A method for producing titanosilicate ion exchangers, Patent UA48457U, 2012. (Ukrainian)

4. Ivanets, A.I., Kitikova, N.V., Shashkova, I.L., Oleksiienko, O.V., Levchuk, I. and Sillanpää, M., Using of phosphatized dolomite for treatment of real mine water from metal ions. Journal of Water Process Engineering, 2016, 9, pp. 246-253.

Nomenclature

Latin alphabet

m	mass	g
p	pressure	Pa
r	radius	m
T	temperature	K
t	time	s
$t_{½}$	half life	a
q	adsorption capacity	mmol/L
q_m	maximum adsorption capacity	mmol/L
V	volume	m^3

Greek alphabet

α	radiation
Δ	change
ε	Polanyi potential
θ	angle

Subscripts

p	particle
g	gas
s	solid
l	liquid
max	maximum
min	minimum
tot	total

Abbreviations

2D	two dimensional
3D	three dimensional
$[Cs^+]$	concentration of Cs^+ in solution
AM	Aveiro and Manchester universities
BET	Brunauer-Emmett-Teller theory
BJH	Barrett-Joyner-Halenda theory
C_0	initial concentration
C_{eq}	concentration at equilibrium
CTS	crystalline titanosilicate material
DF	decontamination factor
DFT	Density functional theory
DR	Dubinin-Radushkevich equation
ETS-10	Engelhard Titanosilicate Number 10

ETS-4	Engelhard Titanosilicate Number 4
EXAFS	extended X-ray absorption fine structure
F	separation factor
FTIR	Fourier transform infrared spectroscopy
GTS-1	Grace titanium silicate-1
HLW	high-level waste
HTT	hydrothermal treatment
ICP-MS	inductively coupled plasma with mass detector
ICP-OES	inductively coupled plasma optical atomic emission spectrometer
ILW	intermediate-level waste
IUPAC	International Union of Pure and Applied Chemistry
K_d	distribution coefficient
K_F	Freundlich constant
K_G	selectivity coefficient according to Gapon
K_L	Langmuir Constant
K_{lm}	selectivity coefficient according to the law of mass action
LLW	low-level waste
LRW	liquid radioactive wastes
N	Avogadro constant
NPP	nuclear power plants
PD	phosphated dolomite
q	sorption capacity
R^2	correlation coefficient
RL	Ringer–Locke's solution
RW	radioactive wastes
S_{BET}	specific surface area cumulated using BET theory
SEM	scanning electron microscopy
SEM-EDX	energy dispersive X-ray spectroscopy
S_{tot}	total surface area
$t_{½}$	half-life time of radionuclide
TiSi	titanosilicate
TiSis	titanosilicates (plural of TiSi to simplify reading and writing)
TiSi(p)	titanosilicates synthesized from a pure precursor
TiSi(t)	titanosilicates synthesized from a technical precursor
VLLW	very low-level wastes
XPS	X-ray photoelectron spectroscopy
XRD	X-ray diffractometry

1 Introduction

1.1 Radioactive pollution and potential problems

Radioactivity, the result of nuclear reactions, was discovered by Henri Becquerel in 1896. It has been used ever since in an increasingly wide range of applications, including nuclear research reactors and isotope laboratories, nuclear medicine, nuclear power plants (NPP) and the defence industry [1-3]. Unfortunately, this great discovery is not only a source of knowledge and progress, but also of radioactive pollution [4-7]. In addition, almost all stages in the nuclear cycle produce radioactive wastes (RW).

Both, the Chernobyl and Fukushima catastrophes evidenced the incapability of the nuclear industry to protect the environment from radionuclide pollution in all circumstances [8-14]. Nevertheless, many countries are continuing to build new nuclear power plants (NPPs). The medical interest in radioactive processes is very high, and energy consumption is growing exponentially. Unfortunately, the renewable energy industry is not yet able to fully replace nuclear energy [15, 16].

Anthropogenic radionuclides increase levels of radioactivity over the natural background where living organisms' mechanisms of self protection are no longer effective. There are numerous studies devoted to the noxious effects of radioactive pollutants on human health including nephrotoxicity [17-19], brain toxicity [20, 21], infant mortality [22-24], skeleton deformation [25, 26] and negative effects on other living organisms [27-36]. Such pernicious effects force people to leave formerly fertile lands, forests and water resources until reliable methods of purifying the polluted sites will be found [37-39].

In order to protect the environment, animals and human settlements from sources of radionuclides, efficient decontaminating processes, techniques and materials must be developed. This thesis focuses on developing such materials.

1.2 Mitigation of radioactive pollution

Radioactive wastes (RW) can be classified by their aggregate state as solid RW, liquid RW (LRW) and gaseous RW, and by the level of radioactivity as low-level waste (LLW), intermediate-level waste (ILW) and high-level waste (HLW). Mitigation activities vary according to the state and radioactivity level of the waste concerned. For example, the depth at which solid RW is buried depends on the radioactivity level. While solid LLW is not considered dangerous to handle, disposal with more care than normal garbage is required. It can be compacted or burned in a closed container and disposed of in a shallow landfill. In contrast, solid ILW and HLW must be stored deep underground [4, 40-45].

Some liquid LLW is disposed off into the sea and can be traced by ^{99}Tc hundreds of kilometres away from its original disposal site. Such discharges are supposed to be strictly regulated so that the maximum dose of radiation released into the environment does not exceed a small fraction of the natural background radiation [42, 46]. Yet the Fukushima disaster made it evident that such a practice must be reconsidered. The French way of storing even very low-level wastes (VLLW) in specifically designed VLLW disposal facilities should be more widely adopted [11, 12]. Liquid ILW and HLW must be treated prior to utilization. This is one of the main issues for radioactive waste management [47-49].

A wide range of methods have been proposed and applied to remediate radioactive pollution in aqueous solutions, such as drinking, sea, mine waters and LRW [2, 4, 36, 37, 49-51]. These include bioremediation, solvent extraction, precipitation, evaporation, adsorption, ion exchange and membrane techniques and combinations thereof [52-56].

Chemical precipitation is suitable for waste in large volumes and with a high salt content; it is easy and inexpensive to operate, but has a low decontamination factor (DF) and its efficiency depends on the solid-liquid separation stage [41, 57, 58]. The thermal evaporation method of concentrating LRW is still in use for large volumes of waste, for example at Chernobyl's Shelter Object, despite its high energy consumption, foaming, corrosion and the volatility of some radionuclides such as ^{137}Cs, ^{106}Ru or ^{3}H [41, 59, 60]. Solvent extraction is selective and makes it possible to recover or recycle actinides, but it generates aqueous and organic secondary wastes [61-64].

Ultrafiltration separates dissolved salts from particulate and colloidal materials. It has good chemical and radiation stability with inorganic membranes, but membrane fouling is a challenge and organic membranes are not always radiation resistant [58, 65, 66]. Microfiltration yields high recovery (99%), but is sensitive to impurities in the waste stream [52, 53, 57, 67, 68]. Reverse osmosis removes dissolved salts, has a medium DF, is economically feasible and established for large scale operations, but it is limited by osmotic pressure and membrane fouling [10, 58, 69, 70]. Membrane distillation carried out at low temperatures decreases the volatility of radionuclides like ^{3}H, some forms of iodine and ruthenium. It is important to note that membrane distillation allows the complete RW purification in one stage. Unfortunately, membranes are liable to fouling, so the module productivity gradually decreases. The need for regular cleaning leads to the interruption of the purification process and production of secondary wastes [41, 52, 53, 57, 58, 68].

Ion exchange and adsorption are the most commonly used methods for LRW chemical processing [71-75]. Obviously, these methods do not have an ideal removal selectivity. Sorption materials sensitive enough to separate individual nuclide ions have not yet been invented. Nevertheless, sorption materials make it possible to decrease LRW levels by retaining the radionuclides in a solid form, while the deactivated water can be reused or safely released to the environment.

Combinations of the abovementioned methods were also tested for treating LRW. Electrically switched ion exchange is an example of a promising combination method. It combines the advantages of selective electrodes and selective ion exchange. Nevertheless, it needs furte her optimization so that a regenerative material can be used and secondary waste minimized [51, 76, 77].

The different origins of LWR define the variety of its composition, which increase the requirements on decontamination processes and materials. This variety makes combined methods and techniques more promising. The most commonly proposed combined processes include sorption materials, which must be ionization radiation resistant, chemically stable in a broad pH range, unaffected by temperature, possess a high kinetic rate, have a high sorption capacity and selectivity to target nuclides and an ability to remain "uncontaminated" by the presence of the other cations in solution. Among all the sorption materials, the inorganic ones meet these requirements best. Metal oxides, phosphates, titanates, ferrocyanides, silica gels, clays, alumosilicates (zeolites), antimony silicates, niobium silicates and titanosilicates have been used for radioactive and stable cation removal from aqueous solutions [49, 74, 78-86].

A comparative study of 28 inorganic sorption materials to Cs^+ showed that the sodium zirconium trisilicate ($Na_2ZrSi_3O_9 \cdot H_2O$) has the highest ion exchange capacity for Cs^+, whereas the highest selectivity was demonstrated by framework titanium silicate (TiSi; $Na_2Ti_2SiO_7 \cdot 2H_2O$), layered titanium silicate ($Na_2TiSi_2O_7 \cdot 2H_2O$) and sodium phlogopite ($NaMg_3[AlSi_3O_{10}](OH)_2$). These exchangers exhibit a high resistance to calcium and sodium competition and retain their selectivity even in the presence of 100–1000 times excess of these ions. Yet only framework titanosilicate, framework niobium silicate ($Na_2Nb_8Si_4O_{29} \cdot 18H_2O$), and layered titanium silicate were suitable for selective strontium uptake in the presence of an excess of calcium. To summarize, two framework silicates (titanosilicate and niobium silicate) and layered titanium silicates showed the best selectivity for Sr^{2+} in calcium neutral media. These exchangers are also selective for Cs^+, suggesting their ability to simultaneously sorb Cs^+ and Sr^{2+} ions from contaminated groundwater and process water. An important observation was that framework TiSi traps the Cs^+ permanently and exhibits irreversible Sr^{2+} ion exchange [86].

2 Sorption theory

2.1 Basic concepts

Sorption is a surface phenomenon of a change in chemical substance concentration (depletion/accumulation) at the common boundary of two neighbouring phases which can be divided into absorption, adsorption and ion exchange. Absorption is the penetration of one phase into another (at least for a few nanometres), while adsorption is the accumulation of a substance on the surface of another phase (in the case of positive adsorption). Ion exchange is an exchange of ions from the boundary surface by ions from the neighbouring, mainly liquid phase. The accumulating substance is called sorbate and the material which causes the concentration change in a system of two phases is the sorbent. Adsorption can be categorized into physisorption and chemisorption depending on the nature of the bonds between the adsorbent and adsorbate: van der Waals forces, hydrogen bonding, hydrophobic and weak electrostatic interactions cause physisorption and covalent or ionic bonds are formed during chemisorption. There are some opinions that ion exchange is an adsorption process with forces of an electrostatic nature [73, 87-91].

Physisorption has low bond energy and heat of adsorption (1–10 kcal/mol). It is a reversible, nonspecific, and spontaneous process, which can occur as a monolayer or multilayer at a temperature close to the critical one. Physical adsorption is an exothermic process that leads to decreasing free energy and entropy of the adsorption system. Chemical sorption is characterized by high bond energy and heat of adsorption (10–100 kcal/mol) and occurs only as a monolayer, usually at temperatures much higher than the critical temperature. It is an irreversible, non-spontaneous, specific process which takes place only on some solid surfaces for a certain substance [89, 92, 93]. The main factors affecting the sorption process in a solid/liquid system are solute concentration, sorbent surface area, sorbent selectivity, solvent effect and pH.

The main characteristics of the ion exchange process are its high rate, stoichiometry, reversibility and selectivity to ions of differing charge and size. The ion selectivity of the exchanger is a function of ionic charge and hydrated radius and functional group-ion chemical interactions. In most cases, the higher the ionic charge, the higher the affinity for a site. The smaller the hydrated radius of the ion, the greater the exchanger affinity to it, which is due to limited pore spaces. In general, cations with a higher valence are sorbed more preferably. Ion exchangers are more selective to a cation with a larger atomic mass if the valence of the cations is equal. With increasing ion concentrations, the general selectivity difference trends are reduced or may reverse. The selectivity coefficient is only applicable over a narrow range of concentrations because the activity coefficients vary with concentration. Selectivity is one of the main exchanger characteristics [94, 95].

Sometimes, absorption–adsorption or adsorption–ion exchange can take place simultaneously, and clear identification of the mechanism is not really possible. In these

cases the term ‘sorption’ is used [73]. Other terms such as retention, adsorption and uptake may be used as alternatives to sorption. In this work the term sorption will be used to describe adsorption or ion exchange processes, or cases where such a clear differentiation is not possible or the mechanism is not defined yet.

Sorption processes can be divided into the following steps (stages): firstly, transport of solute (dissolved component of solution to be sorbed) close to the sorbent surface; secondly, the film diffusion step in which solute passes the diffusion and boundary layers of the counterions (external diffusion) and diffusion of the solute inside the pore space (internal diffusion, if the sorbent has a porous structure); and finally, the surface reaction or binding of the sorbate to the sorbent itself [73, 96]. The contribution of every step and interaction must be investigated and taken into account. The external diffusion step can be neglected and compensated by vigorous shaking or by a flow of liquid, but internal diffusion greatly affects the sorption parameters of sorbents with a porous structure.

Sorption processes can be characterized by their parameters such as capacity, rate, mechanism and selectivity. The maximum amount of substance/ions that can be adsorbed/exchanged by a certain material is called theoretical specific capacity Q (meq/g). Usually, the experimental specific capacity q (mmol/g) that can be calculated using Eq. (2.1) is lower due to the different accessibility of the active sites and steric restrictions in the case of porous materials.

$$q = \left(C_0 - C_t\right)\frac{V_{\mathrm{al}}}{m} \tag{2.1}$$

where C_o and C_{eq} are the initial pollutant concentration and the concentration at the time t in the solution (mmol/L); q is an experimental capacity, the amount of exchanged/sorbed cation on the material surface (mmol/g); V_{al} is an aliquot volume (mL); m is the mass of the adsorbent (g).

Changes in sorption capacity with time define the kinetic parameters of the sorption process. The system reaches equilibrium and can be characterized by its equilibrium capacity q_{eq} (mmol/g) if the sorption capacity remains unchanged with time. The analysis of kinetic and equilibrium parameters of a system can give a suggestion about the mechanism of the sorption process [73, 90, 97, 98]. Sorption theories were developed to describe (model) sorption systems in a state of equilibrium (equilibrium sorption isotherms) and their kinetic parameters (kinetic models), taking into account the contribution of solid/liquid interactions.

2.2 Adsorption isotherms

2.2.1 Classification of isotherms

An adsorption isotherm describes the amount of component adsorbed by the adsorbent surface from the solution with a certain adsorbate concentration at equilibrium and at a constant temperature. Giles (1960) provided the classification of the solution isotherms (Figure 2.1) and directions for diagnosing the sorption mechanism using the isotherm shape [99].

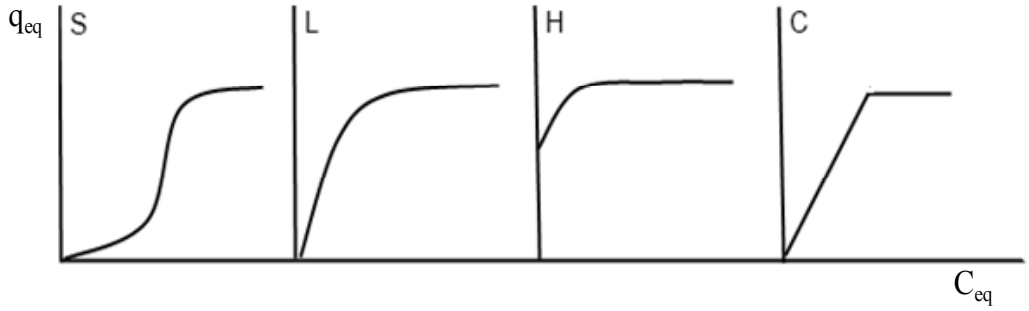

Figure 2.1: The types of solution adsorption isotherm, modified from [99]. The letters S, L, H, and C are the names of the isotherm types.

There are four general types of isotherm (Figure 2.1). The S type isotherm signifies cooperative adsorption and vertical orientation of adsorbate molecules at the sorbent surface. The L type, the normal or "Langmuir" isotherm, is the most common isotherm in the majority of sorptions from dilute solution. It usually indicates preferential adsorption, horizontal adsorbed molecule orientation or vertical orientation of sorbed ions from a particularly strong intermolecular attraction. The H type isotherm curves ("high affinity"), often demonstrated by adsorbed ionic micelles and high-affinity ion exchanging, may suggest chemisorption. The C shape is characteristic of "constant partition" and ion exchange; the linear part is given by solutes which permeate the sorbent better than the solvent does. This can imply that the number of active sites available for the sorption material does not change with concentration up to saturation [99-103].

2.2.2 Equilibrium isotherm models

Sorption isotherm parameters express the sorbent surface properties and affinity. Empirical sorption models were developed to describe experimental data without a theoretical basis, while chemical sorption models describe the sorption process based on the equilibrium approach. Exchange isotherms are an alternative to describe equilibrium by selectivity coefficients and have the same format as adsorption isotherms [73, 87-

91]. The models for the liquid/solid system most frequently used in the literature will be briefly described in this chapter.

Freundlich isotherm

The Freundlich isotherm is one of the earliest empirical non-linear isotherms used for describing adsorption equilibria [98]. It contains only two parameters, allows for multilayer adsorption and represents properly the adsorption data at low and intermediate concentrations on heterogeneous surfaces:

$$q_{eq} = K_F C_{eq}^{1/n_F} \tag{2.2}$$

where q_{eq} and C_{eq} are the equilibrium adsorption capacity (mmol/g) and the equilibrium concentration of the adsorbate (mmol/L), respectively, while K_F ((mmol/g)/(L/mmol)^{n_F}) is the Freundlich constant indicating the adsorption capacity and $1/n_F$ is a function of the strength and intensity of adsorption in the adsorption process. The smaller the $1/n_F$ value, the greater the expected heterogeneity. If n_F is equal to one, the partition between the two phases is independent of the concentration. If the value of $1/n_F$ is below 1, it signifies normal adsorption and where $1/n_F$ is above 1, this indicates cooperative adsorption. Favourable sorption is suggested by $1< n_F <10$ [104].

Langmuir isotherm

The Langmuir model quantitatively represents the formation of an adsorbate monolayer on the adsorbent surface, after which no additional adsorption takes place. The Langmuir isotherm is applicable for monolayer sorption onto a surface with a predetermined number of sites with uniform energies of adsorption. It assumes that adsorption takes place at specific homogeneous sites without any interaction or transmigration within the adsorbate [105]. The non-linear form of the Langmuir isotherm can be expressed as follows:

$$q_{eq} = \frac{q_m K_L C_{eq}}{1 + K_L C_{eq}} \tag{2.3}$$

where q_m is the maximum adsorption capacity of the adsorbent (mmol/g) and K_L is a constant related to the energy of the adsorption called Langmuir constant (L/mmol). K_L indicates the adsorption nature to be unfavourable if $K_L > 1$, linear if K_L is equal to one, favourable if $0 < K_L < 1$ and irreversible if K_L is close to zero.

Bi-Langmuir isotherm (Two-site Langmuir)

The Bi-Langmuir model (two-site Langmuir model) is the simplest four-parameter isotherm that takes into account heterogeneity of the adsorption system by a

combination of two Langmuir equations. The suggested two different surface active sites follow the abovementioned Langmuir assumptions:

$$q_{eq} = \frac{q_{m1} K_{BiL1} C_{eq}}{1 + K_{BiL1} C_{eq}} + \frac{q_{m2} K_{BiL2} C_{eq}}{1 + K_{BiL2} C_{eq}} \tag{2.4}$$

where q_{m1} (mmol/g) is the maximum adsorption capacity of the first active site and K_{BiL1} (L/mmol) the adsorption energy related to the first active site. Equally, q_{m2} and K_{BiL2} are the analogous parameters related to the second adsorption site.

Sips isotherm

Sips [106] proposed an equation which is similar to the Freundlich one, but it has a finite limit when the concentration is sufficiently high:

$$q_{eq} = \frac{q_m (K_S C_{eq})^{n_S}}{1 + (K_S C_{eq})^{n_S}} \tag{2.5}$$

where K_S (L/mmol) is the Sips affinity constant and n_S the surface heterogeneity. If n_S equals one, the Sips isotherm reduces to the Langmuir isotherm and predicts homogeneous adsorption. q_m is the Sips maximum adsorption capacity (mg of sorbate per g of sorbent).

Langmuir-Freundlich model

The Langmuir-Freundlich equation is given by [106]:

$$q_{eq} = \frac{q_{m_{LF}} (K_{LF} C_{eq})^{m_{LF}}}{1 + (K_{LF} C_{eq})^{m_{LF}}} \tag{2.6}$$

where $q_{m_{LF}}$ is the Langmuir-Freundlich maximum adsorption capacity (mg/g), K_{LF} is an equilibrium constant for a heterogeneous solid and m_{LF} is a heterogeneity factor, which ranges between 0 and 1.

Redlich-Peterson isotherm

The Redlich-Peterson isotherm [107] is an empirical model containing three parameters. It combines the basics from both the Langmuir and Freundlich equations. The sorption mechanism is hybrid and sorption does not follow the ideal monolayer model:

$$q_{eq} = \frac{q_m K_{RP} C_{eq}}{1 + (K_{RP} C_{eq})^{n_{RP}}} \tag{2.7}$$

where K_{RP} is the Redlich-Peterson constant and n_{RP} is a Redlich-Peterson constant that ranges between 0 and 1 (L/mg). If the adsorbate concentration is high, the Redlich-Peterson model reduces to the Freundlich equation; when $n_{RP} = 1$, the Redlich-Peterson isotherm returns into the Langmuir equation. If $n_{RP} = 0$, Eq. (2.7) reduces to the Henry equation.

Toth isotherm

The Toth isotherm is an empirical modification of the Langmuir equation which fits at low and high concentrations. Toth reduced the error between experimental data and predicted values of equilibrium adsorption data. The Toth model supposes an asymmetrical quasi-Gaussian energy distribution and is useful in cases of heterogeneous multilayer adsorption [108]:

$$q_{eq} = \frac{q_m C_{eq}}{(a_T + C_{eq}{}^{m_T})^{\frac{1}{m_T}}} \tag{2.8}$$

where a_T is Toth's adsorptive potential constant (mmol/L) and m_T Toth's heterogeneity factor. If the surface is homogeneous, m_T is equal to one, and the Toth model reduces to the Langmuir model.

Temkin isotherm

The Temkin model is based on uniformly distributed binding energies and takes into account the adsorbate–adsorbent interactions. The model presupposes that the heat of adsorption of the adsorbate molecules decrease linearly rather than logarithmically, excluding extremely low and high concentrations [109]:

$$q_{eq} = \frac{R_g T}{b_T} \ln\left(K_T C_{eq}\right) \tag{2.9}$$

where $R_g T/b_T = B_T$ (J/mol) correlates to the heat of the adsorption; R_g is the universal gas constant (kJ/(mol K)), T the temperature (K) and K_T (L/mmol) is the Temkin equilibrium binding constant describing the maximum binding energy. If the adsorption obeys the Temkin equation, the variation of the adsorption energy (b_T) and the Temkin equilibrium constant (K_T) can be calculated from the slope and the intercept of the plot in a coordinate system of q_{eq} versus ln C_{eq}.

Fritz-Schlunder isotherm

The Fritz-Schlunder model proposes the most generalized correlative equation for calculating the adsorption in multisolute systems [83, 110]. It includes four estimated parameters that result in better fitting of the data:

$$q_{eq} = \frac{q_m K_{FS} C_{eq}^{\ n_{FS}}}{1 + K_{FS} C_{eq}^{\ m_{FS}}} \tag{2.10}$$

where K_{FS} (L/mmol) corresponds to the Langmuir affinity constant and n_{FS} and m_{FS} characterize the surface heterogeneity.

Dubinin-Radushkevich isotherm

The Dubinin-Radushkevich isotherm is generally applied to express an adsorption mechanism with a Gaussian energy distribution onto a heterogeneous surface [111, 112]. The model is usually applied to differentiate the physical and chemical adsorption of metal ions with its mean free energy. It can be applied in cases of a high and intermediate range of concentrations:

$$q_{eq} = q_m \exp\left(-K_{DR}\varepsilon^2\right) \tag{2.11}$$

where K_{DR} (mmol^2/J^2) is a constant connected to the mean free energy of adsorption (E_{ads}) per molecule and ε is the Polanyi potential, given as:

$$\varepsilon = RT \ln\left(1 + \frac{1}{C_{eq}}\right) \tag{2.12}$$

The energy of removing a molecule from a sorbent to infinity can be calculated from [83]:

$$E_{ads} = \frac{1}{\sqrt{2K_{DR}}} \tag{2.13}$$

The Dubinin-Radushkevich model is based on the temperature dependence of adsorption and the characteristic curve can be plotted in coordinates of ln q_{eq} versus ε^2 [110]. This model is used to calculate the micropore volume of sorption materials, since it characterizes the microporous adsorbents most precisely and with fewer limitations than the Brunauer, Emmett and Teller theory.

2.2.3 Kinetic models

Kinetic models are usually used to distinguish the sorption rate and the rate limiting step of the sorption mechanism. The most used models in the literature are briefly discussed below.

Pseudo-first order kinetic model (Lagergren's equation)

The pseudo-first order kinetic model (PSO1) was proposed by Lagergren at the end of the 19th century based on the experimental sorption capacities of solids in liquid/solid systems [113, 114]. The model associates the kinetics of sorption at one active site and the equation can be presented as:

$$q_t = q_{eq}\left(1 - e^{-k_1 t}\right) \tag{2.14}$$

where q_{eq} and q_t are the sorbate concentrations on the sorbent surface at equilibrium and at a time t, respectively (mmol/g), and k_1 is the pseudo-first order rate constant (1/h).

Pseudo-second order model

The pseudo-second order (PSO2) model is a modification of the PSO1 for two active adsorption sites. It was proposed by Blanchard to describe the kinetics of metal cation sorption by natural zeolites [115, 116]:

$$q_t = \frac{k_2 q_{eq}^2 t}{1 + k_2 q_{eq} t} \tag{2.15}$$

where k_2 is the PSO2 rate constant (g/(mmol min)) and $k_2 q_{eq}^2$ is the initial sorption rate.

Elovich model

The Elovich model was proposed by Roginsky and Zeldovich in 1934. It is a semi-empirical model and takes into account the heterogeneity of the sorbent surfaces. The model does not suggest any definite sorption mechanism, but it has been widely applied to describe the chemisorption process [117]:

$$q_t = \frac{1}{B_E}\ln\left(1 + A_E B_E t\right) \tag{2.16}$$

where A_E (mmol/(min g)) is the Elovich constant related to the rate of the chemisorption and B_E (g/mmol) is the Elovich constant representing the surface coverage.

Intraparticle diffusion model

The intraparticle diffusion model was proposed by Weber and Morris with the main assumption that the pore diffusion is the rate-limiting step of the sorption process for systems that give a straight line in coordinates of q_t versus $t^{½}$ [90, 118]:

$$q_t = k_{dif} t^{½} + C \tag{2.17}$$

where k_{dif} is the rate constant of intraparticle diffusion (mmol/(g min^{½})) and C is the boundary layer diffusion (mmol/g). If the sorption obeys the intraparticle diffusion model, the k_{dif} value can be calculated from the slope and C can be calculated from the intercepts of the plot q_t versus $t^{½}$.

2.2.4 Brunauer, Emmett and Teller theory (BET)

The Brunauer, Emmett and Teller (BET) theory was formulated in 1938 [119]. The main assumption of the BET model is that the physisorption of gas molecules by a solid can be multilayer, but there is no interaction between the adsorption layers, and the Langmuir theory can be applied to each and every layer:

$$S_{total} = \frac{(v_m N s)}{V} \tag{2.18}$$

$$S_{BET} = \frac{S_{total}}{m} \tag{2.19}$$

where S_{total} is the total surface area and S_{BET} the specific surface area (mL/g), v_m the volume of gas adsorbed at standard temperature and pressure in a monolayer on the sorbent surface (mL); N is the Avogadro constant ($6.022 \cdot 10^{23}$ mol^{-1}); s is an effective cross-sectional area of one adsorbate molecule (m^2); V is the molar volume of the adsorbate (cm^3/mol) and m is the mass of the adsorbent (g).

Despite its many restrictions, the BET theory was the first attempt to create a universal theory of physical adsorption and still is one of the most widely used for specific surface area characterization of porous materials [73, 119]. The IUPAC classification scheme of pore type depending on the isotherm shape was created on the basis of the BET theory [73, 120-122].

2.2.5 Density functional theory (DFT)

Density functional theory (DFT) is currently the most promising method of evaluating the electronic structure of matter [123-126]. It can be applied in a wide range of cases, from atoms and molecules to quantum and classical fluids. The original DFT ascribed a key role to electron density and was then generalized to deal with, for example, time-

dependent phenomena and excited states, bosons, molecular dynamics, relativistic electrons, multicomponent systems such as nuclei and electron-hole droplets, spin-polarized systems, superconductors with electronic pairing mechanisms, or free energy at finite temperatures. The equation is as follows:

$$E \equiv \int V(r)\, n(r)\, \mathrm{d}r + F\left[n(r)\right] \tag{2.20}$$

And the total energy functional can be presented as:

$$E[n] = T[n] + E_H[n] + E_{XC}[n] + \int V(\vec{r})\, n(\vec{r})\, \mathrm{d}^3 r \tag{2.21}$$

where $F[n(r)]$ is the functional of the density; $T[n]$ is kinetic energy; $E_H[n]$ electron-electron repulsion (Hartree energy); $E_{XC}[n]$ is exchange and correlation energies; $V(\vec{r})$ is an external potential.

2.3 Sorption selectivity

Sorbent selectivity can be calculated in a few ways: using the thermodynamic approach based on the law of mass action (K_{lm}), with the empirical equation proposed by Gapon (K_{G}) and via the separation factor (F) [86, 127-131]:

$$K_{\mathrm{lm}}\left(\mathrm{A}^{+n} / \mathrm{B}^{+m}\right) = \frac{q_{\mathrm{A}}^{1/n} C_{\mathrm{B}}^{1/m}}{q_{\mathrm{B}}^{1/m} C_{\mathrm{A}}^{1/n}} \tag{2.22}$$

$$K_{\mathrm{G}}\left(\mathrm{A}^{+} / \mathrm{B}^{2+}\right) = \frac{q_{\mathrm{A}} C_{\mathrm{B}}^{1/2}}{q_{\mathrm{B}} C_{\mathrm{A}}} \tag{2.23}$$

$$F = \frac{K_{\mathrm{d}}(\mathrm{A})}{K_{\mathrm{d}}(\mathrm{B})} \tag{2.24}$$

$$K_{\mathrm{d}} = \frac{\Delta C}{C_{\mathrm{eq}}} \frac{V_{\mathrm{al}}}{m} \tag{2.25}$$

where C_{A} and C_{B} are the equilibrium concentrations of the cations A and B in solution, respectively (mmol/L); q_{A} and q_{B} are the amounts of exchanged cations A or B on a sorbent surface in meq per 100 g of material; K_{lm} is the selectivity coefficient according to the law of mass action; K_{G} is the Gapon's selectivity coefficient; K_{d} is a distribution coefficient; V_{al} is the aliquot volume (mL); m is the mass of adsorbent (g) and C_{eq} is the equilibrium concentration of the target cation (mmol/L).

3 Titanosilicates for radionuclide uptake

3.1 Structural aspects of TiSi sorption materials

Titanosilicates belong to the relatively new class of silicate materials that combine natural minerals and synthesized materials. The history of this class begins with the molecular sieves TS-1 and TS-2 obtained at the end of the 20th century for catalytic purposes. Later, other TiSis were synthesized and have found extensive application in catalysis, optic, ion exchange, adsorption, separation and energy storage as capacitors [132]. The structure of the most promising TiSi sorption materials will be discussed in this chapter (Table 3.1).

In general, TiSi sorption materials are constructed from interconnected polyhedra: octahedra or pentahedra with Ti as the centre atom and tetrahedra of SiO_4. Variations in the incorporation of these structural components lead to the formation of framework, layered and dense structures. The negative charge on the Ti-O groups is compensated by cations that can be exchanged. The TiSi materials with framework and layered structures have the highest ion exchange and sorption potential and will be discussed below.

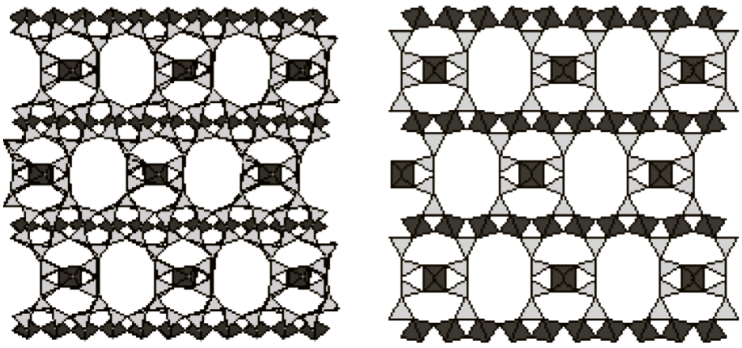

ETS-10 ETS-4

Figure 3.1: Schematic representation of the titanosilicate structures of ETS TiSi materials. The black octahedra and pentahedra have Ti as a central atom and grey tetrahedra are SiO_4, respectively. Extra-framework cations and water molecules were omitted for clarity [133, 134].

The first members of the TiSi sorption family were Engelhard Titanosilicates (Engelhard Corporation) reported by S.M. Kuznicki (US Patent 4 853 202, 1989 and US Patent 4 938 989, 1990). In 1989, the stable microporous crystalline wide-pore (8 Å) TiSi material named Engelhard Titanosilicate Number 10 (ETS-10) was patented. Quasi-cubic ETS-10 crystals with a tendency to agglomeration were observed on SEM

images [135]. This ETS-10 structure was determined only a few years later by Anderson et al. [136] and the chemical formula proposed was $Na_{1.5}K_{0.5}TiSi_5O_{13}\cdot nH_2O$ (Figure 3.1). One of the most interesting aspects of the ETS-10 structure is the alteration of long and short bonds along O-Ti-O-Ti-O chains. These chains are surrounded by SiO_4 tetrahedra linked to the octahedrally coordinated Ti^{4+} through corner-shared oxygen atoms. The pore system consists of an interconnected 12 Si atom channel network (12 member rings) with curvaceous pores in the [001] direction and straight pore in the other directions. The presence of Ti^{4+} in an octahedral coordination generates two negative charges $[TiO_6]^{2-}$ which are balanced by the exchangeable cations Na^+ and K^+. Taking into account the Ti:Si ratio (Ti:Si = 0.2) in the ETS-10 structure, the ion exchange capacity was calculated to be 4.5 meq/g (in dehydrated form). The combination of structural aspects such as a wide pore diameter and developed three-dimensional pore structure with a high ion exchange capacity makes ETS-10 a promising ion-exchanger for high-volume metal cation sorption from aqueous solution.

In 1990, Engelhard Titanosilicate Number 4 (ETS-4) was described. It is a microporous TiSi (pore diameter 3.7 Å) with the following chemical formula: $Na_9Si_{12}Ti_5O_{38}(OH)\cdot 12H_2O$ (Figure 3.1). It was commonly considered that ETS-4 is a synthetic analogue of the zorite mineral until 2001, when a single-crystal study was published by Nair et al. [137]. There are two types of Ti^{4+} coordination in ETS-4: one is coordinated into octahedra and linked into chains and the other is coordinated in pentahedra (semioctahedra with titanyl Ti=O bond) that are isolated by SiO_4 tetrahedra from the chains of TiO_6. In contrast, zorite has a rotating square pyramid form of five coordinated Ti^{4+} and charge balancing protons. The pore structure of ETS-4 can be presented as an intergrowth of 12MR and 8MR channels connected through the short 6MR pores. The important role of water bonds in the channel network structure of ETS-4 must be pointed out, as this makes it a non-thermostable material. At a temperature of about 200 °C water is removed and the framework structure of ETS-4 collapses. Yet the ion exchange capacity of ETS-4 is one of the highest among all reported TiSis (6.3 meq/g in dehydrated form) which makes it an appropriate ion-exchanger within a limited temperature range [137].

The next group of TiSi materials was found by Clearfield and his team [138-141]. The main structural characteristic of this group is the formation of “cubane-like” structures of Ti_4O_4 formed from TiO_6 octahedra in such a way that every octahedron shares three oxygens with neighbouring TiO_6 octahedra inside the cluster (Figure 3.2).

A 1993 report on the synthesis of crystalline titanosilicate material (CTS) with the chemical structure $Na_2Ti_2O_3SiO_4\cdot 2H_2O$ first called this TAM-5 (Figure 3.2) [138, 141]. It has an analogue structure to the material sitinakite and therefore the literature reported synthesis of sitinakite [142]. In CTS, the characteristic “cubane-type” structures are linked to each other by SiO_4 tetrahedrons in the directions of the *a* and *b* axes, while in the direction of the *c* axis, the Ti_4O_{24} clusters are bridged through the top oxygens of octahedrons [80, 141]. Half of the Na^+ are “sandwiched” between the SiO_4 tetrahedra

and called framework cations. This Na^+ can be exchanged only by protons due to space restrictions. The remaining compensation cations are located near the channel centre, and only one of the four of these is exchangeable for Cs^+ due to the same space restrictions. It must be noted that the H form can exchange 2–4 times more Cs^+ and that the size of the CTS tunnels is ideal for selective adsorption of Cs^+. The affinity of CTS can be increased by decreasing the crystallinity. Nevertheless, the presence of competitive ions in solutions decreases the affinity of CTS to Cs^+ [74, 130, 141].

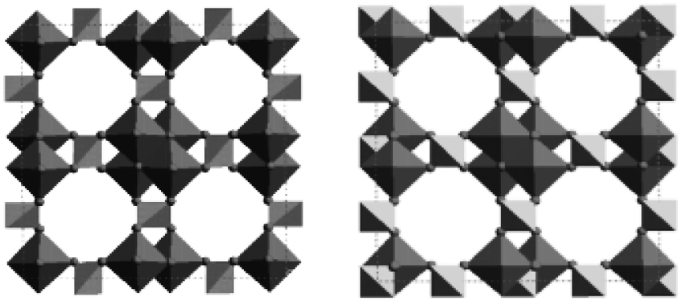

CTS GTS-1

Figure 3.2: Schematic representation of the titanosilicate structures of microporous TiSi materials reported by Clearfield's group. The black octahedra represent TiO_6 groups and the grey tetrahedra illustrate the SiO_4 groups. The dark grey small circles are oxygens [133, 134].

The titanosilicate analogue of the mineral pharmacosiderite was synthesized in 1990 by Chapman and Roe [143]. The material was named Grace Titanium Silicate-1 (GTS-1). The alkali cation analogue of pharmacosiderite with the chemical formula $HM_3Ti_4O_4(SiO_4)_3 \cdot 4H_2O$ (M is an alkali metal cation) was reported by Behrens et al. in 1996 [139]. Thorough studies of the alkali GTS-1 structural and sorption properties have been conducted (Figure 3.2) [74, 139-141, 144]. The main difference to the CTS material is a connection of the cubic Ti_4O_{24} cluster by SiO_4 tetrahedrons in a three-dimensional framework that gives an extra exchangeable space and the tree of four channel cations can be exchanged by Cs^+. X-ray single-crystal studies illustrate the stability of the non-centred position of the exchanged Cs^+ ions in the tunnels of GTS materials [141, 145].

The newest and fundamentally different group of TiSi sorption materials was called the AM-n family because the first member was discovered by researchers from Aveiro and Manchester universities in 1995. In contrast to other TiSis, AM materials contain no Ti-O-Ti bonds (Figure 3.3) [146].

The first member of the AM group was AM-1, which was later described as JDF-L1 in 1996 [147] and as NTS TiSi [148] (Figure 3.3). The chemical formula of AM-1 was

found to be $Na_4Ti_2Si_8O_{22}\cdot 4H_2O$. It contains five-coordinated Ti^{4+} ions in the form of TiO_5 square pyramids connected to SiO_4 tetrahedrons through the oxygen at the pyramid base. Clusters of $TiO\cdot O_4(SiO_3)_4$ form a continuous layer, which is counterbalanced by Na^+ in the interlamellar space and can be exchanged; but this material is mainly used for catalysis.

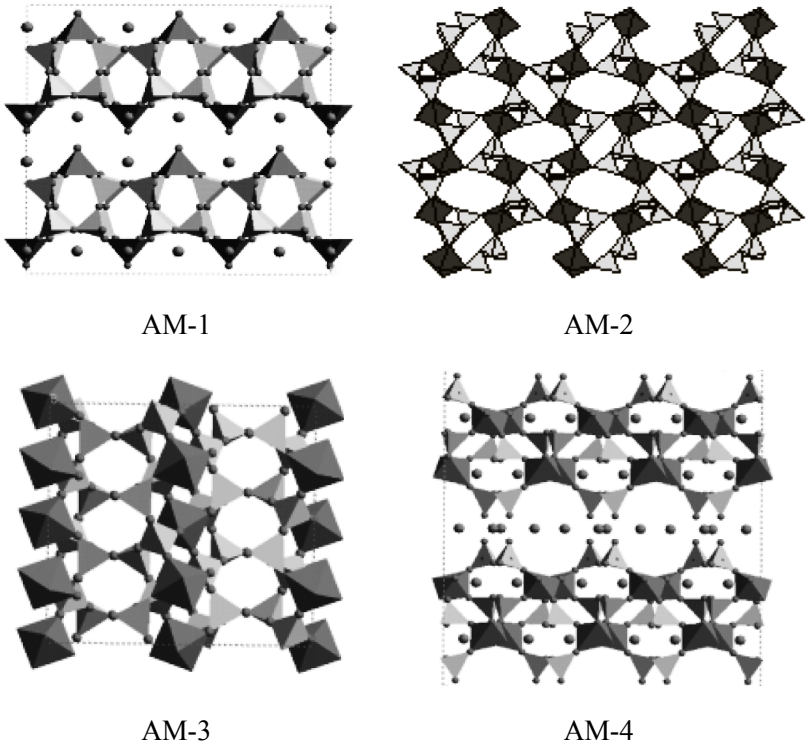

Figure 3.3: Schematic representation of the titanosilicate structures of AM TiSi materials. The black polyhedra show the TiO_n groups and the centres of the grey tetrahedra are occupied by Si atoms. The medium grey circles are the oxygen atoms on AM-3 and the extra framework cations on AM-1 and AM-4 [133, 134].

The titanium substituted synthetic analogue of the mineral umbite has the chemical formula $K_2TiSi_3O_9\cdot H_2O$ and was named AM-2 (STS) [149-151]. The single-crystal X-ray investigation by Zuo and Dadachov in 2000 [152] determined the AM-2 crystal structure (Figure 3.3). Its pore network builds up from TiO_6 octahedrons linked to the six SiO_4 tetrahedrons, forming the open 8MR channel (6.8 Å) along the *c* axis. The charge of TiO_6 octahedrons is balanced by two exchangeable K^+ in the tunnel space.

Table 3.1: Structural aspects of TiSi sorption materials.

Name	Ideal formula	Mineral analogue	Ti/Si	Ti coordination	Structure	r_{pore}, Å	Report in	References
AM-2 (STS)	$K_2TiSi_3O_9 \cdot H_2O$	Ti substituted umbite	0.33	6	microporous framework		1997	[133, 146, 149, 155-157]
AM-3 (penkvilksite-2O)	$Na_2TiSi_4O_{11} \cdot 2H_2O$	penkvilksite	0.25	6	microporous framework		1997	[133, 146, 153, 158-160]
AM-4	$Na_3(Na,H)Ti_2O_2[Si_2O_6]_2 \cdot 2H_2O$		0.5	6	layered		1997	[133, 142, 146, 151, 154]
ETS-4	$Na_9Si_{12}Ti_5O_{38}(OH) \cdot 12H_2O$	zorite	0.42	6, 5	microporous framework	1.85	1990	[133, 142, 151, 161-169]
ETS-10	$Na_{1.5}K_{0.5}TiSi_5O_{13} \cdot nH_2O$		0.2	6	microporous framework	4	1989	[133, 135, 136, 169-171]
CTS (TAM-5)	$Na_2Ti_2O_3SiO_4 \cdot 2H_2O$	sitinakite	2	6	microporous framework	1.75	1993	[74, 79, 80, 80, 82, 86, 130, 133, 138, 140-142, 151, 172-177] **(Paper I–IV)**
GTS-1	$HNa_3Ti_4O_4(SiO_4)_3 \cdot 4H_2O$	pharmacosiderite	1.33	6	microporous framework	5	1996	[74, 86, 133, 139-142, 144, 145, 151, 178-181]

The AM-3 is a microporous synthetic analogue of the orthorhombic penkvilksite mineral (penkvilksite 2O) with the chemical formula $Na_2TiSi_4O_{11}\cdot 2H_2O$ (Figure 3.3). The main structural difference between the AM-2 and AM-3 materials is that SiO_4 tetrahedra linked with isolated TiO_6 octahedra in three-dimensional directions form a developed open pore structure with a pore diameter of 3 Å [133, 146, 153].

The synthesis of a layered TiSi material called AM-4 was reported by Lin et al. in 1997 [146]. The crystal structure was resolved by Dadachov et al. in 1997 [154] and the chemical formula was found to be $Na_3(Na,H)Ti_2O_2[Si_2O_6]_2\cdot 2H_2O$. The Ti atoms in AM-4 are octahedrally coordinated and TiO_6 is connected to the SiO_4 through the oxygens at the edges. The two charges per Ti^{4+} are balanced by Na^+ and K^+ which are located in the interlamellar space (exchangeable) and in the space within the layer (structural cations). The characteristic aspect of the AM-4 material is a five-level structure of layers: SiO_4-TiO_6-SiO_4-TiO_6-SiO_4 (Figure 3.3).

3.2 Synthesis of TiSis

The process of TiSi synthesis can be divided into the following stages: mixing the precursors, hydrothermal treatment (HTT), rinsing the obtained materials and, finally, drying. Practically, TiSi synthesis is carried out under hydrothermal conditions in Teflon-lined autoclaves at 120–230 °C from a few hours up to 30 days in the pH range of 9–13. Exceptionally extreme synthesis conditions were reported by Harrison et al. [145] for growing large crystals in order to conduct single-crystal structure studies of the Cs-phase of GTS-1: 40 h at 750 °C under 200 Pa in a sealed gold tube. Optional stages can include adding the seeds of desirable phases to the mixture of precursors or template substances [182]. Recently, the possibility of replacing the HTT stage by microwave treatment was proposed [166, 183-185]. Microwave synthesis makes it possible to reduce the TiSi synthesis duration by 2–48 times, but this occasionally requires increasing the temperature and produces materials with a smaller crystal size.

Depending on the nature of the precursor, TiSi synthesis can be classified into alkoxide, inorganic or mixed precursor methods. Briefly, the controlled hydrolysis/alcolysis of precursors forces the simultaneous precipitation (coprecipitation) of Ti-O and Si-O groups to form the crystal phase together. All the above mentioned TiSi structures were synthesized as coprecipitated powders.

It is also possible to prepare the same structure using other types of precursor. For example, Kuznicki used $TiCl_3$ as a Ti-containing precursor for the synthesis of ETS-10 [186]. Any reactive source of silicon was allowed in the proposed synthesis approach. The temperature range of 100–175 °C and the time range of 12–15 days were patented as preferred conditions for HTT. The main disadvantage of this method is the use of $TiCl_3$ because it is expensive and has a low stability in air. Das et al. [187] used $TiCl_4$ as a Ti source, sodium silicate as a Si precursor and KF for a faster HTT synthesis (14–16 h) of ETS-10 at 200 °C and a 300 rpm stirrer speed. The drawbacks of using the $TiCl_4$ precursor are its aggressiveness and release of HCl into the atmosphere. The

advantage is that $TiCl_4$ is cheaper, more stable and easier to handle than $TiCl_3$. Titanium sulphate $Ti(SO_4)_2$ was found to be a better Ti source than $TiCl_4$ and $TiCl_3$, yielding the largest ETS-10 crystals when the HTT was at 200 °C under static conditions [188, 189]. Adjusting the Na:K ratio and the reaction water content, without using organic precursors, templates, seeds or F^-, made it possible to control the crystal size of ETS-10. Similar conclusions were reported for the synthesis of all the microporous TiSi by Kostov-Kytin et al. [142, 151] varying only the $Na_2O(K_2O):TiO_2$ ratio using different Ti precursors. Thomas [190] demonstrated how the anatase and rutile phases may be used as a source for TiSi synthesis. The synthesis of ETS-10 reported by Valtchev and Mintova [182] is an example of using the $TiCl_4$ precursor with organic template compounds (tetramethylammonium chloride). It is worth noting that even after HTT for 4–10 days, the products contain the other phases. The approach reported by Chapman and Roe [143] is an example of organic precursors being used for microporous TiSi synthesis. Titanium (IV) ethoxide $Ti(OC_2H_5)_4$ was the chosen precursor for the synthesis of zorite and GTS-1 at 200 °C during 48 h and other organic compounds were tested as templates. The titanium isopropoxide $Ti(OC_3H_7)_4$ with tetraethyl orthosilicate $Si(OC_2H_5)_4$, was used to synthesize CTS by Medvedev et al. [191] and $TiCl_4$ with H_2O_2 was used for CTS synthesis by Clearfield et al. [177].

An advantage of using alkoxide precursors is the high purity of the obtained materials. There are, however, severe drawbacks: these precursors are unstable, toxic, expensive, sensitive to moisture and difficult to handle, requiring special synthesis equipment, ecotoxic solvents, and the results are not readily reproducible. Therefore, inorganic precursors are more commonly used for synthesis due to their ease of handling, stability and lower cost [133]. Usually, H_2O_2 is used as a ligand for slowing down the hydrolysis rate of inorganic Ti-containing salts to the Si-containing sources, which increases the amount of Ti-O-Si bonds in the resulting TiSi materials. There are some benefits of using H_2O_2 as a ligand, such as its non-toxicity and the eco-friendliness of the products (H_2O and O_2). Nonetheless, the main disadvantage is the need for special high-pressure equipment. The autogenous pressure in an autoclave is raised up to 7 Pa

Synthesis of TiSi using organic precursors can be described as in scheme (3.1) and an example of an inorganic synthesis is presented as scheme (3.2):

$$Ti(OR)_4 + Si(OR)_4 + MeOH \xrightarrow{HTT} Me_xTi_ySi_zO_m \cdot nH_2O \qquad (3.1)$$

$$TiCi_4 + Na_2O \cdot SiO_2 + MeOH \xrightarrow{HTT} Me_xTi_ySi_zO_m \cdot nH_2O + NaCl \qquad (3.2)$$

where R is the organic group (the organic part of the elementorganic molecule).

As already mentioned, all reported methods yielded only powdered materials, which can cause many difficulties in practical applications, since agglomeration decreases their working surface and active centre accessibility. Other difficulties with powdered materials include stoppages, a high hydrostatic resistance, bulk compression and poor

wettability [192, 193]. Granulated or particulate materials do not have the same complications. These types of TiSi can be achieved by the sol-gel method, which can be done without binder substances that would decrease the efficiency of the sorbents.

The main advantages of the sol-gel method are [194]:

- excellent homogenization of the precursors during the sol preparation stage,
- the possibility of obtaining high purity materials with an anticipated structure and properties under comparably mild synthesis conditions and
- the ability to choose the form of the materials (powders, fibres, films or particles).

Traditional inorganic synthesis and the sol-gel method of TiSi preparation using H_2O_2 as a ligand were combined in an experiment (**Paper I**). This investigation was based on earlier reported approaches [138, 179]. Unfortunately, H_2O_2 thermal decomposition releases oxygen and damages the gel structure and, consequently, TiSi could only be obtained as a powder.

A new sol-gel synthesis of TiSi from inorganic precursors based on gel preparation at room temperature was developed recently. This method produces stable materials with reproducible properties. The crucial feature of this approach is the use of chemicals at essential concentrations (2–5 M), which greatly increases the material yield. This synthesis can be accomplished using a range of eco-friendly ligands, such as polyalcohols, organic hydroxy-, ceto-, di- and tricarboxylic acids and mixtures of these. Using these ligands solved a few problems. Firstly, the proposed ligands do not ruin the gel structure as traditional H_2O_2 does, and TiSi xerogels with a particle size of ≤ 4 mm are obtained. The second advantage is the decrease in autogenous pressure in the autoclaves by at least an order of magnitude. Finally, substitution of the H_2O_2 ligand makes it possible to increase the amount and quantity of the precursor, which can decrease the costs of the target material. The $TiCl_4$ precursor may also be replaced by a pure and technical $TiOSO_4$ solution [178, 179]. In addition, the pure silica sources Na_2SiO_3 and K_2SiO_3 were replaced with inexpensive bulk liquid glass, and stable porous gels with a high sorption ability were obtained after such precursor substitutions. Using inexpensive precursors (technical $TiOSO_4$, containing iron) would not be possible with H_2O_2, due to the catalytic effect of the Fe^{3+} on the hydrogen peroxide decomposition reaction. In summary, the approach studied and discussed in this thesis is very promising for the large-scale application of TiSi materials.

3.3 Sorption properties of TiSi materials

Due to their thermal and chemical stability, radiation resistance, high ion exchange rate and remarkable capacity, TiSis can effectively decontaminate LRW by retaining long-live nuclides, such as ^{90}Sr ($t_{½}$ = 28.5 a), $^{134,137}Cs$ ($t_{½}$ = 2.065 and 30.1 a)

$^{233\text{-}235,238}$U ($t_{½}$ = 68.9 – 4.471 × 109 a), ^{241}Am ($t_{½}$ = 432.2 a), ^{239,240}Pu ($t_{½}$ = 24110 and 6560 a) and ^{154}Eu ($t_{½}$ = 8.60 a) (**Paper IV**) [130, 167, 174, 195-198]. Since TiSi is a relatively new material class which is currently being very actively explored, many researchers report properties of the same material using different names and abbreviations, as in [153, 158, 159] or [139, 143, 180, 199].

As can be seen, most of the sorption studies were conducted with stable nuclides (Table 3.1). The chemical behaviour of the nuclides of the same element is similar, and therefore this data can be used in a similar way. CTS and ETS-4 have the highest theoretical ion exchange capacity among the reported framework TiSis, while ETS-10 has the largest pore diameter (8 Å), suggesting that it has larger target cations, such as UO_2^{2+}, $^{234}Th^{4+}$, $^{241}Am^{3+}$ or $^{236,239,240}Pu^{3+}$.

ETS-10

The sorption of the U cation from water on ETS-10 was studied by Al-Attar's group in 2000 [198, 209], and the process was analysed again by Pavel et al. [170, 183, 208]. The first study reported the influence of the Ti precursor, contact time, initial sorbate and sorbent concentration on the ability of ETS-10 to retain U. A high DF (about 100%) and K_d (> 10^6 mL/g) were found, and ion exchange, surface precipitation and adsorption of dehydrated uranyl UO_2^{2+} ions were suggested as the predominant mechanisms. In contrast, the second group got a lower K_d (≈ 1900 mL/g) and doubted the mechanisms proposed by the previous study. Based on XRD investigations, the precipitation mechanism was excluded. Sorption of partially dehydrated $[UO_2(H_2O)_5)]^{2+}$, which is connected through sharing oxygen atoms with SiO_4 tetrahedrons, were found during extended X-Ray absorption fine structure (EXAFS) studies of molecular level interactions between the ETS-10 and the U cation [170, 183].

The ability of the ETS-10 to sorb twice as much Th(IV) as U(VI) was explained by the slightly smaller ionic and hydrated Th(IV) radii and associated with a similar role of the silanol group in the Th(IV) sorption process [208]. The role of surface acidity and porosity in the sorption of both the U and Th cations was illustrated.

The role of media composition and competitive ions in the sorption of $^{241}Am^{3+}$ and $^{236,239,240}Pu^{3+}$ by ETS-10, ETS-4, AM-4 and CTS TiSi materials was analysed in comparative studies by Al-Attar et al. [174, 207]. An ion exchange mechanism was suggested for the Am uptake, but no mechanism for Pu was found.

The sorption of smaller cations by ETS-10 has also been studied [135, 174, 207, 211, 212, 230]. The isotope dilution technique was used to study the effects of temperature, surface acidity and porosity modification on the $^{204}Tl^{+}$ sorption ability of ETS-10 [212]. It was found that chemical surface modifications decrease the kinetic and thermodynamic parameters of the sorption process.

The sorption of $^{115}Cd^{2+}$, $^{204}Hg^{2+}$, $^{60}Co^{2+}$, $^{137}Cs^{+}$ radiocations on ETS-10 from monosolutions was investigated using the isotope dilution method by Pavel et al. in

2002 [135]. Sorption was investigated as a function of contact time and temperature under constant batch factors in the absence of competitive ions. The ETS-10 sorption capacity of the studied cations at 20 °C was found to be close to the theoretical exchange capacity (4.5 meq/g) (Table 3.2) and reported values decreased in the following order $^{137}Cs^{+} > {}^{115}Cd^{2+} > {}^{60}Co^{2+} > {}^{204}Hg^{2+}$ [135]. For stable cations, the selectivity of the cation sorption at 20–25 °C was found to be as follows: $Cu^{2+} > Zn^{2+} > Mn^{2+} > Co^{2+}$ and $Pb^{2+} > Cd^{2+} > Cu^{2+}$ from single components and mixed media [211, 230] (Table 3.2). The pH and batch factor dependencies of Cd^{2+} sorption on ETS-10 were described by Chamarinha et al. [231]. They observed that Cd^{2+} sorption increased with an increase in both studied factors. The unusually high sorption capacity of ETS-10 for zeolite type material was emphasized by Zhao et al. using Pb^{2+} [232]. They attributed the extremely high rate and remarkable capacity to the low hydration energy of the sorbate.

Among the investigated TiSis, AM-2 was found to be the best for removing Hg^{2+} in the presence of competitive cations like Mg^{2+} (97.0%), while GTS-1 was the least efficient (72.4%) material of all [134]. ETS-10 demonstrated the best DF of Hg^{2+} from a single solution.

A remarkably high sorption capacity and affinity of ETS-10 to Cs^{+} and Sr^{2+} from single and equivalent mixed cation solutions were reported by Pavel et al. in 2011 (Table 3.2) [196]. They examined the effect of the melting temperature on the retained cation amount in order to test how well ETS-10 solidified for final disposal after retention of Cs^{+} and/or Sr^{2+} radionuclides from LRW. Easy solidification was reported in all studied cases.

ETS-4

Despite its smaller pore radius of 3.7 Å, the ability of ETS-4 to sorb large cations like UO_2^{2+}, $^{241}Am^{3+}$ and $^{236,239,240}Pu^{3+}$ was estimated by Al-Attar et al. from 2000–2003 [174, 198, 207, 209]. The selectivity of ETS-4 to UO_2^{2+} was compared with CTS, AM-4 and ETS-10 titanosilicate materials using the batch K_d. The influence of batch factor, contact time, sorbate concentration and structural aspects on the ion exchange capacity of the studied materials was discussed by Al-Attar and Dyer [198]. A much lower K_d was reported for ETS-4 than for ETS-10 in the first study by Al-Attar (Table 3.2) [209]. For sorption of U on TiSi materials, both surface precipitation and ion exchange mechanisms were suggested. The sorption of trans uranium $^{241}Am^{3+}$ and $^{236}Pu^{3+}$ isotopes on the same type of materials was studied under batch conditions. The K_d was found to be a function of the sorption media composition, concentration and pH, and the effect of structural and surface aspects on ion exchange capacity were also discussed. It was also found that ETS-4 $K_d(^{241}Am^{3+}) > 10^6$, but the AM-4 material was more effective than ETS-4 under the experimental conditions [207].

Table 3.2: Sorption studies using TiSi materials. Alternative names found in the literature are given in brackets.

Name	IEC_t, meq/g	q_{eq}, mmol/g	K_d, mL/g	Target cation	Reference
AM-2 (STS, umbite)	5.6			Na^+, Cs^+, Rb^+, NH_4^+, Mn^{2+}, Mg^{2+}, Ca^{2+}, Sr^{2+}, Co^{2+},	[146, 155] [149, 156]
		$3.5 \cdot 10^{-7}$		UO_2^{2+} Hg^{2+}	
AM-3 (penk-vilksite-2O)	n.r.	0.72		K^+ $^{60}Co^{2+}$, Li^+	[158, 159, 200]
AM-4	7.63		$0.6–4.8 \cdot 10^3$	$^{134,137}Cs^+$,	[142, 151, 174, 198]
			$0.2–1.5 \cdot 10^3$	$^{57,60}Co^{2+}$,	
			2693	Cs^+, Sr^{2+}, Mn^{2+}, $^{110}Ag^+$	
			10–25	$^{125}Sb^{3+}$, $^{238}UO_2^{2+}$	
			$6.7 \cdot 10^4$	Hg^{2+},	
			$1.2 \cdot 10^5$	$^{236}Pu^{3+}$	
			$9 \cdot 10^6$	$^{241}Am^{3+}$	
ETS-4 (zorite-type)	6.4	1.22		Hg^{2+}, Cs^+, Sr^{2+},	[137, 142, 151, 161-169, 174, 198, 201-207]
			2000	UO_2^{2+},	
			732	$^{110}Ag^+$,	
			0	$^{125}Sb^{3+}$,	
			644	$^{204}Hg^{2+}$,	
			$0.1–3.2 \cdot 10^4$	$^{60}Co^{2+}$,	
			583	$^{115m}Cd^{2+}$,	
			$>10^6$	$^{241}Am^{3+}$,	
			$<10^4$	$^{236}Pu^{3+}$	
			$2.8–4.5 \cdot 10^4$	$^{134}Cs^+$,	
			$3.3–2.1 \cdot 10^4$	$^{137}Cs^+$	
ETS-10	4.5		$>10^6$	UO_2^{2+},	[135, 136, 169-171, 174, 183, 196, 198, 207-215]
			5000 800	Th^{4+},	
		4.43	627	$^{115}Cd^{2+}$,	
		3.85	$0.35–4.5 \cdot 10^4$	$^{204}Hg^{2+}$,	
		4.23	$3{,}02 \cdot 10^3$	$^{60}Co^{2+}$,	
			1636	$^{204}Tl^+$,	
		4.5	284	$^{137}Cs^+$, $^{110}Ag^+$,	
		5.5		Cs^+,	
		4.80.7–2.1		Sr^{2+},	
		0.7–1.1	3–13	Zn^{2+}, Pb^{2+},	
		2.1		Cd^{2+},	
			$2.1 \cdot 10^5$	$^{125}Sb^{3+}$	
		0.04	700	Hg^{2+}	
				$^{241}Am^{3+}$	
				$^{236}Pu^{3+}$	
		2.6		Cu^{2+}	

Table 3.2 (continued): Sorption studies using TiSi materials. Alternative names found in the literature are given in brackets.

Name	IEC_t, meq/g	q_{eq}, mmol/g	K_d, mL/g	Target cation	Reference
CTS (TAM-5, sitinakite)	7.5		$0.2–7.2\cdot10^5$ $0.8–7.8\cdot10^5$ $3.2\cdot10^6$ $1.5\cdot10^4$	$^{137}Cs^+$, $^{134,7}Cs^+$, $^{82,90}Sr^{2+}$ $^{90}Y^{3+}$, $^{60}Co^{2+}$, $^{241}Am^{3+}$, $^{152+154}Eu^{3+}$, $^{236,239,240}Pu^{3+}$,	(**Paper IV**) [79, 80, 82, 86, 140, 142, 151, 172-179, 198, 207, 216-228] (**Papers I–III**)
		1.9	11300 22977	Li^+, Na^+, K^+, Cs^+. Rb^+, Ca^{2+}, Sr^{2+}, Eu^{3+},	
GTS-1 (pharmacosiderite)	3.87		 630 260 2580 6190 15360 4530 6050 6487 8800	$^{137}Cs^+$, $^{90}Sr^{2+}$, Li^+, (Na-form) Na^+, (K-form) K^+, (Na-form) Rb^+, (Na-form) Cs^+, (Na-form) Ca^{2+}, (Na-form) Mg^{2+} (Na-form) Sr^{2+},(Na- form) Ba^{2+} (Na- form)	[74, 86, 140, 142, 151, 180, 229]
		$3.55\cdot10^{-7}$		Hg^{2+},	

*n.r.: not reported

The same group of materials was tested for the sorption of $^{110m}Ag^+$, $^{57,60}Co^{2+}$, $^{134,137}Cs^+$, $^{125}Sb^{3+}$ from real NPP waste waters supplied from the Ginna and Diablo Canyon NPP (USA). The selectivity of the materials was evaluated using K_d as a function of NPP solution composition (Table 3.2) [174]. Based on this study, CTS was the most effective TiSi material tested for radiocesium sorption.

The sorption of $^{115m}Cd^{2+}$, $^{60}Co^{2+}$ and $^{203}Hg^{2+}$ radionuclides by ETS-4 from analogues of a radioactive waste water solution was investigated using batch techniques by Popa et al. in 2006 [167]. Using K_d, the selectivity order was estimated as a function of temperature and contact time and the sorption capacity of ETS-4 was found to decrease in the order $^{203}Hg^{2+} > {}^{115m}Cd^{2+} > {}^{60}Co^{2+}$, which is the reverse of the results obtained in the ETS-10 study [135]. No pH or competitive cation studies were conducted.

The process of Cd^{2+} sorption on ETS-4 under batch experimental conditions was reported by the same group in 2009 [233]. Sorption capacity as a function of contact time, sorbent and sorbate concentration was compared with literature data on zeolite A, clinoptilolite and dolomite sorption ability. The experimental data illustrated that ETS-4 was efficient for Cd^{2+} removal from aqueous solution. The pH effect was described by Barreira et al. [215], who reported a high DF of 99.6 % at solution pH 6.

The sorption ability to Hg^{2+} was thoroughly examined by Lopes et al. from 2007–2013 [134, 165, 168, 203, 204, 206]. They studied the sorption ability of ETS-4 materials as a function of batch factor, pH, temperature, contact time, and pollutant concentration in batch mode. They found that the retention of Hg^{2+} by ETS-4 is an exothermic and thermodynamically favourable process strongly affected by solution pH and the presence of chlorine ions. At the same time, the temperature and presence of competitive ions like Na^+, Ca^{2+} or Mg^{2+} did not substantially affect the ability of ETS-4 to sorb Hg^{2+}. The optimal conditions were determined to be pH 4–6 at 21 °C. The column study demonstrated that ETS-4 had a sorption capacity of 0.17 mmol/g during the first two cycles. A comparison by Noh in 2011 found that ETS-4 has the highest selectivity to Hg^{2+} of the materials studied [201].

In 2009–2013, Lopes et al. [206, 234] compared the sorption ability of ETS-4 to Hg^{2+} and Cd^{2+}. The K_d was evaluated as a function of the sorbent concentration from single solutions and equivalent mixtures. The selectivity coefficient was calculated as a ratio between the obtained K_d. It was found that ETS-4 has higher kinetic parameters and selectivity for Cd^{2+}, but slower kinetics and higher sorption capacity for Hg^{2+}.

The fundamental sorption properties of ETS-4 for Sr^{2+} and Ba^{2+} was compared with CTS sorption abilities in 2012 by Noh et al. [202]. The selectivity of the sorption process was studied under batch conditions as a function of the Sr^{2+}/Na^+ or Ba^{2+}/Na^+ ratio. The ETS-4 had a higher selectivity to Ba^{2+} than CTS, but this order was reversed for Sr^{2+} selectivity. This research highlighted the selective sorption ability of ETS-4 to remove both Sr^{2+} and Ba^{2+} from LRW.

AM-2

The microporous titanosilicate $K_2TiSi_3O_9 \cdot H_2O$ was subjected to ion exchange with H^+, NH_4^+, Li^+, Na^+, Rb^+ and Cs^+ under batch conditions. It was demonstrated that the material can be totally exchanged by NH_4^+ and to different extents with the alkaline cations: $NH_4^+ > Rb^+ = Na^+ > Li^+ > Cs^+$ [149]. Li^+, Na^+, K^+, Cs^+, Ca^{2+}, Sr^{2+}, Ba^{2+}, Co^{2+}, Ni^{2+}, Cu^{2+}, and Cr^{3+} ion exchange as a function of pH was studied with AM-2 [157]. Potassium was found to be the most favoured ion in the pH range 3–12 with an ion exchange capacity (IEC) of 5.3 meq/g. An XRD and differential scanning calorimetry studies were done on Na^+-, Cs^+-, Mn^{2+}-, Ca^{2+}-, Sr^{2+}-, and Rb^+-exchanged forms of AM-2. The ion exchange rate followed the sequence $Mn^{2+} > Ca^{2+} > Sr^{2+} > Cs^+$ [155, 156]. Adsorption behaviours of AM-2 and AM-4 were compared with ETS-10, ETS-4, GTS-1 for mercury removal from natural wat

ers. AM-2 was found to be the most efficient in the presence of competitive cations such as Mg^{2+}, with a DF of over 97.0% [134, 235].

AM-3

The ability of AM-3 to sorb the radioactive $^{60}Co^{2+}$ was studied as a function of contact time, target cation and sorbent concentrations using a batch method [159]. The authors linked the significant influence of the batch factor and $^{60}Co^{2+}$ concentration to the equilibrium pH.

The ion exchange capacity of penkvilksite to K^+ was found to be 0.72 meq/g in 1 M KNO_3 at 80 °C after stirring for 24 h [200]. This low result was attributed to the short reaction time. Li^+, Na^+, K^+, Cs^+, Ca^{2+}, Sr^{2+}, Ba^{2+}, Cd^{2+}, Co^{2+}, Hg^{2+}, Pb^{2+}, Cu^{2+}, and Cr^{3+} exchange on AM-3 were recently studied under batch conditions [236]. The dynamic calorimetry method was use to investigate K^+, Cs^+, Sr^{2+} and Cu^{2+} exchange by Chukanov et al. [237]. Frost et al. [238] proposed that AM-3 could be used to incorporate actinides and lanthanides from radioactive waste.

AM-4

The sorption properties of TiSi materials with different framework structures and cation exchange capacities were compared by Al-Attar et al. [198, 207]. Uranium uptake from aqueous solutions by AM-4, ETS-4, ETS-10 and CTS was studied as a function of contact time, uranium concentration and batch factor [198]. The high sorption capacity for U was associated with surface precipitation ($K_d = 6.7 \cdot 10^4$ mL/g). The K_d of $^{241}Am^{3+}$, $^{236}Pu^{3+}$ and $^{110m}Ag^+$, $^{57,60}Co^{2+}$, $^{134,137}Cs^+$, $^{125}Sb^{3+}$, $^{134}Cs^+/^{137}Cs^+$ isotopes was estimated as a function of the retention media composition, concentration and pH. The effects of structural and surface aspects on ion exchange capacity were also discussed. It was established that AM-4 was the most effective for $^{241}Am^{3+}$ sorption at all sodium concentrations studied. Extraordinary suppression of cesium sorption by competitive ions was also reported for AM-4 [174, 207].

In a study of Sr^{2+} uptake as a function of pH and competitive Na^+, K^+, Ca^{2+} and Mg^{2+} concentration from binary solutions, Ca^{2+} was found to be the major competitor. Additionally, AM-4 exhibited a low affinity ($K_d < 640$ mL/g) for the alkali cations and a high affinity for alkaline earths (K_d Sr^{2+} = 66000 mL/g) in neutral and alkaline media [239].

The influence of competitive Na^+, Ca^{2+}, and Mg^{2+} ions on AM-4 uptake of Hg^{2+} was demonstrated by Lopes et al. [134, 235]. In a comparison with ETS-10, ETS-4, AM-2 and AM-4, the last one was found to be the least effective in retaining Hg^{2+} from natural water.

When AM-4 was exchanged with Ag^+, Zn^{2+} and Cu^{2+} and characterized by XRD and TEM, a certain loss of crystallinity was observed on the exchanged AM-4. The best

antimicrobial activity against the bacteria *Staphylococcus aureus* was shown by Ag–AM-4 [240].

CTS

The effect of solution pH on the selectivity order was studied by Clearfield's group. In an acidic medium, CTS selectivity had the following order: $K^+ > Cs^+ >> Na^+ >> Li^+$, while in an alkaline medium it was $Cs^+ > Rb^+ >> K^+ >> Li^+$ The ion exchange properties of CTS was analysed in terms of framework structure and pore space and compared with GTS-1 [86, 141, 177].

The sorption capacity of CTS for Cs^+ and Sr^{2+} has interested several researchers. The role of hydroxyl water, framework structure and pore space in the ion exchange process were determined by X-ray, synchrotron, IR and Raman investigations [74, 82, 86, 138, 141, 173, 175-177, 191, 197, 220, 223, 241-244].

CTS selectivity for radioactive $^{137}Cs^+$ and $^{89}Sr^{2+}$ was studied as a function of contact time, temperature, $NaNO_3$ concentration and Nb^{5+} substitution for Ti^{4+} in the structure. A higher selectivity to Cs^+ than to Sr^{2+} was reported, which increased in Nb-substituted CTS samples. XRD studies identified the position and coordination of the exchanged cations to demonstrate that higher selectivity of the retained cation is correlated with higher coordination in the channel of that cation [241, 242].

The uptake of $^{85}Sr^{2+}$, $^{57}Co^{2+}$ and $^{134}Cs^+$ by CTS was investigated as a function of titanosilicate crystallinity, solution composition and pH [130]. High K_d values were reported for $^{134}Cs^+$ ($2.5 \cdot 10^6$ mL/g) and $^{85}Sr^{2+}$ ($6.8 \cdot 10^4$ mL/g) and the heavy interference of K^+ and Na^+ competing cations at very high pH was highlighted. Affinity was also found to increase with decreasing sample crystallinity [175].

The titanosilicates CTS, ETS-10, ETS-4 and AM-4, layered manganese oxides and an antimony silicate were tested for their ability to decontaminate the reprocessing spent fuel from trans uranium isotopes $^{241}Am^{3+}$ and $^{236}Pu^{3+}$ [207]. The most suitable materials were determined in batch conditions as a function of pH, Na^+ and Ca^{2+} concentration. A negligible variation of CTS K_d $^{241}Am^{3+}$ ($2.6–3.3 \cdot 10^6$ mL/g) was observed at all studied $NaNO_3$ concentrations. For $^{236}Pu^{3+}$ an increase in K_d of one order was established with increasing background salt concentration ($1.6 \cdot 10^4$ mL/g).

The same group of materials was tested for the sorption of $^{110m}Ag^+$, $^{57,60}Co^{2+}$, $^{134,137}Cs^+$, $^{125}Sb^{3+}$ from real NPP waste waters supplied from the Ginna and Diablo Canyon NPP (USA). The selectivity of the materials was evaluated using K_d as a function of NPP solution composition and pH (Table 3.2) [174]. Among the studied materials the CTS was found to be the most effective in radiocesium sorption (K_d $^{134}Cs^+/^{137}Cs^+$ = 7.1–$7.8 \cdot 10^5$).

Sorption of $^{22}Na^+$, $^{134}Cs^+$ and $^{60}Co^{2+}$ radionuclides were studied under batch conditions as a function of contact time, temperature and radionuclide concentration, and a high

sorption rate (3–5 min) was reported [172]. The sorption capacity was found to be higher in Na-CTS form and decreased in the order of $Cs^+ > Co^{2+} > Na^+$. It is noteworthy that the sorption capacity was observed to increase with rising temperature for Cs^+, while the opposite was the case for Co^{2+} and Na^+ uptake.

GTS-1

The ion exchange capacity and selectivity of GTS-1 decreases in the order $Cs^+ > K^+ > Na^+ > Li^+$ according to Behrens et al. [82, 141, 143, 229]. Great affinity for Cs^+ was found by Clearfield's group [86, 138]. Later, Cs^+ and Sr^{2+} selectivity was investigated in the presence of Na^+, K^+, Mg^{2+} and Ca^{2+} competitive cations [74, 82, 85, 86, 139-141, 144, 229, 245]. The removal of $^{137}Cs^+$ and $^{89}Sr^{2+}$ by different cationic forms of synthetic pharmacosiderite was also reported by Dyer et al. [180].

The capacity of GTS-1 to adsorb Hg from natural waters was compared with AM-2, AM-4, ETS-10 and ETS-4. GTS-1 was found to be the least efficient material of all, with a DF of 72.4% [134].

In general, all this research demonstrated that TiSi are efficient sorption materials. Temperature dependence and thermodynamic parameters were evaluated, but few column studies have been conducted. At the same time, the most informative investigations are the comparative studies from solutions that contain sorbates and competitive ions simultaneously or tests from real radionuclide polluted water. For example, in a comparative study of 28 sorption materials including TiSis using LRW (Cs^+ and Sr^{2+}) as the main pollutant, Bortun et al. [86] demonstrated that CTS had the highest capacity, selectivity and retentivity of Cs^+ and Sr^{2+} among the framework and layered TiSis. A comparative study of 60 sorption materials carried out at the Los Alamos National Laboratory and Pacific Northwest Laboratory demonstrated that CTS materials are the most promising for Cs^+ retention from an acid-dissolved sludge simulant and slightly neutralized acidic and basic simulants of Hanford tank wastes [216]. Based on these positive results, CTS materials became the object of this study and are discussed hereafter.

4 Objectives and structure of the work

The main aim of this study was to investigate the physico-chemical properties of sol-gel synthesized titanosilicates for radionuclide uptake from aqueous solutions. Four key investigations were conducted and published in **Papers I** to **IV** (see page 49).

The first objective of the present study was to determine the effect of synthesis conditions on the structural and sorption parameters of TiSis obtained by the sol-gel method in order to obtain a highly efficient sorption material (**Paper I**). The effect of precursor substitution on structural and sorption properties was studied in order to increase the amount of precursor used and reduce the cost of the final product (**Papers II–IV**).

The second stage of the work was to assess the ability of the obtained TiSis to retain stable Cs^{+} and Sr^{2+} nuclides (**Papers I–IV**) and potentially toxic metal cations (presented in the experimental section) from the aqueous solutions. A comparison of the sorption ability of TiSi and cheap dolomite materials was conducted and is presented in the experimental section and **Paper V**.

The third aim of this research was to investigate the sorption behaviour and sorption mechanisms using theoretical models and material characterization techniques, since knowledge of the sorption mechanism is crucial for real application of the TiSi materials (**Papers II** and **III**).

The fourth and final part of the study was devoted to real application: the TiSi materials were tested in real mine water (presented in the experimental section). Specifically, the sorption properties of TiSis were tested with radionuclides (presented in the experimental section and **Paper IV**).

5 Experimental section

5.1 Sol-gel synthesis of TiSis

Titanosilicates were prepared by sol-gel synthesis according to the scheme and procedure given in **Paper I** and [178, 179]:

$$\text{inorganic salt Ti} + Na_2O{\times}SiO_2 + MOH \xrightarrow[\text{ligand}]{\text{HTT}} \underset{\text{gel}}{M_xTi_ySi_zO_m} \times nH_2O \qquad (5.1)$$

where $TiCl_4$ and a pure or technical solution of $TiOSO_4$ can be used as an inorganic salt of Ti, HTT is hydrothermal treatment and MOH are alkali or alkaline earth hydroxides.

The TiSi hydrogels were obtained by magnetic stirring at room temperature. Next, the hydrogels were agitated at room temperature and then hydrothermally (HT) treated in Teflon-lined steel autoclaves under autogenous pressure. Finally, the HT treated gels were rinsed with water, dried, ground and sieved. Thereafter, the fraction with a size of 0.25–0.5 mm was used in the sorption studies.

5.2 Material characterization

X-ray diffraction (XRD) was used for sample phase identification; patterns were collected using a DRON 407 (CuKα; $2\theta = 5 - 80°$ step $\Delta 2\theta = 0.02°$). A Quantachrome NOVA 2200 surface area analyser with NOVAWin software was used to evaluate the gel pore structure and BET specific surface area. To estimate the pore volume and pore size distribution of the TiSi xerogels, the DR equations (2.11-2.13) and Density functional theory were used (2.20-2.21). A Thermo Fisher Scientific ESCALAB 250Xi was used for collecting the X-ray photoelectron spectroscopy (XPS) data. A Bruker Vertex 70v spectrometer was used for recording the FTIR spectra. A Nova Nano SEM 200 FEI with an attachment for chemical analysis of a specimen in micro areas with energy dispersive X-ray spectroscopy (EDX, EDAX) was used to determine the microstructure of the obtained materials by scanning electron microscopy (SEM) (**Papers I–V**). Exsiccator porosimetry was applied as an express test method (**Paper I**).

5.3 Sorption experiments

The sorption capability of the synthesized TiSi gels was studied as a function of pH, adsorbent mass, initial concentration of target ion, contact time, temperature and the composition and concentration of the background solution. All sorption experiments are described in detail in **Papers I–V**. Briefly, the chosen amount of the obtained material was mixed with the sorbate containing solution. Solids were separated from liquids using polypropylene syringe filters. Filtrates were analysed for pH and cation content, while solids were dried and investigated with XRD, FTIR, SEM-EDX and XPS in order to understand the sorption mechanism.

The cation concentrations (except Cs^+) in the solutions of the sorption tests were estimated with an inductively coupled plasma optical atomic emission spectrometer (ICP-OES) model iCAP 6300 (Thermo Electron Corporation, USA), and the Cs^+ concentrations were determined by inductively coupled plasma with mass detector (ICP-MS) model Agilent 7500ce. The sorption capacity (q) was estimated by Eq. (2.1), the separation factor (F), distribution coefficient (K_d), thermodynamic and Gapon's selectivity coefficients were evaluated with Eq. (2.22–2.25) and the decontamination factor (DF) was calculated using the following equation (**Papers I–V**) [86, 127-131]:

$$\mathrm{DF} = \frac{(\Delta C \cdot 100\%)}{C_0} \tag{5.2}$$

In order to identify the source of the heterophase on the sample surface, four series of sorption tests were conducted in an inert atmosphere (N_2/Ar) (Table 5.1). The first series of samples had all the same sorption experiment conditions and only drying was done under an inert atmosphere. For the second series, the Milli-Q water was decarbonized before the Sr^{2+} solution preparation; drying was also in an inert atmosphere. In the third series, the surface of the xerogels was degassed by boiling in decarbonized Milli-Q water with following ultrasonication; the Sr^{2+} solution was prepared with non-decarbonized Milli-Q water; and drying followed in an inert atmosphere. The fourth test was carried out with degassed materials and decarbonized Milli-Q water before the Sr^{2+} solution was prepared, again with drying in an inert atmosphere.

Table 5.1: Test conditions for the 4 sorption tests in inert atmosphere. -: condition not applied, +: condition applied in the test.

Conditions	Series N1	Series N2	Series N3	Series N4
Decarbonized Milli-Q water	-	+	-	+
Degassed xerogels	-	-	+	+
Drying in an inert atmosphere	+	+	+	+

5.4 Theoretical modelling and mechanism investigation

In order to gain an insight into the mechanism of cation sorption on the TiSi xerogel surface, the sorption theories discussed in Chapter 2 were applied. One of the most popular and reliable criteria for fitting a theoretical model to experimental data is the correlation coefficient (R^2). This was calculated using the following equation:

$$R^2 = \frac{\sum (q_{\mathrm{eq,\,exp}} - \bar{q}_{\mathrm{eq,\,exp}})^2 - \sum (q_{\mathrm{eq,\,exp}} - q_{\mathrm{eq,\,calc}})^2}{\sum (q_{\mathrm{eq,\,exp}} - \bar{q}_{\mathrm{eq,\,exp}})^2} \tag{5.3}$$

where, $q_{eq,exp}$ is equilibrium capacity obtained experimentally and $\overline{q}_{eq.exp}$ is mean value of experimental capacity; $q_{eq,calc}$ is equilibrium capacity, calculated from the isotherm equation

The models which best fit to the experimental data ($R^2 \geq 0.9$) were reported in **Papers II–III** and will be discussed briefly in Chapter 6.

6 Results and discussion

6.1 Material characterization before sorption studies

The effect of synthesis conditions on the structural and sorption properties of TiSi is described in detail in **Papers I–IV** and the corresponding patents [178, 179]. Based on these investigations, the most efficient synthesis conditions that yielded material selective to Sr^{2+} were identified. The most effective was found to be the TiSi xerogel prepared under HTT at 150 °C for 6 h. The sorption ability to other potential pollutants of these chosen TiSi xerogels was tested and the materials were characterized before and after the sorption tests in order to understand the nature of the material and sorption process.

All TiSi materials prepared using chemically pure and technical solutions of titanyl sulphate ($TiOSO_4$) were characterized by XRD, FTIR and XPS, but the focus here is on the chosen TiSi samples. It could be demonstrated that the described synthetic approach yields titanosilicate with the same peak positions and broadness as poorly crystalline sodium titanosilicate (Figure 3.2, Table 3.1) [175]. According to the findings, the size of the crystallites becomes detectable after HTT at 200 °C for 12 h (Figure 6.1).

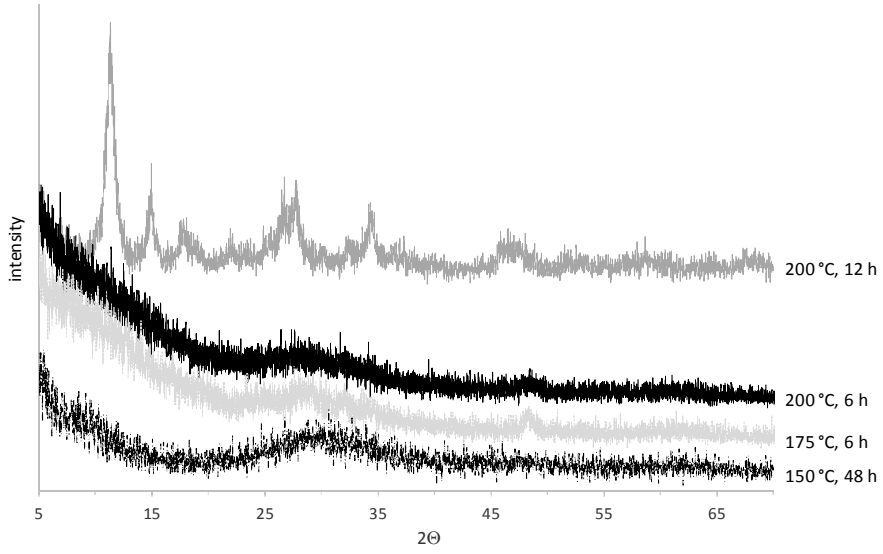

Figure 6.1: Influence of hydrothermal treatment temperature and duration on the phase composition of TiSi xerogels.

The FTIR spectra of the studied xerogels with the suggested functional groups superimposed is presented Figure 6.2. A detailed analysis of the main band positions

was presented in **Papers II–III.** The summary of FTIR spectroscopy is given in Table 6.1. It is important to emphasize that amorphous samples contain bridged Si-O-Ti functional groups as well, confirming that the obtained gels are titanosilicates.

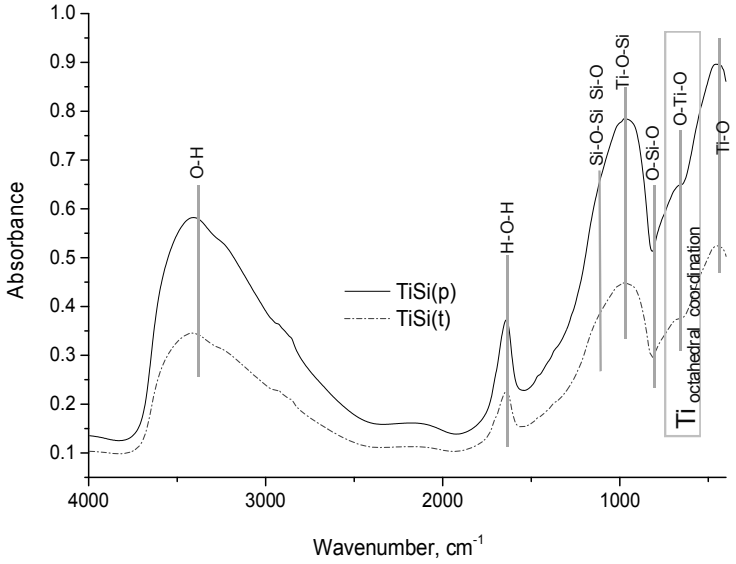

Figure 6.2: FTIR spectra of the synthesized TiSi materials.

Table 6.1: Major functional groups of the TiSi xerogels.

Band position, cm^{-1}	Functional group
3433–3417	O-H
1640	H-O-H
1110–800	Si-O
1068	Si-O-Si
971–956	Bridged Si-O-Ti
450	Ti-O, O-Si-O and O-Ti-O
654 and 546	Ti in octacoordination

The surface chemistry of the TiSi samples was determined by XPS (Figure 6.3), SEM-EDX and mapping (Figure 6.4). The presence of the main elements Ti, Si, O and Na was confirmed (Table 6.2; **Paper II**). As can be seen, C is present on the surface of both materials, which is important for understanding the Sr sorption mechanism. K, Fe and Mg were observed in the data for TiSi(t) (TiSi synthesized from a technical precursor), which can be attributed to the composition of the technical precursor. Interestingly, K^+ is preferred over Na^+ during the gel structure formation of TiSi(t).

Table 6.2: Element content of the TiSi xerogel surface.

Element	Atomic %	
	TiSi(t)	TiSi(p)
Si 2p	15.21	13.76
Ti 2p	6.75	6.71
O 1s	52.28	48.80
K 2p	5.86	n.d.
Mg 1s	0.24	n.d.
Fe 2p	0.51	n.d.
C 1s	16.19	22.53
Na 1s	2.95	8.20

n.d. – not detected

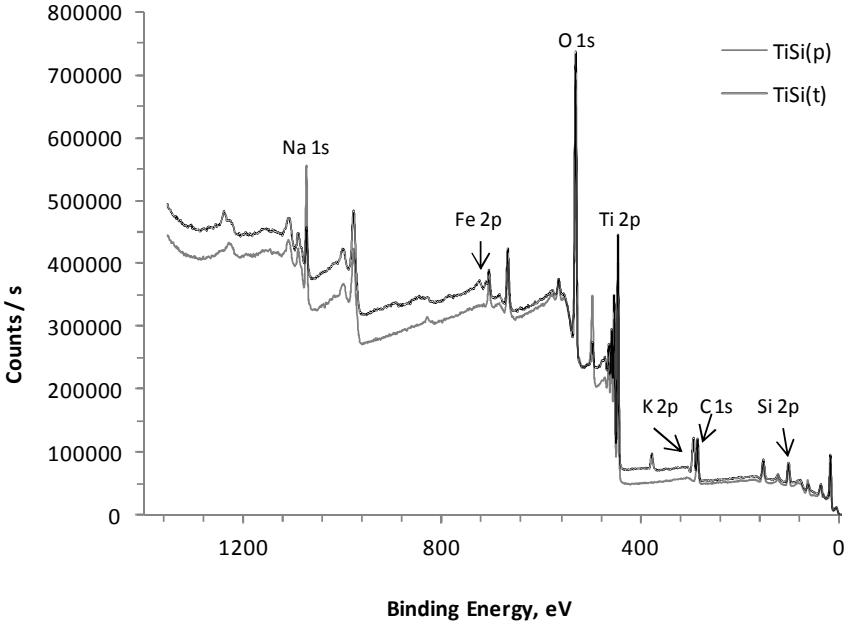

Figure 6.3: XPS spectra of the TiSi xerogels.

The morphology and microstructure of the chosen samples were estimated by SEM and the uniformity of the chemical element distribution was determined by SEM-EDX technique (Figure 6.4, **Paper II**). The isotherm data indicates that the surfaces of both materials are uneven, have pore openings and that elements like Ti, K and Fe are distributed homogeneously on the sample surfaces (Figure 6.4). Based on the FTIR, SEM-EDX and mapping data, the most active ion-exchangeable groups of the obtained TiSi materials were suggested: ≡Ti-O-Si-ONa, ≡Si-O-Ti-ONa and NaO-Si-O-Ti-ONa. Based on the literature, the role of surface ion exchange centres like ≡Si-O-Si-ONa and

≡Ti-O-Ti-ONa are supposed to be less relevant for estimating the TiSi sorption ability and selectivity [138, 139, 162, 241, 242].

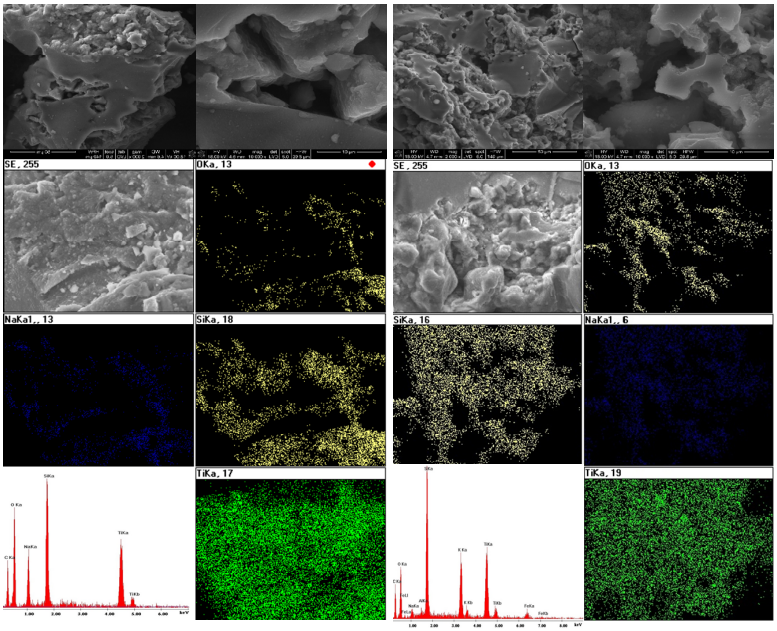

Figure 6.4: SEM images, SEM-EDX and mapping data of TiSi(p) (left) and TiSi(t) (right).

The pore structure of the TiSi xerogels was defined by a low-temperature nitrogen sorption/desorption technique (Figure 6.5, Table 6.3). Isotherms and the pore size distribution (DFT) demonstrate the developed porous structure of the produced TiSi. According to the IUPAC, the obtained isotherm shapes can be classified as type IV with H2 hysteresis loops, designating the micro-mesopore structure of the TiSi materials [120]. It is interesting to note that the TiSi(t) hysteresis loop is closer in shape to the H1 loop type, which suggests a micro-meso-macropore structure of the TiSi(t) sample. The pore size distribution confirmed the abovementioned assumptions: the micro-mesopore structure is characteristic for TiSi(p) (TiSi synthesized from a pure precursor), while the micro-meso-macropore structure is typical for TiSi(t).

Table 6.3: Textural properties of selected TiSis.

Sample name	S, m^2/g	V_{total}, cm^3/g	$V_{DR\ micro}$, cm^3/g	R_{pore}, nm	$R_{micropore}$, nm
TiSi(t)	158.7	0.47	0.05	8.40	1.6
TiSi(p)	270.3	0.42	0.10	3.52	2.5

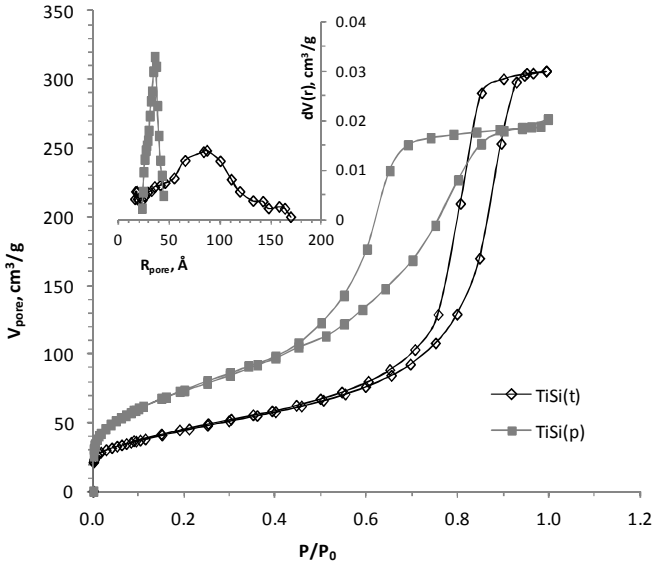

Figure 6.5: Isotherms of nitrogen low-temperature sorption/desorption and DFT pore size distribution of prepared TiSis.

6.2 Sorption capabilities of TiSis

6.2.1 Affinity of TiSis to Sr^{2+} and Cs^{+} stable nuclides

Influence of adsorbent dose

Details of the efficient dose estimation process are described in **Papers II–III**. Both technical and pure TiSi were found to be efficient sorption materials for Sr^{2+} (DF ≥ 90%) in all the studied ranges of 20–0.25 mg/L (the volume to the solid mass ratio, *V*:*m*, ranges from 50 to 4000). Variations of DF were less than 9%, which is within the batch method error range. The TiSi(t) demonstrated the same high affinity to Cs^{+} (DF over 90%). Hence, the TiSi(p) sorption capacity for Cs^{+} was suppressed by the presence of the competitive Na^{+} background and a TiSi(p) dose of 10 mg/L (*V*:*m* = 100) was found to be efficient. Such a difference in Cs^{+} sorption ability is attributed to the alterations in pore structure of the technical and pure TiSi (Table 6.3). The sorbent dose of 10 mg/L (*V*:*m* = 100) was therefore used for further investigations for all materials and solutions.

Effect of pH

The literature indicates [197, 243] that cation exchange increases with pH. The observation of a negligible (in the case of Sr^{2+} at pH ≥ 4) and reverse (in the case of Cs^{+}) dependency suggests a sorption mechanism which is different from both the typical

cation exchange and from each other retention mechanism for these two sorbates (Figure 6.7).

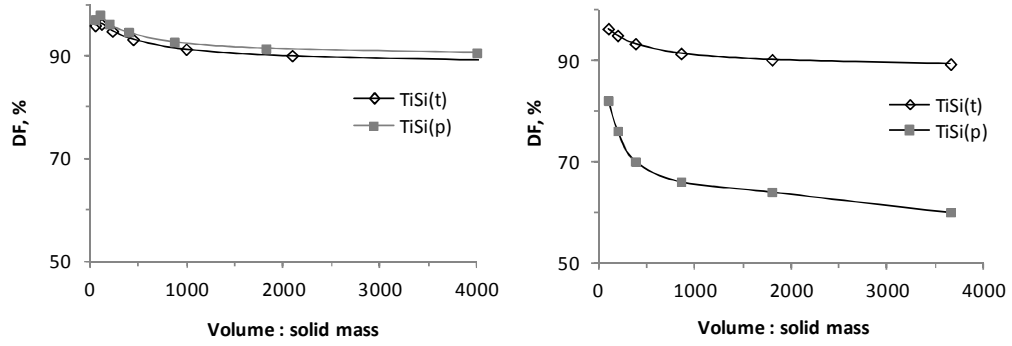

Figure 6.6: Effect of volume to sorbent mass ratio on the decontamination factor of Sr^{2+} (left) and Cs^{+} (right) from a 0.1N NaCl background.

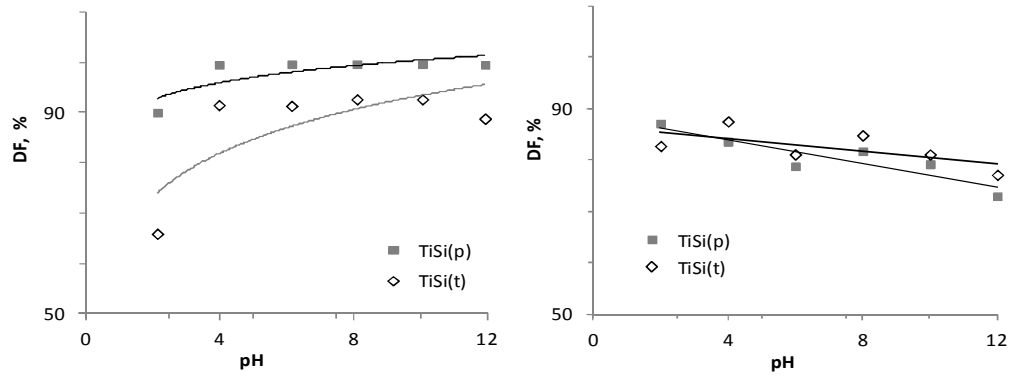

Figure 6.7: Effect of pH on TiSi sorption of Sr^{2+} (left) and Cs^{+} (right) from water.

Influence of the initial cation concentration

A detailed description of the influence of the initial concentration of the target cation and background solution and the composition of the latter on the sorption parameters of TiSi xerogels is presented in **Papers I–III.** Briefly, a water medium was selected for collecting the reference data, a NaCl background solution was used to evaluate the Na^{+} competition effect on the Sr^{2+} or Cs^{+} uptake and Ringer–Locke's solution was used to assess the effect of the Na^{+}, K^{+} and Ca^{2+} competitive ions on the sorption capacity and selectivity of the synthesized xerogels. The obtained data is intended for use to envisage the TiSi behaviour in aqueous media containing Sr^{2+}, Ca^{2+}, Cs^{+}, K^{+} and Na^{+} such as drinking, ground, sea and mine water, blood plasma and LRW.

It was expected that the TiSi xerogels would demonstrate a higher capacity and selectivity to Sr^{2+} than to Na^{+}, K^{+}, Cs^{+} and Ca^{2+}, based on the well-known general trend that cations with a higher valence and a bigger atomic mass are preferentially sorbed [94, 95].

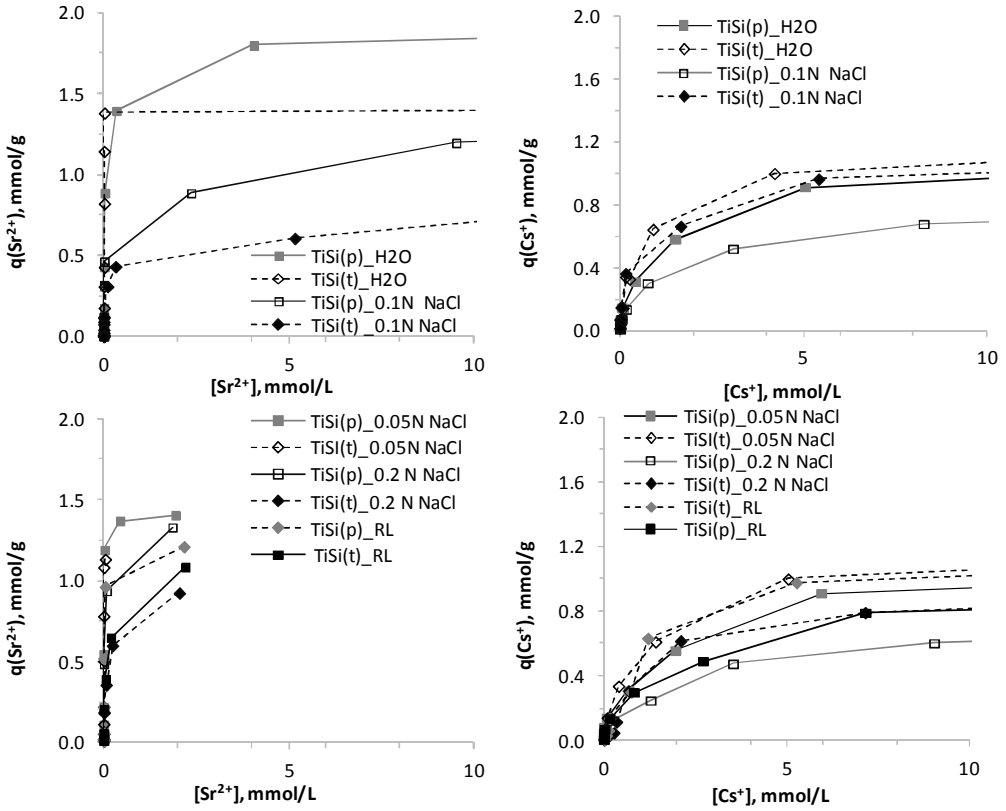

Figure 6.8: Sorption isotherms of Sr^{2+} (left column) and Cs^{+} (right column) from solutions with only one potential pollutant. Experimental conditions: initial Sr^{2+} or Cs^{+} concentration range 10–5000 mg/L; *V*:*m* ratio 100; contact time 24 h, media: water (pH = 6.78); 0.05 M, 0.1 M, 0.2 M NaCl and Ringer–Lock's solution (RL, 153.85 mmol/L of NaCl; 2.38 mmol/L of $NaHCO_3$; 2.68 mmol/L of KCl; 1.8 mmol/L of $CaCl_2$ and 5.55 mmol/L of D-glucose; pH = 8.07); ambient temperature.

Comparing the sorption capacities of the TiSi xerogels, they do indeed seem to fit this general trend, since $q(Sr^{2+}) > q(Cs^{+})$ in all studied media (Table 6.4). Yet some interesting facts need to be discussed. First of all, according to the Giles classification, the sorption isotherms can be classified as H2 shape, which indicates the high affinity and selectivity to both target cations even in the presence of competitive ions (Figure 6.8) [99-102]. Secondly, no effect of the medium composition and concentration of competitive ions was detectable for the Sr^{2+} retention ability of both TiSi xerogels up to

Sr^{2+} and Cs^{+} initial concentrations of 500 mg/L. In contrast, a decrease in the precipitated CTS sorption ability was reported with much lower initial Sr^{2+} and Cs^{+} concentrations (10^{-9} – 10^{-3} M) in the same media concentrations [86, 130, 138, 177, 195]. Thirdly, the adsorption isotherms had the same shape in different background solutions for both the Sr^{2+} and Cs^{+} sorbates. On the one hand, it is evident that sorption of the target cations by TiSi xerogels had a greater energy benefit than that of Ca^{2+}, K^{+} or Na^{+}. On the other hand, however, a mechanism of uptake other than ion exchange may be involved.

Table 6.4: Maximum sorption capacity of TiSi materials to Sr^{2+} and Cs^{+} from different background solutions.

Background solution / Sample name	H_2O	NaCl			Ringer–Locke's solution
		0.05 M	0.1 M	0.2 M	
		q_{eq} (Sr^{2+}), mmol/g			
TiSi(p)	1.95	1.40	1.38	1.32	1.21
TiSi(t)	1.42	1.13	1.02	0.92	1.08
		q_{eq} (Cs^{+}), mmol/g			
TiSi(p)	1.13	1.091	0.83	0.75	0.92
TiSi(t)	1.21	1.203	1.13	0.98	1.16

Interestingly, TiSi(p) has a higher maximum sorption capacity for Sr^{2+} than TiSi(t), while for Cs^{+} the opposite situation was observed in all studied media. The first observation was attributed to a less specific surface area, which results in fewer accessible active centres and half the micropore volume, while the second observation is ascribed to the less steric restrictions for the big Cs^{+} cation in pores with a wider radius (Table 6.4 and Table 6.3).

In order to compare the selectivity of the TiSi xerogels to the target ions, the selectivity coefficients and separation factors were evaluated for different media containing both Sr^{2+} and Cs^{+} simultaneously. It was found that the TiSi xerogels have a higher selectivity to Sr^{2+} and the separation factor has a smaller deviation from experimental observations than the calculated selectivity coefficients (Table 6.5). Nevertheless, the obtained TiSi xerogels demonstrated a high sorption ability, DF and selectivity to Cs^{+} even in the presence of competing cations such as Na^{+}, K^{+}, Sr^{2+} and Ca^{2+} (Figure 6.9, Table 6.5). A detailed description of the experiment can be found in **Paper I.** Interestingly, the synthesized TiSis from media containing both Sr^{2+} and Cs^{+} simultaneously demonstrated the similar high values of $q(Sr^{2+})$ and $q(Cs^{+})$ that were obtained in solutions with only one target cation (Table 6.4 and **Papers II–III**). This fact may also suggest that the sorption of Sr^{2+} and Cs^{+} takes place on different active centres, or that different sorption mechanisms are involved.

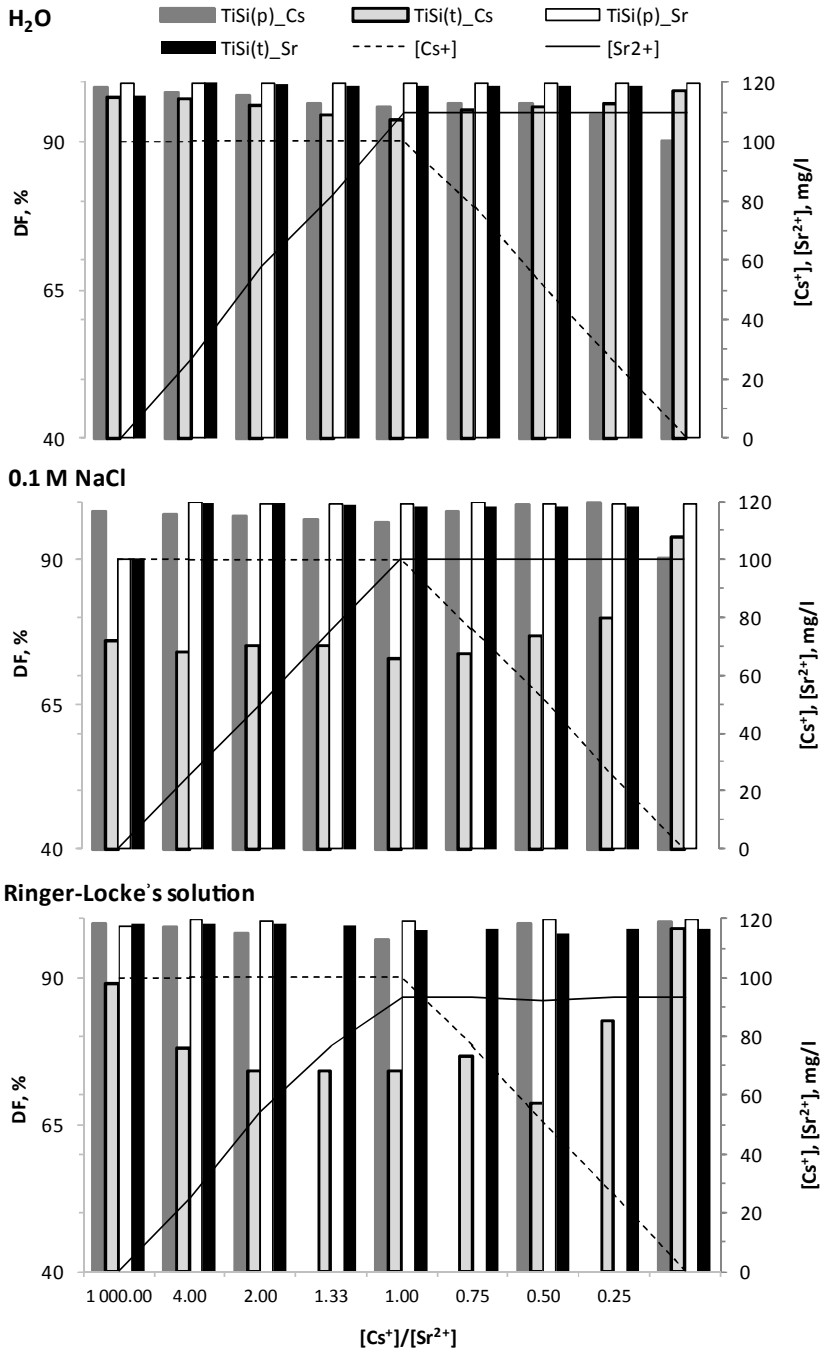

Figure 6.9: Effect of the initial concentration of Sr^{2+} and Cs^{+} present together in solution on decontamination factor of TiSi xerogels. Experimental conditions: water, 0.1 M NaCl and Ringer–Locke's solution media; *V*:*m* ratio 100; contact time 24 h; ambient temperature.

Table 6.5: Selectivity coefficient of TiSi xerogels from different media and different mass concentration ratios (* in column 1) of Cs^+ and Sr^{2+}.

$\frac{c_{in}Cs^+}{c_{in}Sr^{2+}}$ *	q (Sr^{2+}), mmol/g	K_d (Sr^{2+})	Sr^{2+}/Cs^+			q (Cs^+), mmol/g	K_d (Cs^+)	Cs^+/Sr^{2+}		
			K_{Im}	K_G	F			K_{Im}	K_G	F
TiSi(p) H_2O										
$2.56 \cdot 10^3$	$4.45 \cdot 10^{-5}$	43294	0.53	0.03	3.49	0.07	12417	1.89	30.23	0.29
3.70	0.03	33744	0.94	1.55	5.47	0.07	6167	1.06	0.65	0.18
1.72	0.07	41362	1.51	3.64	9.73	0.07	4251	0.66	0.27	0.10
1.22	0.09	50997	2.67	7.64	19.10	0.07	2667	0.37	0.13	0.05
0.91	0.12	52073	3.10	10.24	22.35	0.07	2330	0.32	0.10	0.04
0.71	0.13	47726	2.57	8.52	17.77	0.06	2686	0.39	0.12	0.06
0.46	0.13	45816	2.61	8.67	17.70	0.04	2589	0.38	0.12	0.06
0.23	0.13	39217	3.71	12.30	23.25	0.02	1687	0.27	0.08	0.04
$1.00 \cdot 10^{-5}$	0.13	32292	6.23	20.64	35.40	$6.18 \cdot 10^{-7}$	912	0.16	0.05	0.03
TiSi(t) H_2O										
$2.56 \cdot 10^3$	$4.34 \cdot 10^{-5}$	4227	0.53	0.03	1.09	0.07	3894	1.89	30.71	0.92
3.70	0.03	1585282	11.91	19.56	474.31	0.07	3342	0.08	0.05	0.00
1.72	0.07	230534	1.95	4.69	9.37	0.07	2459	0.51	0.21	0.11
1.22	0.09	20909	2.61	7.46	11.94	0.07	1750	0.38	0.13	0.08
0.91	0.12	19160	2.90	9.58	12.69	0.07	1510	0.34	0.10	0.08
0.71	0.12	1473	1.92	6.32	7.35	0.06	2004	0.52	0.16	0.14
0.46	0.12	16557	1.75	5.78	7.11	0.04	2327	0.57	0.17	0.14
0.23	0.12	14870	1.50	4.94	5.78	0.02	2576	0.67	0.20	0.17
$1.00 \cdot 10^{-5}$	0.12	18233	0.62	2.05	2.64	$6.75 \cdot 10^{-7}$	6900	1.62	0.49	0.38
TiSi(p) 0.1 M NaCl										
$1.10 \cdot 10^5$	$9.35 \cdot 10^{-7}$	911	0.16	$1 \cdot 10^{-3}$	0.15	0.07	6148	6.44	711.50	6.75
4.00	0.03	45237	1.52	2.390	10.20	0.07	4434	0.66	0.42	0.10
2.00	0.06	31138	1.49	3.330	8.32	0.07	3745	0.67	0.30	0.12
1.33	0.09	23314	1.55	4.220	7.47	0.07	3123	0.65	0.24	0.13
0.76	0.11	20725	1.70	5.360	7.74	0.07	2677	0.59	0.19	0.13
0.52	0.11	41385	1.04	3.270	6.67	0.06	6206	0.97	0.31	0.15
0.25	0.11	35572	0.40	1.280	2.41	0.04	14739	2.47	0.78	0.41
$1.00 \cdot 10^{-5}$	0.11	30053	0.08	0.250	0.44	0.02	68999	12.59	4.00	2.30

Table 6.5 (continued): Selectivity coefficient of TiSi xerogels from different media and different mass concentration ratios (* in column 1) of Cs^+ and Sr^{2+}.

$\frac{c_{in}Cs^+}{c_{in}Sr^{2+}}$*	q (Sr^{2+}), mmol/g	K_d (Sr^{2+})	Sr^{2+}/Cs^+			q (Cs^+), mmol/g	K_d (Cs^+)	Cs^+/Sr^{2+}		
			K_{lm}	K_G	F			K_{lm}	K_G	F
TiSi(t) 0.1 M NaCl										
$1.10 \cdot 10^5$	$9.34 \cdot 10^{-7}$	909	3.02	0.03	2.88	0.06	316	0.33	36.64	0.35
4.00	0.03	34695	20.94	32.87	123.36	0.06	281	0.05	0.03	0.01
2.00	0.06	26184	17.08	38.09	87.39	0.06	300	0.06	0.03	0.01
1.33	0.09	17754	14.05	38.36	59.19	0.06	300	0.07	0.03	0.02
0.76	0.11	12879	13.28	41.83	47.66	0.05	270	0.08	0.02	0.02
0.52	0.11	12226	12.51	39.36	43.73	0.04	280	0.08	0.03	0.02
0.25	0.11	11372	10.14	31.88	34.18	0.03	333	0.10	0.03	0.03
$1.00 \cdot 10^{-5}$	0.11	19793	2.93	9.23	13.05	$6.39 \cdot 10^{-7}$	1517	0.34	0.11	0.08
TiSi(p) Ringer-Locker's solution										
$6.25 \cdot 10^2$	$1.81 \cdot 10^{-4}$	8326	0.22	0.03	0.63	0.07	13241	4.59	36.50	1.59
4.00	0.03	46976	1.05	1.65	7.17	0.07	6554	0.96	0.61	0.14
1.85	0.06	26766	1.39	3.21	7.18	0.07	3728	0.72	0.31	0.14
1.08	0.11	20505	1.75	5.30	7.90	0.07	2595	0.57	0.19	0.13
0.55	0.11	42198	0.63	1.92	4.09	0.04	10314	1.59	0.52	0.24
$1.72 \cdot 10^{-3}$	0.11	40254	0.36	1.09	2.28	$1.19 \cdot 10^{-4}$	17642	2.78	0.91	0.44
TiSi(t) Ringer-Locker's solution										
$6.25 \cdot 10^2$	0.00	13233	4.50	0.57	16.36	0.07	809	0.22	1.76	0.06
4.00	0.03	12378	9.94	15.64	34.97	0.06	354	0.10	0.06	0.03
1.85	0.06	11879	12.13	28.05	41.81	0.06	284	0.08	0.04	0.02
1.30	0.09	8170	10.05	27.71	28.74	0.06	284	0.10	0.04	0.03
1.08	0.10	5365	8.15	24.60	18.87	0.06	284	0.12	0.04	0.05
0.83	0.10	5709	7.29	22.04	17.43	0.04	328	0.14	0.05	0.06
0.55	0.10	3730	8.84	26.44	17.07	0.03	219	0.11	0.04	0.06
0.28	0.10	6100	5.17	15.64	12.77	0.02	478	0.19	0.06	0.08
$1.72 \cdot 10^{-3}$	0.10	5707	0.44	1.33	1.05	$1.18 \cdot 10^{-4}$	5412	2.27	0.75	0.95

The contact time effect

Kinetic studies of the material are important for understanding both its sorption mechanism and potential for real application. An analysis of the DF as a function of contact time is described in **Papers II–III**. In summary, the synthesized TiSi xerogels demonstrated the ability to uptake the target cations with a quite high speed, thus a DF of over 90% was achieved after the first 10–30 min of contact for both materials and both target cations (Figure 6.10). It is noteworthy that in the presence of competitive ions the Cs^+ kinetics is more strongly suppressed than the Sr^{2+} sorption process. This observation may be explained by the different sizes of the cations or may suggest different uptake mechanisms for these two cations by the TiSi xerogels.

The influence of temperature

According to the literature, the kinetics of processes based on ion exchange usually slow down with increasing temperature [113, 114, 246]. Therefore, it was necessary to study the sorption characteristics of the TiSi gels as a function of temperature. The results can indicate the nature of the sorption process and be used to propose new future applications, with an awareness of their potential limitations.

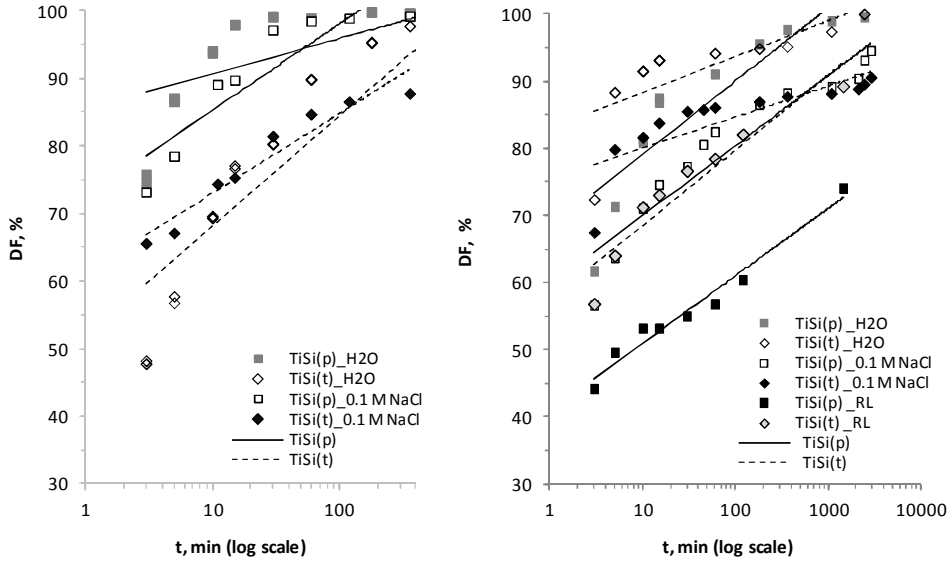

Figure 6.10: Kinetics of Sr^{2+} (left) and Cs^+ (right) sorption on titanosilicates. Experimental conditions: time range 3–2880 min, initial cation concentration 0.5 g/L (Sr^{2+} 5.71 mmol/L; Cs^+ 3.76 mmol/L); V:m ratio 100, background solutions – water (pH = 6.78) and 0.1 M NaCl (pH = 7.08) and Ringer–Locke's (RL, for Cs^+); ambient temperature.

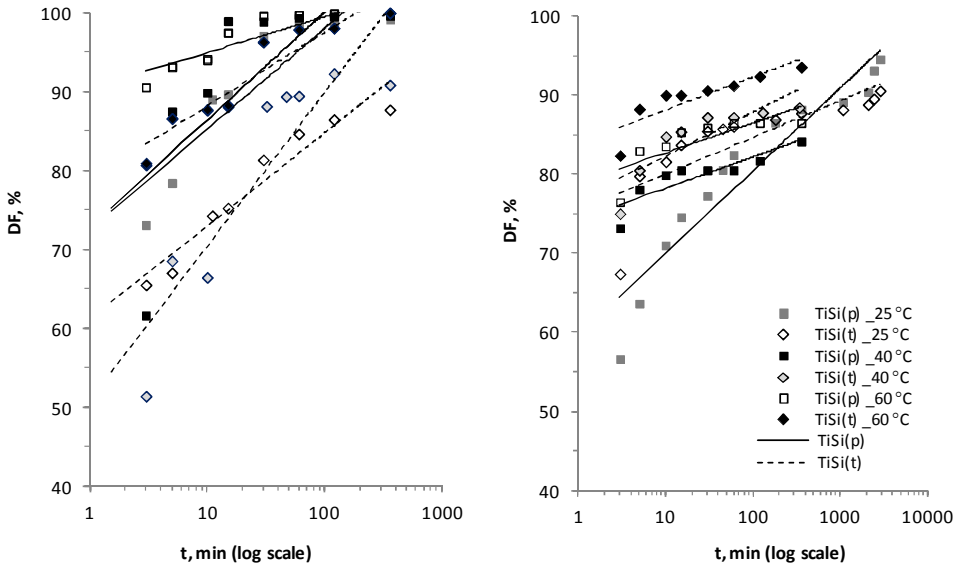

Figure 6.11: Temperature effect on the kinetics of the Sr^{2+} (left) and Cs^{+} (right) sorption. Experimental conditions: contact time 3–360 min, Sr^{2+} initial concentration 0.5 g/L; V:m ratio 100; sorption temperature 25, 40 and 60 °C, medium 0.1 M NaCl, pH = 7.08.

The impact of temperature is presented in **Papers II–III**. In summary, raising the solution temperature increases the TiSi xerogel sorption speed (Figure 6.11), which indicates an endothermic process different from that of ion exchange [247-250]. Due to the endothermic nature of the process, there is no need to cool down polluted aqueous solutions with higher temperatures. These could potentially include blood plasma, bypass or mine water or polluted water from LRW or NPP accidents.

6.2.2 Potentially toxic metal cation uptake from synthetic solution by TiSi

Studies of the sorption abilities of TiSi xerogels to toxic metal cations other than Sr^{2+} and Cs^{+} are presented in this section. The TiSi sorption capability was estimated as a function of sorbent and target cation concentration, pH and contact time from mono- and polycation synthetic solutions. The DF and q_{eq} were calculated to determine the efficiency range of the TiSi materials.

The influence of sorbent dose on TiSi uptake of the studied cations is presented in Figure 6.12. A general trend of increasing DF with raising the sorbent dose can be easily seen. Respectively, the highest DF for all target cations was observed at the highest sorbent dose, 0.1 g L^{-1}. This dose was used for further studies. It follows from the figure that the nature of the precursor does not much affect the sorption ability and selectivity of TiSis. The cation sorption preferences were found to be in the order Mn < Ni < Co < Zn < Cd < Cu < Cr < Pb < Fe for the TiSi(t), while for the pure

material it was only a little different, with Ni < Mn < Co < Zn < Cd < Cu < Cr < Pb < Fe.

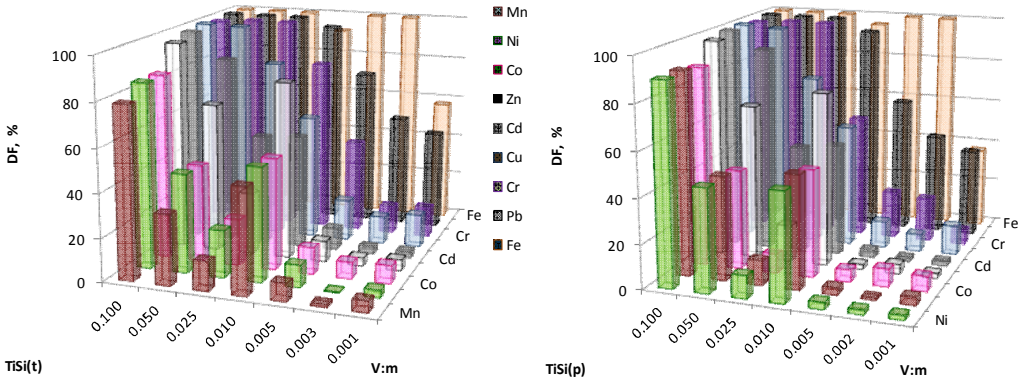

Figure 6.12: Sorbent dose influence on the level of cation retention by TiSis.

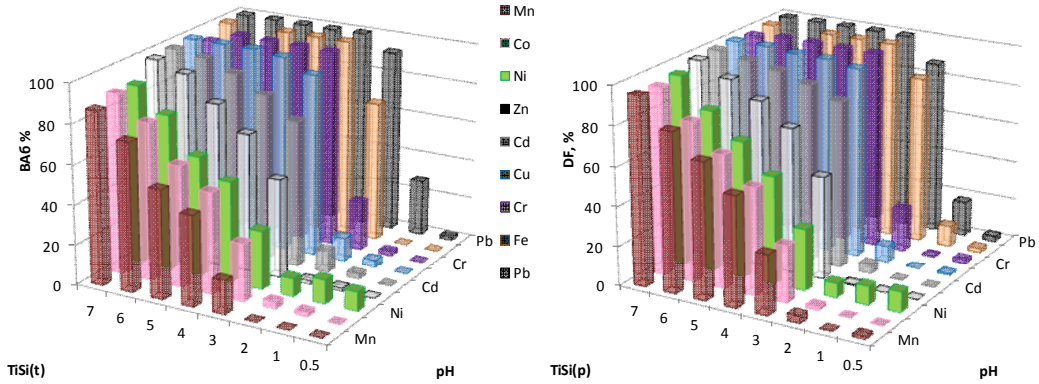

Figure 6.13: Influence of pH on the sorption ability of TiSis.

In terms of solution pH, the broadest range of efficiency was observed for Pb (pH = 2–7) with a DF of over 90% for both TiSi materials. The optimum pH with DF ≥ 90% for all the cations was found to be pH 7 for both TiSi materials. Of course, the cation state changes with pH, which shall be taken into account in explaining the difference in sorption preference and ability of TiSi materials.

The influence of initial cation concentrations on TiSi sorption capacity is presented in Figure 6.14. The shape of the isotherms evidence that TiSi(t) has the highest affinity to Pb, Cd and Cu, while for TiSi(p) the third place in the affinity range was taken by Co. The abrupt increase in sorption capacity at a small initial concentration range was

common for the all cation isotherms except Fe. The figure illustrates this fact by the vertical initial part of the isotherms. According to the Giles classification this fact suggested high sorption capacity and affinity of the studied materials to the target cations. It is noticeable that Fe sorption starts to increase (vertical isotherm part) when the other cation is close to equilibrium. This may suggest that the competitive influence of other cations suppresses the sorption of Fe on TiSi.

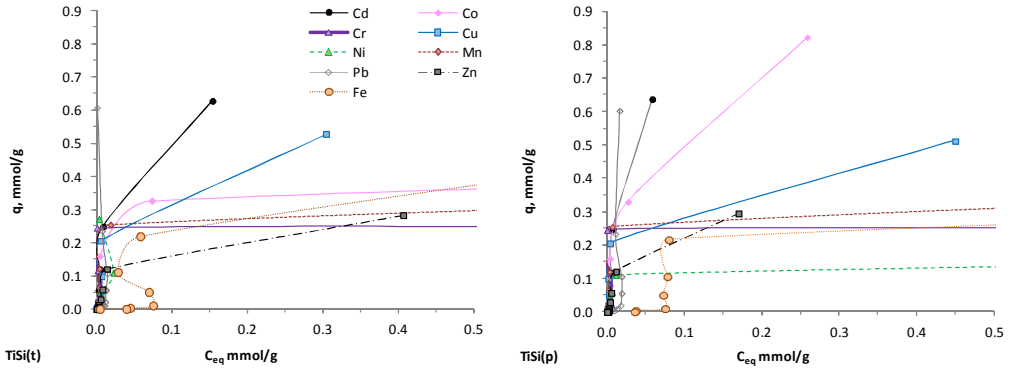

Figure 6.14: Isotherms of cation sorption on TiSi materials.

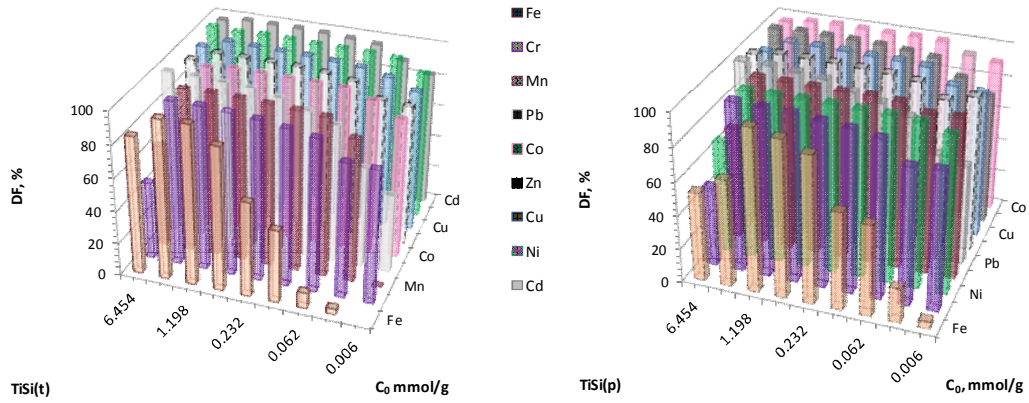

Figure 6.15: Dependence of TiSi decontamination level from initial cation concentration.

As presented in Figure 6.15, the decontamination level is dependent of the initial cation concentration. Both TiSis demonstrated efficient cation uptake across a wide range of concentrations. Concentration variation affected the level of Fe sorption the most, which can suggest a concurrent mechanism of Fe sorption onto TiSi materials. A high sorption efficiency (DF > 90%) was observed for Cd, Co, Cu and Zn throughout the studied concentration range for both TiSis.

The sorption capacity as a function of contact time is presented in Figure 6.16 and Figure 6.17. Interestingly, the highest rate of sorption for both TiSis was observed for Pb, while the highest capacity was observed for Cu. All studied cations achieved a high sorption rate and most reached a stable DF during the first 60 min.

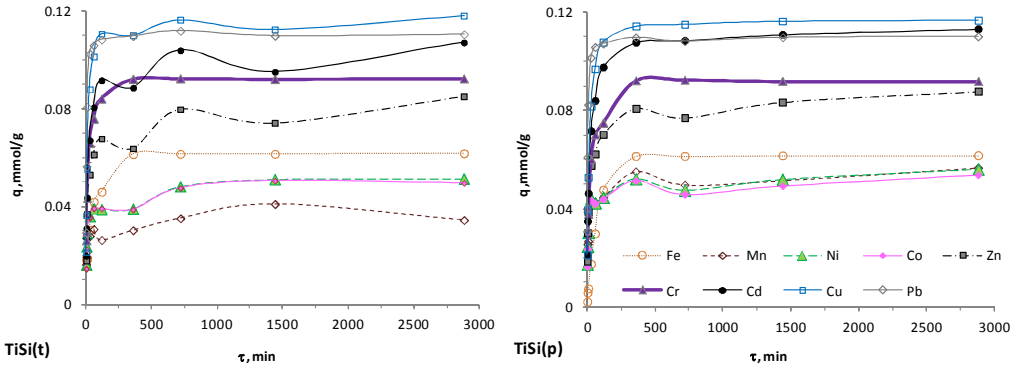

Figure 6.16: Sorption kinetics of cations on TiSi materials.

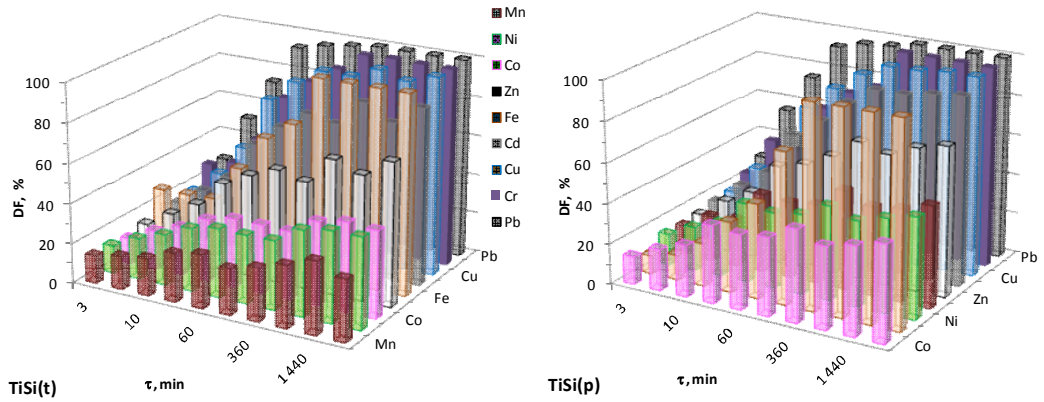

Figure 6.17: TiSi decontamination factor dependence on contact time.

It can be concluded that TiSi materials have the highest efficiency with the studied cations under the following conditions: sorbent dose 0.1 g/L; pH range 3–7 and concentration range 0.05–5.0 mmol/L.

6.2.3 Comparison of TiSi sorption abilities with phosphated dolomite

The inexpensive modified natural material phosphated dolomite (PD) was used to compare the sorption potential of TiSi xerogels for toxic cation uptake from aqueous solutions. The sorption data of the PD were published and discussed in detail in **Paper**

V. Briefly, the optimal conditions were found to be as follows: sorbent dose 10 g/L and pH range 2–6, which is very close to the optimum range for TiSi (Figure 6.18 – Figure 6.21).

It can be concluded that both TiSi and PD materials have relatively good abilities to retain the studied cations in synthetic solution. Sorption tests in real waters will provide more information. It would also be beneficial to compare the production costs of PD and TiSi to determine their commercial potential.

6.3 Studies of the Sr^{2+} and Cs^{+} sorption mechanisms

6.3.1 Theoretical modelling

Studying the mechanism of a reaction is one of the most important stages in any laboratory investigation, as it contributes to understanding the nature of the materials and their potential for future applications. Based on the fitted model parameters in combination with the material characterization after the sorption process, the cation sorption mechanism can be proposed. Full details are reported in **Papers II–III** and are briefly described below.

Different theoretical sorption models were discussed in Chapter 2. The chosen criterion for fitting a theoretical model to the experimental data was the correlation coefficient (R^2). The Langmuir and Freundlich theories were used as the basic models, while the remaining theories were only selected when $R^2 \geq 0.9$ for at least one of the materials (Figure 6.22, Figure 6.23, Table 6.6 and Table 6.7).

As can be seen, the sorption of both target sorbates fits the models better when surface heterogeneity is assumed. In addition, the R^2 is above 0.98 for models which allow for interaction of the adsorbed cations, as implied by the Sips, Toth and Redlich-Peterson models.

The kinetic data show a good correlation with the nonlinear pseudo-first order and pseudo-second order models. The latter of these showed a better correlation for both materials and target cations in most of the studied conditions (R^2 = 0.74…1.00), while the Elovich and intraparticle diffusion theories were not fitted well enough.

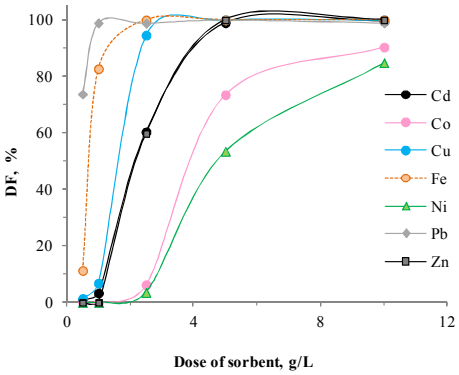

Figure 6.18: Influence of sorbent dose on the decontamination factor of phosphated dolomite materials.

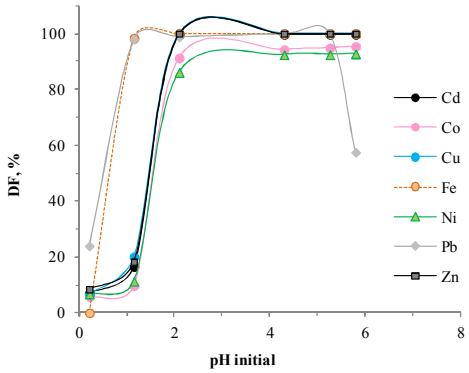

Figure 6.19: The pH dependence of phosphated dolomite materials.

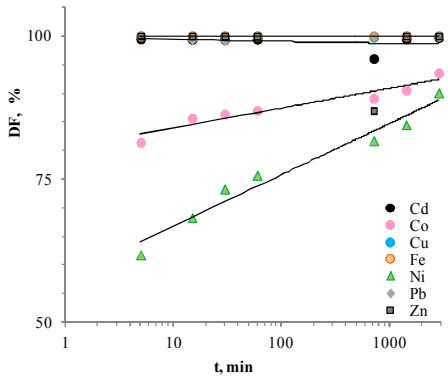

Figure 6.20: Kinetics of cation sorption by phosphated dolomite.

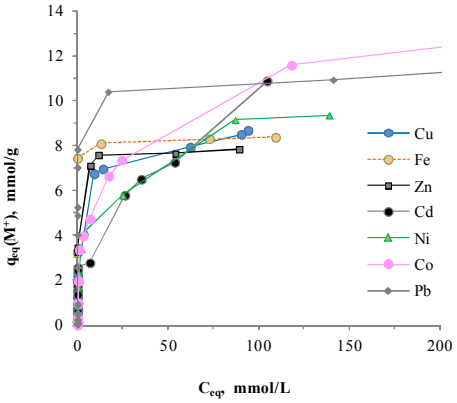

Figure 6.21: Sorption isotherms of phosphated dolomite.

Table 6.6: Adsorption isotherm parameters of synthesized TiSis.

Model	Sr						Cs					
		TiSi(p)			TiSi(t)			TiSi(p)			TiSi(t)	
	q_{exp}, mmol/g	$q_{calc.}$, mmol/g	R^2	q_{exp}, mmol/g	$q_{calc.}$, mmol/g	R^2	q_{exp}, mmol/g	$q_{calc.}$, mmol/g	R^2	q_{exp}, mmol/g	$q_{calc.}$, mmol/g	R^2
H_2O												
Langmuir	1.95	1.81	0.981	1.42	1.23	0.938	1.13	1.10	0.985	1.21	1.16	0.979
Freundlich	1.95	2.24	0.837	1.42	1.69	0.709	1.13	1.23	0.958	1.21	1.31	0.943
Sips	1.95	1.86	0.982	1.42	1.46	0.978	1.13	1.14	0.998	1.21	1.22	0.991
Redlich-Peterson	1.95	1.98	0.990	1.42	1.47	0.967	1.13	1.15	0.993	1.21	1.22	0.988
Toth	1.95	1.89	0.985	1.42	1.46	0.979	1.13	1.15	0.996	1.21	1.22	0.990
0.1 M NaCl												
Langmuir	1.38	1.35	0.917	1.02	0.85	0.943	0.83	0.79	0.987	1.13	1.04	0.966
Freundlich	1.38	1.48	0.971	1.02	1.03	0.987	0.83	0.89	0.973	1.13	1.24	0.934
Sips	1.38	1.36	0.987	1.02	0.99	0.990	0.83	0.83	0.999	1.13	1.13	0.990
Redlich-Peterson	1.38	1.40	0.998	1.02	1.00	0.996	0.83	0.84	0.997	1.13	1.14	0.991
Toth	1.38	1.37	0.992	1.02	0.99	0.993	0.83	0.83	0.998	1.13	1.13	0.991
Ringer-Locke's solution												
Langmuir	1.14	1.19	0.956	1.08	1.11	0.996	0.92	0.92	0.985	1.16	0.91	0.979
Freundlich	1.14	1.31	0.887	1.08	1.20	0.942	0.92	0.99	0.964	1.16	0.96	0.970
Sips	1.14	1.13	0.964	1.08	1.10	0.998	0.92	0.94	0.990	1.16	0.93	0.978
Redlich-Peterson	1.14	1.17	0.957	1.08	1.09	1.000	0.92	0.93	0.985	1.16	0.92	0.979
Toth	1.14	1.13	0.961	1.08	1.09	0.999	0.92	0.94	0.988	1.16	0.93	0.979

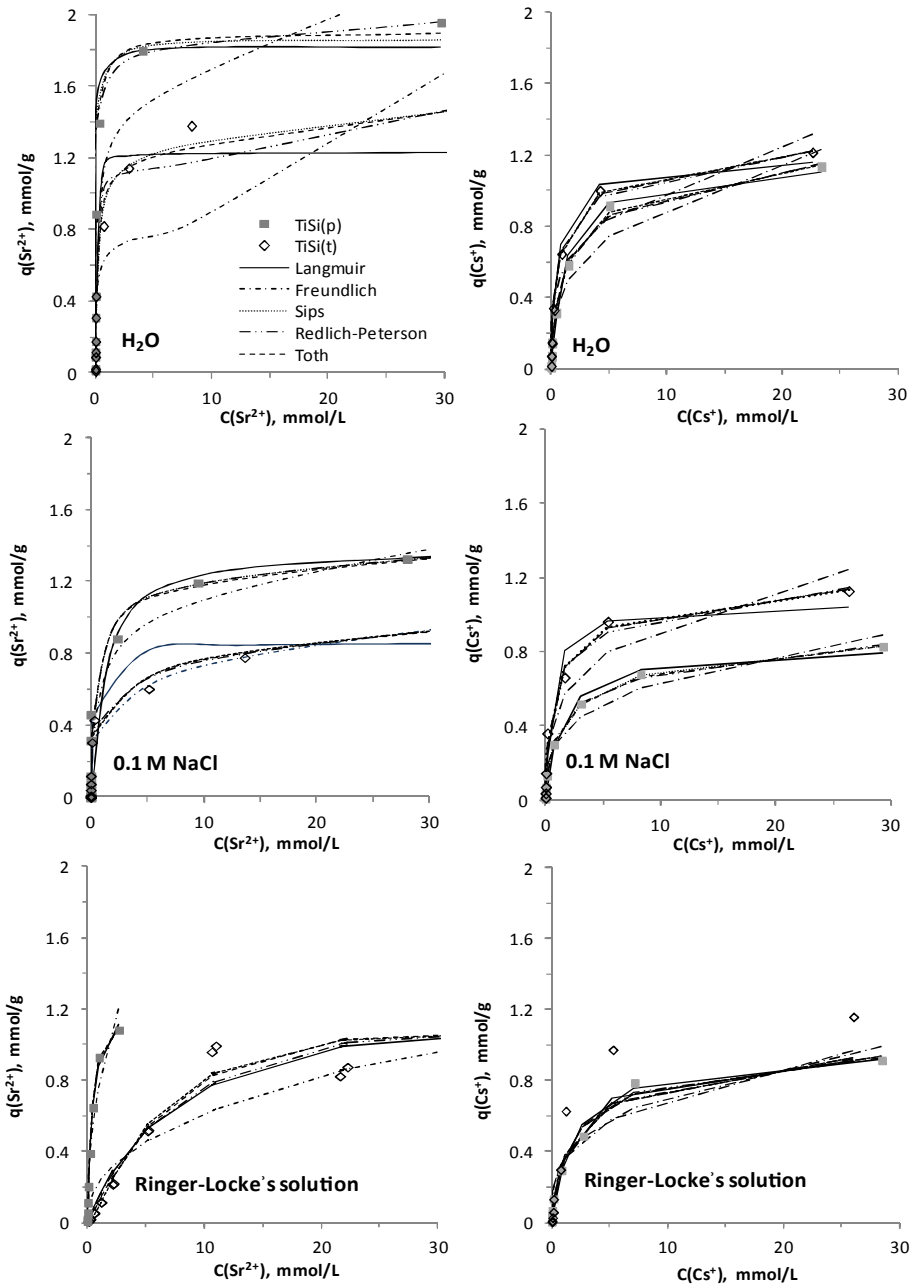

Figure 6.22: Sorption isotherms of Sr^{2+} (left column) and Cs^{+} (right column): dots: experimental results; lines: results of modelling. Experimental conditions: initial strontium concentration range 10–5000 mg/L, *V*:*m* ratio 100, contact time 24 h, ambient temperature.

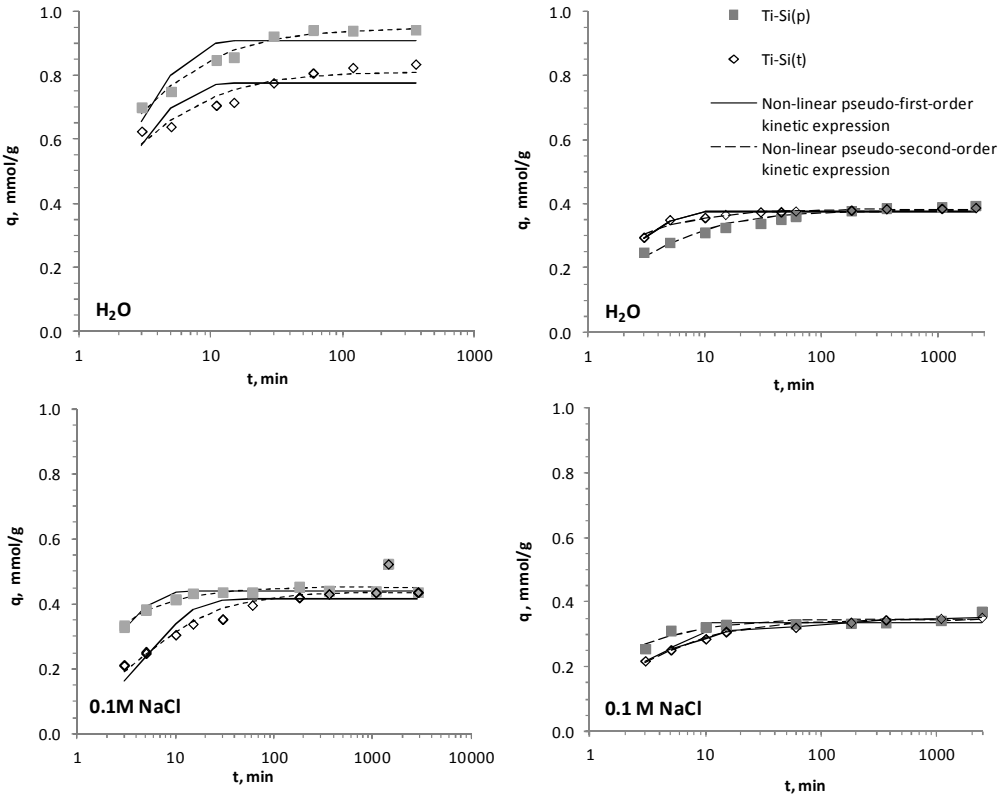

Figure 6.23: Kinetic data fitted to theoretical models of Sr^{2+} (left column) and Cs^{+} (right column): dots: experimental results; lines: results of modelling. Experimental conditions: contact time range 3–2880 min; *V:m* ratio 100; ambient temperature.

Based on the main assumption of the pseudo-second order model, the possible rate-limiting steps of the studied sorption processes are very likely the activated sorption or valence forces involving chemisorption (exchange or sharing of electrons between the sorbate and sorbent) [113, 114. 172, 247, 248]. These mechanisms can be considered as the most suitable because of the following observations: i) the sorption process kinetics follow the pseudo-second order model; ii) the pH dependence for both Sr^{2+} and Cs^{+} is not typical for ion exchange with either TiSi xerogel; iii) the sorption rate increases at elevated temperature iv) the isotherms fitted the models suggesting the interaction between sorbed substances. In order to validate this hypothesis, a material characterization was done after the sorption tests.

Table 6.7: Kinetic parameters for sorption of TiSi xerogels from water and 0.1 M NaCl media.

Model	***t*, °C**	**TiSi(p)**				**TiSi(t)**			
		q_{exp}, mg/g	q_{calc}, mg/g	***k***	***R*²**	q_{exp}, mg/g	q_{calc}, mg/g	***k***	***R*²**
				Sr^{2+}					
Non-linear pseudo-first-order	25*	0.94	0.91	0.44	0.784	0.84	0.78	0.167	0.575
	25	0.52	0.44	0.43	0.747	0.52	0.42	0.462	0.775
	40	0.95	0.96	0.27	0.862	0.86	0.85	0.218	0.932
	60	3.30	3.24	0.76	0.999	3.24	2.70	6.542	0.994
Non-linear pseudo-second-order	25*	0.94	0.95	0.03	0.975	0.84	0.81	0.007	0.885
	25	0.52	0.45	0.01	0.802	0.52	0.44	0.012	0.919
	40	0.95	1.01	0.01	0.740	0.86	0.91	0.004	0.884
	60	3.30	3.29	0.01	1.000	3.24	2.70	379.98	0.993
				Cs^{+}					
Non-linear pseudo-first-order	25*	0.39	0.38	0.51	0.999	0.39	0.38	0.51	0.968
	25	0.37	0.34	0.48	0.794	0.35	0.33	0.29	0.793
	40	0.40	0.36	0.29	0.000	0.35	0.31	0.53	0.575
	60	0.48	0.45	0.46	0.883	0.39	0.39	0.40	0.930
Non-linear pseudo-second-order	25*	0.39	0.38	0.01	0.999	0.39	0.38	0.03	1.000
	25	0.37	0.35	0.03	0.818	0.35	0.34	0.01	0.980
	40	0.40	0.39	0.02	0.962	0.35	0.32	0.03	0.786
	60	0.48	0.47	0.02	0.908	0.39	0.39	0.02	0.912

* adsorption from H_2O

6.3.2 Post-sorption test material characterization

After the sorption tests, the dry xerogel samples were subjected to SEM, XPS and XRD studies. A detailed analysis of the obtained data is provided in **Papers I–III**. In summary, the obtained SEM images show the presence of a heterophase on the sample surface only after sorption tests with Sr^{2+}, while after Cs^{+} and Ca^{2+} uptake, the sample surface appeared unchanged (Figure 6.24). Based on the combination of the collected data from SEM-EDX, mapping, XPS (Figure 6.25**)** and XRD (Figure 6.26)**,** the observed crystals are attributed to the mineral strontianite ($Sr_x(OH)_y(CO_3)_z$).

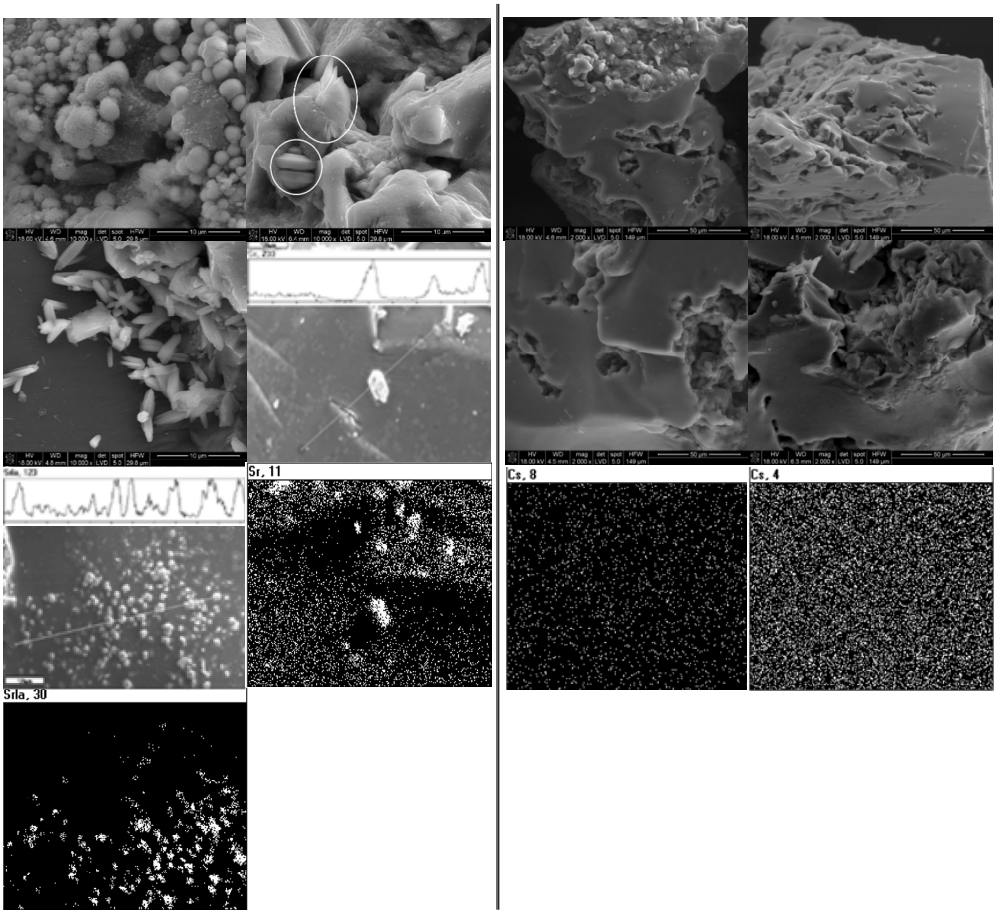

Figure 6.24: SEM images with EDX and mapping data of the TiSi surfaces: a: TiSi(p), b: TiSi(t) after Sr^{2+} sorption, c: TiSi(p), d: TiSi(t) after Cs^{+} sorption.

In order to identify the source of the heterophase, four series of sorption tests in an inert atmosphere (N_2/Ar) were performed (Table 5.1). The assumptions were as follows: i)

the heterophase was formed as a result of the epitaxial growth of $Sr_x(OH)_y(CO_3)_z$ while the samples were drying in air; ii) the phases were formed during the sorption process. It was found that the crystals of the heterophase grow on the TiSi xerogel surface with varying intensity, and in the cases of HCO_3^- or CO_3^{2-} they are available in the solution or on the surface. Based on experimental observations i–iv and the suggested theoretical models, the following mechanism of the Sr^{2+} sorption process was proposed: The ion exchange step in the presence of HCO_3^- or CO_3^{2-} in the solution or on the TiSi surface is followed by the interaction of retained Sr^{2+} with the available HCO_3^- or CO_3^{2-}. In the scheme (Figure 6.27), this rapid ion exchange process is presented as the first kinetic step, and the heterophase growing process is proposed as the second kinetic step. For Cs^+, an activated sorption mechanism is suggested.

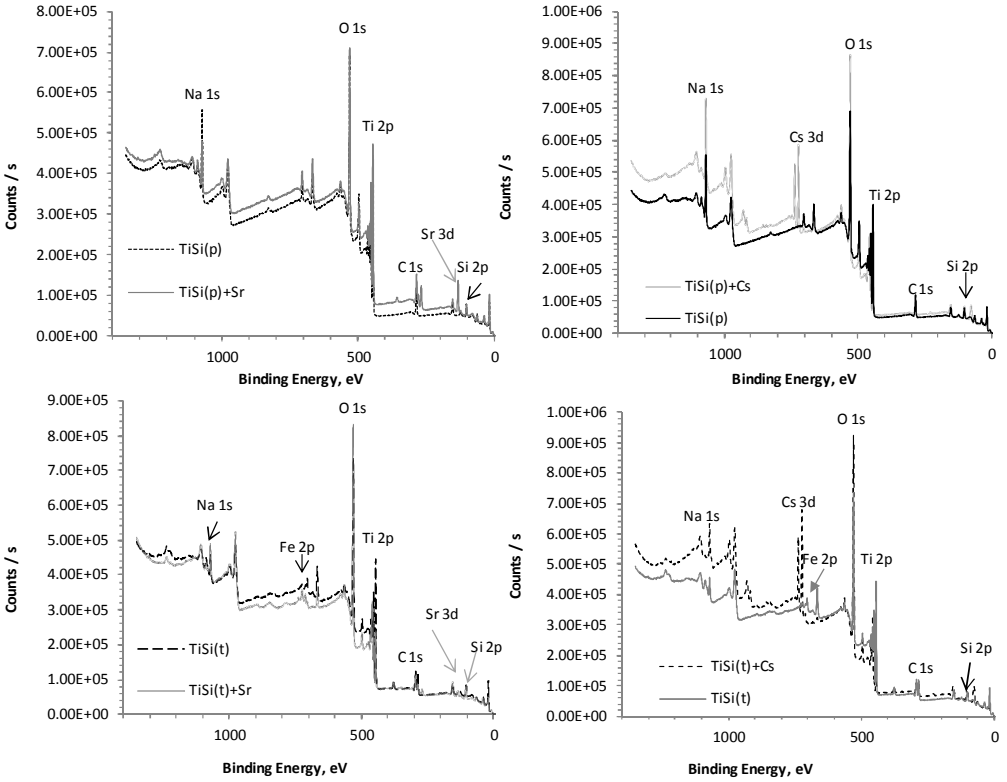

Figure 6.25: XPS spectra of TiSi before and after sorption tests with Sr^{2+} (left column) and Cs^+ (right column) containing solution.

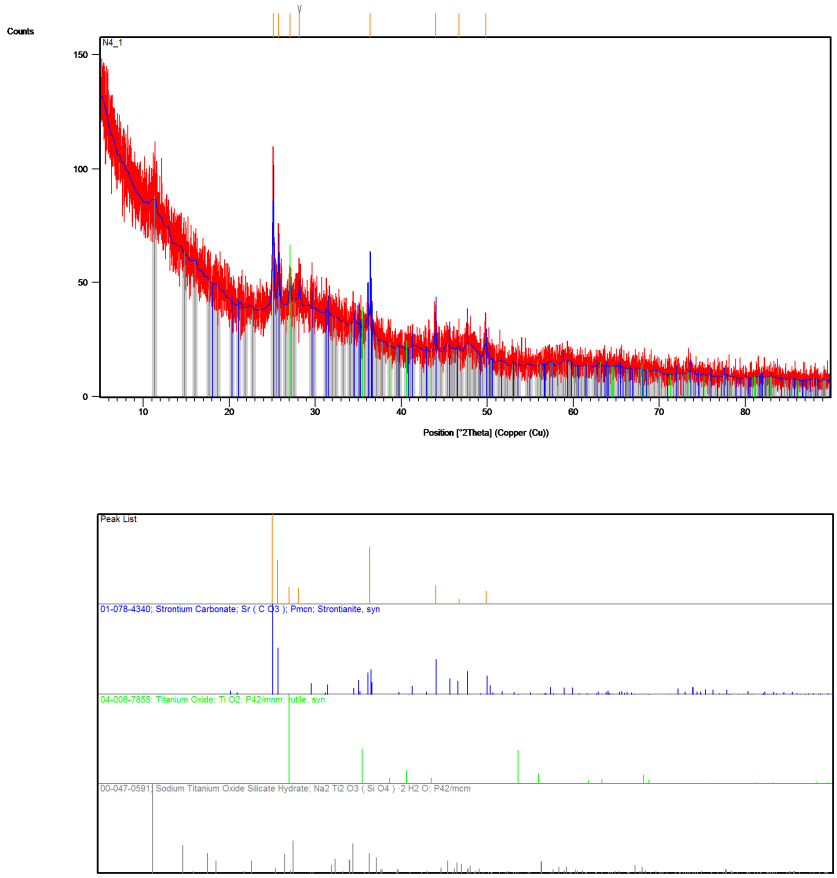

Figure 6.26: XRD pattern of TiSi(p) after Sr^{2+} adsorption.

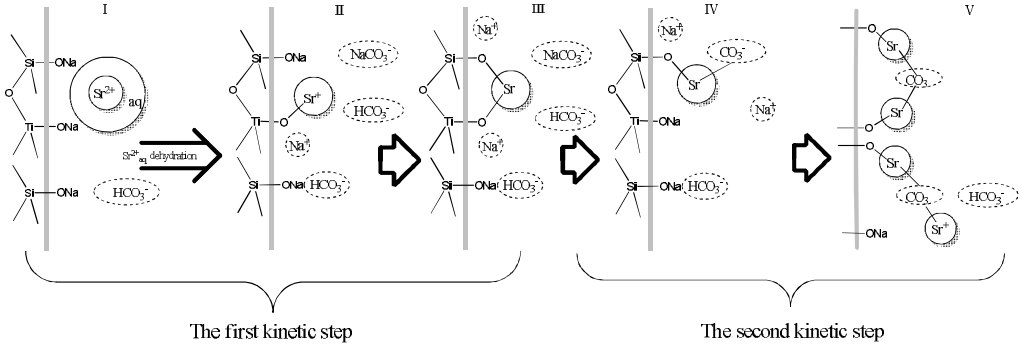

Figure 6.27: Scheme of the proposed sorption mechanism of Sr^{2+} on the TiSi xerogel.

6.4 Practical application

6.4.1 Sorption tests with real Cu-Zn mine water

Real mine water was used to compare the sorption capabilities of the synthesized TiSi xerogels and phosphated dolomite materials. The mine water was sampled at a Finnish underground Cu-Zn mine at the working levels +270 m, +500 m and +720 m and analysed with ICP-MS (Table 6.8).

Table 6.8: Metal ion content in the mine water samples. All concentrations in mg/L.

	mine water and level	Al^{3+}	Cd^{2+}	Co^{2+}	Cr^{3+}	Cu^{2+}	Fe^{3+}	Mn^{2+}	Ni^{2+}	Pb^{2+}	Zn^{2+}
1	**+720**	270	0.25	0.37	0.09	6.4	350	34	0.48	0.0030	310
2	**+500**	1300	4.80	2.50	0.40	110	1300	120	3.80	0.0004	2800
3	**+270**	1300	15	2.9	0.32	140	980	130	30	0.0004	610

Phosphated dolomite materials were efficient only with water from the +720 m level. The obtained results are presented and discussed in detail in the related publication [251]. Briefly, cation uptake efficiency was evaluated as a function of the batch factor, temperature, contact time, nature of the sorbate and sorbent. The optimal sorption conditions were found to be as follows: a sorbent dose of 25 g/L, temperature above 25 °C and contact time over 10 min. Tertiary phosphated material proved to be more efficient in mine water treatment than hydrogen phosphated dolomite.

The efficiency of TiSi xerogels for cation uptake from real mine water is shown in Figure 6.28. The removal efficiency of Fe^{3+}, Pb^{2+}, Cs^{+} and Al^{3+} was quite high, while for other metals it was not of relevance (DF < 60%). It must be noted that TiSi(p) demonstrated higher DF for Cs^{+} in all studied waters and DF(Cs^{+}) varied by around 10% according to the nature of the precursor. Interestingly, TiSi xerogels provide almost full Cs^{+} decontamination even in such a complicated background and the presence of so many competitors.

Basically, we can conclude that the tested TiSi sorbent is not efficient enough to fully purify the considered mine waters of all toxic cations. Therefore the use of cheaper phosphated dolomite materials appears more rational. At the same time, utilization of TiSi for Cs^{+} retention from mine water is proved to be efficient.

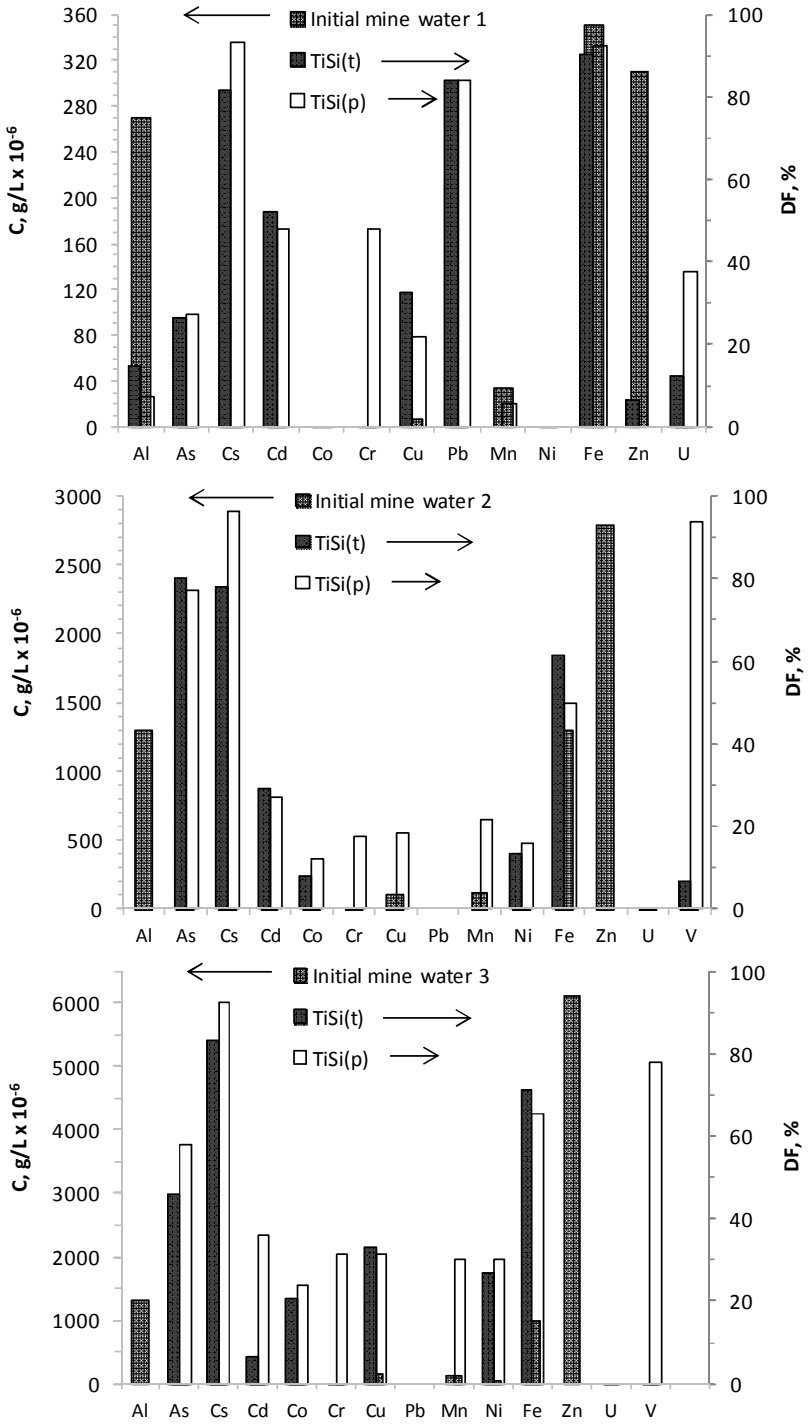

Figure 6.28: Cation sorption by TiSi materials from real mine water.

6.4.2 Radionuclide uptake by TiSi

A comparative sorption investigation was conducted and is described in detail in **Paper IV**. This study included the long-lived radionuclides $^{134}Cs^{+}$, $^{84,89,90}Sr^{2+}$, $^{238,239,240,241,242}Pu^{3+}$ and $^{243}Am^{3+}$ and sorption on titanosilicate, iron oxides and natural clay materials with 14% montmorillonite, using natural groundwater, 0.1 mol/L $NaNO_3$ solution and spent fuel pond water. Briefly, it was found that TiSi materials have a higher sorption capacity for all studied radionuclides than the other materials (Table 6.9). Thus, 90% of ^{134}Cs was retained in the first 10 min (Figure 6.29), while for ∑Pu full sorption takes around an hour. This difference in kinetic data is attributed to the steric limitation of big ions like Pu^{3+} and Am^{3+} in the pore structure of TiSi.

Laboratory batch investigations demonstrated the high sorption capacity, kinetic rate, selectivity and radioactive resistance of the obtained TiSi materials. This, consequently, encouraged to perform further tests with real radioactive aqueous solutions. Preliminary sorption column studies with real LRW in the Shelter Object of Chernobyl NPP, natural ground and river water sampled near Chernobyl confirmed the high efficiency of the TiSi xerogels in real conditions (publication of the detailed experimental data was not permitted by the relevant state authorities).

Table 6.9: The TiSi sorption capacity for long-lived radionuclides.

c_0, mol/L	$^{137}Cs^{+}$	$^{90}Sr^{2+}$	$\sum Pu^{3+}$	$^{241}Am^{3+}$
	$6.8\cdot10^{-5}$	$2.3\cdot10^{-10}$	$1.10\cdot10^{-9}$	$3.20\cdot10^{-11}$
K_d	$4.1\cdot10^{4}$	$1.6\cdot10^{5}$	$2.6\cdot10^{5}$	$1.6\cdot10^{4}$

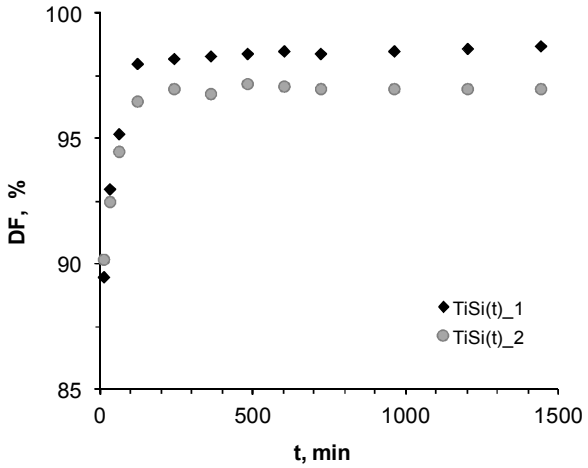

Figure 6.29: Kinetics of ^{134}Cs sorption on TiSi xerogels from 0.1 mol L^{-1} $NaNO_3$ solution. Experimental conditions: contact time range 5–1440 min; *V*:*m* ratio 1000; pH 5.6–6.2±0.1, ambient temperature.

7 Synopsis and Conclusions

In this thesis, the recently developed and for industrial applications highly promising sol-gel method was used to prepare titanosilicate xerogel particles. The applied sol-gel approach of titanosilicates yielded materials with a poorly crystalline sodium titanosilicate structure under relatively mild synthesis conditions. All effects of the synthesis parameter were studied. The temperature of HTT has the strongest influence on the structure of the materials and consequently was concluded to be the control factor for the preparation of gels with the desired properties. Under the selected synthesis conditions, TiSi xerogels with a high affinity, selectivity and sorption rate for both Sr^{2+} and Cs^{+} pollutants was prepared and proved to be effective and selective for both Sr^{2+} and Cs^{+} decontamination from synthetic and real aqueous solutions of various compositions. In addition, a higher sorption capacity was observed for the amorphous xerogel samples, as reported by Möller et al. [130] for coprecipitated TiSi analogues.

The sorption mechanisms for both target cations were found to be an activated sorption mechanism for Cs^{+} and a two step sorption mechanism for Sr^{2+}. In the latter, the first step is an ion exchange and the second step an interaction between the retained Sr^{2+} with the available HCO_3^{-} or CO_3^{2-} and heterophase formation. No influence of the precursor on the sorption mechanism for Sr^{2+} and Cs^{+} could be observed. Yet, the precursor quality might be relevant for toxicology tests on titanosilicate materials before blood plasma testing. This is an important and highly interesting aspect to consider in future studies.

The effect of precursors on the final sorption properties was tested and described. A decreasing precursor quality influenced the TiSi sorption abilities ambiguously. While xerogels with a technical precursor have a smaller micropore radius and volume, the main pore radius and the total volume increased causing an improved sorption rate, decreasing the steric restriction inside the pore space and increasing the number of possible target cations. The obtained TiSis have a slightly higher selectivity and sorption ability for Sr^{2+} than Cs^{+}. A difference of over 10% DF for Cs^{+} between the technical and pure TiSi xerogel material was observed in the presence of competitive ions, while no alterations were noticed for the Sr^{2+} retention process. The cost-benefit analysis of Cs^{+} sorption by technical or pure material may be calculated for each case specifically, based on the pure precursor price and 10–20% DF of this pollutant. Since the sorption capacity of both TiSi xerogel materials increased with rising temperature, both materials can be used without a preceding cooling stage in normal treatment procedures and in cases of emergency.

The efficiency of the obtained TiSi xerogels could be proved, but the techniques and approaches to synthesize it on a pilot and industrial scale still need to be developed. Thereafter, a further pilot scale or industrial scale sorption studies will be required.

The main conclusion is that an effective titanosilicate sorption material for Sr^{2+} and Cs^{+} decontamination from aqueous solutions can be produced in highly promising for

industrial application particle form utilizing the chosen condition of sol-gel approach. It can be used in a broad range of applications to purify drinking, ground, sea and mine waters, blood plasma and liquid radioactive wastes.

Based on the investigation conducted, it is easy to believe that utilizing described profitable sol-gel synthesis, which yielded more efficient and easy-to-use sorption materials will soon be applied in industrial scale that will result in better environmental and health protection from radioactive pollutions.

8 References

[1] M.R. de Andrade, *Henri Becquerel and Radioactivity: A Critical Revision*. *Brazilian Studies in Philosophy and History of Science*. Springer Netherlands, 290 (2011), pp. 107-117.

[2] A.G. Chmielewski and M. Haji-Saeid, *Radiation Technologies: Past, Present and Future*, Radiat. Phys. Chem. 71 (2004), pp. 17-21.

[3] C. Fry and M. Thoennessen, *Discovery of Actinium, Thorium, Protactinium, and Uranium Isotopes*, Atomic Data and Nuclear Data Tables. 99 (2013), pp. 345-364.

[4] IAEA, *Improvements of Radioactive Waste Management at WWER Nuclear Power Plants*, TECDOC-1492, (2006), pp. 1-95.

[5] G.N. Kelly, V. Golikov, L.S. Constine, H.D. Nage, l.D. Nosske and R. Shore, *Sources and Effects of Ionizing Radiation.* UNSCEAR, A68/46, New York, (2013).

[6] C. Beghin, *European and International Standards regarding Radioactive Waste Disposal*, Nucl. Eng. Des. 176 (1997), pp. 121-139.

[7] R. Pravalie, *Nuclear Weapons Tests and Environmental Consequences: A Global Perspective*, Ambio. 43 (2014), pp. 729-744.

[8] K. Katashi, N. Kazutoshi, K. Hiroyuki, K. Yasushi, H. Hirohide, M. Hisaya, E. Tetsuya, O. Takeshi, K. Shoji, K. Takeshi and S. Takuro, *Analyses and Countermeasures for Decreasing Radioactive Cesium in Buckwheat in Areas Affected by the Nuclear Accident in 2011*, Field Crops Res. 170 (2015), pp. 40-46.

[9] S.V. Fesenko, R.M. Alexakhin, M.I. Balonov, I.M. Bogdevitch, B.J. Howard, V.A. Kashparov, N.I. Sanzharova, A.V. Panov, G. Voigt and Y.M. Zhuchenka, *An Extended Critical Review of Twenty Years of Countermeasures used in Agriculture After the Chernobyl Accident*, Sci. Total Environ. 383 (2007), pp. 1-24.

[10] A. Manu, V. Santhanakrishnan, S. Rajaram and P.M. Ravi, *Concentration of Natural Radionuclides in Raw Water and Packaged Drinking Water and the Effect of Water Treatment*, J. Environ. Radioact. 138 (2014), pp. 456-459.

[11] C.V. Srinivas, P.T. Rakesh, K.B.R.R. Hari Prasad, R. Venkatesan, R. Baskaran and B. Venkatraman, *Assessment of Atmospheric Dispersion and Radiological Impact from the Fukushima Accident in a 40-km Range using a Simulation Approach*, Air Qual. Atmos. Hlth. 7 (2014), pp. 209-227.

[12] T. Wada, Y. Nemoto, S. Shimamura, T. Fujita, T. Mizuno, T. Sohtome, K. Kamiyama, T. Morita and S. Igarashi, *Effects of the Nuclear Disaster on Marine Products in Fukushima*, J. Environ. Radioact. 124 (2013), pp. 246-254.

[13] N. Evangeliou, Y. Balkanski, A. Cozic and A.P. Møller, *How "lucky" we are that the Fukushima Disaster Occurred in Early Spring: Predictions on the Contamination Levels from various Fission Products Released from the Accident and Updates on the Risk Assessment for Solid and Thyroid Cancers*, Sci. Total Environ. 500–501 (2014), pp. 155-172.

[14] M. Yamaguchi, A. Kitamura, Y. Oda and Y. Onishi, *Predicting the Long-Term 137Cs Distribution in Fukushima after the Fukushima Dai-Ichi Nuclear Power Plant Accident: A Parameter Sensitivity Analysis*, J. Environ. Radioact. 135 (2014), pp. 135-146.

[15] M. Schneider, A. Froggatt, K. Hosokawa, S. Thomas, Y. Yamaguchi and J. Hazemann, *World Nuclear Industry Status Report 2013*, Project Report. Mycle Schneider Consulting, Paris, France & London, UK. (2013), 2013-V4, pp. 1-139.

[16] E. Schneider, B. Carlsen, E. Tavrides, C. van der Hoeven and U. Phathanapirom, *A Top-Down Assessment of Energy, Water and Land use in Uranium Mining, Milling, and Refining*, Energy Econ. 40 (2013), pp. 911-926.

[17] E.V. Dubovsky and C.D. Russell, *Radionuclide Evaluation of Renal Transplants*, Semin. Nucl. Med. 18 (1988), pp. 181-198.

[18] B. Lambert, M. Cybulla, S.M. Weiner, C. Wiele, H. Ham, R.A. Dierckx and A. Otte, *Renal Toxicity After Radionuclide Therapy*, Radiat. Res. 161 (2004), pp. 607-611.

[19] J. Svensson, J. Mölne, E. Forssell-Aronsson, M. Konijnenberg and P. Bernhardt, *Nephrotoxicity Profiles and Threshold Dose Values for ^{177}Lu-DOTATATE in Nude Mice*, Nucl. Med. Biol. 39 (2012), pp. 756-762.

[20] G. Paganelli, M. Bartolomei, C. Grana, M. Ferrari, P. Rocca and M. Chinol, *Radioimmunotherapy of Brain Tumor*, Neurol. Res. 28 (2006), pp. 518-522.

[21] M. Zalutsky, *Current Status of Therapy of Solid Tumors: Brain Tumor Therapy*, J. Nucl. Med. 46 (2005), pp. 151S-156S.

[22] A.R. Joffe, H. Kolski, J. Duff and A.R. deCaen, *A 10-Month-Old Infant with Reversible Findings of Brain Death*, Pediatr. Neurol. 41 (2009), pp. 378-382.

[23] L.M. Tatham, F.J. Bove, W.E. Kaye and R.F. Spengler, *Population Exposures to I-131 Releases from Hanford Nuclear Reservation and Preterm Birth, Infant Mortality, and Fetal Deaths*, Int. J. Hyg. Environ. Health. 205 (2002), pp. 41-48.

[24] S. Ashwal, A.J.K. Smith, F. Torres, M. Loken and S.N. Chou, *Radionuclide Bolus Angiography: A Technique for Verification of Brain Death in Infants and Children*, J. Pediatr. 91 (1977), pp. 722-727.

[25] F.J. Frassica, N. Inoue, P. Virolainen and E.Y.S. Chao, *Skeletal System: Biomechanical Concepts and Relationships to Normal and Abnormal Conditions*, Semin. Nucl. Med. 27 (1997), pp. 321-327.

[26] M. Jangoux, *Diseases of Echinoderms*, Helgoländer Meeresuntersuchungen. 37 (1984), pp. 207-216.

[27] H.N. Lee, *Radionuclides: Their Biogeochemical Cycles and the Impacts on the Biosphere*, in *Encyclopedia of Ecology*, S.E. Jørgensen and B.D. Fath, eds., Academic Press, Oxford, (2008), pp. 2966-2975.

[28] A. Aarkrog, *Translocation of Radionuclides in Cereal Crops*, Blackwell Scientific Publications, United Kingdom, (1983), pp. 1-279.

[29] N. Adams, B.W. Hunt and J.A. Reissland, *Annual Limits of Intake of Radionuclides for Workers*, NRPB, Harwell, United Kingdom, (1978), NRPB-R-82, pp. 1-42.

[30] J. Garnier-Laplace, M. Gilek, S. Sundell-Bergman and C. Larsson, *Assessing Ecological Effects of Radionuclides: Data Gaps and Extrapolation Issues*, J. Radiol. Prot. 24 (2004), pp. A139-A155.

[31] R.J. Pentreath and D.J. Allington, *Dose to Man from the Consumption of Marine Seafoods: A Comparison of the Naturally-Occurring ^{210}Po with Artificially-Produced Radionuclides*, Pergamon, Australia, (1988), pp. 1582-1585.

[32] V.N. Shutov, G.Y. Bruk, M.I. Balonov, V.I. Parkhomenko and I.Y. Pavlov, *Cesium and Strontium Radionuclide Migration in the Agricultural Ecosystem and Estimation of Internal Doses to the Population*, Research Enterprises, United States, (1993), pp. 167-218.

[33] J.R. Sty and R.J. Starshak, *The Role of Radionuclide Studies in Pediatric Gastrointestinal Disorders*, Semin. Nucl. Med. 12 (1982), pp. 156-172.

[34] T.E. Kozhakhanov, S.N. Lukashenko and N.V. Larionova, *Accumulation of Artificial Radionuclides in Agricultural Plants in the Area used for Surface Nuclear Tests*, J. Environ. Radioact. 137 (2014), pp. 217-226.

[35] I.N. Onishchenko, *Multisensing in Chernobyl: The State and Monitoring of Object "Shelter"*. Multisensor Fusion. Springer Netherlands. 70 (2002), pp. 779-797.

[36] A.J. Gonzalez, *International Policies and Strategies for the Remediation of Land Contaminated by Radioactive Material Residues*, J. Environ. Radioact. 119 (2013), pp. 5-12.

[37] S. Fesenko, P. Jacob, A. Ulanovsky, A. Chupov, I. Bogdevich, N. Sanzharova, V. Kashparov, A. Panov and Y. Zhuchenka, *Justification of Remediation Strategies in the Long Term After the Chernobyl Accident*, J. Environ. Radioact. 119 (2013), pp. 39-47.

[38] P. Jacob, S. Fesenko, I. Bogdevitch, V. Kashparov, N. Sanzharova, N. Grebenshikova, N. Isamov, N. Lazarev, A. Panov, A. Ulanovsky, Y. Zhuchenko and M. Zhurba, *Rural Areas Affected by the Chernobyl Accident: Radiation Exposure and Remediation Strategies*, Sci. Total Environ. 408 (2009), pp. 14-25.

[39] M. Nakano and R.N. Yong, *Overview of Rehabilitation Schemes for Farmlands Contaminated with Radioactive Cesium Released from Fukushima Power Plant*, Eng. Geol. 155 (2013), pp. 87-93.

[40] R.C. Ausness, *High-Level Radioactive Waste Management: The Nuclear Dilemma*, Wis. L. Rev. (1979), pp. 707-767.

[41] R.O.A. Rahman, H.A. Ibrahium and Y. Hung, *Liquid Radioactive Wastes Treatment: A Review*, Water. 3 (2011), pp. 551-565.

[42] INSC (International Nuclear Societies Council), *Current Issues in Nuclear Energy. Radioactive Waste*, USA, (2002), pp. 1-90.

[43] Nuclear Energy Agency, *Features, Events and Processes (FEPs) for Geologic Disposal of Radioactive Waste*, NEA. (1986), pp. 1-90.

[44] Nuclear Energy Agency, *Low-Level Radioactive Waste Repositories*, NEA (1999), pp. 1-180.

[45] P. Landais, *Advances in Geochemical Research for the Underground Disposal of High-Level, Long-Lived Radioactive Waste in a Clay Formation*, J. Geochem. Explor. 88 (2006), pp. 32-36.

[46] E.R. Vance, *Sol-Gel Production of Titanosilicate Glass-Ceramics for Nuclear Waste Immobilization*, J. Mater. Sci. 21 (1986), pp. 1413-1416.

[47] IAEA, *Developing Multinational Radioactive Waste Repositories: Infrastructural Framework and Scenarios of Cooperation*, IAEA-TECDOC-1413, (2014), pp. 1-62.

[48] IAEA, *Multilateral Approaches to the Nuclear Fuel Cycle*, (2005), pp. 1-201.

[49] IAEA, *Technologies for Remediation of Radioactively Contaminated Sites*, TECDOC-1086, IAEA, Austria, (1999), pp. 1-101.

[50] IAEA, *Nuclear Safety Review*, GC(57)/INF/3, Austria, (2013), pp. 1-62.

[51] IAEA, *Technical, Economic and Institutional Aspects of Regional Spent Fuel Storage Facilities*, IAEA-TECDOC-1482, (2005), pp. 1-43.

[52] L. Buckley, S. Bushart, V. Efremenkov, Y. Karlin, R. Kohout, A. Pabby and G. Tapsell, *Application of Membrane Technology for Liquid Radioactive Waste Processing*, IAEA-TRS No. 431, (2004), 145p.

[53] G. Zakrzewska-Trznadel and M. Harasimowicz, *Application of Ceramic Membranes for Hazardous Wastes Processing: Pilot Plant Experiments with Radioactive Solutions*, Desalination. 162 (2004), pp. 191-199.

[54] D.T. Hobbs, *Evaluation of Alternate Materials and Methods for Strontium and Alpha Removal from Savannah River Site High-Level Waste Solutions,* WSRC, WSRC-TR-2000-00229 (2000), pp. 1-15.

[55] D.V. Marinin and G.N. Brown, *Studies of sorbent/ion-Exchange Materials for the Removal of Radioactive Strontium from Liquid Radioactive Waste and High Hardness Groundwaters*, Waste Manage. 20 (2000), pp. 545-553.

[56] U. İpek, E. Öbek, L. Akca, E.I. Arslan, H. Hasar, M. Doğru and O. Bayk, *Determination of Degradation of Radioactivity and its Kinetics in Aerobic Composting*, Bioresour. Technol. 84 (2002), pp. 283-286.

[57] D. Rana, T. Matsuura, M.A. Kassim and A.F. Ismail, *Radioactive Decontamination of Water by Membrane Processes – A Review*, Desalination. 321 (2013), pp. 77-92.

[58] R.D. Ambashta and M.E.T. Sillanpää, *Membrane Purification in Radioactive Waste Management: A Short Review*, J. Environ. Radioact. 105 (2012), pp. 76-84.

[59] L.I. Rudenko, V.E. Khan and N.I. Panasyuk, *Physicochemical Study of the Mechanism of Radionuclide Migration from the Shelter Object and its Service Area to Groundwater*, Radiochemistry. 45 (2003), pp. 293-297.

[60] L.I. Rudenko, O.V. Dzhuzha and V.E. Khan, *Semipermeable Dynamic Membranes for Ultrafiltration Treatment of Ground Waters to Remove Radionuclides*, Radiochemistry. 49 (2007), pp. 201-203.

[61] V.N. Romanovskiy, I.V. Smirnov, V.A. Babain, T.A. Todd, R.S. Herbst, J.D. Law and K.N. Brewer, *The Universal Solvent Extraction (UNEX) Process. I. Development of the UNEX Process Solvent for the Separation of Cesium, Strontium, and the Actinides from Acidic Radioactive Waste*, Solv. Extr. Ion Exch. 19 (2001), pp. 1-21.

[62] S. Dai, Y.H. Ju and C.E. Barnes, *Solvent Extraction of Strontium Nitrate by a Crown Ether using Room-Temperature Ionic Liquids*, J. Chem. Soc., Dalton Trans. (1999), pp. 1201-1202.

[63] E.P. Horwitz, M.L. Dietz, R. Chiarizia, H. Diamond, S.L. Maxwell and M.R. Nelson, *Separation and Preconcentration of Actinides by Extraction Chromatography using a Supported Liquid Anion Exchanger: Application to the Characterization of High-Level Nuclear Waste Solutions*, Anal. Chim. Acta. 310 (1995), pp. 63-78.

[64] A.E. Visser and R.D. Rogers, *Room-Temperature Ionic Liquids: New Solvents for f-Element Separations and Associated Solution Chemistry*, Solid State Sci. 171 (2003), pp. 109-113.

[65] L.I. Rudenko and V.E. Khan, *Membrane Methods for Treating Liquid Radioactive Wastes from the Shelter to Remove Transuranic Elements*, Radiochemistry. 47 (2005), pp. 89-92.

[66] L.I. Rudenko, O.A. Gumennaya, V.E. Khan and O.V. Dzhuzha, *A Mechanism of Purification of Liquid Radioactive Waste from Transuranium Elements and Uranium by the Method of Complex-Formation and Ultrafiltration*, Dop. NASU. 11 (2009), pp. 145-148.

[67] A.K. Pabby, *Membrane Techniques for Treatment in Nuclear Waste Processing: Global Experience*, Membr. Tech. 2008 (2008), pp. 9-13.

[68] G. Zakrzewska-Trznadel, M. Harasimowicz and A.G. Chmielewski, *Membrane Processes in Nuclear Technology-Application for Liquid Radioactive Waste Treatment*, Sep. Purif. Technol. 22–23 (2001), pp. 617-625.

[69] C. Fritzmann, J. Löwenberg, T. Wintgens and T. Melin, *State-of-the-Art of Reverse Osmosis Desalination*, Desalination. 216 (2007), pp. 1-76.

[70] R.J. Petersen, *Composite Reverse Osmosis and Nanofiltration Membranes*, J. Membr. Sci. 83 (1993), pp. 81-150.

[71] P. Rajec, J. Orechovská, J. Šúcha and I. Novák, *Sorption of Radionuclides on Inorganic Sorbents*, J. Radioanal. Nucl. Chem. 208 (1996), pp. 477-486.

[72] B.T. Kim, H.K. Lee, H. Moon and K.J. Lee, *Adsorption of Radionuclides from Aqueous Solutions by Inorganic Adsorbents*, Sep. Sci. Technol. 30 (1995), pp. 3165-3182.

[73] A. Dąbrowski, *Adsorption – from Theory to Practice*, Adv. Colloid Interface Sci. 93 (2001), pp. 135-224.

[74] A. Clearfield, *Inorganic Ion-Exchangers, Past, Present and Future*, Solv. Extr. Ion Exch. 18 (2000), pp. 655-678.

[75] A.E. Osmanlioglu, *Treatment of Radioactive Liquid Waste by Sorption on Natural Zeolite in Turkey*, J. Hazard. Mater. 137 (2006), pp. 332-335.

[76] M.A. Lilga, R.J. Orth, J.P.H. Sukamto, S.M. Haight and D.T. Schwartz, *Metal Ion Separations using Electrically Switched Ion Exchange*, Sep. Purif. Technol. 11 (1997), pp. 147-158.

[77] IAEA, *Combined Methods for Liquid Radioactive Waste Treatment*, IAEA-TECDOC-1336, (2003), pp. 851-859.

[78] V.V. Milyutin, S.V. Mikheev, V.M. Gelis and E.A. Kozlitin, *Sorption of Cesium on Ferrocyanide Sorbents from Highly Saline Solutions*, Radiochemistry. 51 (2009), pp. 298-300.

[79] L. Oji, K. Martin and D. Hobbs, *Development of Prototype Titanate Ion-Exchange Loaded-Membranes for Strontium, Cesium and Actinide Decontamination from Aqueous Media*, J. Radioanal. Nucl. Chem. 279 (2009), pp. 847-854.

[80] A. Clearfield, A. Tripathi, D. Medvedev, A.J. Celestian and J.B. Parise, *In Situ Type Study of Hydrothermally Prepared Titanates and Silicotitanates*, J. Mater. Sci. 41 (2006), pp. 1325-1333.

[81] I.M. El-Naggar, E.A. Mowafy, I.M. Ali and H.F. Aly, *Synthesis and Sorption Behaviour of some Radioactive Nuclides on Sodium Titanate as Cation Exchanger*, Adsorption. 8 (2002), pp. 225-234.

[82] E.A. Behrens, P. Sylvester, G. Graziano and A. Clearfield, *Evaluation of a Sodium Nonatitanate, Sodium Titanosilicate, and Pharmacosiderite-Type Ion Exchangers for Strontium Removal from DOE Waste and Hanford N-Springs Groundwater Simulants*, in *Science and Technology for Disposal of Radioactive Tank Wastes*, Springer, (1998), pp. 287-299.

[83] F. Han, G. Zhang and P. Gu, *Adsorption Kinetics and Equilibrium Modeling of Cesium on Copper Ferrocyanide*, J. Radioanal. Nucl. Chem. 295 (2013), pp. 369-377.

[84] T.D. Clarke and C.M. Wai, *Selective Removal of Cesium from Acid Solutions with Immobilized Copper Ferrocyanides*, J. Anal. Chem. 70 (1998), pp. 3708-3711.

[85] P. Sylvester, E.A. Behrens, G.M. Granziano and A. Clearfield, *An Assessment of Inorganic Ion-Exchange Materials for the Removal of Strontium from Simulated Hanford Tank Wastes*, Sep. Sci. Technol. 34 (1999), pp. 1981-1992.

[86] A.I. Bortun, L.N. Bortun and A. Clearfield, *Evaluation of Synthetic Inorganic Ion Exchangers for Cesium and Strontium Removal from Contaminated Groundwater and Wastewater*, Solv. Extr. Ion. Exch. 5 (1997), pp. 909-929.

[87] C.E. Harland, *Ion Exchange: Theory and Practice* Vol. 6, RSC, UK, (1994).

[88] N. Krishnamurthy, P. Vallinayagam and D. Madhavan, *Engineering Chemistry*, PHI Learning Pvt. Ltd., Delhi, (2014).

[89] M.-C. Desjonquères and D. Spanjaard, *Concepts in Surface Physics* Vol. 30, Springer, Berlin, (2012).

[90] W.J. Weber, P.M. McGinley and L.E. Katz, *Sorption Phenomena in Subsurface Systems: Concepts, Models and Effects on Contaminant Fate and Transport*, Water Res. 25 (1991), pp. 499-528.

[91] G. Sposito, *The Surface Chemistry of Natural Particles*, Oxford University Press, New York, (2004).

[92] A.W. Adamson, *Physical Chemistry of Surfaces*, Wiley-Blackwell, New York, (1990).

[93] G.H. Bolt, M.F. De Boodt, M.H.B. Hayes, M.B. McBride and E.B.A. De Strooper, *Interactions at the Soil Colloid: Soil Solution Interface* Vol. 190, Springer, Berlin, (2013).

[94] D.L. Sparks, *Environmental Soil Chemistry*, Academic press, 2003.

[95] J.E. Huheey, E.A. Keiter and R.L. Keiter, *Inorganic Chemistry: Principles of Structure and Reactivity*, Prentice Hall, (1983).

[96] Colloidal Dynamics Pty Ltd., *Electroacoustics Tutorials, Zeta Potential, Colloidal Dynamics Leaders in Colloid Measurement*, Technology Park, Australia, (1999).

[97] S. Barany and V. Strelko, *Laws and Mechanism of Adsorption of Cations by Different Ion-Exchange Forms of Silica Gel*, Adsorption. 19 (2013), pp. 769-776.

[98] H.M.F. Freundlich, *Über die Adsorption in Lösungen [Over the Adsorption in Solutions]*, Z. Phys. Chem. 57 (1906), pp. 358-470.

[99] C.H. Giles, T.H. MacEwan, S.N. Nakhwa and D. Smith, *786. Studies in Adsorption. Part XI. A System of Classification of Solution Adsorption Isotherms, and its use in Diagnosis of Adsorption Mechanisms and in Measurement of Specific Surface Areas of Solids*, J. Chem. Soc. (1960), pp. 3973-3993.

[100] C.H. Giles, A.P. D'Silva and I.A. Easton, *A General Treatment and Classification of the Solute Adsorption Isotherm Part. II. Experimental Interpretation*, J. Colloid Interface Sci. 47 (1974), pp. 766-778.

[101] C.H. Giles, D. Smith and A. Huitson, *A General Treatment and Classification of the Solute Adsorption Isotherm. I. Theoretical*, J. Colloid Interface Sci. 47 (1974), pp. 755-765.

[102] C.H. Giles and R.B. Mackay, *Adsorption of Cationic (Basic) Dyes by Fixed Yeast Cells*, J. Bacteriol. 89 (1965), pp. 390-397.

[103] G. Limousin, J. Gaudet, L. Charlet, S. Szenknect, V. Barthes and M. Krimissa, *Sorption Isotherms: A Review on Physical Bases, Modeling and Measurement*, Appl. Geochem. 22 (2007), pp. 249-275.

[104] S. Goldberg, *Equations and Models Describing Adsorption Processes in Soils*, in M.A. Tabatabai, D.L. Sparks, L. Al-Amoodi and W.A. Dick, eds., Soil Sci. Soc. Am. J, 2005, pp. 489-517.

[105] I. Langmuir, *The Constitution and Fundamental Properties of Solids and Liquids*, J. Am. Chem. Soc. 38 (1916), pp. 2221-2295.

[106] R. Sips, *On the Structure of a Catalyst Surface*, J. Chem. Phys. 16 (1948), pp. 490-495.

[107] O.J.D.L. Redlich and D.L. Peterson, *A Useful Adsorption Isotherm*, J. Phys. Chem. 63 (1959), pp. 1024-1024.

[108] J. Tóth, *Calculation of the BET-Compatible Surface Area from any Type I Isotherms Measured Above the Critical Temperature*, J. Colloid Interface Sci. 225 (2000), pp. 378-383.

[109] M. Temkin, *Adsorption Equilibrium and the Kinetics of Processes on Nonhomogeneous Surfaces and in the Interaction between Adsorbed Molecules*, Zh. Fiz. Chim. 15 (1941), pp. 296-332.

[110] A. Dada, A. Olalekan, A. Olatunya and O. Dada, *Langmuir, Freundlich, Temkin and Dubinin-Radushkevich Isotherms Studies of Equilibrium Sorption of Zn^{2+} Unto Phosphoric Acid Modified Rice Husk*, J. App. Chem. 3 (2012), pp. 38-45.

[111] M.M. Dubinin and L.V. Radushkevich, *The Equation of the Characteristic Curve of the Activated Charcoal*, Compt. Rend. Acad. Sci. 55 (1947), pp. 327.

[112] M.M. Dubinin, *Fundamentals of the Theory of Adsorption in Micropores of Carbon Adsorbents: Characteristics of their Adsorption Properties and Microporous Structures*, IUPAC. 61 (1989), pp. 1841-1843.

[113] Y.S. Ho and G. McKay, *Pseudo-Second Order Model for Sorption Processes*, Process Biochem. 34 (1999), pp. 451-465.

[114] Y.S. Ho, J.F. Porter and G. McKay, *Equilibrium Isotherm Studies for the Sorption of Divalent Metal Ions Onto Peat: Copper, Nickel and Lead Single Component Systems*, Water Air Soil Poll. 141 (2002), pp. 1-33.

[115] G. Blanchard, M. Maunaye and G. Martin, *Removal of Heavy Metals from Waters by Means of Natural Zeolites*, Water Res. 18 (1984), pp. 1501-1507.

[116] W. Plazinski, W. Rudzinski and A. Plazinska, *Theoretical Models of Sorption Kinetics Including a Surface Reaction Mechanism: A Review*, Adv. Colloid Interface Sci. 152 (2009), pp. 2-13.

[117] I.S. McLintock, *Comments on the Elovich Equation*, J. Catal. 16 (1970), pp. 126-128.

[118] W.J. Weber and J.C. Morris, *Kinetics of Adsorption on Carbon from Solution*, J. Sanit. Eng.Div. Am. Soc. Civ. Eng. 89 (1963), pp. 31-60.

[119] S. Brunauer, P.H. Emmett and E. Teller, *Adsorption of Gases in Multimolecular Layers*, J. Am. Chem. Soc. 60 (1938), pp. 309-319.

[120] K.S.W. Sing, *Adsorption Methods for the Characterization of Porous Materials*, Adv. Colloid Interface Sci. 76 (1998), pp. 3-11.

[121] K.S.W. Sing, *Reporting Physisorption Data for gas/solid Systems with Special Reference to the Determination of Surface Area and Porosity*, Pure Appl. Chem. 11 (1982), pp. 2201-2218.

[122] F. Rodríguez-Reinoso, J. Rouquerol, K.K. Unger and K.S.W. Sing, *Characterization of Porous Solids III*, Elsevier, Netherlands, (1994).

[123] P. Hohenberg and W. Kohn, *Inhomogeneous Electron Gas*, Phys. rev. 136 (1964), pp. B864-B871.

[124] W. Kohn and L.J. Sham, *Self-Consistent Equations Including Exchange and Correlation Effects*, Phys. Rev. 140 (1965), pp. A1133-A1138.

[125] W. Koch, M.C. Holthausen and M.C. Holthausen, *A Chemist's Guide to Density Functional Theory* Vol. 2, Wiley-VCH, Weinheim, (2001).

[126] P. Tarazona, U.M.B. Marconi and R. Evans, *Phase Equilibria of Fluid Interfaces and Confined Fluids: Non-Local Versus Local Density Functionals*, Mol. Phys. 60 (1987), pp. 573-595.

[127] I. Shainberg, N.I. Alperovitch and R. Keren, *Charge Density and Na-K-Ca Exchange of Smectites*, Clay. Clay Miner. 35 (1987), pp. 68-73.

[128] V.P. Evangelou and F.J. Coale, *Dependence of the Gapon Coefficient on Exchangeable Sodium for Mineralogically Different Soils*, Soil Sci. Soc. Am. J. 51 (1987), pp. 69-72.

[129] A.D. McNaught and A.D. McNaught, *Compendium of Chemical Terminology* Vol. 1669, Blackwell, Oxford, (1997).

[130] T. Möller, R. Harjula and J. Lehto, *Ion Exchange of ^{85}Sr, ^{134}Cs and ^{57}Co in Sodium Titanosilicate and the Effect of Crystallinity on Selectivity*, Sep. Purif. Technol. 28 (2002), pp. 13-23.

[131] J. Lehto and R. Harjula, *Selective Separation of Radionuclides from Nuclear Waste Solutions with Inorganic Ion Exchangers*, Radiochim. Acta. 86 (1999), pp. 65-70.

[132] K. Popa and C.C. Pavel, *Radioactive Wastewaters Purification using Titanosilicates Materials: State of the Art and Perspectives*, Desalination. 293 (2012), pp. 78-86.

[133] J. Rocha and M.W. Anderson, *Microporous Titanosilicates and Other Novel Mixed Octahedral – Tetrahedral Framework Oxides*, Eur. J. Inorg. Chem. (2000), pp. 801-818.

[134] C.B. Lopes, J. Coimbra, M. Otero, E. Pereira, A.C. Duarte, Z. Lin and J. Rocha, *Uptake of Hg^{2+} from Aqueous Solutions by Microporous Titano-and Zircono-Silicates*, Quimica Nova. 31 (2008), pp. 321-325.

[135] C.C. Pavel, K. Popa, N. Bilba, A. Cecal, D. Cozma and A. Pui, *The Sorption of some Radiocations on Microporous Titanosilicate ETS-10*, J. Radioanal. Nucl. Chem. 258 (2003), pp. 243-248.

[136] M.W. Anderson, O. Terasaki, T. Ohsuna, A. Philippou, S.P. MacKay, A. Ferreira, J. Rocha and S. Lidin, *Structure of the Microporous Titanosilicate ETS-10*, Nature. 367 (1994), pp. 347-351.

[137] S. Nair, H.K. Jeong, A. Chandrasekaran, C.M. Braunbarth, M. Tsapatsis and S.M. Kuznicki, *Synthesis and Structure Determination of ETS-4 Single Crystals*, Chem. Mater. 13 (2001), pp. 4247-4254.

[138] D.M. Poojary, R.A. Cahill and A. Clearfield, *Synthesis, Crystal Structures, and Ion-Exchange Properties of a Novel Porous Titanosilicate*, Chem. Mater. 6 (1994), pp. 2364-2368.

[139] E.A. Behrens, D.M. Poojary and A. Clearfield, *Syntheses, Crystal Structures, and Ion-Exchange Properties of Porous Titanosilicates, $HM_3Ti4O_4(SiO_4)_3 \cdot 4H_2O$ ($M = H^+$, K^+, Cs^+), Structural Analogues of the Mineral Pharmacosiderite*, Chem. Mater. 8 (1996), pp. 1236-1244.

[140] E.A. Behrens and A. Clearfield, *Titanium Silicates, $M_3HTi_4O_4(SiO_4)_3 \cdot 4H_2O$($M = Na^+$, K^+) with Three-Dimensional Tunnel Structures for the Selective Removal of*

Strontium and Cesium from Wastewater Solutions, Microporous Mater. 11 (1997), pp. 65-75.

[141] A. Clearfield, *Structure and Ion Exchange Properties of Tunnel Type Titanium Silicates*, Solid State Sci. 3 (2001), pp. 103-112.

[142] V. Kostov-Kytin, B. Mihailova, Y. Kalvachev and M. Tarassov, *Atomic Arrangements in Amorphous Sodium Titanosilicate Precursor Powders*, Micropor. Mesopor. Mat. 86 (2005), pp. 223-230.

[143] D.M. Chapman and A.L. Roe, *Synthesis, Characterization and Crystal Chemistry of Microporous Titanium-Silicate Materials*, Zeolites. 10 (1990), pp. 730-737.

[144] E.A. Behrens, P. Sylvester and A. Clearfield, *Assessment of a Sodium Nonatitanate and Pharmacosiderite-Type Ion Exchangers for Strontium and Cesium Removal from DOE Waste Simulants*, Environ. Sci. Technol. 32 (1998), pp. 101-107.

[145] W.T.A. Harrison, T.E. Gier and G.D. Stucky, *Single-Crystal Structure of Cs $HTi_4O_4(SiO_4)_3 \cdot 4H_2O$, a Titanosilicate Pharmacosiderite Analog*, Zeolites. 15 (1995), pp. 408-412.

[146] Z. Lin, J. Rocha, P. Brandão, F. Ferreira, A.P. Esculcas, J. Pedrosa de Jesus, A. Philippou and M.W. Anderson, *Synthesis and Structural Characterization of Microporous Umbite, Penkvilksite, and Other Titanosilicates*, J. Phys. Chem. B. 101 (1997), pp. 7114-7120.

[147] M.A. Roberts, G. Sankar, J.M. Thomas, R.H. Jones, H. Du, J. Chen, W. Pang and R. Xu, *Synthesis and Structure of a Layered Titanosilicate Catalyst with Five-Coordinate Titanium*, Nature. 381 (1996), pp. 401-404.

[148] G. Sankar, J.M. Thomas, C.R.A. Catlow, C.M. Barker, D. Gleeson and N. Kaltsoyannis, *The Three-Dimensional Structure of the Titanium-Centered Active Site during Steady-State Catalytic Epoxidation of Alkenes*, J. Phys. Chem. B. 105 (2001), pp. 9028-9030.

[149] V. Valtchev, J.-. Paillaud, S. Mintova and H. Kessler, *Investigation of the Ion-Exchanged Forms of the Microporous Titanosilicate $K_2TiSi_3O_9 \cdot H_2O$*, Micropor. Mesopor. Mat. 32 (1999), pp. 287-296.

[150] V. Kostov-Kytin and S. Ferdov, *Investigations in the System Na_2O-K_2O-TiO_2-$SiO_2 \times H_2O$*, Comptes Rendus de l'Academie Bulgare des Sciences. 54 (2001), pp. 51-54.

[151] V. Kostov-Kytin, S. Ferdov, Y. Kalvachev, B. Mihailova and O. Petrov, *Hydrothermal Synthesis of Microporous Titanosilicates*, Micropor. Mesopor. Mat. 105 (2007), pp. 232-238.

[152] X. Zou and M.S. Dadachov, *$K_2TiSi_3O_9 \cdot H_2O$*, Acta Crystallogr. C: Cryst. Struct. Commun. 56 (2000), pp. 738-739.

[153] S.P. Cardoso, P.F. Lito, J. Rocha, Z. Lin and C.M. Silva, *Synthesis and Permeation Properties of Small-Pore Titanosilicate AM-3 Membranes*, Procedia Engineering. 44 (2012), pp. 926-927.

[154] M.S. Dadachov, J. Rocha, A. Ferreira, Z. Lin and M.W. Anderson, *Ab Initio Structure Determination of Layered Sodium Titanium Silicate Containing Edge-Sharing Titanate Chains (AM-4) $Na_3(Na,H)Ti_2O_2[Si_2O_6]_2 \times 2H_2O$*, Chem. Comm. (1997), pp. 2371-2372.

[155] N. Döbelin and T. Armbruster, *Microporous Titanosilicate AM-2: Ion-Exchange and Thermal Stability*, Micropor. Mesopor. Mat. 99 (2007), pp. 279-287.

[156] N. Döbelin and T. Armbruster, *Microporous Titanosilicate AM-2: Rb-Exchange and Thermal Behaviour*, Mater. Res. Bull. 42 (2007), pp. 113-125.

[157] A.I. Bortun, L.N. Bortun, D.M. Poojary, O. Xiang and A. Clearfield, *Synthesis, Characterization, and Ion Exchange Behavior of a Framework Potassium Titanium Trisilicate $K_2TiSi_3O_9 \times H_2O$ and its Protonated Phases*, Chem. Mater. 12 (2000), pp. 294-305.

[158] M. Cadoni and G. Ferraris, *Penkvilksite-2O: $Na_2TiSi_4O_{11} \cdot 2H_2O$*, Acta Crystallogr. C, Cryst. Struct. Commun. 64 (2008), pp. 87-90.

[159] Y. Koudsi and A. Dyer, *Sorption of ^{60}Co on a Synthetic Titanosilicate Analogue of the Mineral Penkvilksite-2O and Antimonysilicate*, J. Radioanal. Nucl. Chem. 247 (2001), pp. 209-219.

[160] S. Merlino, M. Pasero, G. Artioli and A.P. Khomyakov, *Penkvilksite, a New Kind of Silicate Structure: OD Character, X-Ray Single-Crystal (lM), and Powder Rietveld (2O) Refinements of Two MDO Polytypes*, Am. Mineral. 79 (1994), pp. 1185-1193.

[161] B. Yilmaz, P.Q. Miraglia, J. Warzywoda and A. Sacco Jr., *Synthesis of Titanosilicate ETS-4 with Controlled Morphology and Investigation of its Crystallization Kinetics*, Micropor. Mesopor. Mat. 71 (2004), pp. 167-175.

[162] R.P. Nikolova, B.L. Shivachev and S. Ferdov, *Crystal Structures of Mg^{2+}, Ba^{2+} and Cs^{+} Exchanged K–Na–ETS-4*, Micropor. Mesopor. Mat. 165 (2013), pp. 121-126.

[163] L. Liu, W. Tan, P. Xiao and Y. Zhai, *A Novel Synthesis Process of ETS-4 Titanosilicate using Commercial Anatase in the Absence of Fluoride Ions*, Int. J. Miner. Metall. Mater. 19 (2012), pp. 675-678.

[164] M. Sacerdoti and G. Cruciani, *Comparison of Structural Changes upon Heating of Zorite and Na-ETS-4 by in Situ Synchrotron Powder Diffraction Minerals as Advanced Materials II.* Springer, Berlin, (2012), pp. 187-197.

[165] C.B. Lopes, M. Otero, Z. Lin, C.M.l. Silva, E. Pereira, J. Rocha and A.C. Duarte, *Effect of pH and Temperature on Hg^{2+} Water Decontamination using ETS-4 Titanosilicate*, J. Hazard. Mater. 175 (2010), pp. 439-444.

[166] D. Coutinho, J.A. Losilla, J. Balkus and J. Kenneth, *Microwave Synthesis of ETS-4 and ETS-4 Thin Films*, Micropor. Mesopor. Mat. 90 (2006), pp. 229-236.

[167] K. Popa, C.C. Pavel, N. Bilba and A. Cecal, *Purification of Waste Waters Containing $^{60}Co^{2+}$, $^{115m}Cd^{2+}$ and $^{203}Hg^{2+}$ Radioactive Ions by ETS-4 Titanosilicate*, J. Radioanal. Nucl. Chem. 269 (2006), pp. 155-160.

[168] C.B. Lopes, E. Pereira, Z. Lin, P. Pato, M. Otero, C.M. Silva, J. Rocha and A.C. Duarte, *Fixed-Bed Removal of Hg^{2+} from Contaminated Water by Microporous Titanosilicate ETS-4: Experimental and Theoretical Breakthrough Curves*, Micropor. Mesopor. Mat. 145 (2011), pp. 32-40.

[169] C.C. Pavel, D. Vuono, L. Catanzaro, P. De Luca, N. Bilba, A. Nastro and J.B. Nagy, *Synthesis and Characterization of the Microporous Titanosilicates ETS-4 and ETS-10*, Micropor. Mesopor. Mat. 56 (2002), pp. 227-239.

[170] C.C. Pavel, L.V. Pavel, I. Cretescu and K. Popa, *Some Aspects Concerning the Interaction between Uranium and ETS-10 Titanosilicate*, Rev. Chim. (Bucharest). 60 (2009), pp. 19-22.

[171] C.C. Pavel, H. Park, A. Dreier, B. Tesche and S. Schmidt, *Structural Defects Induced in ETS-10 by Postsynthesis Treatment with H_2O_2 Solution*, Chem. Mater. 18 (2006), pp. 3813-3820.

[172] I.M. Ali, E.S. Zakaria and H.F. Aly, *Highly Effective Removal of ^{22}Na, ^{134}Cs and ^{60}Co from Aqueous Solutions by Titanosilicate: A Radiotracer Study*, J. Radioanal. Nucl. Chem. 285 (2010), pp. 483-489.

[173] A.J. Celestian and A. Clearfield, *The Origin of Ion Exchange Selectivity in a Porous Framework Titanium Silicate*, J. Mater. Chem. 17 (2007), pp. 4839-4842.

[174] L. Al-Attar, A. Dyer, A. Paajanen and R. Harjula, *Purification of Nuclear Wastes by Novel Inorganic Ion Exchangers*, J. Mater. Chem. 13 (2003), pp. 2969-2974.

[175] A. Clearfield, D.G. Medvedev, S. Kerlegon, T. Bosser, J.D. Burns and J. Milton, *Rates of Exchange of Cs^{+} and Sr^{2+} for Poorly Crystalline Sodium Titanium Silicate (CST) in Nuclear Waste Systems*, Solv. Extr. Ion Exch. 30 (2012), pp. 229-243.

[176] A.J. Celestian, J.B. Parise and A. Clearfield, *Crystal Growth and Ion Exchange in Titanium Silicates*, in *Springer Handbook of Crystal Growth*, Springer, (2010), pp. 1637-1662.

[177] A. Clearfield, L.N. Bortun and A.I. Bortun, *Alkali Metal Ion Exchange by the Framework Titanium Silicate $M_2Ti_2O_3SiO_4 \cdot nH_2O$ (M=H, Na)*, React. Funct. Polym. 43 (2000), pp. 85-95.

[178] V.V. Strelko, S.V. Meleshevych, V.A. Kanibolotsky and O.V. Oleksiienko, *A Method for Producing Titanosilicate Ionexchanger*, UA patent. 66489 (2012).

[179] V.G. Kalenchuk, S.V. Meleshevych, V.A. Kanibolotsky, V.V. Strelko, O.V. Oleksiienko and N.M. Patryliak, *A Method for Producing Titanosilicate Ionexchanger*, UA patent. 48457 (2010).

[180] A. Dyer, M. Pillinger and S. Amin, *Ion Exchange of Caesium and Strontium on a Titanosilicate Analogue of the Mineral Pharmacosiderite*, J. Mater. Chem. 9 (1999), pp. 2481-2487.

[181] M.S. Dadachov and W.T.A. Harrison, *Synthesis and Crystal Structure of $Na_4[(TiO)_4(SiO_4)_3] \cdot 6H_2O$, a Rhombohedrally Distorted Sodium Titanium Silicate Pharmacosiderite Analogue*, J. Solid State Chem. 134 (1997), pp. 409-415.

[182] V. Valtchev and S. Mintova, *Synthesis of Titanium Silicate ETS-10: The Effect of Tetrametylammonium on the Crystallization Kinetics*, Zeolites. 14 (1994), pp. 697-700.

[183] C.C. Pavel, M. Walter and K. Popa, *Improvement of Retention Capacity of ETS-10 for Uranyl Ions by Porosity Modification and their Immobilization into a Titanosilicate Matrix*, J. Mater. Chem. 18 (2008), pp. 3342-3346.

[184] J.A. Losilla and K.J. Balkus Jr., *Microwave Assisted Synthesis of ETS-10*, J. Porous Mat. 16 (2009), pp. 487-496.

[185] H.J. Sung, J. Taihuan, K.H. Young and C. Jong-San, *Microwave Effect in the Fast Synthesis of Microporous Materials: Which Stage between Nucleation and Crystal Growth is Accelerated by Microwave Irradiation?*, Chem. Eur. J. 13 (2007), pp. 4410-4417.

[186] S.M. Kuznicki, *Large-Pored Crystalline Titanium Molecular Sieve Zeolites*, US Patent. US 07/094,237 (1989).

[187] T.K. Das, A.J. Chandwadkar and S. Sivasanker, *A Rapid Method of Synthesizing the Titanium Silicate ETS-10*, Chem. Commun. (1996), pp. 1105-1106.

[188] Z. Ji, J. Warzywoda and A. Sacco, *Synthesis and Morphological Control of Large Titanosilicate ETS-10 Crystals*, Micropor. Mesopor. Mat. 109 (2008), pp. 1-11.

[189] Z. Ji, B. Yilmaz, J. Warzywoda and A. Sacco, *Hydrothermal Synthesis of Titanosilicate ETS-10 using $Ti(SO_4)_2$*, Micropor. Mesopor. Mat. 81 (2005), pp. 1-10.

[190] J.K. Thomas, *Synthesis of Microporous Titanosilicates ETS-10 and ETS-4 using Solid TiO_2 as the Source of Titanium*, Chem. Commun. (1996), pp. 1435-1436.

[191] D.G. Medvedev, A. Tripathi, A. Clearfield, A.J. Celestian, J.B. Parise and J. Hanson, *Crystallization of Sodium Titanium Silicate with Sitinakite Topology: Evolution from the Sodium Nonatitanate Phase*, Chem. Mater. 16 (2004), pp. 3659-3666.

[192] R. Freeman, *Measuring the Flow Properties of Consolidated, Conditioned and Aerated Powders – A Comparative Study using a Powder Rheometer and a Rotational Shear Cell*, Powder Technol. 174 (2007), pp. 25-33.

[193] J. Bridgwater, *Fundamental Powder Mixing Mechanisms*, Powder Technol. 15 (1976), pp. 215-236.

[194] C.J. Brinker and G.W. Scherer, *Sol-Gel Science: The Physics and Chemistry of Sol-Gel Processing*, Academic Press, United States, (1990).

[195] T. Möller, *Selective Crystaline Inorganic Materials as Ion Exchangers in the Treatment of Nuclear Waste Solutions*, Academic Dissertation, University of Helsinki, Finland. (2002).

[196] C.C. Pavel, M. Walter, P. Pöml, D. Bouëxière and K. Popa, *Contrasting Immobilization Behavior of Cs^+ and Sr^{2+} Cations in a Titanosilicate Matrix*, J. Mater. Chem. 21 (2011), pp. 3831-3837.

[197] A. Dyer, J. Newton, L. O'Brien and S. Owens, *Studies on a Synthetic Sitinakite-Type Silicotitanate Cation Exchanger. Part 2. Effect of Alkaline Earth and Alkali Metals on the Uptake of Cs and Sr Radioisotopes*, Micropor. Mesopor. Mat. 120 (2009), pp. 272-277.

[198] L. Al-Attar and A. Dyer, *Sorption of Uranium Onto Titanosilicate Materials*, J. Radioanal. Nucl. Chem. 247 (2001), pp. 121-128.

[199] S. Ferdov, C. Lengauer, O. Petrov and V. Kostov-Kytin, *A Rapid Method for Low-Temperature Synthesis of the Na Analogue of the Microporous Titanosilicate GTS-1*, J. Mater. Sci. 39 (2004), pp. 4343-4344.

[200] Y. Liu, H. Du, F. Zhou and W. Pang, *Synthesis of a New Titanosilicate: An Analogue of the Mineral Penkvilksite*, Chem. Commun. (1997), pp. 1467-1468.

[201] Y.D. Noh and S. Komarneni, *Mercury (II) Exchange by Highly Charged Swelling Micas, Sodium Engelhard Titanosilicate-4, and Sodium Titanosilicate*, Environ. Sci. Technol. 45 (2011), pp. 6954-6960.

[202] Y.D. Noh, S. Komarneni and K.J.D. Mackenzie, *Titanosilicates: Giant Exchange Capacity and Selectivity for Sr and Ba*, Sep. Purif. Technol. 95 (2012), pp. 222-226.

[203] C.B. Lopes, M. Otero, Z. Lin, C.M. Silva, J. Rocha, E. Pereira and A.C. Duarte, *Removal of Hg^{2+} Ions from Aqueous Solution by ETS-4 Microporous titanosilicate—Kinetic and Equilibrium Studies*, Chem. Eng. J. 151 (2009), pp. 247-254.

[204] C.B. Lopes, P.F. Lito, M. Otero, Z. Lin, J. Rocha, C.M. Silva, E. Pereira and A.C. Duarte, *Mercury Removal with Titanosilicate ETS-4: Batch Experiments and Modelling*, Micropor. Mesopor. Mat. 115 (2008), pp. 98-105.

[205] S. Cavenati, C.A. Grande, F.V.S. Lopes and A.E. Rodrigues, *Adsorption of Small Molecules on Alkali-Earth Modified Titanosilicates*, Micropor. Mesopor. Mat. 121 (2009), pp. 114-120.

[206] M. Otero, C.B. Lopes, J. Coimbra, T.R. Ferreira, C.M. Silva, Z. Lin, J. Rocha, E. Pereira, A.C. Duarte and A.C. Duarte, *Priority Pollutants (Hg^{2+} and Cd^{2+}) Removal from Water by ETS-4 Titanosilicate*, Desalination. 249 (2009), pp. 742-747.

[207] L. Al-Attar, A. Dyer and R. Harjula, *Uptake of Radionuclides on Microporous and Layered Ion Exchange Materials*, J. Mater. Chem. 13 (2003), pp. 2963-2968.

[208] R. Grădinaru, S.O. Vălu, Ş. Postolache, C.C. Pavel, I. Sandu and K. Popa, *On the Influence of ETS-10 Porosity and Surface Properties in Retention of some Nanoions and Nanomolecules*, Environ. Eng. Manag. J. 8 (2009), pp. 901-905.

[209] L. Al-Attar, A. Dyer and R. Blackburn, *Uptake of Uranium on ETS-10 Microporous Titanosilicate*, J. Radioanal. Nucl. Chem. 246 (2000), pp. 451-455.

[210] R. Tykva, K.S. Din, C. Pavel, A. Cecal and K. Popa, *Contribution to the External Surface of a Titanium-Rich Sand (Abou-Khashaba, Egypt) in the Uranium Uptake Processes*, J. Radioanal. Nucl. Chem. 279 (2009), pp. 811-816.

[211] J.H. Choi, S.D. Kim, Y.J. Kwon and W.J. Kim, *Adsorption Behaviors of ETS-10 and its Variant, ETAS-10 on the Removal of Heavy Metals, Cu^{2+}, Co^{2+}, Mn^{2+} and Zn^{2+} from a Waste Water*, Micropor. Mesopor. Mat. 96 (2006), pp. 157-167.

[212] C. Borcia, K. Popa, C.C. Pavel, A. Dascălu, C. Vitelaru and B.A. Apetrăchioaei, *Sorption of Thallous Ion from Acidic Aqueous Solutions Onto ETS-10 Titanosilicate*, J. Radioanal. Nucl. Chem. 288 (2011), pp. 25-30.

[213] L. Lv, M.P. Hor, F. Su and X.S. Zhao, *Competitive Adsorption of Pb^{2+}, Cu^{2+}, and Cd^{2+} Ions on Microporous Titanosilicate ETS-10*, J. Colloid Interface Sci. 287 (2005), pp. 178-184.

[214] L. Lv, G. Tsoi and X.S. Zhao, *Uptake Equilibria and Mechanisms of Heavy Metal Ions on Microporous Titanosilicate ETS-10*, Ind. Eng. Chem. Res. 43 (2004), pp. 7900-7906.

[215] L.D. Barreira, P.F. Lito, B.M. Antunes, M. Otero, Z. Lin, J. Rocha, E. Pereira, A.C. Duarte and C.M. Silva, *Effect of pH on Cadmium (II) Removal from Aqueous Solution using Titanosilicate ETS-4*, Chem. Eng. J. 155 (2009), pp. 728-735.

[216] R.G. Anthony, R.G. Dosch, D. Gu and C.V. Philip, *Use of Silicotitanates for Removing Cesium and Strontium from Defense Waste*, Ind. Eng. Chem. Res. 33 (1994), pp. 2702-2705.

[217] Z. Zheng, C.V. Philip, R.G. Anthony, J.L. Krumhansl, D.E. Trudell and J.E. Miller, *Ion Exchange of Group I Metals by Hydrous Crystalline Silicotitanates*, Ind. Eng. Chem. Res. 35 (1996), pp. 4246-4256.

[218] Z. Zheng, D. Gu, R.G. Anthony and E. Klavetter, *Estimation of Cesium Ion Exchange Distribution Coefficients for Concentrated Electrolytic Solutions when using Crystalline Silicotitanates*, Ind. Eng. Chem. Res. 34 (1995), pp. 2142-2147.

[219] Z. Zheng, R.G. Anthony and J.E. Miller, *Modeling Multicomponent Ion Exchange Equilibrium Utilizing Hydrous Crystalline Silicotitanates by a Multiple Interactive Ion Exchange Site Model*, Ind. Eng. Chem. Res. 36 (1997), pp. 2427-2434.

[220] V. Luca, J.V. Hanna, M.E. Smith, M. James, D.R.G. Mitchell and J.R. Bartlett, *Nb-Substitution and Cs Ion-Exchange in the Titanosilicate Sitinakite*, Micropor. Mesopor. Mat. 55 (2002), pp. 1-13.

[221] I.M. Latheef, M.E. Huckman and R.G. Anthony, *Modeling Cesium Ion Exchange on Fixed-Bed Columns of Crystalline Silicotitanate Granules*, Ind. Eng. Chem. Res. 39 (2000), pp. 1356-1363.

[222] K.A. Venkatesan, V. Sukumaran, M.P. Antony and T.G. Srinivasan, *Studies on the Feasibility of using Crystalline Silicotitanates for the Separation of Cesium-137 from Fast Reactor High-Level Liquid Waste*, J. Radioanal. Nucl. Chem. 280 (2009), pp. 129-136.

[223] A.J. Celestian, J.D. Kubicki, J. Hanson, A. Clearfield and J.B. Parise, *The Mechanism Responsible for Extraordinary Cs Ion Selectivity in Crystalline Silicotitanate*, J. Am. Chem. Soc. 130 (2008), pp. 11689-11694.

[224] T.M. Nenoff, J.E. Miller, S.G. Thoma and D.E. Trudell, *Highly Selective Inorganic Crystalline Ion Exchange Material for Sr^2 in Acidic Solutions*, Environ. Sci. Technol. 30 (1996), pp. 3630-3633.

[225] N.R. Mann and T.A. Todd, *Removal of Cesium from Acidic Radioactive Tank Waste by using Ionsiv IE-911*, Sep. Sci. Technol. 39 (2005), pp. 2351-2371.

[226] I.M. El-Naggar, E.A. Mowafy and E.A. Abdel-Galil, *Diffusion Mechanism of Certain Fission Products in the Particles of Silico(IV)Titanate*, Colloid. Surface A. 307 (2007), pp. 77-82.

[227] L.M. Wang, J. Chen and R.C. Ewing, *Radiation and Thermal Effects on Porous and Layer Structured Materials as Getters of Radionuclides*, Curr. Opin. Solid St. M. 8 (2004), pp. 405-418.

[228] T.A. Todd, T.A. Batcheller, J.D. Law and R.S. Herbst, *Cesium and Strontium Separation Technologies*, INEEL/EXT-04-01895, 2004.

[229] N. Lihareva and V. Kostov-Kytin, *Sorption of Cs by Nano-Sized Microporous Titanium Silicates with Pharmacosiderite Structure*, Bulgarian Chem. Commun. 46 (2014), pp. 569-575.

[230] A. Nalaparaju, Z.Q. Hu, X.S. Zhao and J.W. Jiang, *Exchange of Heavy Metal Ions in Titanosilicate Na-ETS-10 Membrane from Molecular Dynamics Simulations*, J. Membr. Sci. 335 (2009), pp. 89-95.

[231] E.D. Camarinha, P.F. Lito, B.M. Antunes, M. Otero, Z. Lin, J. Rocha, E. Pereira, A.C. Duarte and C.M. Silva, *Cadmium(II) Removal from Aqueous Solution using Microporous Titanosilicate ETS-10*, Chem. Eng. J. 155 (2009), pp. 108-114.

[232] G.X.S. Zhao, J.L. Lee and P.A. Chia, *Unusual Adsorption Properties of Microporous Titanosilicate ETS-10 Toward Heavy Metal Lead*, Langmuir. 19 (2003), pp. 1977-1979.

[233] T.R. Ferreira, C.B. Lopes, P.F. Lito, M. Otero, Z. Lin, J. Rocha, E. Pereira, C.M. Silva and A. Duarte, *Cadmium (II) Removal from Aqueous Solution using Microporous Titanosilicate ETS-4*, Chem. Eng. J. 147 (2009), pp. 173-179.

[234] S.P. Cardoso, C.B. Lopes, E. Pereira, A.C. Duarte and C.M. Silva, *Competitive Removal of Cd^{2+} and Hg^{2+} Ions from Water using Titanosilicate ETS-4: Kinetic Behaviour and Selectivity*, Water Air Soil Poll. 224 (2013), pp. 1-6.

[235] C.B. Lopes, M. Otero, J. Coimbra, E. Pereira, J. Rocha, Z. Lin and A. Duarte, *Removal of Low Concentration Hg^{2+} from Natural Waters by Microporous and Layered Titanosilicates*, Micropor. Mesopor. Mat. 103 (2007), pp. 325-332.

[236] B. El-Gammal, *Adsorption Profiles of some Heavy Metal Ions from Aqueous Waste Solutions using Sodium-Doped Zirconium Titanoslicate*, Desalin. Water Treat. 52 (2014), pp. 5952-5964.

[237] Z. Lin, J. Rocha, P. Brandao, A. Ferreira, A.P. Esculcas, Pedrosa de J., Júlio D., J. Rocha and M.W. Anderson, *Synthesis and Structural Characterization of Microporous Umbite, Penkvilksite, and Other Titanosilicates*, J. Phys. Chem. B. 101 (1997), pp. 7114-7120.

[238] R.L. Frost and Y. Xi, *Vibrational Spectroscopic Study of the Mineral Penkvilksite $Na_2TiSi_4O_{11}\cdot 2H_2O$ – a Mineral used for the Uptake of Radionuclides*, Radiat. Eff. Defects Solids. 168 (2013), pp. 72-79.

[239] J.G. Decaillon, Y. Andres, B.M. Mokili, J.C. Abbe, M. Tournoux and J. Patarin, *Study of the Ion Exchange Selectivity of Layared Titanosilicate $Na_3(Na,H)Ti_2O_2[Si_2O_6]_2\times 2H_2O$, AM-4, for Strontium*, Solv. Extr. Ion Exch. 20 (2002), pp. 273-291.

[240] J. Pérez-Carvajal, P. Lalueza, C. Casado, C. Téllez and J. Coronas, *Layered Titanosilicates JDF-L1 and AM-4 for Biocide Applications*, Appl. Clay. Sci. 56 (2012), pp. 30-35.

[241] A. Tripathi, D.G. Medvedev and A. Clearfield, *The Crystal Structures of Strontium Exchanged Sodium Titanosilicates in Relation to Selectivity for Nuclear Waste Treatment*, J. Solid State Chem. 178 (2005), pp. 253-261.

[242] A. Tripathi, D.G. Medvedev, M. Nyman and A. Clearfield, *Selectivity for Cs and Sr in Nb-Substituted Titanosilicate with Sitinakite Topology*, J. Solid State Chem. 175 (2003), pp. 72-83.

[243] A. Dyer, J. Newton, L. O'Brien and S. Owens, *Studies on a Synthetic Sitinakite-Type Silicotitanate Cation Exchanger: Part 1: Measurement of Cation Exchange Diffusion Coefficients*, Micropor. Mesopor. Mat. 117 (2009), pp. 304-308.

[244] A.J. Celestian, M. Powers and S. Rader, *In Situ Raman Spectroscopic Study of Transient Polyhedral Distortions during Cesium Ion Exchange into Sitinakite*, Am. Mineral. 98 (2013), pp. 1153-1161.

[245] A.M. Puziy, *Cesium and Strontium Exchange by the Framework Potassium Titanium Silicate $K_3HTi_4O_4(SiO_4)_3\cdot 4H_2O$*, J. Radioanal. Nucl. Chem. 237 (1998), pp. 73-80.

[246] W. Zuo, P. Han, Y. Li, X. Liu, X. He and R. Han, *Equilibrium, Kinetic and Mechanism Study for Adsorption of Neutral Red Onto Rise Husk*, Desalin. Water Treat. 12 (2009), pp. 210-218.

[247] T. Wolkenstein, *Electronic Processes on Semiconductor Surfaces during Chemisorption*, translated from Russian by E.M. Yankovskii and edited by R. Morrison New York and London (1991).

[248] T. Wolkenstein, *Activated Adsorption on Semiconductors*, Uspehi Fizicheskih Nauk. 2 (1953), pp. 253-270.

[249] W.G. Pollard, *Use of Surface States to Explain Activated Adsorption*, Phys. Rev. 56 (1939), pp. 324-336.

[250] L.E. Katz, L.J. Criscenti, C. Chen, J.P. Larentzos and H.M. Liljestrand, *Temperature Effects on Alkaline Earth Metal Ions Adsorption on Gibbsite: Approaches from Macroscopic Sorption Experiments and Molecular Dynamics Simulations*, J. Colloid Interface Sci. 399 (2013), pp. 68-76.

[251] A.I. Ivanets, N.V. Kitikova, I.L. Shashkova, O.V. Oleksiienko, I. Levchuk and M. Sillanpää, *Using of Phosphatized Dolomite for Treatment of Real Mine Water from Metal Ions*, J. Water Proc. Eng. 9 (2016), pp. 246-253.

Publication I

Oleksiienko, O., Meleshevych, S., Strelko, V., Wolkersdorfer, Ch., Tsyba, M. M., Kylivnyk, Yu. M., Levchuk, I., Sitarz, M., Sillanpää, M.
Pore structure and sorption characterization of titanosilicates obtained from concentrated precursors by the sol–gel method
Reprinted with permission from
Society of Chemistry Advances
Vol. 5, pp. 72562–72571, 2015

RSC Advances

PAPER

Cite this: *RSC Adv.*, 2015, **5**, 72562

Pore structure and sorption characterization of titanosilicates obtained from concentrated precursors by the sol–gel method

O. Oleksiienko,*[ab] S. Meleshevych,[a] V. Strelko,[a] Ch. Wolkersdorfer,[bc] M. M. Tsyba,[a] Yu. M. Kylivnyk,[a] I. Levchuk,[b] M. Sitarz[d] and M. Sillanpää[b]

A modified approach using the sol–gel synthesis of titanosilicate (TiSi) with a developed pore structure under relatively mild synthesis conditions was developed. To identify the controlling factors for the preparation of gels with the desired properties, the influences of the synthesis parameters on the structure and sorption capacity of the materials were studied. The chosen synthesis conditions allowed the preparation of TiSi xerogels with a high decontamination factor for both Sr^{2+} and Cs^{+}. Effects of competitive ions on the separation factors, distribution and selectivity coefficients were studied from different background solutions containing Sr^{2+} and Cs^{+} simultaneously. It could be shown that it is possible to produce TiSi gels with developed pore structures that are capable of removing Sr^{2+} and Cs^{+} from complex aqueous solutions.

Received 17th April 2015
Accepted 19th August 2015

DOI: 10.1039/c5ra06985h

www.rsc.org/advances

Introduction

Titanosilicates (TiSi) are inorganic compounds widely applied in sorption and ion-exchange processes.[1–11] These chemically and thermally stable and radiation resistant materials with a high ion-exchange rate and remarkable capacity, are able to effectively decontaminate liquid radioactive wastes (LRW) from long-live nuclides, such as ^{90}Sr, $^{134,137}Cs$, $^{233–235,238}U$, ^{241}Am, $^{239,240}Pu$ and ^{154}Eu.[1,3,12,13] In numerous works, different ways of TiSi synthesis, such as hydrolysis of alkoxides and inorganic salts *via* hydrothermal, microwave, mechanochemical and sol–gel routes were proposed.[14–29] Using alkoxides as precursors leads to high purity materials. However, for the synthesis with alkoxides the following drawbacks were observed: toxic, expensive and unstable precursors, ecotoxic solvents and poor reproducibility of results. Consequently, inorganic precursors become now more commonly used for the synthesis due to their stability, easy handling and lower costs.[1,8,15] As a ligand, hydrogen peroxide (H_2O_2) is traditionally used for slowing down the hydrolysis rate of Ti-containing precursors to the silicon precursor rate and increasing the amount of co-precipitated Ti–O–Si bonds. Advantages of using such a ligand are its eco-friendliness and non toxicity of the products H_2O and O_2. The main disadvantage is that the released oxygen during the hydrothermal treatment (HTT) raises the autogenous pressure inside the autoclave to more than 70 bar. Due to this fact, special equipment is required. In preceding works, microwave and mechanochemical routes as well as other reported methods yielded formation of powder titanosilicates.[16–29] However, it is well known that many effective powder materials are not suitable for wide practical applications due to agglomeration, which decreases the working surface and active centre accessibility, difficulties with handling and filtration (stoppages, high hydrostatic resistance, bulk compression and poor wettability).[30,31]

Sol–gel synthesis has numerous benefits in comparison to other methods, such as an excellent homogenization of the precursors during the sol preparation stage, a possibility to obtain high purity materials with the desired composition, structure and properties under comparably mild conditions and an opportunity to choose the form of materials (powders, fibers, films or particles).[32] Synthesis for titanosilicate preparation *via* the sol–gel method using H_2O_2 was based on the approach reported in ref. 33. Previously, decomposition of the peroxide ligand released the oxygen that ruined the formed gel and the titanosilicates could be obtained only in powder form.

Recently, the first authors of this paper developed and patented a new sol–gel synthesis of titanosilicates from inorganic precursors based on gel preparation at room temperature,[34,35] which overcomes several of the before mentioned disadvantages. This synthesis method leads to stable materials with reproducible properties. The crucial point for the proposed approach is the possibility to use chemicals with essential

[a]*Institute of Sorption and Problems of Endoecology NAS of Ukraine, 13 General Naumov str., Kyiv 03164, Ukraine. E-mail: ovalexis@gmail.com; Tel: +380 970870818*
[b]*Laboratory of Green Chemistry, Lappeenranta University of Technology, Sammonkatu 12, 50130 Mikkeli, Finland*
[c]*Tshwane University of Technology, Faculty of Science, Department of Environmental, Water and Earth Science, 175 Nelson Mandela Drive, Pretoria 0001, South Africa*
[d]*AGH University of Science and Technology, Faculty of Materials Science and Ceramics, Al. Mickiewicza 30, 30-059 Kraków, Poland*

concentrations (2–5 M) strongly increasing the material yield. This synthesis route can be accomplished using a range of eco-friendly compounds, such as polyalcohols and organic hydroxy-, ceto-, di- and tricarboxylic acids and its mixtures. Utilization of such ligands solved a few problems: at first, the proposed ligands did not ruin the gel structure as in the traditional H_2O_2 method, and the TiSi xerogels obtained had particle sizes of 4 mm and less, instead of being a fine powder. The second advantage is the decrease of the autogenous pressure in the autoclaves by at least an order of magnitude. Finally, substituting the H_2O_2 ligand offers an opportunity to increase the precursor number and decrease the resulting material costs. The possibility to replace the $TiCl_4$ precursor with pure and technical $TiOSO_4$ solution was shown earlier.[34–37] In addition, the pure silica sources Na_2SiO_3 and K_2SiO_3 have been replaced with cheaper bulk liquid glasses and stable porous gels with a high sorption ability to Sr^{2+} were obtained after such precursor substitutions. Using inexpensive precursors (technical $TiOSO_4$, containing iron cations) would not be possible with H_2O_2, due to the catalytic effect of Fe^{3+} on the hydrogen peroxide decomposition. The modified approach presented in this paper, thus, is very promising for the large-scale application of TiSi materials.

The first part of this paper describes and exemplifies the newly developed approach in the synthesis of TiSi xerogels from pure titanyl sulphate, sodium liquid glass and sodium hydroxide. In the second part, the effect of the synthesis parameters on structural and sorption characteristics is evaluated in order to obtain a sorption material highly efficient for Sr nuclides. The third part is devoted to assessing the ability to uptake stable Cs^+ and Sr^{2+} nuclides from aqueous solutions containing both potential pollutants simultaneously.

Experimental session

Chemicals

Titanium tetrachloride ($TiCl_4$), metatitanic acid (H_2TiO_3) and technical solutions of liquid glass ($Na_2O{\cdot}2.5SiO_2$) were used as precursors (Sumykhimprom and Kremnypolymer, Ukraine). A bulk solution of $Na_2O{\cdot}2.5SiO_2$ was taken for synthesis after filtering through a polypropylene filter (0.5–1.0 mm). D-Sorbitol ((2*S*,3*R*,4*R*,5*R*)-hexane-1,2,3,4,5,6-hexol ($C_6H_{14}O_6$)), L-lactic acid (2-hydroxypropanoic acid ($C_3H_6O_3$)), benzene (C_6H_6), Trilon B (disodium ethylenediaminetetraacetic acid (EDTA)) or (2-({2-[bis(carboxymethyl)amino]ethyl}(carboxymethyl)amino)acetic acid) and calcein (fluorexon) indicator (2-[[7′-[[bis(carboxymethyl)amino]methyl]-3′,6′-dihydroxy-3-oxospiro[2-benzofuran-1,9′-xanthene]-2′-yl]methyl-(carboxymethyl)amino]acetic acid) with an assay of 95–98% (Chimlaborreaktiv, Macrochem and Synbias, Ukraine) were used without further purification. Pure solutions of $TiOSO_4$ were achieved by replacing Cl^- with SO_4^{2-} in $TiCl_4$ or by dissolving the metatitanic acid in H_2SO_4. All chemicals used for the sorption tests (CsCl, $SrCl_2{\cdot}6H_2O$; NaCl, $NaHCO_3$, KCl, $CaCl_2$, D-glucose, H_2SO_4, NaOH) were of analytical grade (Sigma-Aldrich) and used without further purification. Laboratory glassware was rinsed with concentrated HCl or HNO_3, and Milli-Q water (resistance 18.2 MΩ) was used for all studies.

Synthesis

Titanosilicate sols were obtained by mixing two initial solutions at room temperature using a magnetic stirrer. The first solution was prepared by mixing pure (3.4 M) $TiOSO_4$ and the ligand, a mixture with D-sorbitol and L-lactic acid. The second initial solution was obtained by mixing a technical liquid glass solution (3.81 M of Si) with 5 M NaOH. Gels for the present study were achieved by mixing the precursor at the molar ratio of Ti : Si : ligand : NaOH = 1 : 1 : 0.5 : 4. The obtained colourless transparent sols were transformed into milky homogeneous gels after 7 s to 15 min (depending on the pH). Fresh gels were aged at room temperature under a polyethylene cover for 0–7 d (days) in order to investigate the effects of aging time (T_{ag}) before hydrothermal treatment (HTT) on the gel properties. Syneresis liquids were taken for pH measurements and gels were then subject to HTT in Teflon-lined steel autoclaves under autogenous pressure. Influences of the HTT parameters were studied in the temperature range of 120–200 °C during 6–48 h.[34,35] The proposed synthesis can be described as follows:

$$TiOSO_4 + Na_2O \times 2.5SiO_2 + NaOH \xrightarrow[\text{ligand}]{\text{HTT}} Na_xTi_ySi_zO_m \times nH_2O(\text{gel}) \quad (1)$$

The HTT gels were rinsed with water to remove salts and ligands. Thereafter, the hydrogels were dried at 80 °C, ground, sieved and fractionated.

Characterization

Sample phase identification was done using X-ray diffraction (XRD), patterns collected using DRON-4-07 (CuKα; 2θ = 5–80° step $\Delta 2\theta = 0.02°$). The Brunauer–Emmett–Teller's (BET) specific surface area and pore structure were determined using a Quantachrome NOVA 2200 surface area analyser and calculated with the NOVAWin software. The pore size distribution, micropore and total pore volume of TiSi xerogels were evaluated by density functional theory (DFT) and Dubinin–Radushkevich (DR) equations.[38,39] The following express-test methods were used: exsiccator porosimetry and trilonometric titration of Sr^{2+}. TiSi xerogels were dried at 105 °C until constant weight was achieved and thereafter saturated with distilled water and benzene vapours in an exsiccator to constant weight at room temperature. The maximum specific sorption pore volume V_p, which is relevant for the characterization and sorption capacity of the studied material, was calculated with eqn (2) ($cm^3\ g^{-1}$). A single point measurement of maximum sorption capacity q to Sr^{2+} from 0.05 M $SrCl_2$ solution was used as an express-test of the sorption ability (eqn (3)). Experimental conditions of the sorption test were: room temperature (25 ± 2 °C), contact time 24 h, 0.1 M NaCl background solution. The concentration of Sr^{2+} in solution was estimated by trilonometric titration with a calcein (fluorexon) indicator and calculated with eqn (4):

$$V_p = \frac{(m_{st} - m_0)}{m_0 \rho} \quad (2)$$

$$q = (C_0 - C_{eq}) \frac{V_{al}}{m_0} \quad (3)$$

$$C(Sr^{2+}) = \frac{\left(V_i m_{e_{Sr^{2+}}} C_i\right)}{V_{al}} \quad (4)$$

where V_p is the maximum specific sorption pore volume ($cm^3\ g^{-1}$), which can be measured by water vapour ($V_{p(w)}$) or by benzene vapour ($V_{p(b)}$); m_0 and m_{st} are the initial and stable sample masses before and after vapour sorption, respectively (g); ρ water or benzene mass density ($g\ cm^{-3}$), V_i is the volume of the Trilon B solution used for titration and V_{al} is the aliquot volume (mL); C_i is the concentration of Trilon B solution used for titration; $m_{e_{Sr^{2+}}}$ is the mass equivalent of Sr^{2+} (meq L^{-1}); C_0 and C_{eq} are the initial and equilibrium concentrations of Sr^{2+} in solution (mg L^{-1}, mmol L^{-1} or meq L^{-1}).

The sorption ability in regards to Sr^{2+} and Cs^+ present simultaneously in aqueous solutions was evaluated by batch experiments. Initial Sr^{2+} concentrations were varied from 4.45×10^{-4} to 1.26 mmol L^{-1}, while the initial Cs^+ concentration was kept constant at 0.752 mmol L^{-1}. Furthermore, initial Cs^+ concentrations varied from 6.85×10^{-6} to 0.75 mmol L^{-1} with a constant initial Sr^{2+} concentration of 1.26 mmol L^{-1}. Milli-Q water, 0.1 M NaCl and Ringer–Locke's solution (0.15 mol L^{-1} of NaCl, 2.38 mmol L^{-1} of $NaHCO_3$, 2.68 mmol L^{-1} of KCl, 0.2 g L^{-1} of $CaCl_2$ and 1.8 mmol L^{-1} of D-glucose; pH = 8.07 (ref. 40 and 41)) were used as media for the sorption tests. An IKA KS 4000i control shaker-incubator was used at 200 rpm (rotations per minute) to overcome the slow diffusion rate; the aliquot volume to sorbent material mass ratio ($V : m$) was 100; contact time 24 h; ambient temperature. The Cs^+ and Sr^{2+} concentrations during the sorption experiments were determined by inductively coupled plasma with mass detector (ICP-MS) model Agilent 7500ce. Distribution coefficients (K_d) and decontamination factors (DF) were calculated using the following equations:

$$K_d = \frac{\Delta C}{C_{eq}} \frac{V_{al}}{m_s} \quad (5)$$

$$DF = \frac{\Delta C \times 100\%}{C_0} \quad (6)$$

$$\Delta C = C_0 - C_{eq} \quad (7)$$

Separation factor F and selectivity coefficients were calculated using the following equations:[42–44]

$$K_{lm}(A^{+n}/B^{+m}) = \frac{{q_A}^{1/n} {C_B}^{1/m}}{{q_B}^{1/m} {C_A}^{1/n}} \quad (8)$$

$$K_G\left(A^+/B^{2+}\right) = \frac{q_A {C_B}^{1/2}}{q_B C_A} \quad (9)$$

$$F = \frac{K_d(A)}{K_d(B)} \quad (10)$$

where C_A and C_B are the equilibrium concentrations of the potential cation pollutants in solution (mg L^{-1}, mmol L^{-1} or meq L^{-1}); q is the amount of the exchanged cation on the material in meq per 100 g of material; K_{lm} is the selectivity coefficient according to the law of mass action form; K_G is the Gapon's selectivity coefficient.

Results and discussion

To identify the crucial synthesis parameters for creating materials with the anticipated properties, the fresh homogenous TiSi hydrogels were subjected to various post synthesis treatments. Altering parameters such as pH or pressure of the HTT yielded material with poor sorption characteristics of Sr^{2+} as well as decomposed gel structures resulting in powder like materials. Drying the fresh hydrogels before HTT produced materials with $DF(Sr^{2+}) \leq 80\%$. Therefore, these synthesis factors were excluded from the present study. Yet, variations of the aging time T_{ag} before HTT, the duration or temperature of HTT resulted in TiSi materials with a high affinity to Sr^{2+}. In order to understand the influence of the abovementioned factors on the TiSi gels' structure, studies using the low temperature nitrogen sorption/desorption technique and X-ray diffraction were conducted subsequently.

Fig. 1 and Table 1 illustrate the influence of aging time (T_{ag}) before HTT on the TiSi gel structural and sorption properties. Pore structure parameters measured with the surface area analyser were compared with data obtained by express-analysis methods (sorption pore volume by water and benzene vapours and sorption capacity to Sr^{2+}). The results presented are for xerogels HTT under 150 °C during 6 h.

It was found that the isotherms obtained from TiSi gels belong to the IV type. According to the IUPAC classification[45] such an isotherm form is typical for materials with a developed pore structure. The shape of the hysteresis loops can be attributed to the H2 type that suggested the "ink-bottle" pore form.

A statistical test with SPSS (22.0) investigated if there are statistically significant differences in the TiSi gel properties or sorption capacities of the HT treatments with different aging times. The Shapiro–Wilk test for normality showed that for 7 of the 8 parameters the zero-hypothesis for normality can't be rejected and that the aging time has no measurable effect on the TiSi properties. Yet, TiSi no. 2, relating to one day of aging, has a R_{pore} value that is different from the other 4 aging steps. Based on the statistical investigation that sample is an outlier and the difference is very likely due to random processes during the HTT.

Sorption tests with Sr^{2+} proved that the reported synthesis approach led to TiSi gels with a high sorption capacity. The sorption data for Sr^{2+} shows a gradual increase of the TiSi sorption capacity (q) of 18% during the first four days and decreases thereafter. Yet, based on the statistical investigation it cannot be excluded that this observation is due to random behaviour. Since the statistical investigation shows that the

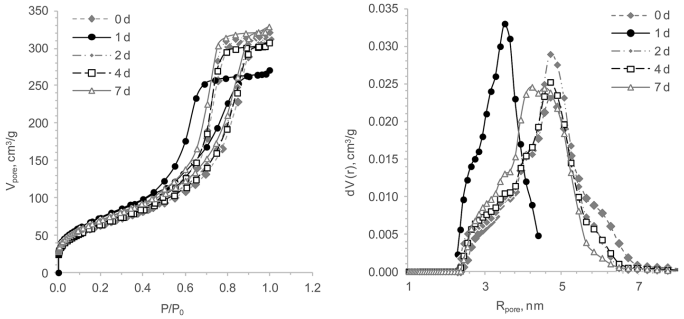

Fig. 1 Effects of the aging time before HTT on the TiSi xerogels' structural and sorption properties: isotherms of nitrogen sorption/desorption (left) and DFT pore size distribution (right).

Table 1 The influence of the aging time before HTT on TiSi xerogels' properties and p-values for the Shapiro–Wilk test for normality ($\alpha = 0.05$)

		HTT								
No.	T_{ag}, d	t, °C	τ, h	S_{BET}[a], m² g⁻¹	$V_{pore\ total}$[a], cm³ g⁻¹	$V_{DR\ micro}$[a], cm³ g⁻¹	R_{pore}[a], nm	V_w[b], cm³ g⁻¹	V_b[b], cm³ g⁻¹	$q(Sr^{2+})$[b], mmol g⁻¹
1	0	150	6	229.2	0.48	0.09	4.71	0.34	0.48	0.86
2	1	150	6	270.3	0.41	0.10	3.52	0.31	0.40	0.91
3	2	150	6	244.1	0.50	0.06	4.71	0.37	0.45	0.98
4	4	150	6	233.6	0.48	0.06	4.71	0.33	0.41	1.04
5	7	150	6	257.0	0.51	0.07	4.39	0.31	0.40	0.85
p	—	—	—	0.715	0.140	0.254	0.012	0.384	0.159	0.511

[a] The instrumental error was 1–3%. [b] The experimental error was up to 10%.

sorption capacity does not depend on the aging period T_{ag}, a one day aging period was chosen for all further investigations to simplify sample handling.

Effects of the HTT duration were studied at 150 °C using hydrogels aged one day. It became clear that the studied variation has an essential effect on the pore structure and is reflected in the sorption pore volume evaluated by benzene vapour (Fig. 2 and Table 2). Between 6 and 24 h HTT, the total pore volume and pore radius increased, while the specific surface area decreased. This observation indicates that the HTT conditions catalyse the ripening processes while the syneresis cannot compensate it since water vapour has less adhesive properties than liquid water at normal conditions. As a result, the mean pore radius rose while the micropore volume and

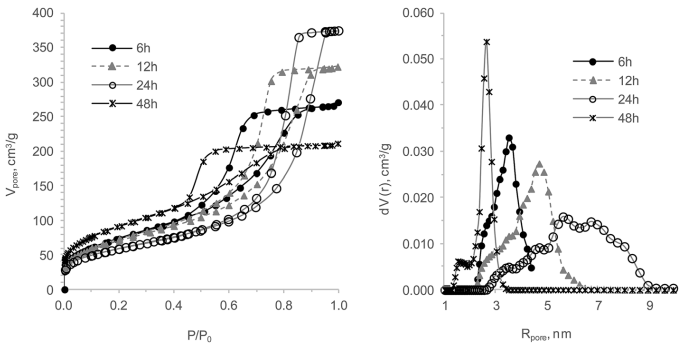

Fig. 2 The effect of the HTT duration on the TiSi xerogels' structural and sorption properties: isotherms of nitrogen sorption/desorption (left) and DFT pore size distribution (right).

Table 2 Effects of the HTT duration on the TiSi xerogels' properties

		HTT								
No.	T_{ag}, d	t, °C	τ, h	S_{BET}, $m^2\ g^{-1}$	$V_{pore\ total}$, $cm^3\ g^{-1}$	$V_{DR\ micro}$, $cm^3\ g^{-1}$	R_{pore}, nm	V_w, $cm^3\ g^{-1}$	V_b, $cm^3\ g^{-1}$	$q(Sr^{2+})$, mmol g^{-1}
2	1	150	6	270.3	0.42	0.10	3.52	0.31	0.40	0.91
6	1	150	12	256.2	0.50	0.07	4.81	0.31	0.47	0.93
7	1	150	24	209.4	0.58	0.08	5.64	0.31	0.94	0.89
8	1	150	48	326.0	0.33	0.08	2.64	0.32	0.31	0.96

sorption capability to Sr^{2+} did not change. These suggestions are based on express-test data and were confirmed with low temperature nitrogen studies.

The data shows that an increase of the HTT duration from 6 to 12 h is similar to 7 d of aging before HTT, as the samples for 1, 2 and 7 aging days with 6 and 12 h show almost identical isotherms (Fig. 3). The pore size distributions of these gels illustrate stiffness (less sensitivity to HTT influence) of the hydrogel structure after one week of aging before HTT. The sample with the highest specific surface area and the widest hysteresis loop had been prepared during 48 h of HTT (Fig. 2). The size and shape of the hysteresis loop indicates an essential difference between the pores "necks" and "bodies". The pore size distribution curve of the sample with 48 h HTT confirms a biporous structure. The biggest shift of the isotherm in a region of lower relative pressure is an indication for a structure with small mean pore sizes. Consequently, a hydrogel with an analogous structure would be obtained after a few months of aging. Interestingly, the maximal Sr^{2+} sorption capacity varies around 7% within the limits of the experimental error. It can therefore be concluded that the effect of both studied factors on the micropore volume and developed transport (mesopore) structure of all obtained gels is insignificant. This observation agrees with earlier works[11,14,33,46–48] stating that the ion-exchange of small cations like Cs^+ and Sr^{2+} takes place in micropores and crystal channels with micropore size. Consequently, it was decided to use 6 h of HTT for further studies as the least energy consuming synthesis of the effective sorption materials investigated. Because of the small number of observations (4), a statistical test with Shapiro–Wilk for normality did not provide useful results.

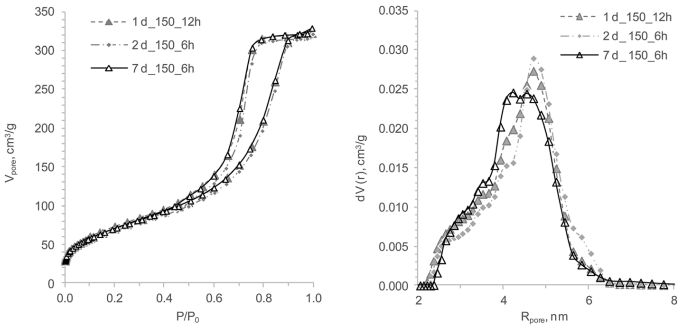

Fig. 3 The influence of the HTT duration and the aging time before HTT on the TiSi xerogels' structural and sorption properties: isotherms of nitrogen sorption/desorption (left) and DFT pore size distribution (right).

Table 3 Effects of temperature of HTT on TiSi xerogels' properties. n.d.: not detected

		HTT								
No.	T_{ag}, d	t, °C	τ, h	S_{BET}, $m^2\ g^{-1}$	$V_{pore\ total}$, $cm^3\ g^{-1}$	$V_{DR\ micro}$, $cm^3\ g^{-1}$	R_{pore}, nm	V_w, $cm^3\ g^{-1}$	V_b, $cm^3\ g^{-1}$	$q(Sr^{2+})$, mmol g^{-1}
9	1	120	6	186.9	0.007	0.0001	1.77	0.12	0.05	0.49
2	1	150	6	270.3	0.419	0.101	3.52	0.31	0.40	0.91
10	1	175	6	176.2	0.70	0.05	8.96	0.26	0.64	0.83
11	1	200	6	236.3	0.44	n.d.	4.10	0.30	0.42	0.47
12	7	200	6	292.7	0.53	0.07	4.07	0.28	0.46	0.65

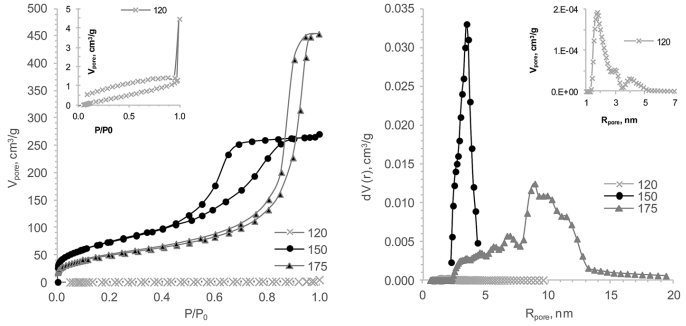

Fig. 4 The influence of the HTT temperature on the TiSi xerogels' properties: isotherms of nitrogen sorption/desorption (left) and DFT pore size distribution (right).

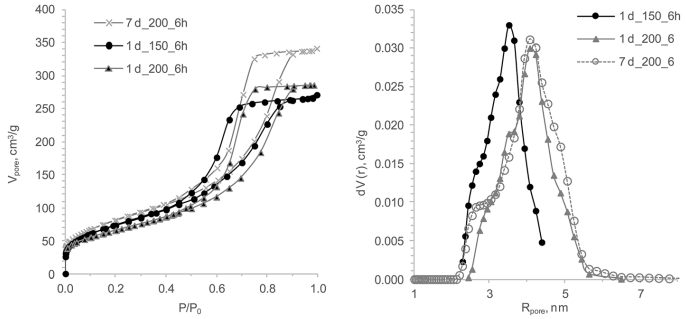

Fig. 5 The influence of the HTT temperature and the aging before HTT on the TiSi xerogels' properties: isotherms of nitrogen sorption/desorption (left) and DFT pore size distribution (right).

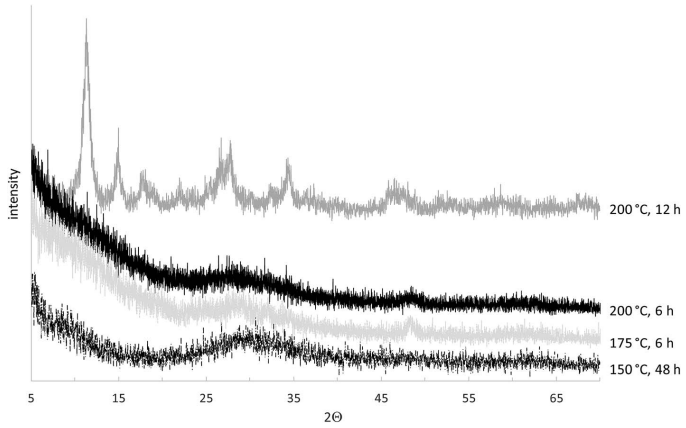

Fig. 6 Temperature influence on the phase structure of TiSi xerogels.

Influences of the HTT temperature on the hydrogels' structure aged one day are presented in Fig. 4 and Table 3. It could be shown that HTT at 120 °C promoted the formation of a TiSi hydrogel structure with an atypical isotherm attributed to the V type. This type and the "open" shape of the hysteresis loop are indicative of a microporous structure of the sample and consequently a small pore volume. Using pore distribution data, the micropore sample structure was evaluated. The sorption pore volume by water vapour and the sorption capacity to Sr^{2+} of this xerogel are half as large as those of sample no. 2 at 150 °C. The HTT at 150–200 °C results in hydrogels with a type IV isotherm. It should be noted that a hydrogel with an H1 hysteresis loop shape was formed at 175 °C HTT. This fact testifies the presence of a macropore or mesopore structure with a big pore radius. The pore size distribution of this sample is wide and the mean pore radius is about 9 nm. Samples with 150 and 200 °C have an H2 shape of the hysteresis loop (Fig. 4).

The influence of temperature on the xerogels' pore structure differs substantially from that of varying HTT durations and aging times (Fig. 5). Temperature clearly predetermined the pore structure and, as a result, the xerogels' sorption capacity. It was found that rising the HTT temperature from 120 °C to 150 °C almost doubled $q(Sr^{2+})$ while in the temperature interval from 175 to 200 °C, $q(Sr^{2+})$ decreased by 76%. This can be explained

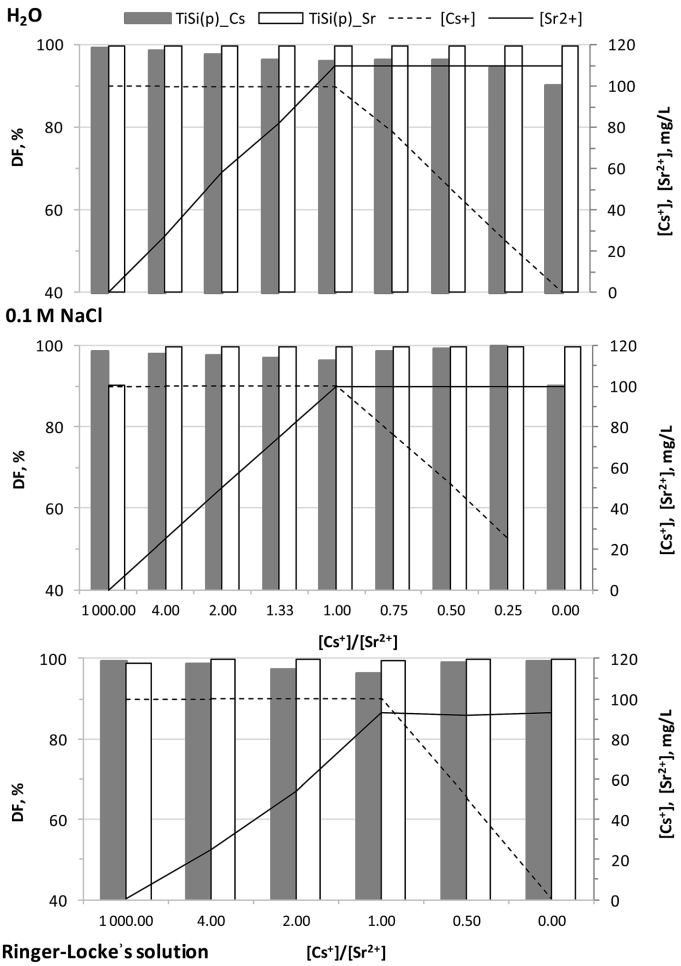

Fig. 7 The influence of the initial concentration of Sr^{2+} and Cs^{+} on the decontamination factor by sorption on TiSi xerogels. Experimental conditions: water, 0.1 M NaCl and Ringer–Locke's solution media; $V : m$ ratio was 100; contact time 24 h; ambient temperature.

with the fact that the 200 °C samples have only half of the micropore volume. Consequently, 175 °C is the temperature where polycondensation, hydrolysis and coarsening processes have the highest rate and/or the basic pH of the syneresis liquid has a catalytic effect on the abovementioned processes. Because of the different modifications in the treatment (aging and temperature), a statistical test with the data did not provide additional information (Table 3).

Unexpectedly low $q(Sr^{2+})$ were obtained for the samples treated at 200 °C HTT and after one and seven days of aging prior to HTT. The shape of the isotherms, hysteresis loops and pore distributions suggests that the developed porosity with micropore volume should be enough for a high sorption ability. Yet, the decline of the sorption capacity might be ascribed to changes in the surface chemistry of the hydrogels under higher temperatures or a decreasing accessibility of the ion-exchange centres due to an increasing order of the structure.

For justification of this assumption, an XRD investigation was performed. The effect of the temperature on structural changes is reflected in the XRD patterns (Fig. 6). The spectrum peaks have the same position and broadness as *poorly* crystalline sodium titanosilicate.[49] Consequently, the described synthetic approach lead to a TiSi which would have the ideal formula $Na_2Ti_2O_3(SiO_4)\cdot 2H_2O$ were it a highly crystalline sodium titanosilicate. According to the results, crystallites become detectable after HTT at 200 °C and the molar ratio of the Ti : Si would be an important parameter in the sorption study. Yet, in this study, even after 48 h of HTT at 150 °C, no detectable crystalline phase was found and the molar ratio is of no known relevance. Thus, it can be concluded that the temperature had the strongest effect on the TiSi hydrogel structure. It was further assumed that the duration of the HTT could be used instead of pre-HTT aging to reduce the synthesis time for the final product. Detailed structural and sorption studies should be done around 175 °C HTT in order to obtain sorption material for big cation pollutants. Following the synthesis conditions: $T_{ag} \geq 1$ day and HTT at 150 °C for 6 h make it possible to obtain materials with the highest sorption capacity in regards to Sr^{2+}, consuming a minimum of time and energy. Samples prepared under the chosen regime were synthesized for further sorption investigations.

Sorption study

The effects of the synthesis conditions on the studied materials' sorption capacity in relation to Sr^{2+} were evaluated from 0.1 M NaCl by trilonometric titration. For determining the sorption capability and selectivity of the obtained xerogels, sorption tests

Table 4 The selectivity coefficient of titanosilicate xerogels' in different solutions and different mass concentration ratios of Cs^+ and Sr^{2+}

			Cs^+/Sr^{2+}					Sr^{2+}/Cs^+		
$\frac{C_{in}Cs^+}{C_{in}Sr^{2+}}$[a]	$q(Cs^+)$, mmol g^{-1}	$K_d(Cs^+)$	K_{lm}	K_G	F	$q(Sr^{2+})$, mmol g^{-1}	$K_d(Sr^{2+})$	K_{lm}	K_G	F
H_2O										
10^3	0.07	12 417	1.89	30.23	0.29	4.45×10^{-5}	43 294	0.53	0.03	3.49
4	0.07	6167	1.06	0.65	0.18	0.03	33 744	0.94	1.55	5.47
2	0.07	4251	0.66	0.27	0.10	0.07	41 362	1.51	3.64	9.73
1.33	0.07	2667	0.37	0.13	0.05	0.09	50 997	2.67	7.64	19.10
1	0.07	2330	0.32	0.10	0.04	0.12	52 073	3.10	10.24	22.35
0.75	0.06	2686	0.39	0.12	0.06	0.13	47 726	2.57	8.52	17.77
0.5	0.04	2589	0.38	0.12	0.06	0.13	45 816	2.61	8.67	17.70
0.25	0.02	1687	0.27	0.08	0.04	0.13	39 217	3.71	12.30	23.25
10^{-4}	6.18×10^{-7}	912	0.16	0.05	0.03	0.13	32 292	6.23	20.64	35.40
0.1 N NaCl										
10^3	0.07	6148	6.44	711.50	6.75	9.35×10^{-7}	911	0.16	0.001	0.15
4	0.07	4434	0.66	0.42	0.10	0.03	45 237	1.52	2.390	10.20
2	0.07	3745	0.67	0.30	0.12	0.06	31 138	1.49	3.330	8.32
1.33	0.07	3123	0.65	0.24	0.13	0.09	23 314	1.55	4.220	7.47
1	0.07	2677	0.59	0.19	0.13	0.11	20 725	1.70	5.360	7.74
0.75	0.06	6206	0.97	0.31	0.15	0.11	41 385	1.04	3.270	6.67
0.5	0.04	14 739	2.47	0.78	0.41	0.11	35 572	0.40	1.280	2.41
0.25	0.02	68 999	12.59	4.00	2.30	0.11	30 053	0.08	0.250	0.44
10^{-4}	6.17×10^{-7}	911	0.18	0.06	0.03	0.11	26 932	5.69	17.980	29.55
Ringer–Locke's solution										
10^3	0.07	13 241	4.59	36.50	1.59	1.81×10^{-4}	8326	0.22	0.03	0.63
4	0.07	6554	0.96	0.61	0.14	0.03	46 976	1.05	1.65	7.17
2	0.07	3728	0.72	0.31	0.14	0.06	26 766	1.39	3.21	7.18
1	0.07	2595	0.57	0.19	0.13	0.11	20 505	1.75	5.30	7.90
0.5	0.04	10 314	1.59	0.52	0.24	0.11	42 198	0.63	1.92	4.09
10^{-3}	1.19×10^{-4}	17 642	2.78	0.91	0.44	0.11	40 254	0.36	1.09	2.28

[a] Mass concentration ratio.

were performed from solutions containing both Sr^{2+} and Cs^{+} simultaneously. The 0.1 M NaCl background solution was used to assess the Na^{+} competition effect on the potential pollutants' uptake. A Ringer–Locke's solution was used to evaluate the effect of Na^{+}, K^{+} and Ca^{2+} competitive ions on the sorption capacity and the selectivity of the synthesized xerogels. There were two reasons to expect a higher affinity and selectivity to Sr^{2+} compared to the cations Na^{+}, K^{+} and Ca^{2+}. Firstly, it is well known that in general, cations with a higher valence more preferably sorb compared to those with lower ones. When the valence is equal, the cation with a bigger atomic mass is sorbed.[41,42] Secondly, studies of TiSi xerogel sorption capacities in the same background solutions with only one cation (Sr^{2+} or Cs^{+}) indicate different sorption mechanisms for these cations (chemisorption for Sr^{2+} and activated sorption for Cs^{+}).[36,37] Coefficients of selectivity and separation factors were calculated in order to evaluate these assumptions. The collected data is expected to be useful for predicting the TiSi behaviour in aqueous media containing Sr^{2+}, Cs^{+}, Na^{+}, K^{+} and Ca^{2+} such as drinking, ground, sea and mine water, blood plasma and liquid radioactive wastes.

Titanosilicates synthesized *via* the sol–gel method have a high sorption affinity to both Sr^{2+} and Cs^{+} (Fig. 7). Varying the initial concentration of one potential pollutant cation has a weak effect on the decontamination factor DF of both cations. Generally, the synthesized material has a higher affinity and sorption capacity to Sr^{2+}: $q(Sr^{2+}) > q(Cs^{+})$ and $K_d(Sr^{2+}) > K_d(Cs^{+})$. It is worth to note, that the same values of $q(Sr^{2+})$ and $q(Cs^{+})$ were obtained during sorption studies in the same background solutions with only one cation (Sr^{2+} or Cs^{+}). It could be shown that the separation factor has a lesser deviation from experimental observations than the calculated selectivity coefficients (Table 4). The selectivity to Sr^{2+} in water increased with increasing initial Sr and decreasing Cs concentrations. The presence of competitive ions in the background solutions reduced both, the selectivity coefficients and separation factors. For example, the Gapon's selectivity coefficient K_G for the mass concentration ratio of $Sr^{2+} : Cs^{+} = 1$ in media with dissolved salts was only half of that one in water. Nevertheless, the synthesized TiSi xerogels demonstrated a high sorption ability, DF and selectivity to Cs^{+} even in the presence of competing cations such as Na^{+}, K^{+}, Sr^{2+} and Ca^{2+}. These good characteristics could be observed even from trace initial concentrations of the potential pollutant ($C_0 \leq 10^{-3}$ mmol L^{-1}).

Conclusions

In the presented study, a synthetic approach yielding in materials with a poorly crystalline sodium titanosilicate structure at relatively mild conditions is described. The work showed that the temperature of the HTT has the strongest influence on the structure of the materials and consequently, it can be used as the controlling factor for the preparation of gels with the desired properties. The chosen synthesis conditions allow for the preparation of TiSi with a high decontamination factor for both Sr^{2+} and Cs^{+}, and competitive ions have a weak influence on the ability and sorption capacity of the obtained TiSi xerogels. Based on the results, it could be shown that the presence of competitive ions reduced the selectivity coefficients and separation factors, but TiSi illustrates a higher affinity and selectivity to Sr^{2+} than to Cs^{+} in all studied media and concentrations. Hence, it can be concluded that the prepared materials could be used as an effective sorption material for Sr^{2+} and Cs^{+} decontamination from drinking, ground, sea and mine waters, blood plasma and LRW. Further studies need to show that the material can also be used in a pilot scale or industrial scale application.

Acknowledgements

The authors thank Elisa Alasuvanto for her assistance with the sorption experiments. Also, we thank N. M. Patryliak, for assistance with the single point measurement of maximum sorption capacity to Sr^{2+}. We are also grateful to Valerij I. Yakovlev for assisting with the precursor preparation and for our fruitful discussions. Furthermore, we thank Mykola P. Ryzhuk for supporting the hydrothermal experiment. Comments from two anonymous reviewers helped to emphasize the novelties described in this paper.

References

1 K. Popa and C. C. Pavel, *Desalination*, 2012, **293**, 78–86.
2 Y. D. Noh, S. Komarneni and K. J. D. Mackenzie, *Sep. Purif. Technol.*, 2012, **95**, 222–226.
3 T. Möller, R. Harjula and J. Lehto, *Sep. Purif. Technol.*, 2002, **28**, 13–23.
4 L. Lv, M. P. Hor, F. Su and X. S. Zhao, *J. Colloid Interface Sci.*, 2005, **287**, 178–184.
5 C. B. Lopes, M. Otero, Z. Lin, C. M. Silva, E. Pereira, J. Rocha and A. C. Duarte, *J. Hazard. Mater.*, 2010, **175**, 439–444.
6 S. Cavenati, C. A. Grande, F. V. S. Lopes and A. E. Rodrigues, *Microporous Mesoporous Mater.*, 2009, **121**, 114–120.
7 C. B. Lopes, M. Otero, Z. Lin, C. M. Silva, J. Rocha, E. Pereira and A. C. Duarte, *Chem. Eng. J.*, 2009, **151**, 247–254.
8 A. Clearfield, *Solvent Extr. Ion Exch.*, 2000, **18**, 655–678.
9 A. Clearfield, L. N. Bortun and A. I. Bortun, *React. Funct. Polym.*, 2000, **43**, 85–95.
10 J. H. Choi, S. D. Kim, Y. J. Kwon and W. J. Kim, *Microporous Mesoporous Mater.*, 2006, **96**, 157–167.
11 A. Anson, C. C. H. Lin, S. M. Kuznicki and J. A. Sawada, *Chem. Eng. Sci.*, 2009, **64**, 3683–3687.
12 P. Sylvester, E. A. Behrens, G. M. Granziano and A. Clearfield, *Sep. Sci. Technol.*, 1999, **34**, 1981–1992.
13 G. Lujaniene, S. Meleshevych, V. Kanibolotskyy, J. Sapolaite, V. Strelko, V. Remeikis, O. Oleksiienko, K. Ribokaite and T. Sciglo, *J. Radioanal. Nucl. Chem.*, 2009, **282**, 787–791.
14 A. Clearfield, *Solvent Extr. Ion Exch.*, 2000, **18**, 655–678.
15 J. Rocha and M. W. Anderson, *Eur. J. Inorg. Chem.*, 2000, **5**, 801–818.
16 S. E. B. Garcia, K. Yamamoto and A. Muramatsu, *J. Mater. Sci.*, 2008, **43**, 2367–2371.
17 K. Yamamoto, S. E. B. Garcia, F. Saito and A. Muramatsu, *Chem. Lett.*, 2006, **35**, 570–571.

18 D. Coutinho, J. A. Losilla, J. Balkus and J. Kenneth, *Microporous Mesoporous Mater.*, 2006, **90**, 229–236.
19 X. Deng, Y. Wang, L. Shen, H. Wu, Y. Liu and M. He, *Ind. Eng. Chem. Res.*, 2013, **52**, 1190–1196.
20 T. Fernandez, U. K. Samersen, X. Joseph and N. V. Unnikrishnan, *J. Mater. Process. Technol.*, 2008, **202**, 528–535.
21 F. Figueras and J. L. Flores Moreno, in *Emerging Fields in Sol–Gel Science and Technology*, ed. T. Lopez, D. Avnir and M. Aegerter, Springer, US, 2003, pp. 37–48.
22 S. E. B. García, K. Yamamoto, F. Saito and A. Muramatsu, *J. Jpn. Pet. Inst.*, 2007, **50**, 53–60.
23 T. Iwasaki, M. Isaka, H. Nakamura, M. Yasuda and S. Watano, *Microporous Mesoporous Mater.*, 2012, **150**, 1–6.
24 L. Liu, W. Tan, P. Xiao and Y. Zhai, *Int. J. Miner., Metall. Mater.*, 2012, **19**, 675–678.
25 M. Muthuraman and K. C. Patil, *Mater. Res. Bull.*, 1998, **33**, 655–661.
26 Z. Shan, E. Gianotti, J. C. Jansen, J. A. Peters, L. Marchese and T. Maschmeyer, *Chem.–Eur. J.*, 2001, **7**, 1437–1443.
27 S. Sivakumar, C. P. Sibu, P. Mukundan, P. K. Pillai and K. G. K. Warrier, *Mater. Lett.*, 2004, **58**, 2664–2669.
28 K. Yamamoto, S. E. Borjas García and A. Muramatsu, *Microporous Mesoporous Mater.*, 2007, **101**, 90–96.
29 K. Yamamoto, S. E. B. Garcia, F. Saito and A. Muramatsu, *Chem. Lett.*, 2006, **35**, 570–571.
30 J. Bridgwater, *Powder Technol.*, 1976, **15**, 215–236.
31 R. Freeman, *Powder Technol.*, 2007, **174**, 25–33.
32 C. J. Brinker and G. W. Scherer, *Sol–gel science: the physics and chemistry of sol–gel processing*, Academic Press, United States, 1990.
33 O. V. Oleksiienko, S. I. Meleshevych, V. V. Strelko, O. I. V'yunov, O. K. Matkovsky, V. G. Milgrandt, M. M. Tsyba and V. A. Kanibolotsky, *Prob. Chem. Chem. Technol.*, 2013, **2**, 101–105.
34 V. G. Kalenchuk, S. V. Meleshevych, V. A. Kanibolotsky, V. V. Strelko, O. V. Oleksiienko and N. M. Patryliak, A method for producing titanosilicate ion exchangers, Patent UA48457U, 2010.
35 V. V. Strelko, S. V. Meleshevych, V. A. Kanibolotsky and O. V. Oleksiienko, A method for producing titanosilicate ion exchangers, Patent UA48457U, 2012.
36 O. Oleksiienko, I. Levchuk, M. Sitarz, S. Meleshevych, V. Strelko and M. Sillanpää, *J. Colloid Interface Sci.*, 2015, **438**, 159–168.
37 O. Oleksiienko, I. Levchuk, M. Sitarz, S. Meleshevych, V. Strelko and M. Sillanpää, *Desalin. Water Treat.*, 2015, DOI: 10.1080/19443994.2014.1003103.
38 A. Dada, A. Olalekan, A. Olatunya and O. Dada, *J. Appl. Chem.*, 2012, **3**, 38–45.
39 A. Dąbrowski, *Adv. Colloid Interface Sci.*, 2001, **93**, 135–224.
40 W. R. Amberson, J. Flexner, F. R. Steggerda, A. G. Mulder, M. J. Tendler, D. S. Pankratz and E. P. Laug, *J. Cell. Comp. Physiol.*, 1934, **5**, 359–382.
41 J. P. Steel, *Br. Med. J.*, 1927, **2**, 1177–1178.
42 A. I. Bortun, L. N. Bortun and A. Clearfield, *Solvent Extr. Ion Exch.*, 1997, **5**, 909–929.
43 I. Shainberg, N. I. Alperovitch and R. Keren, *Clays Clay Miner.*, 1987, **35**, 68–73.
44 V. P. Evangelou and F. J. Coale, *Soil Sci. Soc. Am. J.*, 1987, **51**, 69–72.
45 K. S. W. Sing, *Pure Appl. Chem.*, 1982, **54**(11), 2201–2218.
46 A. Clearfield, *Solid State Sci.*, 2001, **3**, 103–112.
47 E. A. Behrens, D. M. Poojary and A. Clearfield, *Chem. Mater.*, 1996, **8**, 1236–1244.
48 A. Tripathi, D. G. Medvedev and A. Clearfield, *J. Solid State Chem.*, 2005, **178**, 253–261.
49 A. Clearfield, D. G. Medvedev, S. Kerlegon, T. Bosser, J. D. Burns and J. Milton, *Solvent Extr. Ion Exch.*, 2012, **30**, 229–243.

Publication II

Oleksiienko, O., Levchuk, I., Sitarz, M., Meleshevych, S., Strelko, V., Sillanpää, M.
Removal of strontium (Sr^{2+}) from aqueous solutions with titanosilicates obtained by sol-gel method
Reprinted with permission from
Journal of Colloid and Interface Science
Vol. 438, pp. 159–168, 2015

Journal of Colloid and Interface Science 438 (2015) 159–168

Contents lists available at ScienceDirect

Journal of Colloid and Interface Science

www.elsevier.com/locate/jcis

Removal of strontium (Sr^{2+}) from aqueous solutions with titanosilicates obtained by the sol–gel method

Olga Oleksiienko [a,b,*], Irina Levchuk [b], Maciej Sitarz [c], Svitlana Meleshevych [a], Volodymyr Strelko [a], Mika Sillanpää [b]

[a] Institute of Sorption and Problems of Endoecology NAS of Ukraine, 13 General Naumov str., Kyiv 03164, Ukraine
[b] Laboratory of Green Chemistry, Lappeenranta University of Technology, Sammonkatu 12, Mikkeli 50130, Finland
[c] AGH University of Science and Technology, Faculty of Materials Science and Ceramics, Al. Mickiewicza 30, 30-059 Kraków, Poland

ARTICLE INFO

Article history:
Received 5 August 2014
Accepted 27 September 2014
Available online 8 October 2014

Keywords:
Titanosilicate
Sol–gel synthesis
Porous structure
Adsorption
Kinetic study

ABSTRACT

Titanosilicates (TiSis) were synthesized from pure and technical precursors by the sol–gel method. X-ray diffraction (XRD) studies of TiSi identified amorphous phases. The Brunauer, Emmett and Teller (BET) surface area of TiSis obtained from pure and technical precursors measured using the low-temperature nitrogen adsorption/desorption technique were 270.3 and 158.7 $m^2 g^{-1}$, respectively. Micro-mesopore and micro- meso- macropore structures were attributed to TiSi prepared from pure and technical precursors, correspondingly. TiSis mass, solution pH, contact time, initial Sr^{2+} concentration, temperature and background solution were investigated for their effect on sorption properties. TiSis were observed to have a high affinity for strontium in the pH range of 4–12. Strontium adsorption isotherms were established and fitted to the Langmuir, Freundlich, Redlich–Peterson, Sips and Toth models. Pseudo-first and pseudo-second models were used to describe experimental kinetic data. X-ray photoelectron spectroscopy (XPS) and scanning electron microscopy with energy dispersive X-ray spectroscopy (SEM–EDX) data for TiSis were collected before and after adsorption. Heterophase was observed on the surfaces of both types of TiSi material after Sr^{2+} uptake. The mechanism of Sr^{2+} sorption on titanosilicates was suggested.

1. Introduction

Nuclear disasters such as Chernobyl and Fukushima lead to the release of radionuclides into the environment, which in turn has a harmful effect on all living organisms. This makes the removal of radionuclides from water and wastewater a key issue for today [1,2]. The development of new materials for contaminated wastewater treatment is thus attracting significant attention [3–7]. Titanosilicates are known as the most promising inorganic adsorbents for the decontamination of liquid radioactive wastes from long-lived radionuclides such as caesium and strontium. This can be explained by their high selectivity and stability over a wide pH range, high immutability with temperature variations and resistance to ionizing radiation [8,9]. Numerous studies of framework TiSis have reported on their various synthesis methods, structural and sorption properties [10,11]. Yet all known synthesis methods lead to titanosilicates in powder form only, which raises difficulties for their practical application. Granulated and particulate materials could be used in order to achieve a measure of success. One way of applying these kinds of material without any binders is by sol–gel method. Sol–gel synthesis has a number of benefits in comparison with conventional methods, such as synthesis at relatively low temperatures and the possibility synthesizing composite materials. These are difficult to achieve by traditional means due to the problems associated with volatilization, high melting temperatures or crystallization. Other important advantages of the sol–gel method are high purity and excellent homogeneity. This method can also be used to prepare a wide range of materials such as thin and thick films, fibres and bulk materials. Finally, sol–gel synthesis can obtain materials with the desired properties [12]. A novel approach to the sol–gel synthesis of titanosilicates was developed recently [13,14]. This method leads to the preparation of a stable gel with reproducible properties using simple inorganic salts, acids and alkali or alkaline earth hydroxides, and particles are then obtained by gel crushing. The influence of synthesis parameters on the crystal-chemical structure and adsorption capacity of the abovementioned materials have also been investigated [5,15,16]. The possibility to conduct a synthesis with technical precursors instead of pure chemicals was reported in [13,14]. It was found that a complexing cations (contained in technical precursor as a pollutants)

* Corresponding author at: Laboratory of Green Chemistry, Lappeenranta University of Technology, Sammonkatu 12, Mikkeli 50130, Finland.
E-mail address: ovalexis@gmail.com (O. Oleksiienko).

http://dx.doi.org/10.1016/j.jcis.2014.09.075
0021-9797/

affected the sol–gel processing. The present work seeks to investigate the influence of precursor substitution on the TiSi materials properties. Since obtained materials supposed to be used as adsorbents, the main attention of current study was paid to difference in sorption abilities and understanding the sorption mechanism on titanosilicates synthesized by sol–gel method with pure and technical precursors.

2. Experimental procedure

2.1. Chemicals

All chemicals used for analysis ($SrCl_2{\cdot}6H_2O$; NaCl, $NaHCO_3$, KCl, $CaCl_2$, D-glucose, H_2SO_4, HNO_3, HCl, NaOH) were of analytical grade (Sigma–Aldrich) and used without further purification. Technical liquid glass solution ($Na_2O{\cdot}2.5\ SiO_2$) and technical solution of $TiOSO_4$ were purchased from Ukrainian enterprises. Laboratory glassware was washed with concentrated HCl or HNO_3. Milli-Q water (resistance 18.2 M Ω cm) was used for all experiments.

2.2. Synthesis

Titanosilicates were prepared by sol–gel synthesis according to the scheme and procedure given in [13,14].

$$\text{inorganic salt Ti} + Na_2O \cdot SiO_2 + MOH \overset{HTT}{\rightarrow} \underset{gel}{M_xTi_ySi_zO_m \cdot nH_2O} \quad (1)$$

where HTT is hydrothermal treatment and MOH is alkali or alkaline earth hydroxides.

Pure and technical solutions of $TiOSO_4$ were used as an inorganic titanium salt and NaOH as MOH. Technical liquid glass solution was used as a source of silicon for titanosilicate synthesis.

Pure solution of $TiOSO_4$ was achieved by replacing Cl^- with SO_4^{2-} in $TiCl_4$. All chemicals used in this reaction were of analytical grade. A technical solution of $TiOSO_4$ was taken for synthesis after filtering through a polypropylene filter (0.5–1.0 mm). Pure or technical solutions of $TiOSO_4$, liquid glass and NaOH with the molar ratio Ti:Si:NaOH = 1:1:4 were used. TiSi gels were obtained at room temperature after magnetic stirring. The gels were then hydrothermally treated (HTT) in Teflon-lined steel autoclaves under autogenous pressure. The HTT gels were then rinsed with water and dried at 80 °C. Particles of prepared xerogel were ground, sieved and fractions with a size of 0.25–0.5 mm were used in the sorption studies.

2.3. Instrumentation

Measurements of pH were taken using a 340i pH-metre. The BET specific surface area, Barrett–Joyner–Halenda (BJH) and density functional theory (DFT) pore size distribution, DFT and Dubinin–Radushkevich (DR) micropore volume of TiSi were measured using a Quantachrome NOVA 2200 surface area analyser. The X-ray diffraction (XRD) patterns were recorded using DRON-4-07 (Cu Kα; 2θ = 5–80° step $\Delta 2\theta$ = 0.02°). An IKA KS 4000i control shaker–incubator was used for sorption tests at 200 rtp. The cation concentrations in solutions during sorption tests were investigated with an inductively coupled plasma optical atomic emission spectrometer (ICP–OES) model iCAP 6300 (Thermo Electron Corporation, USA). X-ray photoelectron spectroscopy (XPS) data were collected using a Thermo Fisher Scientific ESCALAB 250Xi. FTIR spectra were recorded with a Bruker Vertex 70v spectrometer. Spectra were collected in the mid (MIR) regions (4000–100 cm^{-1}) after 128 scans at 4 cm^{-1} resolution. Samples were prepared by the standard KBr pellets methods. Microstructure of the produced materials was examined by means of scanning electron microscope (SEM, Nova Nano SEM 200, FEI Company) with an attachment for chemical analysis of specimen in microareas with energy dispersive X-ray spectroscopy (EDX, EDAX). The experiment was carried out in low vacuum condition in secondary electron mode.

2.4. Adsorption experiments

Initial strontium solutions for the sorption experiments were prepared from solids of strontium chloride hexahydrate. Experiments were performed in batch tests using a shaker–incubator, and aqueous solutions of Sr^{2+} with different media such as water, NaCl and Ringer–Locke's (RL) solution. All batch tests were performed in polypropylene tubes. Polypropylene syringe membranes (0.45 μm) were used for sorbent separation. Adsorption capacity was investigated as a function of adsorbent mass, initial concentration, time, pH, temperature, composition and concentration of background solution. Control experiments (without sorbent material) were conducted at the same time with sorption experiment in order to illustrate, that sorption take place on the sorbent surface and not on the dish's surface.

The effect of ratio between adsorbent mass (m) and solution volume (V) on the adsorption capacity of TiSi was studied at V/m ratios from 50 to 2000. The initial concentration of Sr^{2+} was 0.5 g L^{-1}, the solution medium was 0.1 M NaCl and the pH was 7.08.

The influence of initial Sr^{2+} concentration on the sorption properties of TiSi was investigated in solutions with different media, such as water (pH = 6.78); NaCl at concentrations 0.01 M, 0.05 M, 0.1 M and 0.2 M (pH = 7.08) and Ringer–Locke's solution (9 g L^{-1} of NaCl, 0.2 g L^{-1} of $NaHCO_3$, 0.2 g L^{-1} of KCl, 0.2 g L^{-1} of $CaCl_2$ and 1 g L^{-1} of D–glucose; pH = 8.07). Initial strontium concentrations were varied from 10 to 5000 mg L^{-1}, the solution volume was 5 mL and the contact time was 24 h.

The effect of pH on the sorption properties of TiSi was evaluated from strontium solutions in water medium. Experiments were conducted at pH ranging from 1 to 12, with an initial Sr^{2+} concentration of 0.5 g L^{-1}, 5 mL solution volume and 24 h contact time.

The impact of contact time (t) on the adsorption capacity of TiSi was estimated using strontium solutions with water (pH = 6.78) and 0.1 M NaCl (pH = 7.08) media. The contact time ranged from 3 to 2880 min at ambient temperature (24 °C ± 2) and from 3 to 360 min at elevated temperatures. The initial Sr^{2+} concentration was 0.5 g L^{-1} and the solution volume was 5 mL.

The effect of temperature was studied with strontium solutions with 0.1 M NaCl (pH = 7.08 ± 0.02) as a medium. Sorption tests were conducted at temperatures of 40, 60 and 70 °C, at a contact time of 3–360 min, an initial Sr^{2+} concentration of 0.5 g L^{-1} and a solution volume of 10 mL.

Adsorption capacity (q), distribution coefficient (K_d) and decontamination factor (DF) were calculated using the following equations:

$$q = (C_o - C_t) \cdot \frac{V}{m} \quad (2)$$

$$K_d = \frac{(C_o - C_t)}{C_t} \cdot \frac{V}{m} \quad (3)$$

$$DF = (\Delta C \cdot 100\%)/C_0 \quad (4)$$

$$\Delta C = C_o - C_t$$

where C_o and C_t are initial concentration and concentration of strontium in solution (mmol L^{-1}) for time t, V is the aliquot volume (mL) and m is the mass of adsorbent (g).

Experimental data were fitted to the Langmuir, Freundlich, Sips (Langmuir–Freundlich), Redlich–Peterson and Toth models, which

are commonly used to describe liquid–solid systems [17–20]. The equations for these models are presented below:

$$q_e = \frac{q_m K_L C_e}{1 + K_L C_e} \quad (5)$$

$$q_e = K_F C_e^{1/n_F} \quad (6)$$

$$q_e = \frac{q_m (K_S C_e)^{n_S}}{1 + (K_S C_e)^{n_S}} \quad (7)$$

$$q_e = \frac{q_m K_{RP} C_e}{1 + (K_{RP} C_e)^{n_{RP}}} \quad (8)$$

$$q_e = \frac{q_m C_e}{(a_T + C_e^{m_T})^{\frac{1}{m_T}}} \quad (9)$$

where

q_e is the adsorption capacity (mg g^{-1} or mmol g^{-1}),
C_e is the equilibrium concentration,
K_L is the Langmuir sorption equilibrium constant (L mg^{-1} or L $mmol^{-1}$),
q_m is the maximum capacity (mg g^{-1} or mmol g^{-1}),
K_F is the Freundlich parameter in $mg^{1-1/n}$ $L^{1/n}$ g^{-1} ((mmol g^{-1})/(L $mmol^{-1}$)^{nF}),
n_F is the Freundlich parameter,
K_S is the affinity constant in (L $mmol^{-1}$),
n_S is the Sips parameter for surface heterogeneity description,
K_{RP} and n_{RP} are the Redlich–Peterson constants,
α_T is the adsorptive potential constant (mmol L^{-1}) and,
m_T is the Toth's heterogeneity factor.

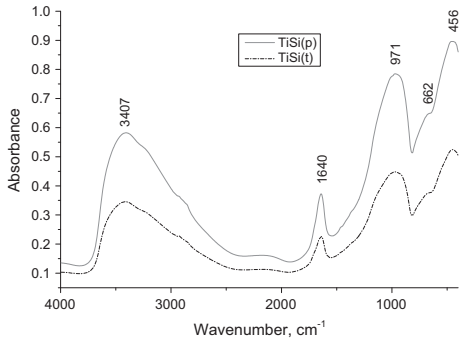

Fig. 1. MIR spectra of prepared TiSi materials.

The experimental kinetic data were fitted to the non-linear pseudo-first order model (PS1) and non-linear pseudo-second order model (PS2).

$$q_t = q_e^{-k_1 t} \quad (10)$$

$$q_t = \frac{k_2 q_e^2 t}{1 + k_2 q_e t} \quad (11)$$

where q_t and q_e are the adsorption capacity (mmol g^{-1}) at time t and at equilibrium respectively, while k_1 represents the PS1 rate constant (L min^{-1}), k_2 is the PS2 rate constant (g $mmol^{-1}$ min^{-1}) and $k_2 q_e^2$ represents the initial sorption rate.

The correlation between the experimental data and theoretical models was evaluated using the coefficient of determination (R^2). Calculations were carried out in Microsoft Excel.

$$R^2 = \frac{\sum (q_{e,exp} - \bar{q}_{e,exp})^2 - \sum (q_{e,exp} - q_{e,calc})^2}{\sum (q_{e,exp} - \bar{q}_{e,exp})^2} \quad (12)$$

where $q_{e,calc}$ is equilibrium capacity, calculated from the isotherm equation, $q_{e,exp}$ is equilibrium capacity obtained experimentally and $\bar{q}_{e,exp}$ is mean value of $q_{e,exp}$.

3. Results and discussion

3.1. Characterization of the adsorbent materials

The titanosilicate materials prepared using chemically pure and technical solutions of titanyl sulphate ($TiOSO_4$) were characterized by XRD and FTIR. The X-ray patterns of the obtained materials were found to be amorphous (not shown). Fig. 1 presents a summary of the MIR spectra of output xerogels. On both spectra, two intense bands are shown at about 1640 and 3407–3327 cm^{-1} respectively. These bands are associated with stretching and bending vibrations of O–H bonds in the molecules of H_2O. An intense large band half-width is also shown at about 1110–800 cm^{-1} and 450 cm^{-1}. These bands are related to the presence of Si–O and Ti–O bonds. On TiSi xerogel spectra, the most characteristic feature is the presence of a band at 971–956 cm^{-1}, which is related to the presence of oxygen bridged Si–O–Ti bonds. In addition, however, a shoulder is also visible at about 1068 cm^{-1} which indicates the presence of Si–O–Si bonds. A very broad band with a maximum at about 450 cm^{-1} is related to the bending vibrations of O–Si–O and O–Ti–O bonds [21,22]. The morphology of the chosen samples was estimated by SEM (Fig. 2). As the images indicate the surfaces of both the technical and the pure samples are uneven and porous.

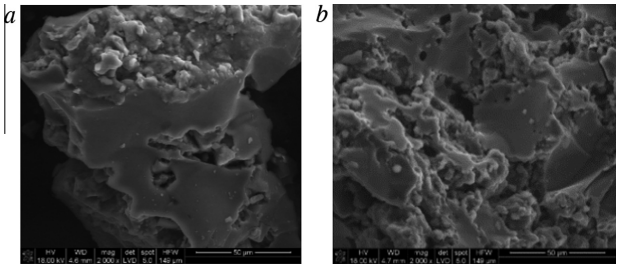

Fig. 2. SEM pictures of synthesized samples: (a) TiSi(p), and (b) TiSi(t).

The pore structure of the selected sorbents was defined by a low-temperature nitrogen adsorption/desorption technique. The isotherms and pore size distribution (DFT) are presented in Fig. 3. The titanosilicates produced are shown to have developed a porous structure. Type IV nitrogen adsorption isotherms with H2 hysteresis loops were derived from TiSi(p) IUPAC [23]. Isotherm and loop shape indicate the micro-mesopore structure of TiSi synthesized from a pure precursor. The H2 type of hysteresis loop suggests that the mesopores are ink-bottle shaped, with narrow necks and wide bodies. Type IV nitrogen adsorption isotherms with H1 hysteresis loops were derived from TiSi(t). The loops were narrow and not fully vertical over an appreciable range of N_2 uptake, suggesting a micro- meso- macropore structure for TiSi(t). It is probable that iron cations in the technical precursor promote the formation of a gel structure with minor differences between the mesopore necks and bodies. The pore size distribution verified the micro-mesopore structure of TiSi(p) and micro- meso- macropore structure of TiSi obtained from a technical precursor. The porous parameters were calculated using NOVAWin Surface Area Analyzer Quantachrome NOVA 2200 software. The results are presented in Table 1.

3.2. Adsorption experiments

In order to illustrate the effect of adsorbent mass on adsorption capacity, the ratio of adsorbent mass to aliquot volume is presented as a function of decontamination factor (DF). Decontamination factor was studied for ratios 50, 100, 200, 500, 1000, 2000 and 4000. Fig. 4 indicates that the maximum DF was observed at mass–volume ratio 100. Hence this value was used in subsequent adsorption investigations. It was worth to note that even at concentration of adsorbent 0.25 g L^{-1} (volume to mass ratio 4000) TiSis demonstrated high adsorption capacity to Sr^{2+} DF $\geqslant$ 90%.

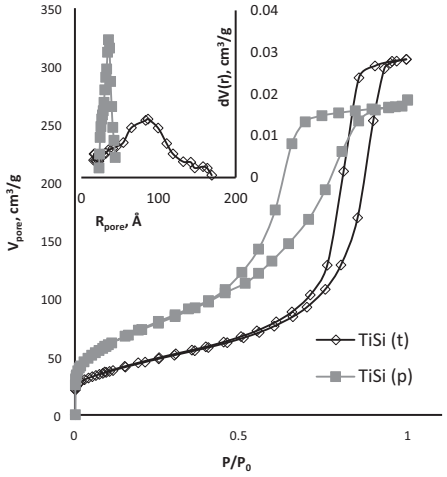

Fig. 3. Isotherms of nitrogen adsorption/desorption and pore size distribution of prepared titanosilicates.

Table 1
Structural properties of synthesized titanosilicates.

Sample name	S (m^2/g)	V_{total} (cm^3/g)	$V_{DR\ micro}$ (cm^3/g)	R_{pore} (nm)	$R_{micropore}$ (nm)
TiSi(t)	158.7	0.47	0.05	8.4	1.6
TiSi(p)	270.3	0.42	0.1	3.52	2.5

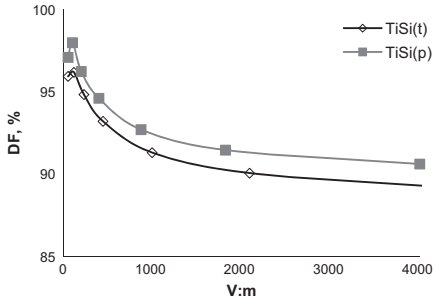

Fig. 4. Effect of volume to sorbent mass ratio on DF. Experimental conditions: initial concentrations of Sr^{2+} 0.5 g/l, background solution 0.1 M NaCl (pH = 7.08), ambient temperature.

The influence of initial strontium concentration on sorption properties was studied using solutions with different media in order to assess the impact of composition and concentration of background solution on titanosilicate ability to absorb Sr^{2+}. Data obtained with a water medium were used as a reference. High concentrations of sodium compounds in liquid radioactive wastes have been reported elsewhere [3,24], so the behavior of the material in the presence of these competitive ions was investigated. The simplest model solution, NaCl solution, was used to determine the competition effect of Na^+ and Sr^{2+} on the adsorption affinity of TiSi to Sr^{2+}. Ringer–Locke's solution was used to model both warm-blooded animal plasma [25] and seawater. A study of adsorbent affinity to Sr^{2+} in the presence of three competitive ions (Na^+, K^+, Ca^{2+}) was particularly interesting due to availability of these cations in seawater, blood plasma and drinking water. Concentrations of these cations are clearly lower in drinking water than in seawater, but it is possible to use the obtained data for predicting the sorption behavior of TiSi. As Fig. 5 shows, adsorption isotherms for different media have the H2 shape according to the Giles classification [26], which indicates the high affinity and selectivity to the adsorbate. It should be noted that background solution composition or concentration of competitive ions did not have any detectable effect on sorption capacity and the DF for both types of material was higher than 91% with initial strontium concentrations of up to 500 mg L^{-1}. Suppression of TiSi sorption capacity was observed in the presence of competitive ions at high initial strontium concentrations (1–5 g L^{-1}). Various reports indicate that sorption capacity of powder titanosilicate analogues (synthesised by precipitation method) decreases in the presence of high concentrations of competitive ions with much lower initial pollutant concentrations (10^{-9} ÷ 10^{-3} M) [24,27,28].

A combination of stereochemical and physicochemical factors affect the selectivity of the adsorbent, including hydrated and ionic radius, hydration energy and complexing ability, valency and electrostatic interaction, cation mobility and space requirement. On the one hand Na^+ has smaller ionic radii and higher mobility compared to K^+, Ca^{2+} and Sr^{2+} and lower hydration energy than Ca^{2+} and Sr^{2+}. On the other hand, Sr^{2+} has higher valency and complexing ability than Na+, but also higher hydration energy [29–33]. Since the adsorption isotherms had the same shape in different background solutions, the Sr^{2+} sorption process was of greater energy benefit than that of Na^+, K^+ or Ca^{2+}.

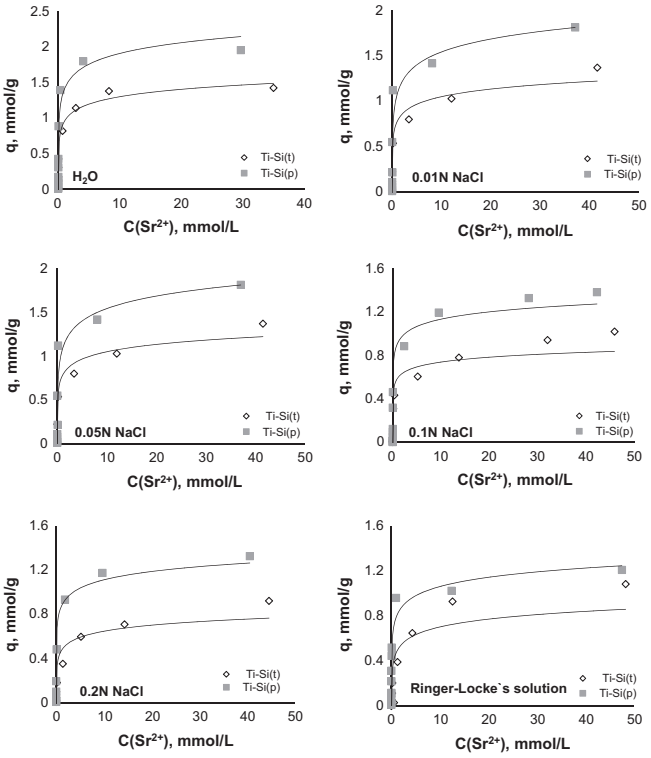

Fig. 5. Adsorption isotherms. Experimental conditions: initial strontium concentration range 10–5000 mg/l, solution volume 5 ml, contact time 24 h, media: water (pH = 6.78); 0.01 M, 0.05 M, 0.1 M, 0.2 M NaCl (pH = 7.08) and Ringer–Locke's solution (9 g L^{-1} of NaCl, 0.2 g L^{-1} of $NaHCO_3$, 0.2 g L^{-1} of KCl, 0.2 g L^{-1} of $CaCl_2$ and 1 g L^{-1} of D–glucose; pH = 8.07).

The maximum adsorption capacity of TiSi synthesized from pure precursors proved to be higher than that of TiSi obtained from technical precursors (Table 2). This could be ascribed to the lower specific surface of TiSi(t), resulting in a lower number of sorption active centres. Previous investigations with analogous materials synthesized by precipitation method with followed HTT [16] demonstrated that mesopores play a role in transporting small cations and that the sorption process mainly occurs in micropores. The micropore volume of TiSi samples declined steeply or was not available for N_2 and H_2O detecting molecules at all after adsorption tests [16]. Micropores and tunnels have been proposed as a sorption location for other crystalline TiSi ion-exchangers [10,34,35]. Thus reduction sorption also could be attributed to the lower micropore volume of TiSi synthesised from a technical precursor.

The sorption capacity of TiSi as a function of pH is presented in Fig. 6. The effect of pH ranging from 4 to 12 on the sorption properties of TiSi appears to be negligible. It is known that cation adsorption (cation exchange) increases with pH [28,36]. The high DF and low influence of pH illustrate the selectivity and chemical stability of the obtained amorphous materials. Below pH 4 sorption capacity suppression occurs, which can be explained by competition between Sr^{2+} and increased concentrations of anomalous mobile H^+ [28,36,37]. For example at pH 2 the DF for TiSi(p) declined by 10% and the DF of TiSi(t) by 27% compared to data at pH 4. An analogous effect has also been observed for powder titanosilicates [3,24].

The effect of contact time on the DF of Sr^{2+} was studied in time range 3–2880 min. The kinetic curves presented in Fig. 7 illustrate

Table 2
The maximum adsorption capacities of titanosilicate materials to Sr^{2+} at different background solutions.

q_{eq} (mmol/g)						
Background solution	H_2O	NaCl				Ringer–Locke's solution
		0.01 M	0.05 M	0.1 M	0.2 M	
Sample name						
TiSi(p)	1.95	1.81	1.40	1.38	1.32	1.21
TiSi(t)	1.42	1.37	1.13	1.02	0.92	1.08

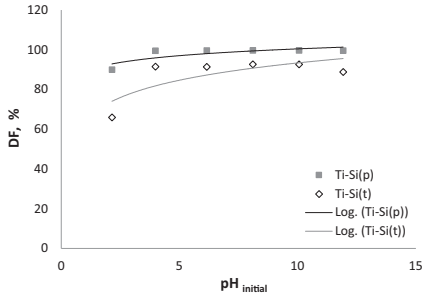

Fig. 6. Effect of pH on DF. Experimental conditions: pH from 2 to 12, Sr^{2+} initial concentration 0.5 g/l, solution volume 5 ml, contact time 24 h, ambient temperature.

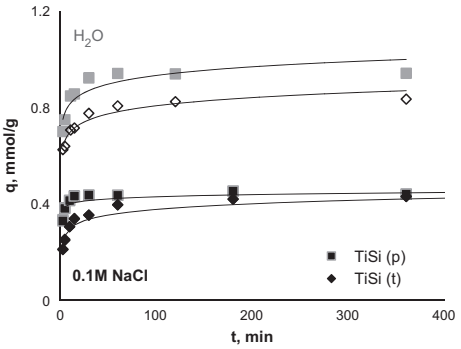

Fig. 7. Kinetics of Sr^{2+} sorption on titanosilicates. Experimental conditions: time range 3–2880 min, initial concentration of Sr^{2+} 0.5 g/l; solution volume 5 ml, background solutions – water (pH = 6.78) and 0.1 M NaCl (pH = 7.08), ambient temperature.

that both titanosilicate materials have the ability to remove Sr^{2+} from water at a relatively high rate. A DF of more than 70% was observed already after the first 3 min. Equilibrium was reached for TiSi(p) after a contact time of only 30 min while for TiSi(t) it took 60 min. The shape of the kinetic curves suggests that the sorption process could be separated into at least two steps: a high rate stage (the first 10–30 min) followed by a slow rate stage. The variation in Sr^{2+} uptake for different materials can be attributed to the microporous widths and micropore volume of these materials (Table 1). Consequently, TiSi(t) has smaller diameter and volume of micropores, which resulting in slower Sr^{2+} uptake.

A 0.1 M NaCl background illustrates the effect of Na^+/Sr^{2+} competition on the adsorption rate (Fig. 7). The medium impacted significantly: the presence of Na^+ decreases the uptake rate of TiSi(t) dramatically in the first 5 min. The initial parts of the kinetics curves became more vertical and the sorption capacity of both materials was suppressed. Nevertheless, both samples had reached equilibrium after the same length of time as in water. It was concluded that Na^+/Sr^{2+} competition affects titanosilicate sorption kinetics only during the high rate stage, i.e. in the first 10–30 min, while it does not have a significant impact on the slow rate stage.

Decontamination factor as a function of time at different temperatures is shown in Fig. 8. This figure indicates that sorption capacity and rate increase with increasing temperature. For instance, at 60 °C the DF was 91% after just 3 min of sorption. The graph showing $K_d(Sr^{2+})$ plotted against contact time illustrates that at elevated temperatures the sorption rate is higher on TiSi(p) than on TiSi(t), which could be attributed to the larger volume and width of micropores available in pure materials. The higher Sr^{2+} sorption rate and capacity at elevated temperatures illustrate the endothermic nature of sorption process on obtained TiSis and may suggest an activated sorption [38–41] mechanism. It is known that physisorption and ion exchange decrease with increasing temperature [42,43].

3.3. Reaction mechanism

In order to understand the mechanism of sorption on synthesized titanosilicates, the obtained experimental data were fitted to theoretical models. The samples were collected after adsorption tests and studied with SEM, XRD and XPS. The adsorption isotherm

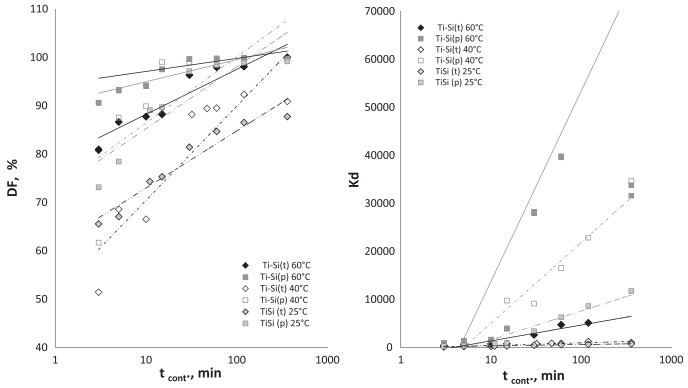

Fig. 8. Temperature effect on kinetics of Sr^{2+} sorption. Experimental conditions: contact time 3–360 min, Sr^{2+} initial concentration 0.5 g/l; solution volume 10 ml; adsorption temperature 25, 40 and 60 °C for medium 0.1 M NaCl (pH = 7.08).

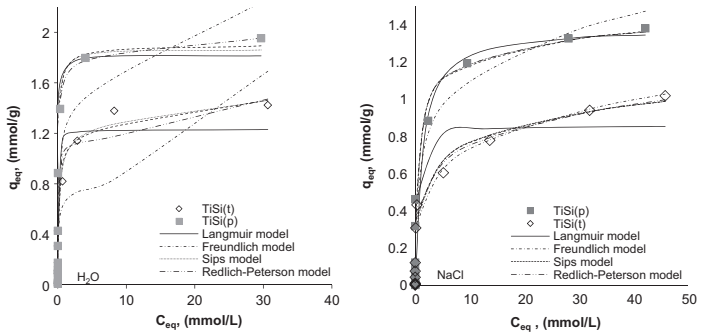

Fig. 9. Results of adsorption isotherm data modelling. Media: water and 0.1 M NaCl.

Table 3
Adsorption isotherm parameters obtained for synthesized TiSi.

Model	H_2O						0.01 M NaCl					
	TiSi(p)			TiSi(t)			TiSi(p)			TiSi(t)		
	q_{exp} (mmol/g)	$q_{calc.}$ (mmol/g)	R^2	q_{exp} (mmol/g)	$q_{calc.}$ (mmol/g)	R^2	q_{exp} (mmol/g)	$q_{calc.}$ (mmol/g)	R^2	q_{exp} (mmol/g)	$q_{calc.}$ (mmol/g)	R^2
Langmuir	1.95	1.81	0.981	1.42	1.23	0.938	1.38	1.35	0.917	1.02	0.85	0.943
Freundlich	1.95	2.24	0.837	1.42	1.69	0.709	1.38	1.48	0.971	1.02	1.03	0.987
Sips	1.95	1.86	0.982	1.42	1.46	0.978	1.38	1.36	0.987	1.02	0.99	0.990
Redlich–Peterson	1.95	1.98	0.990	1.42	1.47	0.967	1.38	1.40	0.998	1.02	1.0	0.996
Toth	1.95	1.89	0.985	1.42	1.46	0.979	1.38	1.37	0.992	1.02	0.99	0.993

data were fitted to the Langmuir, Freundlich, Sips, Redlich–Peterson and Toth models as shown in Fig. 9. This figure and Table 3 indicate that the Sips, Toth and Redlich–Peterson models, which consider surface heterogeneity assumptions and the possibility of interaction between the adsorbed substances, describe the experimental data better than the Langmuir and Freundlich models. The determination coefficient values were in the range of 0.967–0.996. The kinetic data were described using nonlinear pseudo-first order and pseudo-second order equations; the latter clearly described the data better ($R^2 \geqslant 0.993$; see Fig. 10 and Table 4). The pseudo-second order model assumes that the rate-limiting step is likely to be activated sorption or chemisorption involving valence forces, due to the exchange or sharing of electrons between the sorbent and sorbate [31,38,39,43].

The SEM images illustrate heterophase on the surfaces of both TiSi samples after sorption tests (Fig. 11). Acicular crystals in spherical aggregates measuring 2–5.5 μm were observed on both TiSi(p) and TiSi(t). Hexagonal crystals were 1–7 μm in size on TiSi(p) and 5–15 μm on TiSi(t). SEM–EDX mapping data showed the localization of more strontium at crystal regions than in any other area (Fig. 11). XPS data confirm the presence of strontium and carbon on both TiSi spectra after sorption tests (Fig. 12). Both crystal morphologies are typical for strontium carbonate [44–46]. The XRD pattern confirms the presence of the same strontianite mineral phase for both types of heterophase on the TiSi(p) sample after Sr^{2+} adsorption. At first this was attributed to epitaxial growth of $Sr_x(OH)_y(CO_3)_z$ on the alkalic sorbent surface during drying in air. Since no precipitation or changes in the Sr^{2+} concentration were detected during the control experiments and for initial tested solutions, it was concluded that strontium carbonate formation was possible only in the presence of TiSis for the studied Sr^{2+} concentrations and during the studied time. After the same tests for adsorption Cs^+ with Ca^{2+} cations and drying in air, however, no heterophase was detected. Therefore it was suggested that

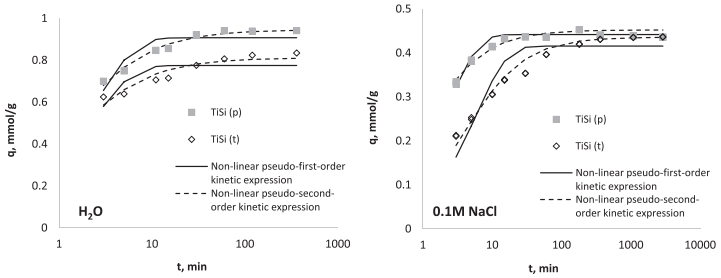

Fig. 10. Results of kinetic data modelling. Background solutions: water and 0.1 M NaCl.

Table 4
Kinetic parameters for strontium sorption on TiSi from 0.1 M NaCl.

Model	*t*, (°C)	TiSi(p)			TiSi(t)		
		$q_{exp.}$ (mmol/g)	$q_{calc.}$ (mmol/g)	R^2	$q_{exp.}$ (mmol/g)	$q_{calc.}$ (mmol/g)	R^2
Non-linear pseudo-first-order expression	25 [a]	0.941	0.907	0.784	0.835	0.775	0.575
	25	0.524	0.442	0.747	0.523	0.416	0.775
	40	0.950	0.956	0.862	0.864	0.852	0.932
	60	3.304	3.237	0.999	3.241	2.698	0.994
Non-linear pseudo-second-order expression	25 [a]	0.941	0.946	0.975	0.835	0.812	0.885
	25	0.524	0.452	0.802	0.523	0.436	0.919
	40	0.950	1.006	0.740	0.864	0.912	0.884
	60	3.304	3.291	1.0	3.241	2.698	0.993

[a] Adsorption from H_2O.

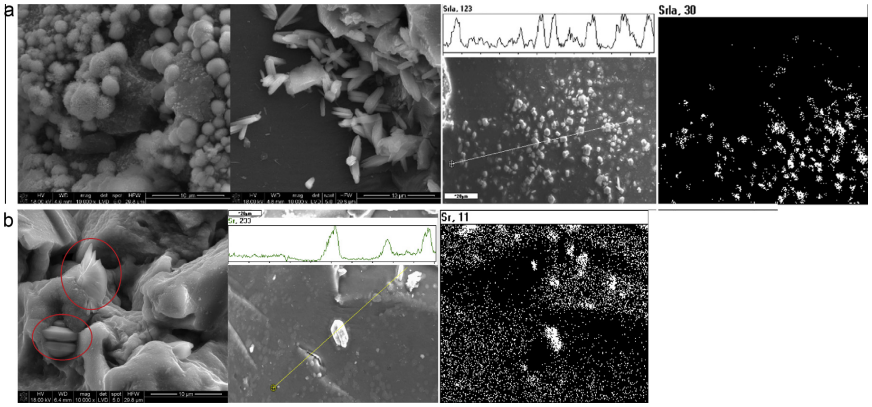

Fig. 11. SEM images with EDX of TiSis after Sr^{2+} adsorption: (a) TiSi(p), and (b) TiSi(t).

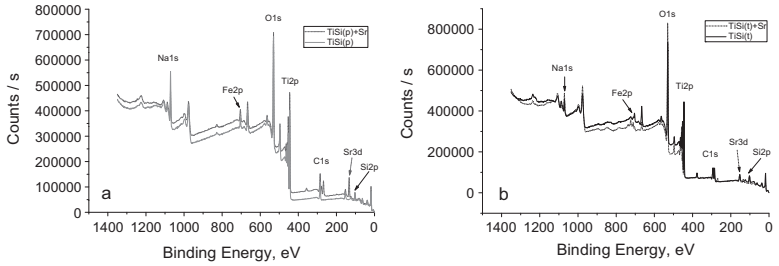

Fig. 12. XPS spectra of TiSi before and after sorption tests: (a) TiSi(p), and (b) TiSi(t).

one possible reason for Sr^{2+} selective sorption by TiSis could be participation of the CO_3^{2-}, $NaCO_3^-$ and HCO_3^- ions in the surface sorption process. Thus a hypothetical sorption mechanism was proposed.

Based on the FTIR results it was suggested that titanosilicate materials have the following surface ion-exchangeable groups: ≡Ti–O–Si–ONa, ≡Si–O–Ti–ONa and NaO–Si–O–Ti–ONa. It was entertained a possibility of the presence of the surface ion-exchange centres like ≡Si–O–Si–ONa and ≡Ti–O–Ti–ONa, but their role in titanosilicate adsorption capacity and selectivity was supposed negligibly. Based on literature data [9,35,47–49] it was assumed that the most active ion-exchange centres are ≡Ti–O–Si–ONa, ≡Si–O–Ti–ONa and NaO–Si–O–Ti–ONa.

The low dependence of TiSi sorption capacity on pH (pH ⩾ 4) and medium composition and concentration (up to 500 mg L^{-1} initial strontium concentration) suggests that Sr^{2+} sorption is dominated by inner sphere complexation [50]. It was reported elsewhere [29,30,33,40] that alkali and alkaline metals exchanged in dehydrated or partially dehydrated form. It follows from this assumption that cations reach the dehydration stage before the exchange. Dehydration is an endothermic process and its rate should increase with increasing temperature. This suggestion is in good agreement with

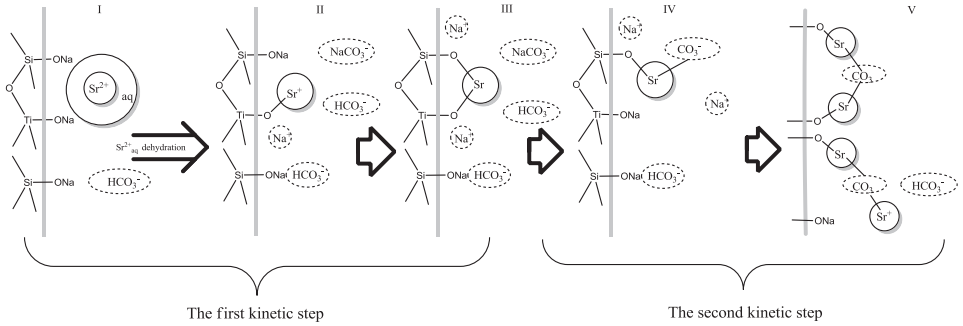

Fig. 13. Scheme of hypothetical sorption mechanism of Sr^{2+} on sol–gel prepared Titanosilicates.

the obtained kinetic data at elevated temperatures: sorption rates increased at the initial 'fast' parts of the kinetic curves.

During adsorption experiments pH rose by 2 ± 0.5, this was attributed to ion exchange between Sr^{2+} and Na^{+}. It is therefore proposed that the first step of the suggested mechanism is dehydration of hydrated strontium cation (Sr^{2+}_{aq}) near the exchange centre and ion exchange followed by inner sphere complexation. This step could represent the first kinetic stage with a high sorption rate while dehydration and/or inner sphere complexation could be the rate-limiting stages.

An interaction between the complexed by surface strontium and carbonate ions, which are usually present in aqueous solutions, was ascribed to the second step, at which the formation of strontium carbonate heterophase was observed. This step could represent the second part of the kinetic curve, with slow sorption rate and heterophase formation as a rate-limiting stage. This suggestion is in good agreement with the obtained sorption data at an elevated temperature: the rate and capacity of Sr^{2+} sorption were increased with increasing temperature. Fig. 13 presents a hypothetical scheme of the proposed mechanism. Additional studies of the sorption tests and sample drying in an inert atmosphere are needed, however, in order to confirm the proposed mechanism.

4. Conclusions

It was found that grade of precursor affected the pore structure of obtained titanosilicates, what reflected in different sorption capacity and uptake rate. TiSi prepared from a pure precursor had a higher adsorption capacity than material obtained from a technical precursor, estimated to be 1.95 mmol g^{-1} and 1.42 mmol g^{-1}, respectively. It was established that the Sr^{2+} uptake process on studied materials is rapid at ambient temperature and the rate increases at elevated temperatures. At room temperature the sorption process for both pure and technical TiSi follows pseudo-second order kinetic models. Scheme of possible Sr^{2+} sorption mechanism was proposed. The effect of competitive ions was investigated and no detectable effect on sorption capacity was observed for either type of material up to 500 mg L^{-1} initial strontium concentrations. Titanosilicates synthesized by the sol–gel method from pure and technical precursors proved to be highly efficient for strontium removal from aqueous solutions across a wide pH range. Obtained results lead to the conclusion that sol–gel synthesized TiSi can be effectively used for liquid radioactive wastewater decontamination instead of powder crystalline analogues TiSi [51,52]. Furthermore, it was suggested that proposed materials should be tested for blood plasma, mining, sea and drinking water purification from strontium.

Acknowledgments

The authors wish to thank Elisa Alasuvanto for her assistance with the sorption experiments. We are also grateful to Yurij M. Kylivnyk and Valerij I. Yakovlev for assisting with the precursor preparation and for our fruitful discussions. Furthermore, we thank Mukola M. Tsyba for supporting the porous investigations.

References

[1] H.N. Lee, in: S.E. Jørgensen, B.D. Fath (Eds.), Academic Press, Oxford, 2008. p. 2966.
[2] IAEA, IAEA, GC(57)/INF/3, 2013, 1.
[3] A.I. Bortun, L.N. Bortun, A. Clearfield, Solvent Extr. Ion Exch. 5 (1997) 909–929. http://dx.doi.org/10.1080/0736629970893451.
[4] A. Clearfield, Solvent Extr. Ion Exch. 18 (2000) 655. http://dx.doi.org/10.1080/073662900089347.
[5] F.J. Maringer, J. Šuráň, P. Kovář, B. Chauvenet, V. Peyres, E. García-Toraño, M.L. Cozzella, P. De Felice, B. Vodenik, M. Hult, U. Rosengård, M. Merimaa, L. Szücs, C. Jeffery, J.C.J. Dean, Z. Tymiński, D. Arnold, R. Hinca, G. Mirescu, Appl. Radiat. Isot. 81 (2013) 255. http://dx.doi.org/10.1016/j.apradiso.2013.03.046.
[6] N. Bolong, A.F. Ismail, M.R. Salim, T. Matsuura, Desalination 239 (2009) 229. http://dx.doi.org/10.1016/j.desal.2008.03.020.
[7] R.D. Ambashta, M.E.T. Sillanpää, J. Environ. Radioact. 105 (2012) 76. http://dx.doi.org/10.1016/j.jenvrad.2011.12.002.
[8] A. Clearfield, D.G. Medvedev, S. Kerlegon, T. Bosser, J.D. Burns, J. Milton, Solvent Extr. Ion Exch. 30 (2012) 229. http://dx.doi.org/10.1080/07366299.2011.639256.
[9] A. Tripathi, D.G. Medvedev, A. Clearfield, J. Solid State Chem. 178 (2005) 253. http://dx.doi.org/10.1016/j.jssc.2004.06.047.
[10] A. Clearfield, Solid State Sci. 3 (2001) 103. http://dx.doi.org/10.1016/S1293-2558(00)01113-4.
[11] J. Rocha, M.W. Anderson, Eur. J. Inorg. Chem. (2000) 801. doi:10.1002/(SICI)1099-0682(200005)2000:5<801::AID-EJIC801>3.0.CO;2-E.
[12] V.V. Strelko, J. Sol-Gel Sci. Technol. 68 (2013) 438. http://dx.doi.org/10.1007/s10971-013-2990-0.
[13] V.G. Kalenchuk, S.V. Meleshevych, V.A. Kanibolotsky, V.V. Strelko, O.V. Oleksienko, N.M. Patryliak, UA Patent 48457, 2010.
[14] V.V. Strelko, S.V. Meleshevych, V.A. Kanibolotsky, O.V. Oleksienko, UA Patent 66489, 2012.
[15] G. Lujaniene, S. Meleshevych, V. Kanibolotskyy, J. Sapolaite, V. Strelko, V. Remeikis, O. Oleksiienko, K. Ribokaite, T. Sciglo, J. Radioanal. Nucl. Chem. 282 (2009) 787. http://dx.doi.org/10.1007/s10967-009-0170-z.
[16] O.V. Oleksiienko, S.I. Meleshevych, V.V. Strelko, O.I. V'yunov, O.K. Matkovsky, V.G. Milgrandt, M.M. Tsyba, V.A. Kanibolotsky, Problems Chem. Chem. Technol. 2 (2013) 101.
[17] Y.S. Ho, J.F. Porter, G. McKay, Water Air Soil Poll. 141 (2002) 1.
[18] H.M.F. Freundlich, Z. Phys. Chem. 57A (1906) 358.
[19] Y. Liu, Y. Liu, Sep. Purif. Technol. 61 (2008) 229. http://dx.doi.org/10.1016/j.seppur.2007.10.002.
[20] K.Y. Foo, B.H. Hameed, Chem. Eng. J. 156 (2010) 2. http://dx.doi.org/10.1016/j.cej.2009.09.013.
[21] A.K. Brisdon, Inorganic Spectroscopic Methods, Oxford University Press, Oxford, 1998.
[22] K. Nakamoto, Infrared and Raman Spectra of Inorganic and Coordination Compounds, fifth ed., vol. A, Wiley-Interscience, New Jersey, U.S.A., 1997.
[23] K.S.W. Sing, Pure Appl. Chem. (1982) 2201. http://dx.doi.org/10.1351/pac198254112201.

[24] T. Möller, R. Harjula, J. Lehto, Sep. Purif. Technol. 28 (2002) 13. http://dx.doi.org/10.1016/S1383-5866(02)00004-7.
[25] L. Sehulster, R.Y.W. Chinn, MMWR 52 (RR10) (2003) 1.
[26] C.H. Giles, R.B. Mackay, J. Bacteriol. 89 (1965) 390.
[27] A. Clearfield, L.N. Bortun, A.I. Bortun, React. Funct. Polym. 43 (2000) 85. http://dx.doi.org/10.1016/S1381-5148(99)00005-X.
[28] A. Dyer, J. Newton, L. O'Brien, S. Owens, Microporous Mesoporous Mater. 120 (2009) 272. http://dx.doi.org/10.1016/j.micromeso.2008.11.016.
[29] I.M. El-Naggar, E.A. Mowafy, E.A. Abdel-Galil, Colloids Surf Physicochem. Eng. Aspects. 307 (2007) 77. http://dx.doi.org/10.1016/j.colsurfa.2007.05.004.
[30] J. Lehto, R. Harjula, Radiochim. Acta 86 (1999) 65. http://dx.doi.org/10.1524/ract.1999.86.12.65.
[31] I.M. Ali, E.S. Zakaria, H.F. Aly, J. Radioanal. Nucl. Chem. 285 (2010) 483. http://dx.doi.org/10.1007/s10967-010-0612-7.
[32] J. Burgess, Metal Ions in Solutions, Ellis Horwood, Chichester, England, 1978.
[33] I.M. El-Naggar, E.A. Mowafy, I.M. Ali, H.F. Aly, Adsorption 8 (2002) 225. http://dx.doi.org/10.1023/A:1021212617839.
[34] P. Sylvester, E.A. Behrens, G.M. Granziano, A. Clearfield, Sep. Sci. Technol. 34 (1999) 1981. http://dx.doi.org/10.1081/SS-100100750.
[35] E.A. Behrens, D.M. Poojary, A. Clearfield, Chem. Mater. 8 (1996) 1236. http://dx.doi.org/10.1021/cm950534c.
[36] A. Dyer, J. Newton, L. O'Brien, S. Owens, Microporous Mesoporous Mater. 117 (2009) 304. http://dx.doi.org/10.1016/j.micromeso.2008.07.003.
[37] A. Gierer, K. Wirtz, J. Chem. Phys. 17 (1949) 745. http://dx.doi.org/10.1063/1.1747388.
[38] T. Wolkenstein, Uspehi Fizicheskih Nauk. 2 (1953) 253.
[39] T. Wolkenstein, Electronic Processes on Semiconductor Surfaces during Chemisorption, Bureau, New York, 1991.
[40] W.G. Pollard, Phys. Rev. 56 (1939) 324. http://dx.doi.org/10.1103/PhysRev.56.324.
[41] L.E. Katz, L.J. Criscenti, C. Chen, J.P. Larentzos, H.M. Liljestrand, J. Colloid Interface Sci. 399 (2013) 68. http://dx.doi.org/10.1016/j.jcis.2012.05.011.
[42] W. Zuo, P. Han, Y. Li, X. Liu, X. He, R. Han, Water Treat. 12 (2009) 210. http://dx.doi.org/10.5004/dwt.2009.935.
[43] Y.S. Ho, G. McKay, Process Biochem. 34 (1999) 451. http://dx.doi.org/10.1016/S0032-9592(98)00112-5.
[44] M.A. Alavi, A. Morsali, Ultrason Sonochem. 17 (2010) 132. http://dx.doi.org/10.1016/j.ultsonch.2009.05.004.
[45] L. Li, R. Lin, Z. Tong, Q. Feng, Nanoscale Res. Lett. 7 (2012). http://dx.doi.org/10.1186/1556-276X-7-305.
[46] G. Guo, G. Yan, L. Wang, J. Huang, Mater Lett. 62 (2008) 4018. http://dx.doi.org/10.1016/j.matlet.2008.05.052.
[47] A. Tripathi, D.G. Medvedev, M. Nyman, A. Clearfield, J. Solid State Chem. 175 (2003). http://dx.doi.org/10.1016/S0022-4596(03)00145-2.
[48] D.M. Poojary, R.A. Cahill, A. Clearfield, Chem. Mater. 6 (1994) 2364. http://dx.doi.org/10.1021/cm00048a024.
[49] R.P. Nikolova, B.L. Shivachev, S. Ferdov, Microporous Mesoporous Mater. 165 (2013) 121. http://dx.doi.org/10.1016/j.micromeso.2012.07.053.
[50] W. Stumm, Chemistry of the Solid-Water Interface Processes at the Mineral-Water and Particle-Water Interface in Natural Systems, Wiley, New York, 1992.
[51] K. Popa, C.C. Pavel, Desalination 293 (2012) 78. http://dx.doi.org/10.1016/j.desal.2012.02.027.
[52] J.E. Miller, N.E. Brown, Sandia National Laboratories, SAND97-0771 l UC-721, UC-510, 1997.

Publication III

Oleksiienko, O., Levchuk, I., Sitarz, M., Meleshevych, S., Strelko, V., Sillanpää, M.

Adsorption of caesium (Cs^+) from aqueous solution by porous titanosilicate xerogels

Reprinted with permission from
Desalination and Water Treatment
Vol. 1, pp. 1–13, 2015

Desalination and Water Treatment
www.deswater.com
doi: 10.1080/19443994.2014.1003103

57 (2016) 5554–5566
March

Taylor & Francis
Taylor & Francis Group

Adsorption of caesium (Cs^+) from aqueous solution by porous titanosilicate xerogels

Olga Oleksiienko[a,b,*], Irina Levchuk[a], Maciej Sitarz[c], Svitlana Meleshevych[b], Volodymyr Strelko[b], Mika Sillanpää[a]

[a]*Laboratory of Green Chemistry, Lappeenranta University of Technology, Sammonkatu 12, Mikkeli 50130, Finland, Tel. +358 466297873; emails: ovalexis@gmail.com (O. Oleksiienko), Irina.Levchuk@lut.fi (I. Levchuk), Mika.Sillanpaa@lut.fi (M. Sillanpää)*
[b]*Institute of Sorption and Problems of Endoecology NAS of Ukraine, 13 General Naumov str., Kyiv 03164, Ukraine, emails: melesh@ispe.kiev.ua (S. Meleshevych), ispe@ispe.ldc.net (V. Strelko)*
[c]*Faculty of Materials Science and Ceramics, AGH University of Science and Technology, Al. Mickiewicza 30, Kraków 30059, Poland, email: msitarz@agh.edu.pl*

Received 12 September 2014; Accepted 21 December 2014

ABSTRACT

Two types of titanosilicate (TiSi) materials were synthesized by the sol–gel method using pure and technical precursors. All samples obtained were characterized using X-ray diffraction, FTIR in the mid-region and the low-temperature nitrogen adsorption/desorption technique. The synthesized xerogels were found to be amorphous with a developed porous structure. Solution pH, sample mass, initial Cs^+ concentration, competitive ions, contact time and temperature were studied for their influence on TiSi sorption ability. Both samples demonstrated a high capacity for caesium across a broad pH range of 2–12, and the adsorption isotherms were fitted to the Langmuir, Freundlich, Sips, Toth and Redlich–Peterson models, while the kinetic data were described using pseudo-first and pseudo-second models. All the TiSi samples were characterized by X-ray photoelectron spectroscopy and scanning electron microscopy with energy dispersive X-ray spectroscopy before and after the adsorption tests. Activated adsorption was proposed as a stage in the adsorption mechanism.

Keywords: Titanosilicates; Synthesis precursor; Xerogel pore structure; Adsorption capacity; Kinetic study

1. Introduction

Liquid radioactive waste (LRW) originates from many sources, including nuclear power plants, the mining industry, defence industry, nuclear medicine, nuclear research reactors and isotope laboratories [1,2]. The differences in the origins of LRW define the variety of its composition, which increase the requirements on decontamination materials and processes. There are many LRW treatment methods, including ion exchange, thermal evaporation, chemical precipitation, sedimentation and biological methods, and of those, ion exchange is currently the most commonly used method of LRW chemical processing [3–5]. Consequently, the synthesis of effective and stable ion exchange materials is a topical issue.

*Corresponding author.

It is well known that of the ion exchangers, ferrocyanides are the most selective for caesium, but they are efficient only in acidic medium [6–8]. In contrast, crystalline and poorly crystalline porous titanosilicates (TiSi) are effective and stable ion exchangers across a broad pH range [9–13]. Yet, both of these materials can be obtained in powder form only, which raises challenges for practical industrial applications. Recently, TiSi was synthesized by the sol–gel method [14,15], allowing to control the porosity, crystallinity, form and cost of the material. With the proposed method, it is possible to choose the fraction of sorbent particles (from 0.01 to 4 mm) after graining the xerogels. Sol–gel synthesis does not require cementation agents, which usually decrease the efficiency of sorption material. Therefore, the preparation time and the final cost of the product can also be reduced. Variation of the synthesis precursors broadened the field of sorbent application. For example, using an inexpensive (bulk grade) precursor yielded an ion exchanger for LRW mine and sea water. A pure precursor could achieve TiSi material for drinking water or blood plasma purification. This study seeks to investigate the influence of precursors on the sorption affinity and selectivity to Cs^+ of TiSi obtained by sol–gel synthesis using a chemically pure and technical solution of titanyl sulphate.

2. Experimental procedure

2.1. Chemicals

All chemicals used for the sorption tests (CsCl, NaCl, $NaHCO_3$, KCl, $CaCl_2$, H_2SO_4, HNO_3, HCl, NaOH, D-glucose) were of analytical grade (Sigma-Aldrich) and were used without further purification. Laboratory glassware washed with concentrated HCl or HNO_3 Milli-Q water (resistance 18.2 $M\Omega cm^{-1}$) was used for all experiments. Analytical grade solution of $TiCl_4$, technical solution of $TiOSO_4$ and technical solution of liquid glass ($Na_2O{\cdot}2.5SiO_2$) were bought from Ukrainian enterprises. Pure solution of $TiOSO_4$ was prepared by replacing Cl^- with SO_4^{2-} in $TiCl_4$.

2.2. Synthesis

TiSi samples were synthesized using the sol–gel method [14,15]. TiSi gels were obtained after a few minutes of intensive magnetic stirring of pure or technical $TiOSO_4$ solution (0.1 mmol), liquid glass (0.1 mmol) and NaOH (0.4 mmol) at room temperature. Thereafter, the prepared gels were hydrothermally treated (HTT) in steel autoclaves with Teflon beakers under autogenous pressure, and the synthesized TiSi gels were rinsed with water after HTT and dried at 80°C. Finally, the obtained xerogels were ground and sieved, and the fraction of 0.25–0.5 mm was used for the sorption tests.

2.3. Instrumentation

Specific surface area, pore size distribution and pore volume of TiSi xerogels were measured using a Quantachrome NOVA 2,200 surface area analyser. X-ray diffraction (XRD) patterns were obtained using DRON-4–07 (CuKα; 2θ = 5–80° step $\Delta 2\theta$ = 0.02°). FTIR spectra were recorded with a Bruker Vertex 70v spectrometer and collected in the mid (MIR)-region (4,000–100 cm^{-1}) after 128 scans at 4 cm^{-1} resolution. All samples were prepared by the standard KBr pellet method, and the microstructure of the produced materials was determined by scanning electron microscopy (SEM, Nova Nano SEM 200, FEI Company) with an attachment for the chemical analysis of specimens in micro-areas with energy dispersive X-ray spectroscopy. The experiment was carried out under low vacuum conditions in secondary electron mode. X-ray photoelectron spectroscopy (XPS) data were collected using a Thermo Fisher Scientific ESCALAB 250Xi Photoelectron Spectrometer. Measurements of pH were taken with a calibrated WTW 340i pH meter (WTW, Weilheim, Germany). A ST15 rotary shaker (CAT, M. Zipperer GmbH, Staufen, Germany) and IKA KS 4000i control shaker–incubator were used for sorption tests. To determine cation concentrations during the adsorption tests, an Agilent 7500ce inductively coupled plasma with mass detector was used.

2.4. Adsorption Experiments

Adsorption tests were conducted in batch technique using a shaker–incubator and rotary shaker with initial solutions prepared from solids. Aqueous solutions of caesium were used with different media: water, NaCl and Ringer–Locke's (RL) solution. All batch tests were performed in polypropylene tubes. Polypropylene syringe filters (size 0.45 μm) were used for sorbent separation. Adsorption capacity was studied as a function of pH, adsorbent mass, initial concentration, contact time, temperature, composition and concentration of background solution.

The influence of pH on the TiSi adsorption capacity (q) in Cs^+ solutions with water and 0.1 M NaCl media was evaluated, and experiments were conducted at a pH range of 2–12, with an initial Cs^+ concentration of 3.76 mmol L^{-1}. The solution volume to sorbent mass ratio (V:m) was 100, and the contact time was 24 h at ambient temperature (25 ± 2°C).

Effects of V:m ratio on the sorption capacity of TiSi were studied at V:m ratios ranging from 100 to 2,000 with an initial Cs^+ concentration of 3.76 mmol L^{-1}, water and 0.1 M NaCl as the solution media. pH was kept at 6.1 ± 0.2 and the contact time was 24 h at ambient temperature.

Influences of initial Cs^+ concentrations on q_{TiSi} were investigated in solutions with different media: water (pH = 6.1 ± 0.2); NaCl at concentrations of 0.05, 0.1 and 0.2 (pH = 6.1 ± 0.2); and RL solution (153.85 mmol L^{-1} of NaCl; 2.38 mmol L^{-1} of $NaHCO_3$; 2.68 mmol L^{-1} of KCl; 1.8 mmol L^{-1} of $CaCl_2$ and 5.55 mmol L^{-1} of D-glucose; pH = 8.07). Initial Cs^+ concentrations varied from 0.075 to 37.62 mmol L^{-1}, the V:m ratio was 100, and the contact time was 24 h at ambient temperature.

Effect of contact time (t) on q_{TiSi} was estimated using Cs^+ solutions with water, 0.1 M NaCl and RL media. Investigations were performed in a time range of 3–2,880 min at ambient temperature using an initial Cs^+ concentration of 3.76 mmol L^{-1} and a V:m ratio of 100.

Temperature effects on the Cs^+ solutions with 0.1 M NaCl and RL matrices were also investigated. Sorption tests were conducted at temperatures of 25, 40 and 60°C. The contact time was 3–180 min, the initial Cs^+ concentration was 3.76 mmol L^{-1}, and the V:m ratio was 100.

Adsorption capacity (q), distribution coefficient (K_d) and decontamination factor (DF) were calculated using the following equations:

$$\text{Adsorption capacity: } q = \Delta C \cdot \frac{V}{m} \tag{1}$$

where $\Delta C = C_o - C_t$, and C_o and C_t are the initial concentration and the concentration at time t of caesium in solution (mg L^{-1} or mmol L^{-1}), V is the aliquot volume (mL), and m is the mass of the adsorbent (g).

$$\text{Distribution coefficient: } K_d = \frac{\Delta C}{C_t} \cdot \frac{V}{m} \tag{2}$$

$$\text{Decontamination factor: } DF = (\Delta C \cdot 100\%)/C_0 \tag{3}$$

Experimental data were fitted to the Langmuir, Freundlich, Sips, Redlich–Peterson and Toth models, which are commonly used to describe liquid–solid systems [16] by the following equations:

$$\text{Langmuir: } q_e = \frac{q_m K_L C_e}{1 + K_L C_e} \tag{4}$$

where q_e is the adsorption capacity (mmol g^{-1}), C_e is the equilibrium concentration of the adsorbate (mmol L^{-1}), q_m is the maximum adsorption capacity of the adsorbent (mmol g^{-1}), and K_L is the Langmuir sorption equilibrium constant (L $mmol^{-1}$).

$$\text{Freundlich: } q_e = K_F C_e^{1/n_F} \tag{5}$$

where K_F ((mmol g^{-1})/(L $mmol^{-1})^{n}_F$) and n_F are the Freundlich adsorption constants.

$$\text{Sips: } q_e = \frac{q_m (K_S C_e)^{n_S}}{1 + (K_S C_e)^{n_S}} \tag{6}$$

where K_S is the affinity constant (L $mmol^{-1}$), and n_S is the Sips parameter for surface heterogeneity description.

$$\text{Redlich–Peterson: } q_e = \frac{q_m K_{RP} C_e}{1 + (K_{RP} C_e)^{n_{RP}}} \tag{7}$$

where K_{RP} and n_{RP} are the Redlich–Peterson constants.

$$\text{Toth: } q_e = \frac{q_m C_e}{(a_T + C_e^{m_T})^{\frac{1}{m_T}}} \tag{8}$$

where a_T is the adsorptive potential constant (mmol L^{-1}), and m_T is the Toth's heterogeneity factor.

The experimental kinetic data were fitted to the following models:

$$\text{nonlinear pseudo-first-order model: } q_t = q_e^{-k_1 t} \tag{9}$$

$$\text{linear pseudo-second-order model: } \frac{t}{q_t} = \frac{1}{k_2 q_e^2} + \frac{t}{q_e} \tag{10}$$

$$\text{and nonlinear pseudo-second-order model: } q_t = \frac{k_2 q_e^2 t}{1 + k_2 q_e t} \tag{11}$$

where q_t and q_e are the adsorption capacity (mmol g^{-1}) at time t and at equilibrium, respectively, while k_1 is the pseudo-first rate constant (L min^{-1}), k_2 is the pseudo-second rate constant (g $mmol^{-1}$ min^{-1}), and $k_2 q_e^2$ is the initial sorption rate.

To evaluate the correlation between the experimental data and the theoretical models, the coefficient of determination (R^2) was maximized with the MS Excel 2007 Solver Add-in:

$$R^2 = \frac{\sum(q_{e,exp} - \bar{q}_{e,exp})^2 - \sum(q_{e,exp} - q_{e,calc})^2}{\sum(q_{e,exp} - \bar{q}_{e,exp})^2} \quad (12)$$

where $q_{e,calc}$ is calculated from the isotherm equation equilibrium capacity, $q_{e,exp}$ is the experimentally obtained equilibrium capacity, and $\bar{q}_{e,exp}$ is the mean value of $q_{e,exp}$.

3. Results and discussion

3.1. Material characterization

The influence of the precursor on the adsorption affinity to Cs^+ was investigated for two types of TiSi xerogels: pure TiSi [TiSi(p)] obtained using a chemically pure solution of titanyl sulphate ($TiOSO_4$) and TiSi [TiSi(t)] synthesized using a technical solution of $TiOSO_4$. Both ion exchange materials were achieved in the amorphous phase, and therefore, no XRD patterns are shown here. FTIR studies were conducted in the mid-region (Fig. 1, with the analysed band positions and the suggested functional groups superimposed). As this figure shows, the bands most characteristic of bridged Si–O–Ti are present on both spectra at 971–956 cm^{-1}.

To investigate the pore structure of the xerogels, a low-temperature nitrogen adsorption/desorption technique was applied obtaining the following structural characteristics: TiSi(p) xerogel: Micro–mesopore structure, specific surface area (S_{BET})—270.3 $m^2 g^{-1}$, total pore volume (V_{total})—0.42 $cm^3 g^{-1}$, Dubinin–Radushkevich's micropore volume ($V_{DR\ micro}$)—0.1 $cm^3 g^{-1}$ and pore radius (R_{pore})—3.52 nm, $R_{micropore}$—2.5 nm; TiSi (t) xerogel: Micro–meso–macropore structure, S_{BET}—158.7 $m^2 g^{-1}$, V_{total}—0.47 $cm^3 g^{-1}$, $V_{DR\ micro}$—0.05 $cm^3 g^{-1}$, R_{pore}—8.4 nm, $R_{micropore}$—1.6 nm [17].

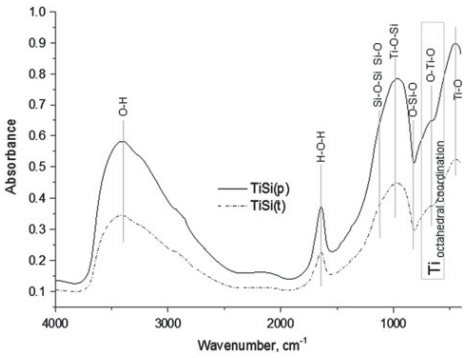

Fig. 1. FTIR spectrum of TiSi samples. Fraction size was 0.25–0.5 mm.

3.2. Sorption experiments

Adsorption studies were carried out with different background solutions in order to investigate the influence of competitive ions on the sorption capacity and selectivity of the obtained TiSi materials. Water was used as a medium for collecting the reference data. Of particular interest was the competition between Cs^+ and Na^+, since Na^+ is present at the highest concentration among the competing ions in real wastewaters and it is also present in drinking, sea and mine water [18–22]. To investigate this influence of the Cs^+/Na^+ competition and concentrations of competitive ions on the TiSi sorption capability, the NaCl background solution was used. With the RL solution, the ability of TiSi xerogels to remove Cs^+ in the presence of three competitive ions was examined: Na^+, K^+, Ca^{2+} [23,24]. Using the obtained data, the sorption ability and sorption mechanism of the synthesized materials in blood plasma, sea and drinking water can be predicted. As concentrations of these cations are substantially lower in drinking water than in sea water, it can be assumed that the TiSi sorption capability in drinking water ranges between the sorption capabilities for pure water and for the RL solution.

The first step of the current investigation was to determine the ability of the sol–gel synthesized TiSis to remove caesium from 3.76 mmol L^{-1} Cs^+ solution in water and 0.1 M NaCl background solution within a pH range from 2 to 12 (Fig. 2). It was found that in contrast to ferrocyanide powders, the obtained TiSi xerogels were able to remove Cs^+ across a broad pH range (2–12) with a high DF (DF ≥ 91% in water medium). It was shown that an increasing pH slightly reduces the DF for both materials in water: in 0.1 M NaCl, the reduction in DF for TiSi(p) was 14% and for TiSi(t) 10%. As has been shown by previous investigators, the cation adsorption, and cation exchange in particular, usually increases with pH [9,19,25–28]. Yet, the observed reverse effect could indicate a more complex Cs^+ removal mechanism than physisorption or ion exchange.

The selectivity of a sorption material is defined as a combination of physicochemical and stereochemical factors, such as ionic and hydrated radius, valency and electrostatic interaction, complexing ability and hydration energy, cation mobility and space requirement [25,26,29–31]. Consequently, sorption suppression could be attributed to an increased concentration of Na^+, since Na^+ has a higher complexing ability,

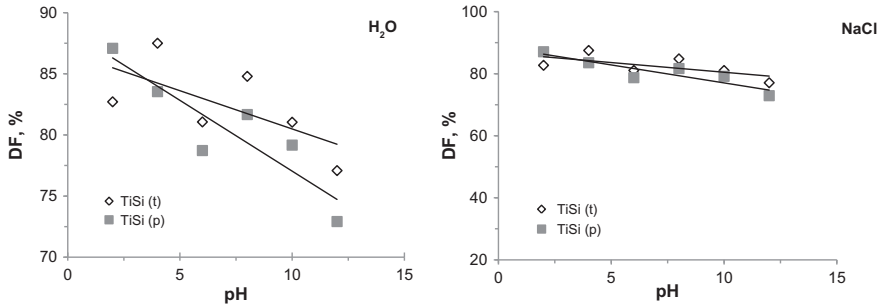

Fig. 2. Effect of pH on the DF of TiSi. Experimental conditions: pH from 2 to 12, initial Cs^+ concentration 3.76 mmol L^{-1}, water and 0.1 M NaCl media, *V:m* ratio 100, contact time 24 h, ambient temperature.

smaller hydrated and ionic radii and higher cation mobility than Cs^+. A similar suppression of H^+ to Cs^+ exchange was observed in the acidic pH region for the H-form of the powder TiSi [9,18]. Yet, such a low suppression at the evaluating concentration of competitive ions could also be related to the fact that Cs^+ has a lower (−263 kJ mol^{-1}) hydration energy than Na^+ (−405 kJ mol^{-1}), which may testify to the greater energy benefit of Cs uptake by TiSi xerogels [26,31,32]. The high DF and low influence of pH indicate the selectivity, chemical stability and capability of the synthesized materials for the effective removal of Cs cations from water and Na^+-containing solutions with a substantial initial Cs^+ concentration.

The second step of the present investigation was to determine the sufficient dose of the studied materials. In both studied background solutions, the adsorption ability decreased by less than 8% at a *V:m* ratio range from 100 to 2,000 for TiSi(t) and for both TiSi in water only (Fig. 3). It was found that the DF for both TiSis was around 90% at a sorbent concentration of 0.5 g L^{-1} and an initial Cs^+ concentration in water of 0.5 g L^{-1} (3.76 mmol L^{-1}). In a 0.1 M NaCl medium, the materials behaved differently: the DF of TiSi(p) decreased by 22% at a *V:m* ratio range from 100 to 2,000, which is 30% less than in water. This observation could be explained by the different porous structures of the obtained materials. Previous studies showed that sorption of Cs^+ and other alkali and alkaline earth cations occurs in micropores [10,11,33–35], and for TiSi with a rigid crystalline structure, less than 55% of ion exchange sites could be occupied by Cs^+ [19,33,36]. Poorly crystalline- or amorphous-structured TiSi with a developed porosity have better accessibility of Cs^+ ion-exchangeable sites [11,19]. An analogous situation was expected to occur with amorphous TiSi

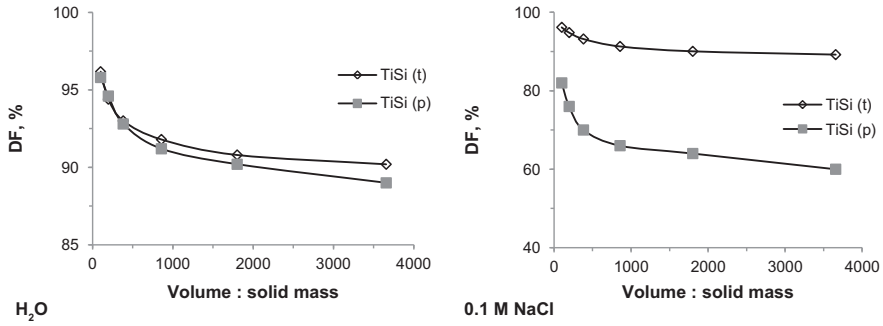

Fig. 3. Effect of the ratio between volume and sorbent mass on DF. Experimental conditions: initial Cs^+ concentrations 3.76 mmol L^{-1}, water and 0.1 M NaCl background solutions, ambient temperature.

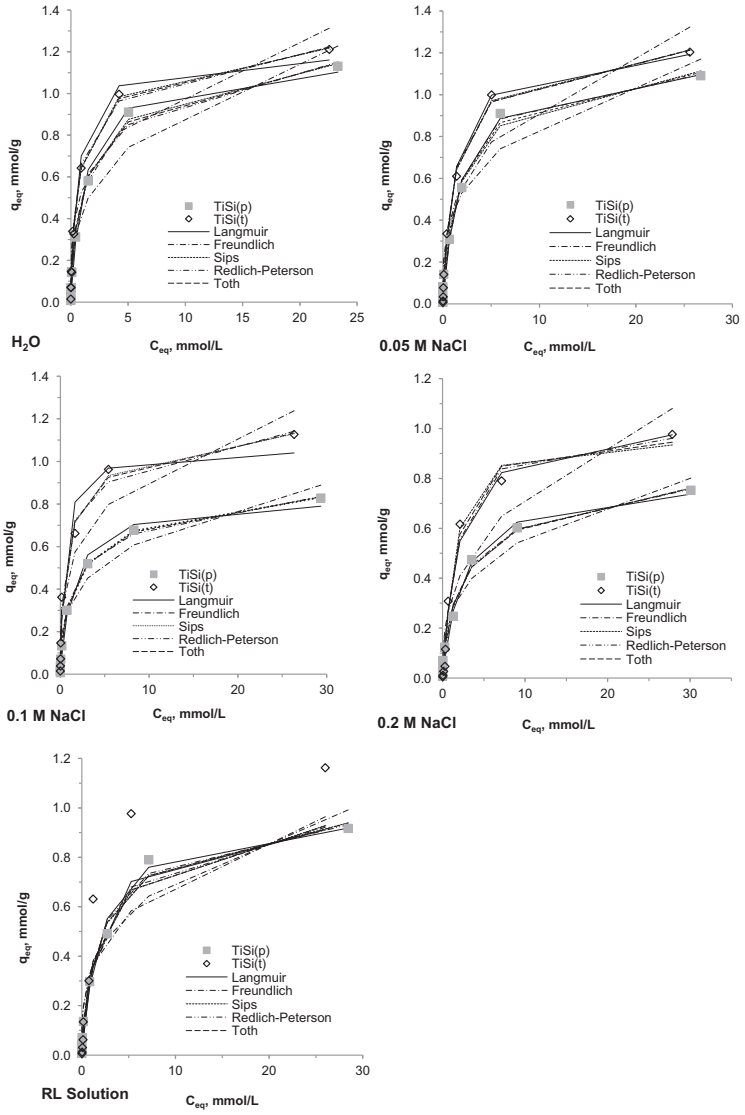

Fig. 4. Adsorption isotherms; experimental results: dots; results of modelling: lines. Experimental conditions: initial Cs^+ concentration range 0.075–37.62 mmol L^{-1}; *V*:*m* ratio 100; contact time 24 h; water; 0.05 M, 0.1 M and 0.2 M NaCl and RL solution media, ambient temperature.

xerogels. Therefore, it was suggested that the lower TiSi(t) micropore volume was compensated by a larger pore size, whereas large Cs^+ cations had fewer steric restrictions. Based on that assumption, it was decided to use a 10 g·L^{-1} dose of sorbent materials (*V*:*m* ratio 100) for further investigations, since at that dose a higher DF was observed.

The influence of the initial Cs^+ concentration on the TiSi adsorption ability was tested in water; 0.05, 0.1, 0.2 M NaCl; and RL solution at ambient temperature (Fig. 4). It was found that the adsorption isotherms for both xerogels synthesized from all studied media belong to the H2 shape according to the Giles classification [37,38]. This indicates the high affinity and selectivity to the adsorbate of the TiSi xerogels, and consequently, since the sorption isotherms were the same shape in different media, supposingly, there was a greater energy benefit in sorption with Cs^+ than with other competitive ions. It is important to note that the medium composition or concentration of competitive ions did not have any detectable influence up to an initial Cs^+ concentration of 3.76 mmol L^{-1}. An essential decrease in the TiSi capacity was observed at high initial Cs^+ concentrations (7.52–37.62 mmol L^{-1}). The results of the equilibrium adsorption capacity (q_{eq}) of the xerogels in different media show that q_{eq} was slightly lower at 0.05 M NaCl than in water (Table 1). In more complex and concentrated media, however, the adsorption capacity was 20–30% lower than in water, an effect that was similarly observed for powder TiSi [9,39]. It was found that TiSi(p) demonstrated $K_d(Cs^+)$ from 1×10^6 to 3×10^6 in all studied background solutions with a 0.075 mmol L^{-1} initial Cs^+ concentration, while TiSi(t) demonstrated $K_d(Cs^+)$ 8×10^6 in water with a 0.75 mmol L^{-1} initial Cs^+ concentration. The same order of K_d values was reported for crystalline powder TiSi analogues and ferrocyanides [7,19,28,36,40–42]. Thus, it can be concluded that (I) the TiSi(p) xerogel can be an efficient sorption material for drinking water and blood plasma and (II) the TiSi(t) xerogel can be used as an efficient sorbent for LRW, sea and mining water due to its higher q_{eq} in all tested media as well as wider pores, allowing the adsorption of cation pollutants both smaller and larger than Cs^+.

Kinetic tests were performed in water, 0.1 M NaCl and RL solution with an initial Cs^+ concentration of 3.76 mmol L^{-1}, the concentration at which the vertical part of the isotherms finished. Obviously, such a high initial concentration is not typical for real wastewaters, but in the vertical isotherm region at concentrations of 0.75 mmol L^{-1} and lower, kinetics is so fast that no substantial influence is observed [11,13]. For all experiments, the contact time ranged from 3 to 2,880 min at

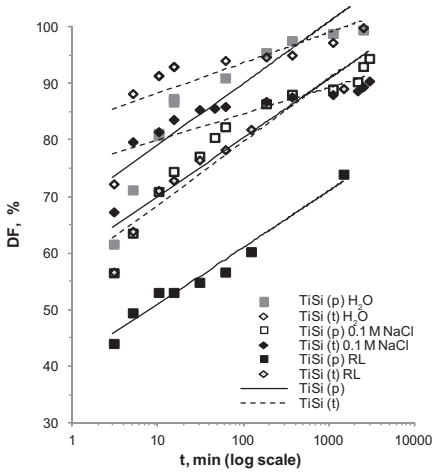

Fig. 5. Kinetics of Cs^+ sorption by TiSis. Experimental conditions: time range 3–2,880 min; initial Cs^+ concentration 3.76 mmol L^{-1}; *V*:*m* ratio 100; water and 0.1 M NaCl and RL background solutions, ambient temperature.

Table 1
The maximum adsorption capacity of Cs^+ by TiSi materials for different background solutions

	Background solution				
	q_{eq}, mmol/g				
		NaCl			
Sample type	H_2O	0.05 M	0.1 M	0.2 M	RL solution
TiSi(p)	1.13	1.091	0.83	0.75	0.92
TiSi(t)	1.21	1.203	1.13	0.98	1.16

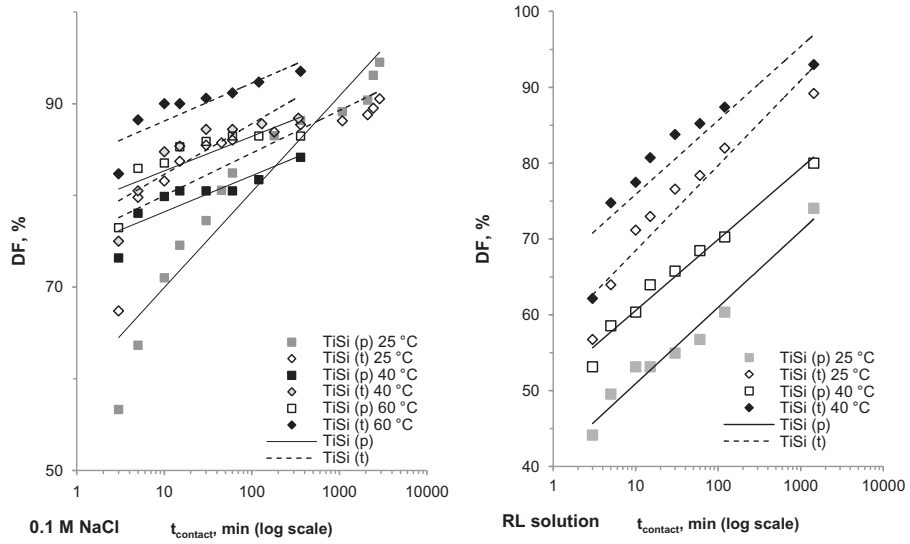

Fig. 6. Temperature effect on the kinetics of Cs^+ sorption. Experimental conditions: contact time 3–120 min; initial Cs^+ concentration 3.76 mmol L^{-1}; *V*:*m* ratio 100; temperature of adsorption 25, 40 and 60˚C for 0.1 M NaCl and RL media.

Table 2
Adsorption isotherm parameters obtained for studied TiSi

	TiSi(p)			TiSi(t)			TiSi(p)			TiSi(t)		
Model	q_{exp} mmol g^{-1}	q_{calc} mmol g^{-1}	R^2	q_{exp} mmol g^{-1}	q_{calc} mmol g^{-1}	R^2	q_{exp} mmol g^{-1}	q_{calc} mmol g^{-1}	R^2	q_{exp} mmol g^{-1}	q_{calc} mmol g^{-1}	R^2
Medium	H_2O						0.05 M NaCl					
Langmuir	1.131	1.102	0.985	1.211	1.161	0.979	1.091	1.096	0.987	1.203	1.193	0.996
Freundlich	1.131	1.228	0.958	1.211	1.313	0.943	1.091	1.170	0.965	1.203	1.324	0.929
Sips	1.131	1.144	0.998	1.211	1.218	0.991	1.091	1.114	0.990	1.203	1.213	0.998
Redlich–Peterson	1.131	1.151	0.993	1.211	1.223	0.988	1.091	1.098	0.987	1.203	1.213	0.997
Toth	1.131	1.148	0.996	1.211	1.22	0.990	1.091	1.107	0.988	1.203	1.215	0.998
Medium	0.1 M NaCl						0.2 M NaCl					
Langmuir	0.828	0.789	0.987	1.127	1.040	0.966	0.753	0.738	0.986	0.977	0.974	0.984
Freundlich	0.828	0.889	0.973	1.127	1.238	0.934	0.753	0.801	0.974	0.977	1.080	0.887
Sips	0.828	0.830	0.999	1.127	1.130	0.990	0.753	0.760	0.993	0.977	0.934	0.990
Redlich–Peterson	0.828	0.836	0.997	1.127	1.142	0.991	0.753	0.758	0.989	0.977	0.985	0.985
Toth	0.828	0.833	0.998	1.127	1.133	0.991	0.753	0.761	0.991	0.977	0.945	0.987
Medium	Ringer–Locke's solution											
Langmuir	0.917	0.918	0.985	1.162	0.912	0.979						
Freundlich	0.917	0.992	0.964	1.162	0.964	0.970						
Sips	0.917	0.940	0.990	1.162	0.929	0.978						
Redlich–Peterson	0.917	0.932	0.985	1.162	0.921	0.979						
Toth	0.917	0.938	0.988	1.162	0.927	0.979						

ambient temperature (Fig. 5), where both TiSi samples were able to remove Cs^+ rapidly and effectively. The difference in the kinetic rates for the obtained materials was attributed to their different porous structure. Fig. 5 illustrates that the TiSi(t) DF reached 91% after only 10 min of contact time, which is attributed to the wider pore distribution and larger average transport pore radius of the technical sample. Yet, pure TiSi showed a slower sorption kinetic and reached a DF of over 91% only after 1 h. In addition, the sorption rate of TiSi(p) was three times slower in a 0.1 M NaCl medium than in water and the sorption capacity of TiSi(t) was decreased in a 0.1 M NaCl medium with the kinetic curve having the same shape as for kinetic tests in water. It is noteworthy that the RL solution reduced the sorption rate and capacity of TiSi(t) only in the first 3 h, after which the DF was higher than that found in a NaCl background solution. In the RL medium, two additional competitive ions decreased the rate of TiSi(p) by two orders in the studied time period. As the TiSi(p) xerogel has wider micropores than TiSi(t), it was concluded that the transport pore radius is a rate-limiting parameter for TiSi xerogels, and presumably, the micropore volume will also play an essential role with increasing contact time.

Fig. 6 shows the effect of temperature on the kinetic of Cs^+ sorption by TiSi. Raising the

Table 3
Kinetic parameters for caesium sorption by TiSi for 0.1 M NaCl

		TiSi(p)				TiSi(t)			
Model	t ℃	q_{exp} mg g^{-1}	q_{calc} mg g^{-1}	k	R^2	q_{exp} mg g^{-1}	q_{calc} mg g^{-1}	k	R^2
Nonlinear pseudo-first-order expression	25*	0.39	0.38	0.51	0.999	0.39	0.38	0.51	0.968
	25	0.37	0.34	0.48	0.794	0.35	0.33	0.29	0.793
	40	0.40	0.36	0.29	0.000	0.35	0.31	0.53	0.575
	60	0.48	0.45	0.46	0.883	0.39	0.39	0.40	0.930
Linear pseudo-second-order expression	25*	0.39	0.41	2.89×10^{-6}	0.988	0.39	0.39	9.34×10^{-7}	0.738
	25	0.37	0.37	1.73×10^{-6}	0.394	0.35	0.37	2.76×10^{-6}	0.315
	40	0.40	0.41	1.05×10^{-5}	0.425	0.35	0.35	1.76×10^{-5}	0.708
	60	0.48	0.49	0.93×10^{-6}	0.367	0.39	0.37	9.37×10^{-6}	0.184
Nonlinear pseudo-second-order expression	25*	0.39	0.38	0.01	0.999	0.39	0.38	0.03	1.000
	25	0.37	0.35	0.03	0.818	0.35	0.34	0.01	0.980
	40	0.40	0.39	0.02	0.962	0.35	0.32	0.03	0.786
	60	0.48	0.47	0.02	0.908	0.39	0.39	0.02	0.912

*Adsorption for H_2O.

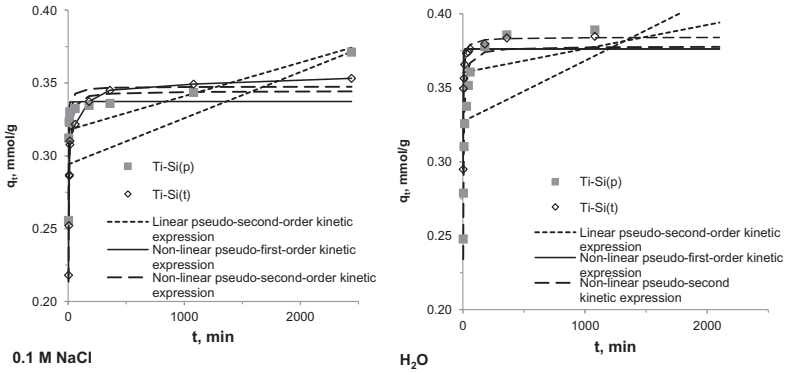

Fig. 7. Kinetic data of Cs^+ sorption fitted to theoretical models; experimental results: dots; results of modelling: lines.

temperature had a substantial impact on the TiSi(p) adsorption rate in the first 10 min. A temperature increase from 25 to 40˚C raises the DF by 20% in the first 3 min, whereas the DF after 10 min at 40˚C reached the same level as after 60 min at 25˚C. It was found that the Cs^+ uptake increased by 10% every 15–20˚C in 0.1 M NaCl and in RL solution for both tested materials. Following the literature, sorption processes based on physical phenomena such as ion exchange decrease with increasing temperature [7,43,44]. The increasing sorption rate could be attributed to the enhanced mobility of caesium ions or suggests that Cs^+ is removed by an activated sorption (when the elevated temperature raises the concentration of dehydrated Cs^+), or chemisorption mechanism [45–48].

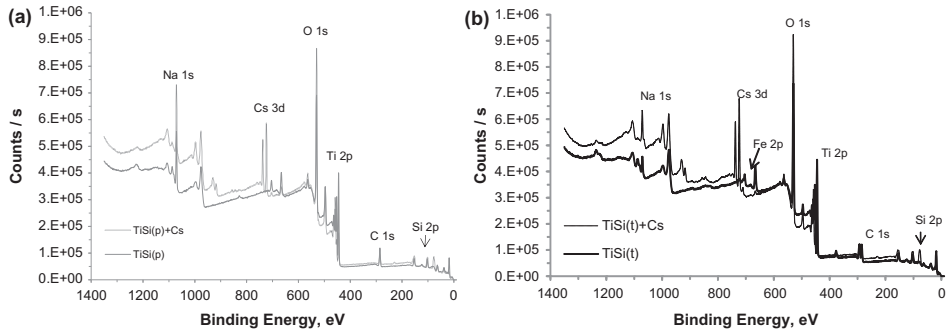

Fig. 8. XPS spectra of TiSi xerogels before and after the adsorption tests: (a) TiSi(p); (b) TiSi(t).

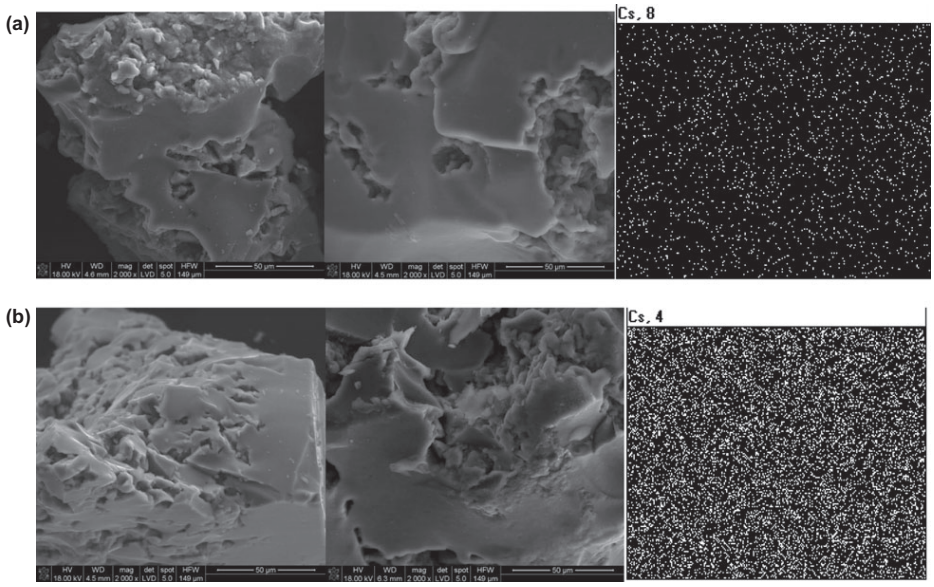

Fig. 9. SEM images of *a*-TiSi(p) and *b*-TiSi(t) xerogels before and after Cs^+ adsorption with mapping data for samples after the sorption tests.

In order to understand the character of the sorption process, the obtained isotherm adsorption data were fitted to theoretical models: the Langmuir, Freundlich, Sips, Redlich–Peterson and Toth models. Table 2 and Fig. 4 demonstrate that the adsorption isotherms of TiSi are better described by models that consider surface heterogeneity. While the Sips model describes TiSi(p) experimental data better than the other models in all matrices ($R^2 \geq 0.99$), the isotherms of TiSi(t) fits best to the Sips, Redlich–Peterson and Toth models ($R^2 \geq 0.98$). Fitting the adsorption kinetic experimental data to nonlinear pseudo-first-order, linear and nonlinear pseudo-second order-theoretical models showed that the nonlinear pseudosecond order model proved to be the most suitable model ($R^2 \geq 0.98$, Table 3 and Fig. 7). This pseudo-second-order model suggests chemisorption involving exchanging or sharing of electrons as a rate-limiting step [45–49]. Since the pH dependence for both TiSi was atypical for a physisorption process and the sorption rate rose with elevated temperature and kinetic data followed pseudo-second-order models, activated sorption or chemisorption mechanisms were considered.

XRD, XPS and SEM data were collected for both TiSi materials before and after the adsorption tests, and the XPS spectra show the presence of caesium on both studied materials (Fig. 8). An XRD is not shown since the samples stayed amorphous and no crystalline heterophase appeared. Fig. 9 illustrates that the sample microstructure did not change during the sorption test and no heterophase was observed. Mapping data demonstrated the homogeneous distribution of Cs across the studied surfaces.

Activated sorption was thus considered as the mechanism of the Cs^+ uptake. Activated adsorption allows to ascribe the obtained temperature dependence to the endothermic nature of the cation dehydrating process. Earlier investigations showed that cations exchanged in dehydrated form for TiSis and for sodium titanate [30,31]. An activated adsorption mechanism implies the presence in the TiSi xerogel structure of micropores whose radius is very similar to that of dehydrated Cs^+ ions. Fine fixation of Cs^+ in channels with an inner radius of similar size to Cs^+ ionic radii was reported for crystalline TiSis with a developed framework structure [11,19].

4. Conclusions

As could been shown, substituting a pure precursor with a technical one not only reduces the final cost of the material but promotes the formation of xerogels with a more developed mesoporous structure. TiSis obtained by sol–gel synthesis from pure and technical precursors proved highly efficient sorbent materials for caesium uptake from aqueous solutions across a broad pH range. The adsorption affinity of TiSi(t) was not substantially higher than that of the material obtained from a pure precursor. Studies of the influence of background solution showed that neither medium composition nor competitive ion concentration had a detectable impact on sorption ability. Selectivity was observed up to an initial Cs^+ concentration of 3.76 mmol L^{-1}. At ambient temperature, the process rate is relatively rapid with slight increases at higher temperatures, and the sorption process for pure and technical TiSi with water and 0.1 M NaCl media follows the pseudo-second-order kinetic model. It is proposed that the Cs^+ uptake occurs via an activated sorption mechanism. Furthermore, it is assumed that the TiSi xerogel structure contained micropores with radii very similar in size to Cs^+ ion radii. In addition, the obtained data proved that synthesized TiSi(p) xerogels can be effective sorption materials for drinking water as well as blood plasma, whereas the TiSi(t) xerogel could be an efficient sorbent for LRW, sea and mine water, due to its high adsorption capacity in all tested media and wide pore size distribution for the adsorption of cationic pollutants both smaller and larger than Cs^+.

Acknowledgements

The authors thank Elisa Alasuvanto for her assistance with the sorption experiments. We are also grateful to Yurij M. Kylivnyk and Valerij I. Yakovlev for assisting with the precursor preparation and for our fruitful discussions. Furthermore, we thank Mukola M. Tsyba for supporting the porous investigations and Kate Sotejeff–Wilson for our fruitful discussions and language support. We greatly acknowledge Prof. Christian Wolkersdorfer for fruitful discussions, language and technical support.

References

[1] R.D. Ambashta, M.E.T. Sillanpää, Membrane purification in radioactive waste management: A short review, J. Environ. Radioact. 105 (2012) 76–84.
[2] UNSCEAR (United Nations Scientific Committee on the Effects of Atomic Radiation), Sources and Effects of Ionizing Radiation, United Nations Scientific Committee on the Effects of Atomic Radiation, UNSCEAR, New York, NY, 2011.
[3] IAEA, Improvements of Radioactive Waste Management at WWER Nuclear Power Plants, IAEA, TECDOC-1492, Vienna, 2006.

[4] IAEA, Nuclear Safety Review, IAEA, GC(57)/INF/3, Vienna, 2013, 1.
[5] R. Harjula, J. Lehto, A. Paajanen, E. Tusa, P. Yarnell, Use inorganic ion exchange materials as precoat filters for nuclear waste effluent treatment, React. Funct. Polym. 60 (2004) 85–95.
[6] IAEA, Technologies for Remediation of Radioactively Contaminated Sites, Technologies for Remediation of Radioactively Contaminated Sites, IAEA, TECDOC-1086, Vienna, 1999.
[7] F. Han, G. Zhang, P. Gu, Adsorption kinetics and equilibrium modeling of cesium on copper ferrocyanide, J. Radioanal. Nucl. Chem. 295 (2013) 369–377.
[8] T.D. Clarke, C.M. Wai, Selective removal of cesium from acid solutions with immobilized copper ferrocyanide, J. Anal. Chem. 70 (1998) 3708–3711.
[9] T. Möller, R. Harjula, J. Lehto, Ion exchange of 85Sr, 134Cs and 57Co in sodium titanosilicate and the effect of crystallinity on selectivity, Sep. Purif. Technol. 28 (2002) 13–23.
[10] A. Clearfield, D.G. Medvedev, S. Kerlegon, T. Bosser, J.D. Burns, J. Milton, Rates of exchange of Cs^+ and Sr^{2+} for poorly crystalline sodium titanium silicate (CST) in nuclear waste systems, Solvent Extr. Ion Exch. 30 (2012) 229–243.
[11] O.V. Oleksiienko, S.I. Meleshevych, V.V. Strelko, O.I. V'yunov, O.K. Matkovsky, V.G. Milgrandt, M.M. Tsyba, V.A. Kanibolotsky, Effect of hydrothermal treatment on the formation of the porous structure titanosilicates, Prob. Chem. Chem. Technol. 2 (2013) 101–105.
[12] K. Popa, C.C. Pavel, Radioactive wastewaters purification using titanosilicates materials: State of the art and perspectives, Desalination 293 (2012) 78–86.
[13] G. Lujaniene, S. Meleshevych, V. Kanibolotskyy, J. Sapolaite, V. Strelko, V. Remeikis, O. Oleksiienko, K. Ribokaite, T. Sciglo, Application of inorganic sorbents for removal of Cs, Sr, Pu and Am from contaminated solutions, J. Radioanal. Nucl. Chem. 282 (2009) 787–791.
[14] V.G. Kalenchuk, S.V. Meleshevych, V.A. Kanibolotsky, V.V. Strelko, O.V. Oleksiienko, N.M. Patryliak, A method for producing titanosilicate ionexchanger, UA patent 48457 (2010).
[15] V.V. Strelko, S.V. Meleshevych, V.A. Kanibolotsky, O.V. Oleksiienko, A method for producing titanosilicate ionexchanger, UA patent 66489 (2012).
[16] K.Y. Foo, B.H. Hameed, Insights into the modeling of adsorption isotherm systems, Chem. Eng. J. 156 (2010) 2–10.
[17] O. Oleksiienko, I. Levchuk, M. Sitarz, S. Meleshevych, V. Strelko, M. Sillanpää, Removal of strontium (Sr^{2+}) from aqueous solutions with titanosilicates obtained by the sol–gel method, J. Colloid Interface Sci. 438 (2015) 159–168.
[18] A.I. Bortun, L.N. Bortun, A. Clearfield, Evaluation of synthetic inorganic ion exchangers for cesium and strontium removal from contaminated groundwater and wastewater, Solvent Extr. Ion Exch. 15 (1997) 909–929.
[19] E.A. Behrens, A. Clearfield, Titanium silicates, $M_3HTi_4O_4(SiO_4)_3{\cdot}4H_2O$ ($M = Na^+$, K^+), with three-dimensional tunnel structures for the selective removal of strontium and cesium from wastewater solutions, Microporous Mater. 11 (1997) 65–75.
[20] A. Tripathi, D.G. Medvedev, A. Clearfield, The crystal structures of strontium exchanged sodium titanosilicates in relation to selectivity for nuclear waste treatment, J. Solid State Chem. 178 (2005) 253–261.
[21] F.J. Maringer, J. Šuráň, P. Kovář, B. Chauvenet, V. Peyres, E. García-Toraño, M.L. Cozzella, P. De Felice, B. Vodenik, M. Hult, U. Rosengård, M. Merimaa, L. Szücs, C. Jeffery, J.C.J. Dean, Z. Tymiński, D. Arnold, R. Hinca, G. Mirescu, Radioactive waste management: Review on clearance levels and acceptance criteria legislation, requirements and standards, Appl. Radiat. Isot. 81 (2013) 255–260.
[22] C. Wolkersdorfer, Water Management at Abandoned Flooded Underground Mines—Fundamentals, Tracer Tests, Modelling, Water Treatment, Springer, Heidelberg, 2008.
[23] J.P. Steel, The treatment of certain mental diseases by Ringer–Locke solution, Br. Med. J. 2 (1927) 1177–1178.
[24] W.R. Amberson, J. Flexner, F.R. Steggerda, A.G. Mulder, M.J. Tendler, D.S. Pankratz, E.P. Laug, On the use of Ringer–Locke solutions containing hemoglobin as a substitute for normal blood in mammals, J. Cell. Comp. Physiol. 5 (1934) 359–382.
[25] A. Dyer, J. Newton, L. O'Brien, S. Owens, Studies on a synthetic sitinakite-type silicotitanate cation exchanger: Part 1: Measurement of cation exchange diffusion coefficients, Microporous Mesoporous Mater. 117 (2009) 304–308.
[26] A. Dyer, J. Newton, L. O'Brien, S. Owens, Studies on a synthetic sitinakite-type silicotitanate cation exchanger. Part 2. Effect of alkaline earth and alkali metals on the uptake of Cs and Sr radioisotopes, Microporous Mesoporous Mater. 120 (2009) 272–277.
[27] N. Bolong, A.F. Ismail, M.R. Salim, T. Matsuura, A review of the effects of emerging contaminants in wastewater and options for their removal, Desalination 239 (2009) 229–246.
[28] V.V. Milyutin, S.V. Mikheev, V.M. Gelis, E.A. Kozlitin, Sorption of cesium on ferrocyanide sorbents from highly saline solutions, Radiochemistry 51 (2009) 298–300.
[29] I.M. El-Naggar, E.A. Mowafy, E.A. Abdel-Galil, Diffusion mechanism of certain fission products in the particles of silico(IV)titanate, Colloids Surf., A 307 (2007) 77–82.
[30] I.M. El-Naggar, E.A. Mowafy, I.M. Ali, H.F. Aly, Synthesis and sorption behaviour of some radioactive nuclides on sodium titanate as cation exchanger, Adsorption 8 (2002) 225–234.
[31] I.M. Ali, E.S. Zakaria, H.F. Aly, Highly effective removal of ^{22}Na, ^{134}Cs and ^{60}Co from aqueous solutions by titanosilicate: A radiotracer study, J. Radioanal. Nucl. Chem. 285 (2010) 483–489.
[32] J. Burgess, Metal ions in solutions, Ellis Horwood, Chichester, 1978.
[33] E.A. Behrens, D.M. Poojary, A. Clearfield, Syntheses, crystal structures, and ion-exchange properties of porous titanosilicates, $HM_3Ti_4O_4(SiO_4)3A\ 4H_2O$ ($M = H^+$, K^+, Cs^+), structural analogues of the mineral pharmacosiderite, Chem. Mater. 8 (1996) 1236–1244.
[34] P. Sylvester, E.A. Behrens, G.M. Graziano, A. Clearfield, An assessment of inorganic ion-exchange materials for the removal of strontium from simulated hanford tank wastes, Sep. Sci. Technol. 34 (1999) 1981–1992.

[35] A. Clearfield, Inorganic ion exchangers, past, present, and future, Solvent Extr. Ion Exch. 18 (2000) 655–678.
[36] D.M. Poojary, R.A. Cahill, A. Clearfield, Synthesis, crystal structures, and ion-exchange properties of a novel porous titanosilicate, Chem. Mater. 6 (1994) 2364–2368.
[37] C.H. Giles, R.B. Mackay, Adsorption of cationic (basic) dyes by fixed yeast cells, J. Bacteriol. 89 (1965) 390–397.
[38] C.H. Giles, T.H. MacEwan, S.N. Nakhwa, D. Smith, 786. Studies in adsorption. Part XI. A system of classification of solution adsorption isotherms, and its use in diagnosis of adsorption mechanisms and in measurement of specific surface areas of solids, J. Chem. Soc. (1960) 3973–3993.
[39] J. Lehto, R. Harjula, Selective separation of radionuclides from nuclear waste solutions with inorganic ion exchangers, Radiochim. Acta 86 (1999) 65–70.
[40] D. Huys, L.H. Baetslé, A new series of synthetic acid stable mineral ion exchangers—I. Ferrocyanide-molybdate (FeMo), J. Inorg. Nucl. Chem. 26 (1964) 1329–1331.
[41] A. Clearfield, L.N. Bortun, A.I. Bortun, Alkali metal ion exchange by the framework titanium silicate $M_2Ti_2O_3SiO_4{\cdot}nH_2O$ (M=H, Na), React. Funct. Polym. 43 (2000) 85–95.
[42] A. Clearfield, Structure and ion exchange properties of tunnel type titanium silicates, Solid State Sci. 3 (2001) 103–112.
[43] L.E. Katz, L.J. Criscenti, C. Chen, J.P. Larentzos, H.M. Liljestrand, Temperature effects on alkaline earth metal ions adsorption on gibbsite: Approaches from macroscopic sorption experiments and molecular dynamics simulations, J. Colloid Interface Sci. 399 (2013) 68–76.
[44] W. Zuo, P. Han, Y. Li, X. Liu, X. He, R. Han, Equilibrium, kinetic and mechanism study for adsorption of neutral red onto rise husk, Desalin. Water Treat. 12 (2009) 210–218.
[45] Y.S. Ho, J.F. Porter, G. McKay, Equilibrium isotherm studies for the sorption of divalent metal ions onto peat: Copper, nickel and lead single component systems, Water Air Soil Pollut. 141 (2002) 1–33.
[46] Y.S. Ho, G. McKay, Pseudo-second order model for sorption processes, Process Biochem. 34 (1999) 451–465.
[47] T. Wolkenstein, Electronic processes on semiconductor surfaces during chemisorption, Bureau, New York, NY, 1991.
[48] T. Wolkenstein, Activated adsorption on semiconductors, Uspehi Fizicheskih Nauk. 2 (1953) 253–270.
[49] W.G. Pollard, Use of surface states to explain activated adsorption, Phys. Rev. 56 (1939) 324–336.

Publication IV

Lujaniene G., Meleshevych S., Kanibolotskyy V., Mazeika K., Strelko V., Remeikis V., Oleksienko O., Sapolaite J.
Application inorganic sorbents for removal Cs, Sr, Pu and Am from contaminated solutions
Reprinted with permission from
Journal of radioanalytical and nuclear chemistry
Vol. 282(3), pp. 787–791, 2009

J Radioanal Nucl Chem (2009) 282:787–791
DOI 10.1007/s10967-009-0170-z

Application of inorganic sorbents for removal of Cs, Sr, Pu and Am from contaminated solutions

G. Lujanienė · S. Meleshevych · V. Kanibolotskyy · J. Šapolaitė · V. Strelko · V. Remeikis · O. Oleksienko · K. Ribokaitė · T. Ščiglo

Received: 19 June 2009 / Published online: 10 July 2009

Abstract A sorption ability of titanium silicates (TiSi) and iron oxides towards Cs, Sr, Pu and Am was tested using the laboratory batch method. The obtained results are expressed as distribution coefficients (K_d). TiSi synthesised using $TiOSO_4$ revealed better sorption ability towards all studied radionuclides in comparison with TiSi produced on the basis of $TiCl_4$. The K_d values ranged from 3.9×10^2 to 1.6×10^5 mL g^{-1} for Sr, from 6 to 4.1×10^4 mL g^{-1} for Cs, from 2.2×10^2 to 2.6×10^5 mL g^{-1} for Pu and from 50 to 1.6×10^4 mL g^{-1} for Am. The highest Pu K_d values (9×10^3–6.2×10^4 mL g^{-1}) and better kinetics were found for iron oxides.

Keywords Titanium silicates · Iron oxides · Cs · Sr · Pu · Am · Distribution coefficients

Introduction

Anthropogenic radionuclides such as ^{137}Cs, ^{90}Sr, $^{239,240}Pu$ and ^{241}Am which originated as global fallout, as discharges from nuclear industry, as well as releases into the environment after various accidents, have recently been studied at ultra-low level concentrations [1–3]. From these studies it is evident that one of the important needs nowadays is development of effective and low-cost water treatment methods, capable of reducing discharges to low-levels for the purpose of protection of the environment from anthropogenic radionuclides and their harmful ecological effects.

The most commonly applied treatment technologies involve precipitation, ion exchange, evaporation and solvent extraction. Recently growing concern about contamination of the environment by radioactive and non-radioactive pollutants resulted in intensive studies related to the development of new technologies for separation of radionuclides from liquid waste. These new technologies should be based on highly selective materials, which are hard to decompose over a wide range of pH, which remain stable at high temperatures, and which are resistant to ionizing radiation. These materials have to be able to operate in the presence of a great excess of competitive ions, organic solvents and oxidants [4–6]. Crystalline TiSi showed high selectivity towards low concentrations of Cs^+ and Sr^{2+} ions in high ionic strength solutions, typical for high level waste cooling ponds, and it also showed a capability of operating under chemically harsh conditions [7].

Complicated technologies, high capital and regeneration costs stimulated studies to develop low-cost and efficient technologies based on naturally occurring minerals such as zeolites and clay minerals [8, 9]. Another option could be an application of amorphous porous mixed oxides—a rapidly developing class of materials prepared by sol-gel procedures, the main benefit of which are very simple procedures conducted under mild reaction conditions in the ambient atmosphere [10].

In addition, ferrites and a variety of iron-containing minerals such as akaganeite, feroxyhyte, ferrihydrite, goethite, hematite, lepidocrocite, maghemite and magnetite have also been widely used as inorganic ion exchangers for

G. Lujanienė (✉) · J. Šapolaitė · V. Remeikis · K. Ribokaitė · T. Ščiglo
Institute of Physics, Savanorių 231, 02300 Vilnius, Lithuania
e-mail: lujaniene@ar.fi.lt

S. Meleshevych · V. Kanibolotskyy · V. Strelko · O. Oleksienko
Institute for Sorption and Problems of Endoecology, Generala Naumova 13, 03164 Kiev, Ukraine

the treatment of liquid wastes containing radioactive and hazardous metals. These materials have certain advantages, and they are also a promising class of materials for radioactive waste treatment. Ferrites possess the property of spontaneous magnetization, they are low-cost crystalline materials soluble only in a strong acid and they can be used for efficient separation by magnetic methods [11, 12].

The aim of this study was to prepare amorphous TiSi by sol-gel procedures under mild conditions using cheap a local technical titanyl sulfate, and organic complexions as stock materials. Further, to carry out a comparative assessment of possible application of these low-cost synthetic inorganic sorbents with conventional and natural sorptive materials in liquid waste treatment technologies to remove long-lived radionuclides such as Cs, Sr, Pu and Am.

Experimental

Synthesis of titanium silicates and iron oxides

The co-precipitation and the sol-gel method followed by the hydrothermal treatment was used for the synthesis of TiSi from alkaline solution Me_2O–TiO_2–SiO_2. The synthesis of TiSi by the precipitation method was conducted under mild conditions. TiSi's were synthesised using cheap raw materials available in the Ukraine—alkali silicate (Na_2SiO_3), potassium/sodium methylsilicates $CH_3Si(OH)_2ONa/K$, titanium tetrachloride ($TiCl_4$) and titanyl sulphate ($TiOSO_4$) [13, 14]. The following prepared ion exchangers were used in sorption experiments: TiSi 17(SO_4), TiSi 20(Cl), TiSi 30(SO_4), TiSi 32(SO_4), TiSi 55(Cl), TiSi 57+58(Cl), TiSi 59(Cl).

The sol-gel method of the TiSi synthesis developed at the Institute for Sorption and Problems of Endoecology of the National Academy of Sciences of Ukraine is based on the use of local technical titanyl sulfate and organic complexions as stock-materials for the synthesis [13]. Ion exchangers TiSi 82-1, TiSi 84-3, TiSi 40, TiSi 86-1, TiSi 84-4, TiSi 82'-1, TiSi 86-4, TiSi 82-3 were tested for their sorption characteristics towards Cs, Sr, Pu and Am.

Iron oxide synthesis was performed using methods described in publications with some modifications. Synthesis details are given in the previously published paper [15].

Physical and chemical analysis of prepared samples

The BET surface area and pore volume of studied sorbents were determined using the nitrogen adsorption/desorption method at a liquid nitrogen temperature by means of a surface area analyzer NOVA 2200. The pore size distribution was determined according to the BJH method using the desorption branch of the isotherms. The X-ray diffraction studies of the prepared Ti–Si sorbents were conducted with an automated diffractometer (DRON -4-07) using Ni-filtered Cu Kα radiation. Synthesised iron oxides were characterised by using Mössbauer spectroscopy [15].

Synthesised sorbents, both titanium silicates and iron oxides, as well as natural clay minerals with 14% of montmorillonite were used in sorption experiments. The laboratory batch method was applied to determine the distribution coefficient values of Cs, Sr, Pu and Am radionuclides (background electrolyte—0.1 mol L^{-1} Na^+) at the 1:100 and 1:1,000 g mL^{-1} liquid : solid.

The total concentrations of caesium in solutions were 2.30×10^{-10} mol L^{-1} and 6.80×10^{-5} mol L^{-1} (the solutions were labelled by ^{134}Cs). A mixture of Pu(IV) isotopes ($^{238,239,\ 240,\ 241}Pu$ prepared from highly contaminated Chernobyl soil) [16] was used in sorption experiments. Starting concentrations of Pu(IV) and ^{241}Am were 1.10×10^{-9} and 3.20×10^{-11} mol L^{-1}, respectively.

pH was measured before and after sorption experiments under continuous Ar flow using WTW pH-electrode SenTix 41, calibrated with standard buffers DIN 19266 (pH values 4.006, 6.865, 9.180) and a WTW inoLab Multi Level 1 m. The solids were separated from the liquid-phase by centrifugation for 20 min at 10,000–20,000 G. ^{134}Cs activities were measured with an intrinsic germanium detector (resolution 1.9 keV @ 1.33 MeV, and efficiency 42%). Plutonium and americium in the solution and the solid-phase were determined after radiochemical separation using UTEVA and TRU (Eichrom Industries) resins, and their activities were measured by alpha spectrometry. ^{242}Pu and ^{243}Am were used as tracers in the separation procedures. Precision of radionuclide measurements by gamma–alphas spectrometry was for Cs $\leq$ 2%, Pu $\leq$ 5%, Am $\leq$ 7%. Sr concentrations in the liquid-phase were measured with a Perkin Elmer Zeeman/3030 AAS-GF. Details of this experiment and the characterization of sorbents are described in previous publications [17, 18].

Results and discussion

Identification and characterization

Typical adsorption isotherm of studied TiSi and distribution of effective pore radii for TiSi synthesised in the presence of chloride and sulphate ions are presented in Fig. 1. Nitrogen adsorption-desorption isotherms belong to type IV in the IUPAC classification. *S*-shaped character indicates the mesoporous structure of synthesised samples. The specific surface area estimated using the BET method varied from 120 to 726 m^2 g^{-1}, the total volume of pores from 0.20 to 0.90 cm^3 g^{-1}, depending on the synthesis

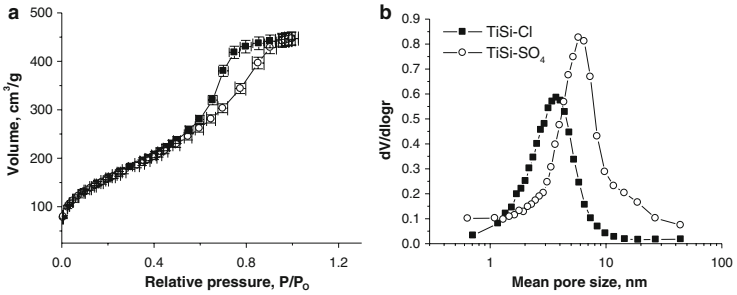

Fig. 1 Typical isotherm of adsorption/desorption N_2 for TiSi samples (**a**), and pore size distribution (*V*-pore volume, *r*-pore radius) of synthesised TiSi (**b**)

conditions, while volume of micropores ranged from 0.02 to 0.09 $m^3\ g^{-1}$, and the effective pores radii from 2.5 to 15.5 nm. It can be seen that the average pores radii in the presence of SO_4-ion increased from 5.7 to 7.8 nm. X-ray investigations of titanium silicates synthesised by different techniques (precipitation and sol-gel methods) showed their amorphous structure.

Preliminary studies were performed in order to determine the sorption ability of synthesised inorganic sorbents towards Sr, Cs, Pu and Am from natural groundwater, 0.1 mol L^{-1} $NaNO_3$ solutions, and fuel pond water. The highest K_d values were found for the system groundwater—TiSi ion exchangers. The data obtained indicated that Sr K_ds varied from 2.9×10^2 to 2.2×10^5 mL g^{-1} for inorganic sorbents and groundwater solutions. Cs K_d for the same sorbents and 0.1 mol L^{-1} $NaNO_3$ solutions varied from 30 to 4.1×10^4 mL g^{-1} whereas Pu K_d varied from 2×10^2 to 4.6×10^3 mL g^{-1}.

The obtained results indicate an effective use of TiSi sorbents during removal of cesium, strontium and plutonium from natural groundwater. It should be noted that a better sorption ability towards studied radionuclides was found for TiSi synthesised using titanilsulfate, whereas the method itself—precipitation or sol-gel—was not important.

Comparably high K_d values found for TiSi-17(SO_4) and TiSi-55(Cl) are promising for particular separations, and it is probably an indication that amorphous TiSi can act as exchangers towards a wide range of cations with dissimilar sizes and charge. On the other hand, the highest Pu K_d value found for sorbent TiSi-17(SO_4) in 0.1 mol L^{-1} $NaNO_3$ solution can be explained by an effect of the methyl groups introduced into the Ti silicate structure using the potassium methyl silicon and the hydrogen peroxide as complexion during the synthesis procedure. The presence of these groups provided formation of sorbent with a mesoporous structure, appropriate for sorption of large size ions.

Data on the Pu sorption kinetics have indicated that a rather short time period is required to reach equilibrium (Figs. 2, 3). Equilibrium was reached after about 2 h of sorption. Kinetic data were fitted to the pseudo-first-order kinetic model: $q_t = q_e(1\text{-}e^{-kadt})$, where q_t and q_e are Pu concentrations (mol/g) at time t and equilibrium, respectively as well as k_{ad} (min^{-1}) is the pseudo-first-order rate constant. It can be seen from the obtained parameters that the iron oxide kinetic data fit well the pseudo-first-order equation, whereas the TiSi's data require additional

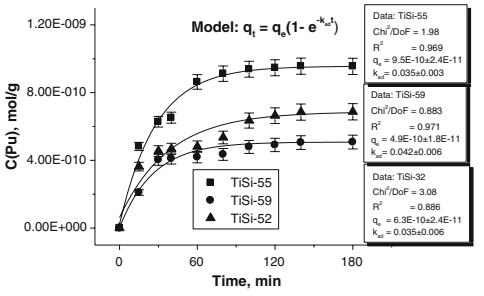

Fig. 2 Kinetics of Pu(IV) sorption to TiSi sorbents (0.1 mol L^{-1} $NaNO_3$ solution, pH 6.08–7.02 ±0.06, solid: liquid ratio 1: 1,000 g/mL)

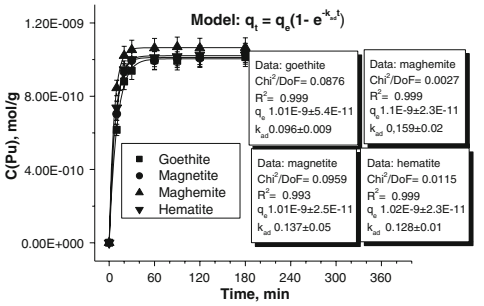

Fig. 3 Kinetics of Pu(IV) sorption to Fe oxides (0.1 mol L^{-1} $NaNO_3$ solution, pH 6.08–7.02 ±0.06, solid: liquid ratio 1: 1,000 g/mL)

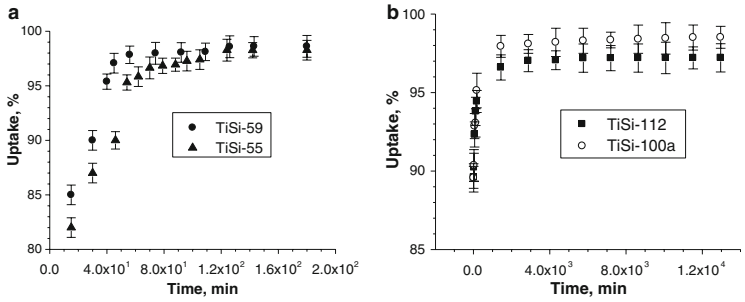

Fig. 4 Kinetics of Cs sorption to Ti–Si sorbents (0.1 mol L^{-1} $NaNO_3$ solution, pH 5.6–6.2 ±0.1, solid: liquid ratio 1: 1,000 g/mL)

analyses. Pu K_d equilibrium ranged from 2.5×10^3 to 4.1×10^3 mL g^{-1} for studied sorbents TiSi-17(SO_4), TiSi-32(SO_4), TiSi-55(Cl) and TiSi-59(Cl).

It should be noted that TiSis are porous materials with pore size distribution from 0.8 to 1.5 nm and their sorption ability towards studied radionuclides depends on their structural parameters. In addition, modification of methods used for preparation of TiSi gives opportunities to change their microstructure and porosity. Despite the fact that TiSi synthesised using the sol-gel methods showed a lower sorption ability towards studied radionuclides, they have great potential for tailoring of the chemical composition, the porosity and the surface properties, as well as for the synthesis of these materials in a granulated form, which is important for practical purposes of natural groundwater treatments.

Pu K_d values ranged from 4.8×10^3 to 1.6×10^4 mL g^{-1}, while Am K_d varied from 9×10^3 to 2.6×10^5 mL g^{-1} for Pu in the system iron minerals—natural groundwater. The obtained values were in a close range as determined for natural clay [17, 18]. An increase in the Pu K_d value by a factor of 6.8 was found for magnetite/hematite composite in comparison with the value for pure magnetite, and lower by a factor of 4 in comparison with the K_d value obtained for pure hematite. Nevertheless, synthesised magnetite/hematite composites possess magnetic properties and comparatively a high sorption ability towards Pu. Therefore, they can be used for separations.

Sorption kinetics is an important parameter of sorbents reflecting their efficiency and cost. Kinetics data for four sorbents are presented in Fig. 4. Better sorption parameters were found for sorbents TiSi-112 and TiSi-100a, when 90% of Cs was removed in the first 10 min. These better sorption parameters can be explained by their structure. Cs kinetics data of sample TiSi-55(Cl) indicated that there is a limitation on Cs ion diffusion into the mesoporous sorbent matrix. Studies of plutonium sorption kinetics indicated a faster plutonium sorption to iron oxides in comparison to TiSi.

Conclusions

The obtained results revealed that the highest sorption ability towards studied radionuclides showed titanium silicates synthesized using $TiOSO_4$ without reference to the chosen method (a co-precipitation or sol-gel). Magnetite and clay minerals showed better sorption ability towards americium. The highest Pu K_d values and better Pu sorption kinetics were found for synthetic iron oxides. An increase in the Pu K_d value by a factor of 6.8 found for magnetite/hematite composite in comparison with the pure magnetite suggests that this sorbent is efficient for plutonium removal and it is promising for its separation from contaminated solutions. Reported K_d values for uptakes of activated corrosion nuclides, fission products and transuranium elements (including ^{241}Am and ^{236}Pu) from 0.1 mol L^{-1} $NaNO_3$ for Am were 7.1×10^4 and 3.2×10^6 mL g^{-1} and for plutonium varied from 1.5×10^4 to 6.7×10^4 mL g^{-1} under similar conditions [19]. The published K_d values obtained using crystalline TiSi for Cs and Sr ranged from 8.9×10^5 to 9×10^5 mL g^{-1} and from 7.4×10^4 to 8.6×10^5 mL g^{-1}, respectively [20, 21]. Thus, TiSi tested in this study showed close sorbtion ability towards studied radionuclides, whereas they were synthesised under mild conditions using cheaper materials. It should be noted that modification of methods used for preparation of TiSi gives great opportunities to change their microstructure and porosity. Thus, despite the lower sorption ability of TiSi prepared by the sol-gel method, it has certain advantages in comparison with the fine powder TsSi. This is because of a huge potential for the tailoring of chemical composition, porosity and surface properties, as well as for the production in the granular form, which is especially important for practical purposes.

Acknowledgments This study was supported by the Ukrainian Ministry of Education, the Lithuanian Ministry of Education and the Lithuanian State Science and Studies Foundation project (grant No. 580 and No. V-35/2007, V-19/2009).

References

1. Povinec PP, Livingston HD, Shima S, Aoyama M, Gastaud J, Goroncy I, Hirose K, Huynh-Ngoc L, Ikeuchi Y, Ito T, La Rosa J, Liong Wee Kwong L, Lee SH, Moriya H, Mulsow S, Oregioni B, Pettersson H, Togawa O (2003) Deep Sea Res Part II 50:2607
2. Laubenstein M, Hult M, Gasparro J, Arnold D, Neumaier S, Heusser G, Ohler MK, Povinec P, Reyss J-L, Schwaiger M, Theodorsson P (2004) Appl Radiat Isot 61:167
3. Egorov VN, Povinec PP, Polikarpov GG, Stokozov NA, Gulin SB, Kulebakina LG, Osvath I (1999) J Environ Radioact 43:137
4. Clearfield A (1982) Inorganic ion exchange materials. CRC Press, Boca Raton, FL
5. Lehto J, Harjula R (1999) Radiochim Acta 86:65
6. Celestian AJ, Medvedev DG, Tripathi A, Parise JB, Clearfield A (2005) Nucl Instr Meth Phys Res 238:61
7. Clearfield A (2001) Solid State Sci 3:103
8. Manohar DM, Noeline BF, Anirudhan TS (2006) Appl Clay Sci 31:194
9. Karamanis D, Assimakopoulos PA (2007) Water Res 41:1897
10. Frenzer G, Maier WF (2006) Annu Rev Mater Res 36:281–331
11. Navratil JD (2001) J Radioanal Nucl Chem 248:571
12. Navratil JD (2001) Arch Oncol 9:257
13. Kanibolotskyy V, Meleshevych S, Strelko V, Kalenchuk V, Shenk N (2006) Patent of Ukraine No 76786A, IPC6 C01B 33/20; claimed 07.05.2004; published 15.09.2006; Bull No 9 (in Russian)
14. Meleshevych S, Kalenchuk V, Kanibolotskyy V, Shenk N, Strelko V, Psaryova T, Zakutevskyy O (2006) Patent of Ukraine No 76886A, IPC6 C01B 33/20; claimed 23.12.2004; published 15.09.2006; Bull No 9 (in Russian)
15. Lujanienė G, Meshevych S, Kanibolotskyy V, Mazeika K, Strelko V, Remeikis V, Kalenchuk V, Šapolaitė J (2008) Lit J Phys 48:107
16. Lujanienė G, Motiejūnas S, Šapolaitė J, Kamarauskas Ž (2005) Lit J Phys 45:273
17. Lujanienė G, Šapolaitė J, Amulevičius A, Mažeika K, Motiejūnas S (2006) Czech J Phys 56:103
18. Lujanienė G, Motiejūnas S, Šapolaitė J (2007) J Radioanal Nucl Chem 274:345
19. Al-Attar L, Dyer A, Harjula R (2003) J Mater Chem 13:2963
20. Bortun AI, Bortun LN, Poojary DM, Ouyang X, Clearfield A (2000) Chem Mater 12:294
21. Sylvester P, Clearfield A (1998) Solv Extr Ion Exch 16:1527

Publication V

Ivanets, A.I., Kitikova, N.V., Shashkova, I.L., Oleksiienko, O.V., Levchuk, I., Sillanpää, M.
Removal of Zn^{2+}, Fe^{2+}, Cu^{2+}, Pb^{2+}, Cd^{2+}, Ni^{2+} and Co^{2+} ions from aqueous solutions using modified phosphate dolomite
Reprinted with permission from
Journal of Environmental Chemical Engineering
Vol. 2, pp. 981–987, 2014

Journal of Environmental Chemical Engineering 2 (2014) 981–987

Contents lists available at ScienceDirect

Journal of Environmental Chemical Engineering

journal homepage: www.elsevier.com/locate/jece

Removal of Zn^{2+}, Fe^{2+}, Cu^{2+}, Pb^{2+}, Cd^{2+}, Ni^{2+} and Co^{2+} ions from aqueous solutions using modified phosphate dolomite

A.I. Ivanets[a,*], N.V. Kitikova[a], I.L. Shashkova[a], O.V. Oleksiienko[b], I. Levchuk[b], M. Sillanpää[b]

[a] Institute of General and Inorganic Chemistry of National Academy of Sciences of Belarus, st. Surganova 9/1, 220072 Minsk, Belarus
[b] Laboratory of Green Chemistry, Lappeenranta University of Technology, Sammonkatu 12, 50130 Mikkeli, Finland

ARTICLE INFO

Article history:
Received 10 December 2013
Accepted 24 March 2014

Keywords:
Phosphate dolomite
Metal ions
Adsorption
Isotherms

ABSTRACT

In the present work, modification of phosphate dolomite was conducted and applied for some bivalent metal ions removal. Physico-chemical properties of sorbent were characterized by means of X-ray diffraction (XRD), Fourier transform infrared spectroscopy (FTIR), differential-thermal analysis (DTA), thermogravimetric analysis (TGA), scanning electron microscopy (SEM) and low temperature adsorption–desorption of nitrogen. Sorption properties of modified dolomite for Zn^{2+}, Fe^{2+}, Cu^{2+}, Pb^{2+}, Cd^{2+}, Ni^{2+} and Co^{2+} removal were studied using model solutions. The highest removal efficiency was observed in pH range from 2 to 5. Among all tested metals, highest adsorption capacity of phosphated dolomite was detected towards Co^{2+} and Pb^{2+} (15 and 12 mmol g^{-1}, respectively) and the lowest towards Zn^{2+}, Fe^{2+} and Cu^{2+} (about 8 mmol g^{-1}). Adsorption isotherms were built for each tested metal ions and were fitted to Langmuir, Freundlich and Redlich–Peterson models.

Introduction

It is well known that bivalent metal ions pollution has become one of the most serious environmental problems today and elevated concentrations have been observed even in the most remote regions [1–3]. The number of methods such as ion exchange, membrane separation, electrolysis, chemical precipitation, and adsorption are used for removal metal ions from aqueous solutions [4–8]. Due to simplicity, effectiveness, and low cost adsorption is widely used technology for heavy metal ions removal [9]. As a rule it has been used as the main method for metal ions removal at low concentrations, or as a final polishing step. Some natural (dolomite, clay and related minerals, i.e., bentonites, montmorillonite, kaolinite [10–14]) or synthetic products (the nanosized metal oxides, metal phosphate, e.g., zirconium or hydroxyl apatite [15–17]) are known to be good adsorbents for metal ions and some of them have excellent ion-exchange properties. However, these materials have a low sorption capacity of 1–2 mmol g^{-1}, and they cannot always be used in acidic environments. Thus, there is a need for the search for novel highly effective sorbents for metal ions.

It has been demonstrated that calcium and magnesium phosphates of non-apatite structure synthesized from chemical reagents have a high sorption properties in processes of some metal ions removal from aqueous solutions [18]. As it was reported in [19], calcium and magnesium phosphates were obtained using natural dolomite – common and low-cost mineral consisting of magnesium and calcium carbonates. However, the obtained Ca–Mg phosphate sorbents were examined only towards Pb^{2+} ions and their sorption capacity was lower than that studied in [18].

The goal of present paper is to improve the method of synthesis of Ca–Mg phosphate sorbent using natural dolomite and to study its sorption properties towards Zn^{2+}, Fe^{2+}, Cu^{2+}, Pb^{2+}, Cd^{2+}, Ni^{2+} and Co^{2+} ions. The above mentioned metals were chosen based on content of real wastewaters from Zn–Cu mines.

Experimental

Preparation of sorbent

Dolomite from the Ruba deposit (Vitebsk region, Belarus) with the following chemical composition (wt.%): SiO_2 1.1, Fe_2O_3 0.4, Al_2O_3 0.5, CaO 30.3, MgO 20.0, SO_3 0.4, calcinations loss 47.0, K_2O 0.2, and Na_2O 0.1 was used as starting material for sorbent preparation. Ca–Mg phosphate was prepared by precipitation from aqueous solution as described in detail elsewhere [15] with several changes. For the synthesis of sorbent with a high content of calcium and magnesium phosphates and high sorption properties at the level of materials obtained in [18] it was previously suggested to activate the natural dolomite by its calcination at 800 °C. This will allow to remove organic impurities contained in the natural dolomite, and also to decompose the dolomites to the magnesium oxide and calcium carbonate [20], which will significantly improve its activity in interaction with nitric acid.

In contrast to previous work, the synthesis was realized by a slow controlled titration (5 mL s^{-1}), and after total addition of the ammonium phosphate solution the suspension was mated during 24 h.

* Corresponding author.
E-mail address: Ivanets@igic.bas-net.by (A.I. Ivanets).

2213-3437/$ - see front matter © 2014 Elsevier Ltd. All rights reserved.
http://dx.doi.org/10.1016/j.jece.2014.03.018

Table 1
Initial concentrations of metals in model solutions.

Metal	Cd^{2+}	Co^{2+}	Cu^{2+}	Fe^{2+}	Ni^{2+}	Pb^{2+}	Zn^{2+}
C (mg L^{-1})	133.7	93.7	94.4	89.5	96.8	2.7	123.1

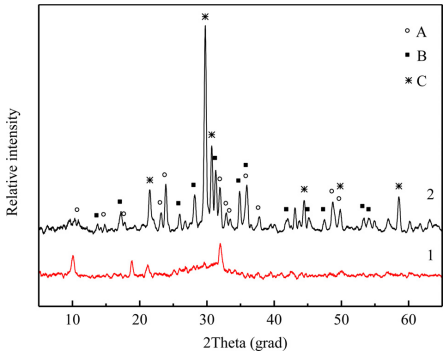

Fig. 1. X-ray diffraction patterns of Ca–Mg-phosphate after heating at 65 °C (1) and after calcination at 1000 °C (2). A – $Ca_4Mg_5(PO_4)_6$ (PDF No. 11-0231); B – $Ca_{2.81}Mg_{0.19}(PO_4)_2$ (PDF No. 70-682); C – $Mg_2P_2O_7$ (PDF No. 72-2042).

After the aging and washing with distilled water the precipitate of Ca–Mg phosphate was rinsed with ethanol. Replacement of intermicellar liquid (water–ethanol) allows to obtain the sorbent with a more developed mesoporous structure, because ethanol has a lower value of the surface tension than water.

Analytical methods

For elemental composition analysis, sorbent was dissolved in 6 M nitric acid. Total calcium and magnesium concentration was determined using complexometric EDTA-titration (±2%), magnesium concentration – by means of atomic-adsorption spectrometer (AAS) ontr AA 300 (Germany) (±3%). The concentration of PO_4^{3-} was defined spectrophotometrically as phosphovanadomolybdate complex at λ = 440 nm (±0.4%). Determination of nitrogen and carbon content was performed with the elemental analyzer Vario Micro. CHNS Mode (Elemetar Analysensysteme GmbH).

X-ray diffractometer (XRD) DRON-3 using Cu Kα radiation (2Θ 5–70°) was used for sorbent phase composition measurements. The morphology and the particle size of the sorbent were examined using a scanning electron microscope (SEM) JEOL-5610 LS (Japan). The Fourier transform infrared spectrum (FTIR) of the sample in KBr pellet was recorded on Midac Fourier transform infrared field spectrometer at room temperature in the range of 400–4000 m^{-1}.

DTA and TGA were performed by means of derivatograph system NETZSCH STA 409 PC/PG, when heated with a speed of 10 °/min from 20 to 1000 ° in air atmosphere.

The adsorption and texture properties of the sorbent were assessed by isotherms of low temperature (−196 °C) physical adsorption–desorption of nitrogen, measured by the volumetric method on an ASAP 2020 MP surface area and porosity analyzer (Micromeritics, US). The surface area of pores per unit mass of the solid or the specific surface area was determined by the methods of a single point (A_{sp}), BET (A_{BET}), and Langmuir (A_L). The single point method was used to calculate not only the specific surface area A_{sp}, but also the adsorption and desorption volumes ($V_{sp.ads}$ and $V_{sp.des}$) of pores and their average adsorption and desorption diameters D_{ads} and D_{des}. The cumulative adsorption and desorption volumes V_{BJHads} and V_{BJHdes} of pores with diameters in the range 1.7–300 nm, and the average adsorption and desorption pore diameters D_{BJHads} and D_{BJHdes} were calculated by the Barrett–Joyner–Halenda (BJH) method. The differential distribution of the mesopore volume over diameters, dV/d log D, was calculated by the Barrett–Joyner–Halenda method. The relative error in determining the pore volume was ±1% for the surface area and ±15% for the pore size.

Concentrations of metals in samples received during adsorption tests were determined by means of inductively coupled plasma optical emission spectrometer (ICP-OES) model iCAP 6300 (Thermo Electron Corporation, USA). Measurements of pH were carried out by means of pH meter 340i (±0.02).

Adsorption studies and modeling

Chemicals

Chemicals used for preparation of model solutions were $ZnSO_4{\cdot}6H_2O$, $FeSO_4{\cdot}7H_2O$, $CuSO_4{\cdot}5H_2O$, $Pb(NO_3)_2$, $CdSO_4$, $NiSO_4{\cdot}6H_2O$, $CoSO_4{\cdot}7H_2O$ and H_2SO_4, which were of analytical grade and utilized as purchased from Sigma–Aldrich without further purification. HNO_3 (Suprapur, 65%) was purchased from Merck Millipore International. Laboratory glassware was washed with strong HCl or HNO_3. For all experiments, Milli-Q water (resistance 18.2 MΩ cm^{-1}) was used.

Dose of sorbent

Purpose of this part of study was to determine the optimum dose of prepared sorbent for maximum removal of Zn^{2+}, Fe^{2+}, Cu^{2+}, Pb^{2+}, Cd^{2+}, Ni^{2+} and Co^{2+} from model solutions, initial concentrations of model solutions are presented in Table 1. Therefore, sorbent with concentrations in range from 0.5 g L^{-1} to 10 g L^{-1} were agitated with 20 mL of model solution (pH = 2.6) for 24 h using rotary shaker ST15 (CAT, M.Zipperer GmbH, Staufen, Germany). After that sorbent was filtered using 0.45 μm polypropylene syringe filter, concentration of metals in solutions was measured with ICP-OES.

Effect of pH on adsorption of metals

Influence of pH on the removal of metals using synthesized sorbent was studied in pH varying from 1 to 6. For pH adjustment H_2SO_4 (98%) and NaOH (5 M) solutions were used. Concentration of sorbent used in these tests was 10 g L^{-1}, volume of model solution, containing Zn^{2+}, Fe^{2+}, Cu^{2+}, Pb^{2+}, Cd^{2+}, Ni^{2+} and Co^{2+} was 10 mL and contact time was 24 h.

Study of metal ions sorption in time

In this study, during which 0.2 g of sorbent was mixed with 20 mL of model solution with pH 2.6 was conducted at ambient temperature. Concentration of metals was measured in samples taken at desired time.

Adsorption isotherms for one-component systems

Experiments were conducted at room temperature for 24 h and volume of 10 mL of model solution was mixed with 0.1 g of sorbent material. Single component model solutions of Zn^{2+}, Fe^{2+}, Cu^{2+}, Pb^{2+}, Cd^{2+}, Ni^{2+} and Co^{2+} with initial concentrations ranging from 0.1 to 2.0 g L^{-1} were tested. Data obtained from these experiments were used for building adsorption equilibrium isotherms in accordance with Langmuir, Freundlich and Redlich–Peterson models,

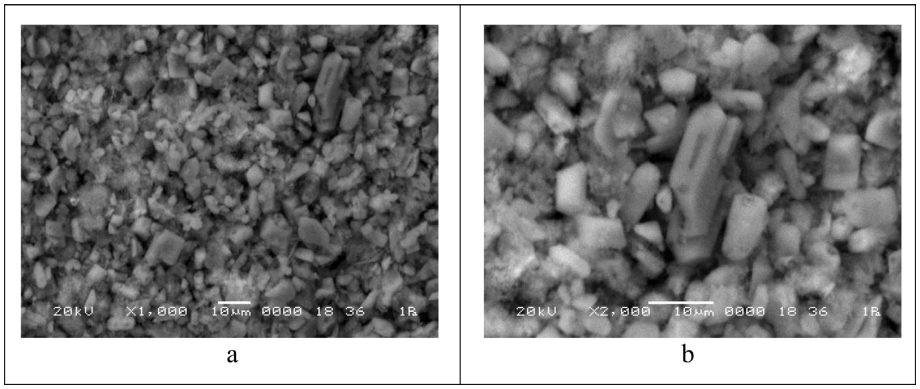

Fig. 2. SEM micrographs of Ca–Mg phosphate after heating at 65 °C, magnified 1000 × (a) and 2000 × (b).

Table 2
Adsorption properties (specific surface area, pore volume and pore diameter) of the sorbent.

Specific surface area ($m^2\ g^{-1}$)			Pore volume ($cm^3\ g^{-1}$)				Pore diameter (nm)			
A_{sp}	A_{BET}	A_L	$V_{sp\ ads}$	$V_{sp\ des}$	$V_{BJH\ ads}$	$V_{BJH\ des}$	$D_{sp\ ads}$	$D_{sp\ des}$	$D_{BJH\ ads}$	$D_{BJH\ des}$
49	54	78	0.182	0.238	0.270	0.272	15	19	23	16

Table 3
Parameters of isotherms.

Metal	Langmuir				Freundlich			
	$q_{exp.}$ (mmol g^{-1})	$q_{calc.}$ (mmol g^{-1})	K_L	R^2	$q_{calc.}$ (mmol g^{-1})	K_F	n	R^2
Cd^{2+}	10.88	6.78	4.23	0.778	9.62	2.30	3.25	0.945
Co^{2+}	15.12	14.19	0.06	0.950	16.68	2.71	3.68	0.961
Cu^{2+}	8.68	7.81	10.07	0.983	9.08	3.30	4.49	0.962
Fe^{2+}	8.37	8.38	2038.14	0.880	8.97	5.49	9.57	0.742
Ni^{2+}	9.35	8.76	0.27	0.944	9.86	2.38	3.47	0.983
Pb^{2+}	12.42	11.49	832.98	0.911	13.13	6.34	8.29	0.704
Zn^{2+}	7.84	7.58	45.48	0.987	8.92	4.08	5.73	0.890

Metal	**Redlich–Peterson**				
	$q_{exp.}$ (mmol g^{-1})	$q_{calc.}$ (mmol g^{-1})	K_{RP}	n_{RP}	R^2
Cd^{2+}	10.88	9.60	9928.0	0.70	0.944
Co^{2+}	15.12	15.70	1.33	0.81	0.992
Cu^{2+}	8.68	8.49	26.73	0.90	0.998
Fe^{2+}	8.37	7.76	768.24	1.07	0.896
Ni^{2+}	9.35	9.59	6.87	0.77	0.992
Pb^{2+}	12.42	11.81	600.20	1.02	0.915
Zn^{2+}	7.84	7.65	49.22	0.99	0.987

which are basically used for the description of adsorption of single component. All isotherms used in this study are presented below [21]:

Langmuir:

$$q_e = \frac{q_m K_L C_e}{1 + K_L C_e} \quad (1)$$

where q_e and C_e are the adsorption capacity (mmol g^{-1}) and the equilibrium concentration of the adsorbate (mmol L^{-1}) respectively, while q_m and K_L represent the maximum adsorption capacity of adsorbents (mmol g^{-1}) and the energy of the adsorption (L $mmol^{-1}$) respectively.

Freundlich:

$$q_e = K_F C_e^{1/n_F} \quad (2)$$

where K_F ((mmol g^{-1})/(L $mmol^{-1})^n{}_F$) and n_F are the Freundlich adsorption constants.

Redlich–Peterson:

$$q_e = \frac{q_m K_{RP} C_e}{1 + (K_{RP} C_e)^{n_{RP}}} \quad (3)$$

where K_{RP} and n_{RP} are the Redlich–Peterson constants.

Fitting of experimental data with mentioned models were carried out using the solver add-in with Microsoft's spreadsheet, Microsoft Excel. In order to check accuracy of the experimental data fitting by isotherms the coefficient of determination (R^2) presented below was

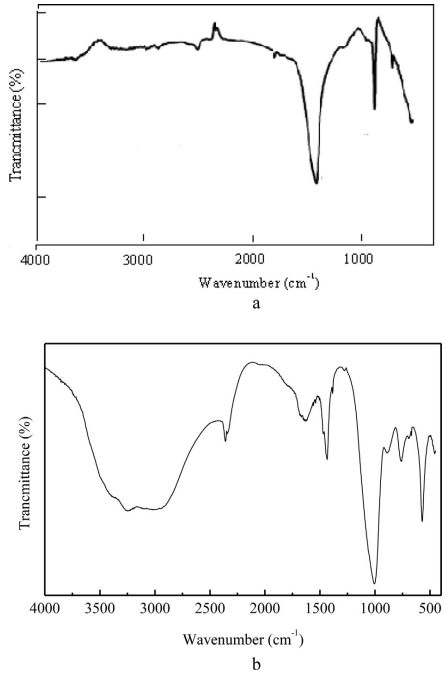

Fig. 3. FTIR spectrum of initial dolomite (a) and Ca–Mg-phosphate after heating at 65 °C (b).

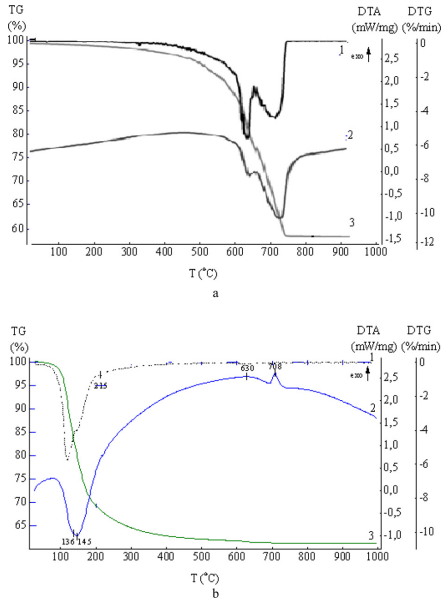

Fig. 4. DTG (1), DTA (2) and TG (3) curves for initial dolomite (a) and Ca–Mg-phosphate sample (b).

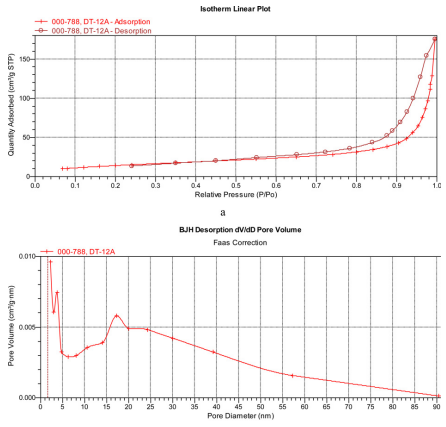

Fig. 5. Isotherms of low-temperature adsorption–desorption of nitrogen in the linear form (a) and pore diameter distribution curves dV/dD–D plotted using BJH method (b) for the sorbent synthesized.

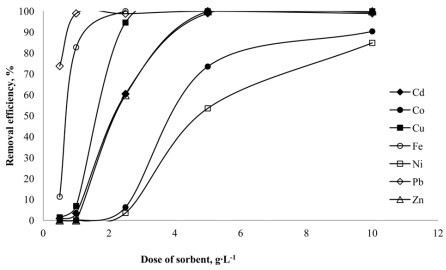

Fig. 6. Dependence of metal removal efficiency on concentration of sorbent.

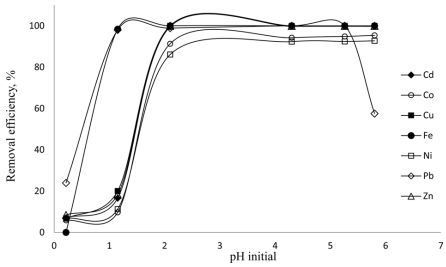

Fig. 7. Elimination of Zn^{2+}, Fe^{2+}, Cu^{2+}, Pb^{2+}, Cd^{2+}, Ni^{2+} and Co^{2+} at various initial pH. Contact time 24 h, dose of sorbent 10 g L^{-1}.

applied.

$$R^2 = \frac{\Sigma(q_{e,exp} - \overline{q}_{e,exp})^2 - \Sigma(q_{e,exp} - \overline{q}_{e,calc})^2}{\Sigma(q_{e,exp} - \overline{q}_{e,exp})^2} \quad (4)$$

where $q_{e,calc}$ is equilibrium capacity, calculated from isotherm equation, $q_{e,exp}$ is equilibrium capacity obtained experimentally and $\overline{q}_{e,exp}$ is mean value of $q_{e,exp}$.

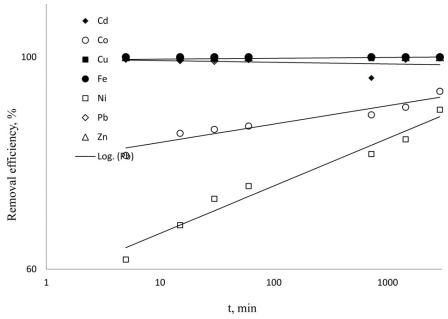

Fig. 8. Dependence of metal removal efficiency on contact time, dose of sorbent 10 g L^{-1}, pH of solution was 2.6.

Results and discussion

Characterization of material

Summing up data of elemental analysis, the composition of prepared sorbent can be described with formula $_3Mg_2(NH_4)_{1.3}(PO_4)_4(CO_3)_{0.3}{\cdot}6H_2O$. The presence of ammonia groups could explain the fact of calcium and magnesium phosphates precipitation performed by ammonia solution. As a result, the obtained sorbent includes the impurities of phase $MgNH_4PO_4{\cdot}6H_2O$ (struvite). The low content of CO_3^{2-} ions in sorbent confirms the almost complete transformation of dolomite to calcium and magnesium phosphates.

The chemical composition is confirmed by the data of the physicochemical analytical methods. From XRD data it can be seen that sorbent is at amorphous state (Fig. 1, curve 1).

As result of heat treatment of sorbent with formula $_3Mg_2(NH_4)_{1.3}(PO_4)_4(CO_3)_{0.3}{\cdot}6H_2O$ at 1000 °, phases , and were crystallized, where and are binary Ca−Mg phosphate with Ca:Mg = 4:5 and Ca:Mg = 2,81:0.19, respectively, is magnesium pyrophosphate – the main product of polymerization of HPO_4^{2-} anion forming after the NH_3 removal from struvite (Fig. 1, curve 2).

$$MgNH_4PO_4 \cdot 6H_2O \rightarrow MgHPO_4 \cdot nH_2O + NH_3 \uparrow \rightarrow Mg_2P_2O_7 + H_2O \quad (5)$$

The low crystallinity and the heterogeneity of composition were confirmed using SEM (Fig. 2). The electron micrographs show that sorbent consisted of both, little oval particles with average dimensions around 2–4 μm and their aggregates and small crystals with a length of 10–16 μm and diameter of 6 μm. Such crystal form is typical for struvite. [22,23]

Fig. 3 shows FTIR spectrums of initial dolomite and after phosphate. The spectrum of Ca−Mg phosphate sample (3b) contains not only the phosphate bands at 570 and 1000 cm^{-1}, but also the bands of NH_4^+ group at 1380, 1435 and 1470 cm^{-1}. The rest bands are attributed to hydrogen bonds of water–phosphate or water–NH_4^+ group [24]. The form of spectrum suggests the amorphous state of the sorbent. The phosphate groups have the unresolved bands that are typical for a poorly crystalline phosphate phase. The O_3^{2-} group has several bands in the same range as NH_4^+ group but carbonate content is very low, therefore, it cannot be observed at FTIR spectrum.

The DTA, DTG and TG curves for the initial dolomite and obtained sample are presented in Fig. 4. The DTA curve (Fig. 4b) shows two endothermic peaks at 136 and 145 °C and exothermic peaks around 630 and at 708 °C. The DTG curve has additional small peak at 215 °C. The peaks at 145, 215 and 630 °C are attributed to the removal of water, then the removal of the ammonia and the formation of $Mg_2P_2O_7$, respectively [24–26]. The peaks at 136 and 708 °C correspond to the removal of crystal hydrate water and the crystallization of Ca- and Mg phosphates [27]. The phases observed by XRD after heating of the sample correspond to thermal analysis data (Fig. 1, curve 2). Thus, it was established that after thermal treatment sorbent consists of mixture of $Mg_2P_2O_7$ and two phosphatic phases, such as $Ca_4Mg_5(PO_4)_6$ and $Ca_{2.81}Mg_{0.19}(PO_4)_2$.

The sorption isotherm in Fig. 5a is mostly type IV and demonstrate that the sample belongs to mesoporous structures. The hysteresis loop in the isotherms is type N3 according to the IUPAC classification. Analysis of the differential curves of the pore diameter distributions by the BJH method (Fig. 5b) makes it possible to identify a mesoporous structure with a predominant pore diameter of 15–20 nm and 2–4 nm.

According to the data from Table 2 the mesopore volumes by single point (ads/des) and BJH (ads/des) are 0.182/0.238 and 0.270/0.272 $cm^3\ g^{-1}$ and the specific surface areas by single point, BET and Langmuir are 49, 54 and 78 $m^2\ g^{-1}$, respectively. The average pore diameter calculated by single point and BJH methods are in the range 15–23 nm.

Adsorption studies

Dose of sorbent

According to Fig. 6, removal efficiency of Fe^{2+}, Pb^{2+} and Cu^{2+} is higher than 90% at sorbent concentration around 2 g L^{-1}. The efficient removal of Zn^{2+} and Cd^{2+} is reached at sorbent dose 5 g L^{-1}. The removal efficiency of Co^{2+} and Ni^{2+} is the lowest from all tested metals – less than 85%. Taking into account that at concentration of sorbent equal to 10 g L^{-1} removal efficiency of all tested metals was the highest, this sorbent dose was chosen as optimum for further studies.

Effect of pH

Aim of this part of study was to determine optimum pH conditions for efficient elimination of all metals presented in model solution. In previous paper [18] it was shown that the removal of bivalent metal ions follows complex mechanism which included physical adsorption, ion exchange and chemisorption. The polyvalent ions interact with Ca−Mg phosphate and obtain compounds with low solubility. It is also clear that different pH of initial solutions determines a different state of metal ions in solution.

Results, which are shown in Fig. 7, suggest that highest removal efficiency for all considered metals was observed within pH range from 2 to 5, which is relatively wide and can be beneficial for the treatment of different types of wastewaters. Fe^{2+} and Pb^{2+} adsorption had the widest pH range – from 1 to 6 and 1–5.2, respectively. The optimal pH value provides the condition for the maximum extraction of polyvalent metal ions from solution. The low efficiency of metal ions removal at pH < 2 was connected with the increased solubility as phosphate-sorbent, and the product of its interaction.

Study of metal ions sorption in time

In order to find out required time for achieving equilibrium, this study was carried out. Model solution was used for this purpose. Samples were taken after 5, 15, 30, 60, 720, 1440 and 2880 min. In Fig. 8 removal efficiency of metals depending on sampling time was shown. As it can be noticed from this plot, already after 5 min of experiment such metals as Cd^{2+}, Cu^{2+}, Fe^{2+}, Pb^{2+} and Zn^{2+} were removed completely. Whereas, sorption of Co^{2+} and Ni^{2+} was not so fast, achieving highest elimination of abovementioned metals after 2880 min. This fact probably related to ionic radii: the kinetics of metal cations slowed with decreases of the ionic radii.

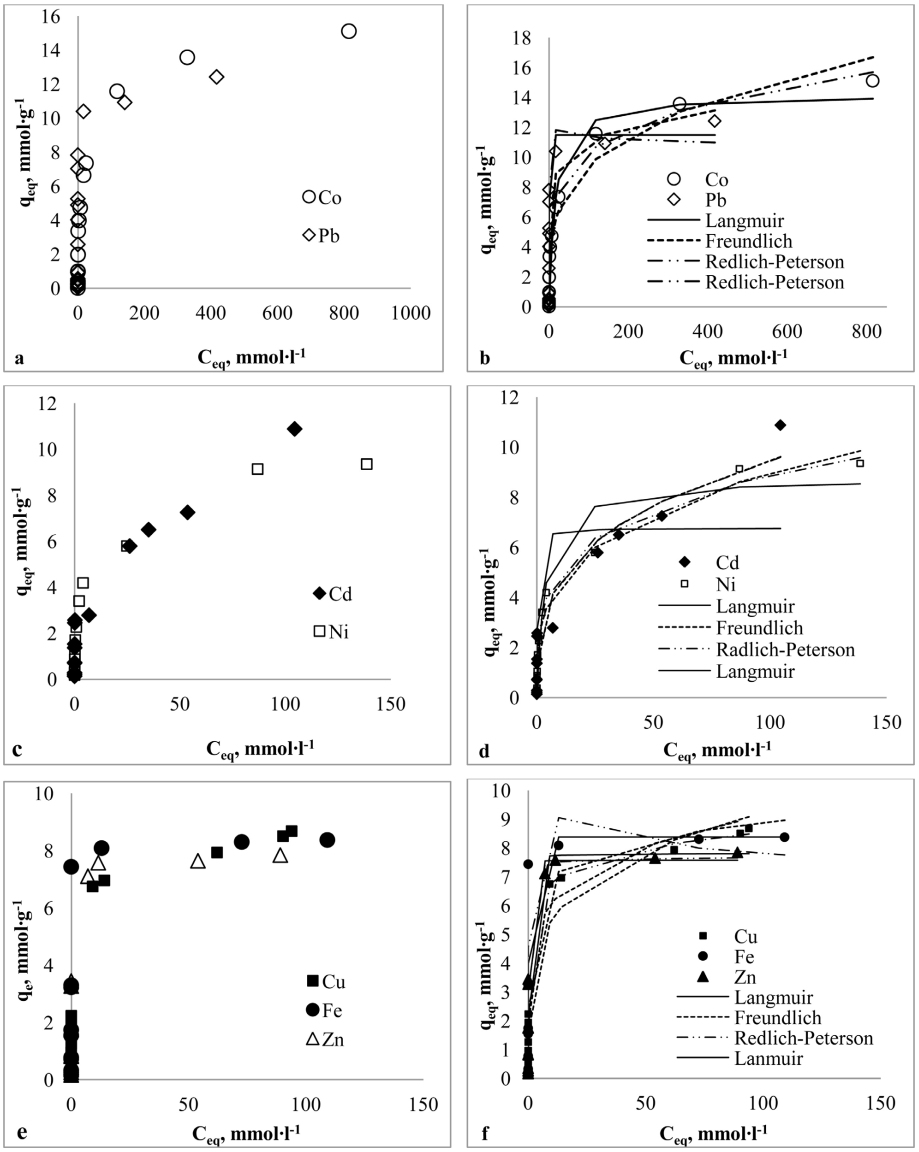

Fig. 9. Adsorption isotherms of cations from aqueous solution. Contact time 24 h, dose of sorbent 10 g L^{-1}, pH of solution 2.6.

Adsorption isotherms

Adsorption isotherms were obtained for each of the following metals: Zn^{2+}, Fe^{2+}, Cu^{2+}, Pb^{2+}, Cd^{2+}, Ni^{2+} and Co^{2+} at different initial concentrations (Fig. 9, curves a, c, and e). All isotherms belong to H type according to Giles classification of adsorption on solids from liquids. This is a case in which the solute has such high affinity that in dilute solutions it is adsorbed completely or till trace amount, which are difficult to detect. It was found that adsorption affinity towards metal cations increases with the rise of the ionic radius. The effect of ionic radii was observed in [28]. The selectivity range of metals for synthesized material can be presented as Ni < Co < Zn˜Fe˜Cu˜Cd˜Pb at low concentration (100 mg L^{-1}) from both model aqueous solutions (Figs. 7 and 8). At higher metal concentrations, the selectivity range changes and can be shown in following form Zn < Fe < Cu < Ni < Cd < Pb < Co. The increasing of maximum adsorption of Ni^{2+} and Co^{2+} could be arised as a summing result of the following factors: 1 – the complex composition of adsorbent (consisting of three cations and two anions), 2 – different forms of finding the ions of these metals in solution; 3 – features of the mechanism of interaction of various metal ions with a sorbent; 4 – different solubility of compound formed as a results of interactions. For example, in works [29–31] observed hiding of adsorption range from directly-proportional of radii either.

Equilibrium data were fit to Langmuir, Freundlich and Redlich–Peterson models (Fig. 9, curves b, d, and f). As it can be seen from Table 3, experimental data can be described more precisely with Redlich–Peterson model for Zn^{2+}, Cu^{2+}, Ni^{2+} and Co^{2+}. The complexity of choosing models for cadmium Cd^{2+}, Fe^{2+} and Pb^{2+} sorption by synthesized sorbent arises due to the complex mechanism of sorption.

Conclusion

The sorption material with high content of calcium and magnesium was synthesized from natural dolomite using the improved method. According to results of physico-chemical analysis established that composition of prepared sorbent can be described with formula $_3Mg_2(NH_4)_{1.3}(PO_4)_4(CO_3)_{0.3}{\cdot}6H_2O$, sorbent has a low crystallinity and developed mesopore structure.

The adsorption studies showed the high sorption properties towards Zn^{2+}, Fe^{2+}, Cu^{2+}, Pb^{2+}, Cd^{2+}, Ni^{2+} and Co^{2+} ions. The highest removal efficiency of chosen metal ions was observed in pH range from 2 to 5 with adsorbent concentration in model solution equal to 10 mg L^{-1}. It was established that obtained material has maximum adsorption capacity (up to 12–15 mmol g^{-1}) towards Co^{2+} and Pb^{2+}, while the adsorption of Co^{2+} and Ni^{2+} were the slowest among the rest cations. Collected data allows to conclude that prepared material can be used as an effective adsorbent for divalent metal cations from acidic water aqueous solutions.

References

[1] F. Fu, Q. Wang, Removal of heavy metal ions from wastewaters: a review, Journal of Environmental Management 92 (2011) 407–18. http://dx.doi.org/10.1016/j.jenvman.2010.11.011, 21138785.

[2] X. Huang, M. Sillanpää, B. Duo, E.T. Gjessing, Water quality in the Tibetan plateau: metal contents of four selected rivers, Environmental Pollution 156 (2008) 270–7. http://dx.doi.org/10.1016/j.envpol.2008.02.014, 18375027.

[3] X. Huang, M. Sillanpää, E.T. Gjessing, R.D. Vogt, Water quality in the Tibetan plateau: major ions and trace elements in the headwaters of four major Asian rivers, Science of the Total Environment 407 (2009) 6242–54. http://dx.doi.org/10.1016/j.scitotenv.2009.09.001, 19783282.

[4] L. Zhang, Y.-H. Zhao, R. Bai, Development of multifunction membrane for chromatic warning and enhanced adsorptive removal of heavy metal ions: application to cadmium, Journal of Membrane Science 379 (2011) 69–79. http://dx.doi.org/10.1016/j.memsci.2011.05.044.

[5] S.O. Kim, S.H. Moon, K.W. Kim, S.T. Yun, Pilot scale study on the ex situ electrokinetic removal of heavy metals from municipal wastewater sludges, Water Research 36 (2002) 4765–74. http://dx.doi.org/10.1016/S0043-1354(02)00141-0, 12448519.

[6] M.J.S. Yabe, E. Oliveria, Heavy metal removal in industrial effluents by sequential adsorbent treatment, Advanced in Environmental Research 7 (2003) 263–72. http://dx.doi.org/10.1016/S1093-0191(01)00128-9.

[7] S.-F. Lo, S.-Y. Wang, M.-J. Tsai, L.-D. Lin, Adsorption capacity and removal efficiency of heavy metal ions by Moso and Ma bamboo activated carbons, Chemical Engineering Research and Design 90 (2012) 1397–406. http://dx.doi.org/10.1016/j.cherd.2011.11.020.

[8] C. Blöcher, J. Dorda, V. Mavrov, H. Chmiel, N.K. Lazaridis, K.A. Matis, Hybrid flotation—membrane filtration process for the removal of heavy metal ions from wastewater, Water Research 37 (2003) 4018–26. http://dx.doi.org/10.1016/S0043-1354(03)00314-2, 12909122.

[9] S. Babel, T.A. Kurniawan, Low-cost adsorbents for heavy metals uptake from contaminated water: a review, Journal of Hazardous Materials 97 (2003) 219–43. http://dx.doi.org/10.1016/S0304-3894(02)00263-7, 12573840.

[10] G.M. Walker, G. Connor, S.J. Allen, Copper(II) removal onto dolomitic sorbents, Chemical Engineering Research and Design 82 (2004) 961–6. http://dx.doi.org/10.1205/0263876041580712.

[11] E. Pehlivan, A.M. Özkan, S. Dinç, Ş. Parlayici, Adsorption of Cu^{2+} and Pb^{2+} ion on dolomite powder, Journal of Hazardous Materials 167 (2009) 1044–9. http://dx.doi.org/10.1016/j.jhazmat.2009.01.096, 19237240.

[12] K.G. Bhattacharyya, S.S. Gupta, Adsorption of a few heavy metals on natural and modified kaolinite and montmorillonite: a review, Advances in Colloid and Interface Science 140 (2008) 114–31. http://dx.doi.org/10.1016/j.cis.2007.12.008, 18319190.

[13] M.G.A. Vieira, A.F.A. Neto, M.L. Gimenes, Removal of nickel on Bofe bentonite calcined clay in porous bed, Journal of Hazardous Materials 176 (2010) 109–18, .

[14] S.M.I. Sajidu, I. Persson, W.R.L. Masamba, et al. Mechanisms of heavy metal sorption on alkaline clays from Tundulu in Malawi as determined by EXAFS, Journal of Hazardous Materials 158 (2008) 401–9. http://dx.doi.org/10.1016/j.jhazmat.2008.01.087, 18329799.

[15] M. Hua, Sh. Zhang, B. Pan, Heavy metal removal from water/wastewater by nanosized metal oxides: a review, Journal of Hazardous Materials 211–212 (2012) 317–31, .

[16] B. Pan, Q. Zhang, W. Du, et al. Selective heavy metals removal from waters by amorphous zirconium phosphate: behavior and mechanism, Water Research 41 (2007) 3103–11. http://dx.doi.org/10.1016/j.watres.2007.03.004, 17433402.

[17] A. Aklil, M. Mouflih, S. Sebti, Removal of heavy metal ions from water by using calcined phosphate as a new adsorbent, Journal of Hazardous Materials 112 (2004) 183–90. http://dx.doi.org/10.1016/j.jhazmat.2004.05.018, 15302439.

[18] I.L. Shashkova, A.I. Rat'ko, N.V. Kitikova, Removal of heavy metal ions from aqueous solutions by alkaline-earth metal phosphate, Colloids and Surfaces, Part A 160 (1999) 207–15. http://dx.doi.org/10.1016/S0927-7757(99)00193-4.

[19] N.V. Kitikova, I.L. Shashkova, A.I. Rat'ko, Synthesis of calcium and magnesium phosphates from natural carbonates and study of their activity in reactions with lead(II) ions, Russian Journal of Applied Chemistry 76 (2003) 368–73. http://dx.doi.org/10.1023/A:1025632213519.

[20] A.I. Rat'ko, A.I. Ivanets, A.I. Kulak, et al. Thermal decomposition of natural dolomite, Journal of Inorganic Materials 47 (2011) 1372–7. http://dx.doi.org/10.1134/S0020168511120156.

[21] K.Y. Foo, B.H. Hameed, A review: insights into the modeling of adsorption isotherm systems, Chemical Engineering Journal 156 (2010) 2–10. http://dx.doi.org/10.1016/j.cej.2009.09.013.

[22] L.N. Schegrov, Phosphaty Dvyhvalentnyh Metallov, Kiev, Nauk. Dumka, 1987, p. 216.

[23] E. Banks, R. Chianelli, R. Korenstein, Crystal chemistry of struvite analogs of the type $MgMPO_4{\cdot}6H_2O$ ($M^+ = K^+$, Rb^+, Cs^+, Tl^+, NH_4^+), Inorganic Chemistry 14 (1975) 1634–9. http://dx.doi.org/10.1021/ic50149a041.

[24] E. Vorndran, A. Ewald, F.A. Müller, et al. Formation and properties of magnesium–ammonium–phosphate hexahydrate biocements in the Ca–Mg–PO_4 system, Journal of Materials Science: Materials in Medicine 22 (2011) 429–36. http://dx.doi.org/10.1007/s10856-010-4220-4.

[25] F. Abbona, A. Baronnet, A XRD and TEM study on the transformation of amorphous calcium phosphate in the presence of magnesium, Journal of Crystal Growth 165 (1996) 98–105. http://dx.doi.org/10.1016/0022-0248(96)00156-X.

[26] R.N. Panda, M.F. Hsieh, R.J. Chung, T.S. Chin, FTIR, XRD, SEM and solid state NMR investigations of carbonate-containing hydroxyapatite nano-particles synthesized by hydroxide-gel technique, Journal of Physics and Chemistry of Solids 64 (2003) 193–9. http://dx.doi.org/10.1016/S0022-3697(02)00257-3.

[27] V.A. Sinyaev, E.S. Shustikova, L.V. Levchenko, et al. Nature and thermal behavior of precipitated calcium–magnesium phosphates, Russian Journal of Applied Chemistry 76 (2003) 1375–9. http://dx.doi.org/10.1023/B:RJAC.0000012650.94921.ee.

[28] E.R. Nightingale, Phenomenological theory of ion solvation. Effective radii of hydrated ions, Journal of Chemical Physics 63 (1959) 1381–8. http://dx.doi.org/10.1021/j150579a011.

[29] J.H. Choi, S.D. Kim, Y.J. Kwon, W.J. Kim, Adsorption behaviors of ETS-10 and its variant, ETAS-10 on the removal of heavy metals, Cu^{2+}, Co^{2+},Mn^{2+} and Zn^{2+} from a waste water, Microporous and Mesoporous Materials 96 (2006) 157–67. http://dx.doi.org/10.1016/j.micromeso.2006.03.050.

[30] M.G. Klimantaviėiūtė, D. Virbalytė, V. Pakštas, R. Juškėnas, A. Pigaga, Interaction of heavy metal ions with cement kiln dust, Ekologija 1 (2005) 31–6.

[31] P. Tzvetkova, R. Nickolov, Modified and unmodified silica gel used for heavy metal ions removal from aqueous solutions, Journal of the University of Chemical Technology and Metallurgy 47 (2012) 498–504.

ACTA UNIVERSITATIS LAPPEENRANTAENSIS

671. SALMINEN, JUHO. The role of collective intelligence in crowdsourcing innovations. 2015. Diss.

672. ROSAS, SAILA. Co-operative acquisitions – the contextual factors and challenges for co-operatives when acquiring an investor-owned firm. 2015. Diss.

673. SINKKONEN, TIINA. Item-level life-cycle model for maintenance networks – from cost to additional value. 2015. Diss.

674. TUUNANEN, JUSSI. Modelling of changes in electricity end-use and their impacts on electricity distribution. 2015. Diss.

675. MIELONEN, KATRIINA. The effect of cationic-anionic polyelectrolyte multilayer surface treatment on inkjet ink spreading and print quality. 2015. Diss.

676. OMAJENE, JOSHUA. Underwater remote welding technology for offshore structures. 2015. Diss.

677. NUUTINEN, PASI. Power electronic converters in low-voltage direct current distribution – analysis and implementation. 2015. Diss.

678. RUSATSI, DENIS. Bayesian analysis of SEIR epidemic models. 2015. Diss.

679. STRAND, ELSI. Enhancement of ultrafiltration process by pretreatment in recovery of hemicelluloses from wood extracts. 2016. Diss.

680. TANNINEN, PANU. Press forming of paperboard – advancement of converting tools and process control. 2015. Diss.

681. VALTONEN, PETRI. Distributed energy resources in an electricity retailer's short-term profit optimization. 2015. Diss.

682. FORSSTRÖM-TUOMINEN, HEIDI. Collectiveness within start up-teams – leading the way to initiating and managing collective pursuit of opportunities in organizational contexts. 2015. Diss.

683. MAGUYA, ALMASI. Use of airborne laser scanner data in demanding forest conditions. 2015. Diss.

684. PEIPPO, JUHA. A modified nominal stress method for fatigue assessment of steel plates with thermally cut edges. 2015. Diss.

685. MURASHKO, KIRILL. Thermal modelling of commercial lithium-ion batteries. 2016. Diss.

686. KÄRKKÄINEN, TOMMI. Observations of acoustic emission in power semiconductors. 2016. Diss.

687. KURVINEN, EMIL. Design and simulation of high-speed rotating electrical machinery. 2016. Diss.

688. RANTAMÄKI, JUKKA. Utilization of statistical methods for management in the forest industry. 2016. Diss.

689. PANOVA, YULIA. Public-private partnership investments in dry ports – Russian logistics markets and risks. 2016. Diss.

690. BAHARUDIN, EZRAL. Real-time simulation of multibody systems with applications for working mobile vehicles. 2016. Diss.

691. MARTIKAINEN, SOILI. Development and effect analysis of the Asteri consultative auditing process – safety and security management in educational institutions. 2016. Diss.

692. TORVINEN, PEKKA. Catching up with competitiveness in emerging markets – An analysis of the role of the firm's technology management strategies. 2016. Diss.

693. NORONTAUS, ANNUKKA. Oppisopimuskoulutus yritysten tuottamana koulutuspalveluna: tavoitteista vaikutuksiin. 2016. Diss.

694. HALMINEN, OSKARI. Multibody models for examination of touchdown bearing systems. 2016. Diss.

695. TALONPOIKA, ANNA-MARIA. Financial working capital – management and measurement. 2016. Diss.

696. INKINEN, HENRI. Intellectual capital, knowledge management practices and firm performance. 2016. Diss.

697. YANG, XIAOCHEN. Development of a welding production quality control and management system model for China. 2016. Diss.

698. LEMINEN, VILLE. Leak-proof heat sealing of press-formed paperboard trays. 2016. Diss.

699. LAAKSONEN, LAURI. Spectral retinal image processing and analysis for ophthalmology. 2016. Diss.

700. OINONEN, MINNA. Management of customer co-development in business-to-business markets. 2016. Diss.

701. ALATALO, SARA-MAARIA. Hydrothermal carbonization in the synthesis of sustainable porous carbon materials. 2016. Diss.

702. UZHEGOV, NIKITA. Design and material selection of high-speed rotating electrical machines. 2016. Diss.

703. RICHTER, CHRIS. Digital collaborations and entrepreneurship – the role of shareconomy and crowdsourcing in the era of smart city. 2016. Diss.

704. JAFARI, SHILA. Investigation of adsorption of dyes onto modified titanium dioxide. 2016. Diss.

705. PATEL, YOGINI. Computational modelling of non-equilibrium condensing steam flows in low-pressure steam turbines. 2016. Diss.

706. LEVCHUK, IRINA. Titanium dioxide based nanomaterials for photocatalytic water treatment. 2016. Diss.

707. AMOUR, IDRISSA. Variational ensemble kalman filtering applied to data assimilation problems in computational fluid dynamics. 2016. Diss.

708. SHESTAKOVA, MARINA. Ultrasound-assisted electrochemical treatment of wastewaters containing organic pollutants by using novel Ti/Ta2O5-SnO2 electrodes. 2016. Diss.